Spring 2003

Understanding wavelet analysis and filters for engineering applications

Chethan Bangalore Parameswariah
Louisiana Tech University

INFORMATION TO USERS

This manuscript has been reproduced from the microfilm master. UMI films the text directly from the original or copy submitted. Thus, some thesis and dissertation copies are in typewriter face, while others may be from any type of computer printer.

The quality of this reproduction is dependent upon the quality of the copy submitted. Broken or indistinct print, colored or poor quality illustrations and photographs, print bleedthrough, substandard margins, and improper alignment can adversely affect reproduction.

In the unlikely event that the author did not send UMI a complete manuscript and there are missing pages, these will be noted. Also, if unauthorized copyright material had to be removed, a note will indicate the deletion.

Oversize materials (e.g., maps, drawings, charts) are reproduced by sectioning the original, beginning at the upper left-hand corner and continuing from left to right in equal sections with small overlaps.

ProQuest Information and Learning
300 North Zeeb Road, Ann Arbor, MI 48106-1346 USA
800-521-0600

UNDERSTANDING WAVELET ANALYSIS AND FILTERS FOR ENGINEERING APPLICATIONS

By

Chethan Parameswariah. B. E., M.S.

A Dissertation Presented in Partial Fulfillment
of the Requirements for the Degree of
Ph. D in Engineering.

COLLEGE OF ENGINEERING AND SCIENCE
LOUISIANA TECH UNIVERSITY

May 2003

LOUISIANA TECH UNIVERSITY

THE GRADUATE SCHOOL

04/04/2003
Date

We hereby recommend that the thesis prepared under our supervision by Chethan Bangalore Parameswariah

entitled Understanding Wavelets Analysis and Filters for Engineering Applications

be accepted in partial fulfillment of the requirements for the Degree of PhD in Engineering

Supervisor of Thesis Research

Head of Department

Department

Recommendation concurred in:

Advisory Committee

Approved:
Director of Graduate Studies

Approved:
Dean of the Graduate School

Dean of the College

GS Form 13
(1/00)

ABSTRACT

Wavelets are signal-processing tools that have been of interest due to their characteristics and properties. Clear understanding of wavelets and their properties are a key to successful applications. Many theoretical and application-oriented papers have been written. Yet the choice of a right wavelet for a given application is an ongoing quest that has not been satisfactorily answered. This research has successfully identified certain issues, and an effort has been made to provide an understanding of wavelets by studying the wavelet filters in terms of their pole-zero and magnitude-phase characteristics. The magnitude characteristics of these filters have flat responses in both the pass band and stop band. The phase characteristics are almost linear. It is interesting to observe that some wavelets have the exact same magnitude characteristics but their phase responses vary in the linear slopes. An application of wavelets for fast detection of the fault current in a transformer and distinguishing from the inrush current clearly shows the advantages of the lower slope and fewer coefficients - Daubechies wavelet D4 over D20. This research has been published in the IEEE transactions on Power systems and is also proposed as an innovative method for protective relaying techniques.

For detecting the frequency composition of the signal being analyzed, an understanding of the energy distribution in the output wavelet decompositions is presented for different wavelet families. The wavelets with fewer coefficients in their filters have more energy leakage into adjacent bands. The frequency bandwidth characteristics display flatness in the middle of the pass band confirming that the frequency of interest should be in the middle of the frequency band when performing a wavelet transform. Symlets exhibit good flatness with minimum ripple but the transition regions do not have sharper cut off. The number of wavelet levels and their frequency ranges are dependent on the two parameters – number of data points and the sampling frequency – and the selection of these is critical to qualitative analysis of signals.

A wavelet seismic event detection method is presented which has been successfully applied to detect the P phase and the S phase waves of earthquakes. This method uses wavelets to classify the seismic signal to different frequency bands and then a simple threshold trigger method is applied to the rms values calculated on one of the wavelet bands.

Further research on the understanding of wavelets is encouraged through this research to provide qualified and clearly understood wavelet solutions to real world problems. The wavelets are a promising tool that will complement the existing signal processing methods and are open for research and exploration.

APPROVAL FOR SCHOLARLY DISSEMINATION

The author grants to the Prescott Memorial Library of Louisiana Tech University the right to reproduce, by appropriate methods, upon request, any or all portions of this Dissertation. It is understood that "proper request" consists of the agreement, on the part of the requesting party, that said reproduction is for his personal use and that subsequent reproduction will not occur without written approval of the author of this Dissertation. Further, any portions of the Dissertation used in books, papers, and other works must be appropriately referenced to this Dissertation.

Finally, the author of this Dissertation reserves the right to publish freely, in the literature, at any time, any or all portions of this Dissertation.

Author chethan B.P.

Date 5/15/2003.

GS Form 14
(5/03)

TABLE OF CONTENTS

LIST OF FIGURES

LIST OF TABLES

ACKNOWLEDGEMENTS

First my thanks go to God for the grace and mercy he has blessed me with. My thanks to my wife Pallavi, for all her support and encouragement, and I appreciate her patience as I spent days on end just working on this research. If not for her, I wouldn't have reached this milestone.

My deepest thanks and gratitude goes to my advisor Dr. Louis Roemer for his encouragement and support through my school years. My deep appreciation goes to Dr Mickey Cox for his continued guidance after my Master's degree. Also, thanks to Dr Natalia Zotov who has always given me invaluable guidance. I extend my sincere appreciation to Dr. David Hall and Dr. Ray Sterling for their professional help.

I do need to mention my parents Umadevi and R. Parameshwaraiah, my brother Vagesh and my sister Sowmya for the whole hearted-love they share with me and who have made me the person that I am through their continued support of my dreams and ambitions.

Also I thank Jinson Erinjeri for all his help and assistance in completing my Ph.D without whom some tasks would have been much more difficult.

CHAPTER 1

INTRODUCTION

On November 25, 1998 moviegoers were treated to wonder with a full-length feature film called "A Bug's Life" released by Walt Disney Pictures and Pixar Animation Studios. One would have wondered about the computer animation and the mathematical modeling required to make such a movie. The movie portrayed a variety of characters in the animated ants' story – not to mention their many textures, their myriad expressions, and the way they jumped, flitted and buzzed around. In this movie, a particular type of computer animation modeling technique that makes use of mathematical procedures called "wavelets" was making its debut [1].

Wavelets are finding use in applications like the one described above and is a rapidly developing area of mathematical and application-oriented research in all fields of science and engineering. They have been widely used in image processing, data compression, denoising, reconstruction of high-resolution images and other communication areas.

The signal processing and engineering study is full of transient phenomena such as seismic earthquake signals, musical instrument signals, electrical transformer inrush currents, aircraft fault signals, switching transients in optical laser systems and many others. Use of wavelets for characterizing and analyzing these transient signals in practical engineering fields is slowly growing.

An engineer or researcher may be more interested in studying the effects of these transient signals on signal quality, power and energy variations, frequency and phase fluctuations, etc. than the effect of steady state signals. The study of these signals becomes more important as they tend to be random, unrepetitive and unpredictable than steady state signals. Detection of these transients to take remedial measures to prevent damage to the system in which they are present is an important aspect of science and engineering. The real time detection of transient signals is significant due to the short, finite duration of the transients and for fast solution and control of the system.

One such transient signal of importance is a seismic signal. Seismic signals obtained from seismometers and accelerometers are continuously being recorded all over the world in hope of measuring and analyzing them for better understanding of the ground below us. Seismic signals from earthquake events provide us valuable information in terms of the pre and post event ground motion. The earthquake event generates a transient signal that just lasts for a short duration and is a good candidate for study by the wavelet transform. A frequency spectrum of the seismic signal is known to have amplitude peaking in the 0.05 Hz to 0.3 Hz frequency band, called the microseism band. The microseism band's peak is understood to change in response to events occurring on the earth and is explained later in this research. Wavelets decompose the signals into

frequency bands keeping the time information intact, providing a good basis for analyzing and obtaining the information of an event. Microseism effects are considerable for any facility or setup that extends to more than a kilometer like water and gas pipelines, large research establishments, urban utility facilities, railroads, etc. This lower frequency band also poses a challenge for the selection of an optimum wavelet. Recent earthquakes in the U.S. and Japan have shown a need for advanced earthquake disaster mitigation management in order to prevent or minimize damage especially in urban areas [2]. Early detection of a oncoming event can help us stop gas and water flow through pipes, cut off electricity, and stop trains to minimize or even prevent major disaster and casualties.

Analysis of seismic signals is still being done using conventional techniques discovered decades ago [3] – [5]. Sweldens, W. in his paper "Wavelets: What next?" quotes "problems not sufficiently explored with wavelets— Prediction: The stock market, earthquakes, weather." [6]. Wavelets have a potential to be an important analysis tool for analysis of signals in ground-based technologies such as trenchless technology, life sciences and geo-sciences.

The Fourier transform has been a very popular signal analysis tool with the signal processing community since its introduction. All kinds of signals have been analyzed, forcing a close examination of the transform method. A drawback was noticed in the Fourier transform: they have trouble reproducing abrupt changes and transients in signals. A music synthesizer, however good it might be, it still can't match the performance of an artist in concert. This is because they cannot reproduce the transient features— such as contact of the bow on the string or the snare of drum. These short

duration events are they are poorly represented by combination of pure sine waves and cannot be reproduced effectively.

The Fourier transform assumes that the signal $f(x)$ is periodic, but most transient signals are non-stationary signals. In Fourier transform, we convert the time-based signal to a frequency-based signal, and hence the time information is lost. As the transient signal is random, unpredictable and unrepetitive, the time of occurrence of a particular disturbance signal is more important. According to Heisenberg Indeterminacy Principle, it is not possible to know simultaneously the exact frequency and the exact time of occurrence of this frequency in a signal.

Researchers came up with a somewhat of a solution where the time of occurrence can be detected by the windowed Fourier Transform or Short Time Fourier Transform (STFT) that has a specific fixed window width of measurement. But the fixed window means a trade-off between frequency resolution and time resolution. The wide window gives a good frequency resolution but a poor time resolution, whereas a narrow window gives a good time resolution but a poor frequency resolution. The relationship between the resolution in time and the resolution in frequency is a concept commonly referred to as the uncertainty principle mentioned above and is given by:

$$\Delta t \times \Delta f \geq \frac{1}{4\pi} \qquad -(1)$$

where Δt is the resolution in time domain and Δf is the resolution in frequency. The equation implies that both the time and frequency cannot be made arbitrarily small: one must be traded for the other [7].

Wavelets are the new analysis tools that are widely being used in signal analysis. Wavelets have been useful in theory for the last two decades but have not been found to have a revolutionary impact upon science and engineering like the Fourier transform. Wavelet transforms do offer many interesting features that the Fourier transform does not posses. The wavelets provide a greater resolution in time for high frequency components of a signal and greater resolution in frequency for the low frequency components. In wavelet analysis, the transients are decomposed into a series of wavelet components, each of which is a time-domain signal that covers a specific octave band of frequency. Hence, the wavelet analysis converts the time-based signal to time-scale regions, where scale is an octave band of frequency. These bands of frequency are non-overlapping bands with constant-Q characteristics. Wavelets do a very good job in detecting the time of the signal, but they give the frequency information in terms of frequency band regions or scales.

The focus of this research is to present the analysis of transient signals using wavelets with an emphasis on the quality and quantity of wavelet decomposition. In some applications, wavelets have been successfully used in identifying the system disturbances, especially with regards to time localization. Tutorial and theoretical papers have been published to address the issue of time localization [8]-[11]. But just identifying the time location of an event is not sufficient for understanding the event. For quality monitoring and analysis, the wavelet transforms must be able to detect, localize, estimate and classify disturbances accurately. Wavelet research is progressing slowly towards this area as the few papers published indicate [12]-[16]. This research looks at the wavelet analysis from an engineer's point of view and answers the questions that arise during analysis such as the choice of wavelets for a particular application, the energy frequency distribution in

each of the wavelet levels, the magnitude and phase of wavelet filters and the frequency bandwidth characteristics of the wavelet levels. This research applies wavelets to transient signals such as motor inrush and fault currents, and seismic signals, in order to understand these characteristics and provides results that are helpful when used for making a selection of a wavelet for a particular application. Advantages, constraints and limitations that arise when applying wavelets to transient seismic and motor current signals, which are relevant to trenchless technology, are discussed.

Part of the above research studying the mentioned characteristics of wavelets was published in a paper authored by Dr. Mickey Cox and Chethan Parameswariah, which has been accepted for publication without comments by the IEEE [17]. The objective of this research is to further the understanding and application of wavelets by engineers in the analysis of transient events. "It is a misunderstanding that any wavelet is suitable for any signal and any applications. Choosing or designing the right wavelet is crucial for a successful WT application" [18].

The applications of wavelets are not limited if they are understood clearly by engineers and researchers. One day, wavelet transforms may be the analysis tool of choice in science and engineering like Fourier transforms. But till that day, more needs to be done to understand them and apply them for practical everyday applications.

CHAPTER 2

WAVELET ANALYSIS – THE BASICS

For an engineer presented with a signal to analyze for its contents, the first tool that probably runs through his mind is the universally accepted Fourier analysis. However, as mentioned before, just knowing the frequency content of the signal is not the complete information, especially if the signal contains transients. Though wavelet analysis cannot completely replace Fourier analysis, it is quickly growing to complement it. But with increased wavelet research, there has been a continued motivation to get the best bases and functions. Unlike Fourier transform where the basis functions are only a combination of sines and cosines of infinite length, these wavelet basis functions have different shapes and finite length. These wavelet bases are mostly grouped according to their inventor and more are being developed even today. Some of the more well-known wavelet families are Daubechies, Haar, Coiflets, Symlets, Mexican hat, and Meyer – to name a few.

To understand wavelet analysis, let us consider a signal with 1024 data points per second sampled using an A/D converter. A small discontinuity

(break) is introduced into the signal at 800th data point due to a transient intermittent cable connection.

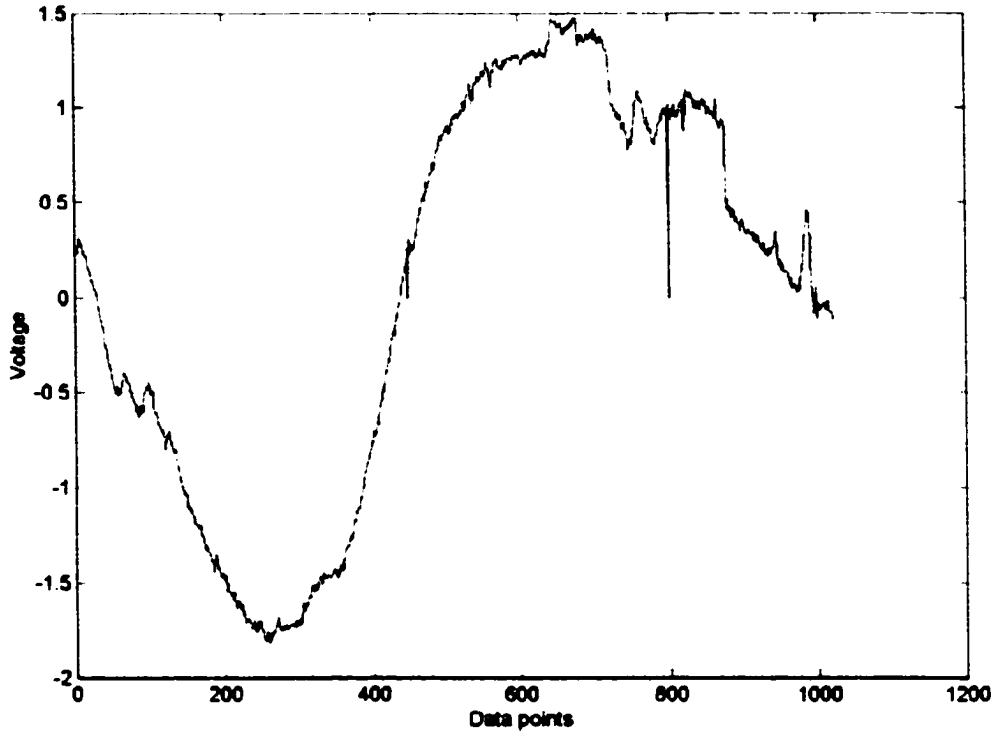

Figure 1: Signal With 1024 Data Points.

FOURIER ANALYSIS:

If we perform a Fourier analysis of the above signal, we transform the time domain signal into frequency domain and display the output as a frequency spectrum. The signal is seen to be made up of an infinite set of sines and cosines which if combined with proper amplitude and phase can reproduce the original signal to certain accuracy. The frequency spectrum output of the Fourier analysis for the signal in figure 1 is shown in figure 2. The maximum frequency is limited to the half the sampling frequency to satisfy Nyquist criteria. The information of the time of occurrence of the break and other characteristics are lost in the frequency spectrum.

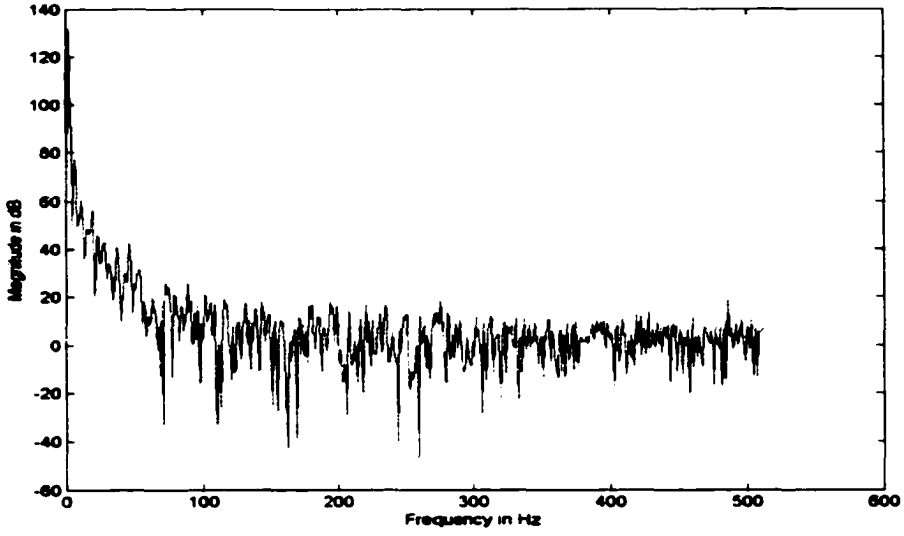

Figure 2: Frequency Spectrum Of The Signal In Figure 1.

WAVELET ANALYSIS:

Performing the wavelet analysis using MATLAB(R) on the same signal with Daubechies D4 wavelet for 10 levels, we get the output as shown in figure 3. Unlike the frequency spectrum where the x and y axes are the frequency and the magnitude respectively, for the wavelet decomposition, x-axis is the time and y-axis is the amplitude of the decomposed signal. Also, the wavelet analysis output provides us with time domain decomposed signals which fall into certain frequency bands or scales. These scales are divided into octave bands of frequency between the ranges: zero on the lower end to half the sampling frequency at the higher end. The lowest frequency-band scale is known as the "*approximation*" of the original signal, and the other scales are known as the "*details*" which are in increasing octave frequency bands. Figure 3 shows 10 scales with the low frequency approximation "a9" signal at the top and the details below it. Detail "d9" is the next higher frequency octave while the detail "d1" is the last octave band within the frequency range and has the highest frequency components.

The number of scales or levels a signal can be fully decomposed into is given by $N = 2^n$, where N is the number of data points and n the number of levels. Hence, for a signal with N = 1024 data points, we have 2^{10} or n =10 levels. Also, as seen from figure 3, wavelet analysis clearly picks out the location of the discontinuity in the signal and can be seen pronounced along the time axis in the high frequency details. The time information of the specifics of the signal is preserved in the wavelet decomposition. However, it is also seen that we cannot pick out specific frequencies, and their amplitudes that make up the original signal.

Figure 3: Wavelet Decompositions Of The Signal In Figure 1.

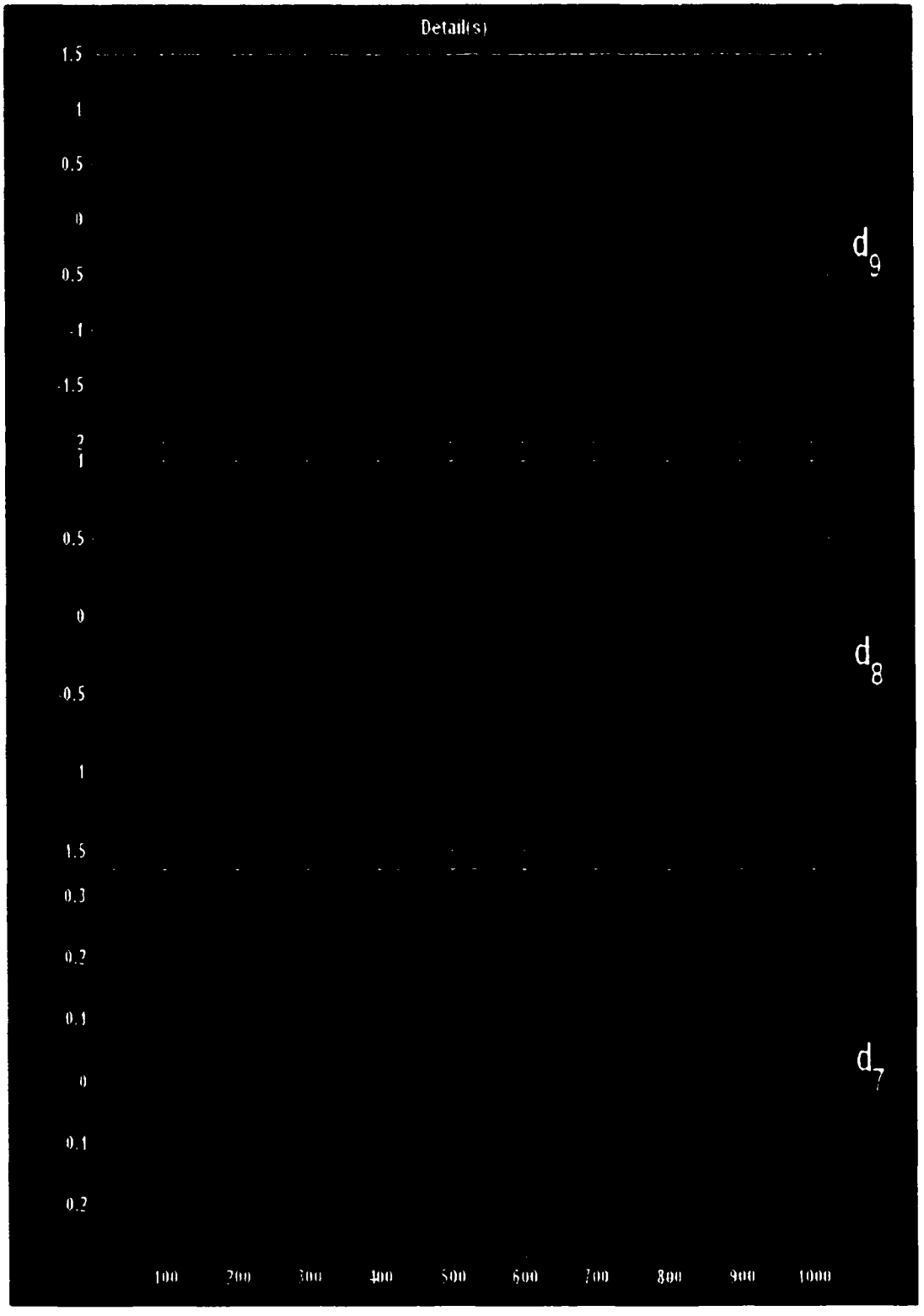

Figure 3 (Continued): Wavelet Decompositions Of The Signal In Figure 1.

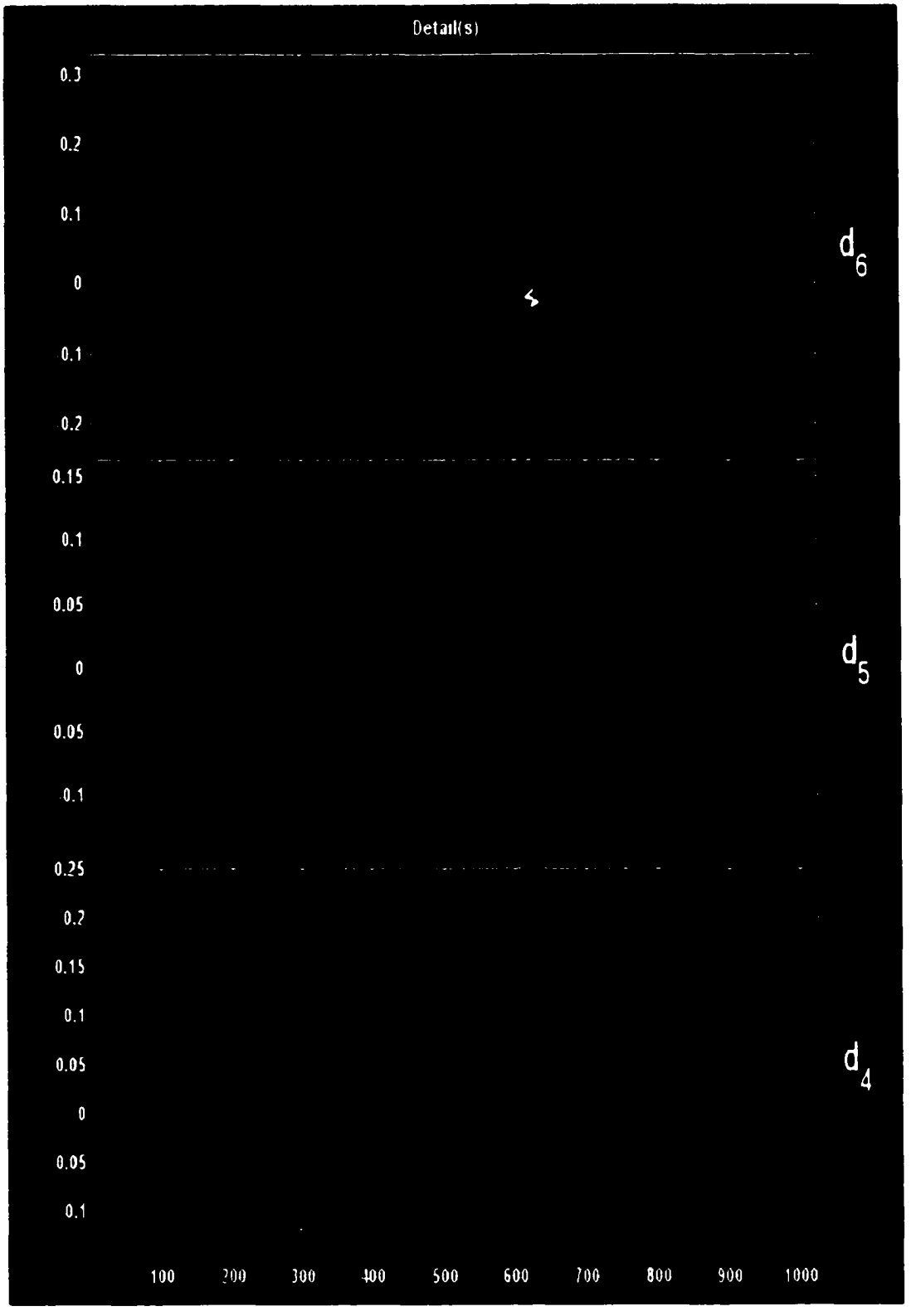

Figure 3 (Continued): Wavelet Decomposition Of The Signal In Figure 1.

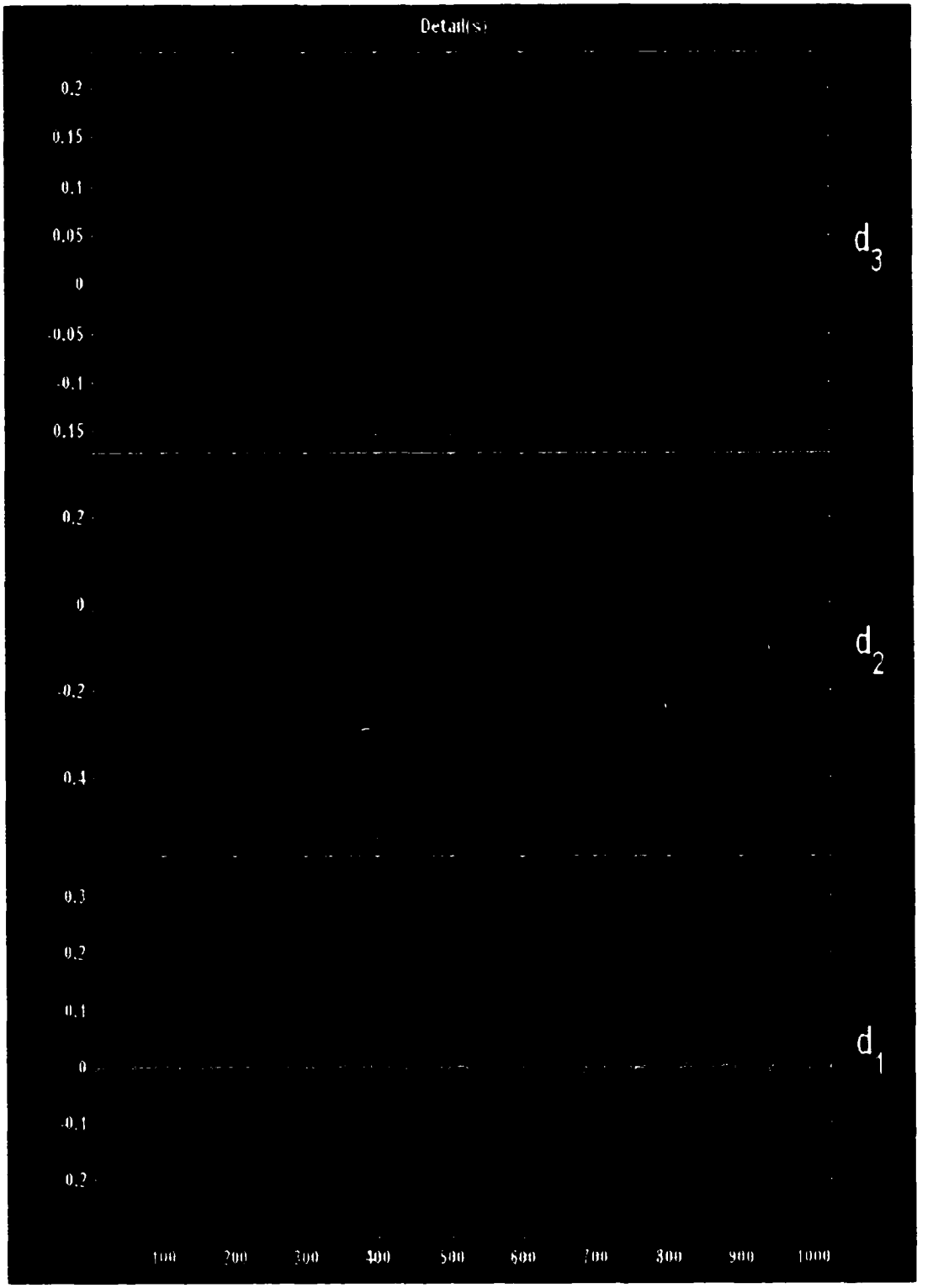

Figure 3 (Continued): Wavelet Decomposition Of The Signal In Figure 1.

The time-frequency resolution is a limitation of the wavelet analysis as imposed by the Heisenberg uncertainty principle which is given by:

$$\Delta t \times \Delta f \geq \frac{1}{4\pi} \qquad -(2)$$

where Δt is the resolution in time domain and Δf is the resolution in frequency. The equation implies that both the time and frequency cannot be made arbitrarily small: one must be traded for the other [7].

The wavelet decomposition achieves the best trade off by having varying resolutions in both the time domain and frequency domain, i.e., the time resolution is very small for high frequency details compared to the longer time resolution for the low frequency approximations. The Short Time Fourier Transform – STFT which tries to localize time by performing Fourier analysis over a short time window is disadvantaged by the time window which is kept constant for all frequencies. Figure 4 shows a pictorial representation of the wavelet time – scale resolution.

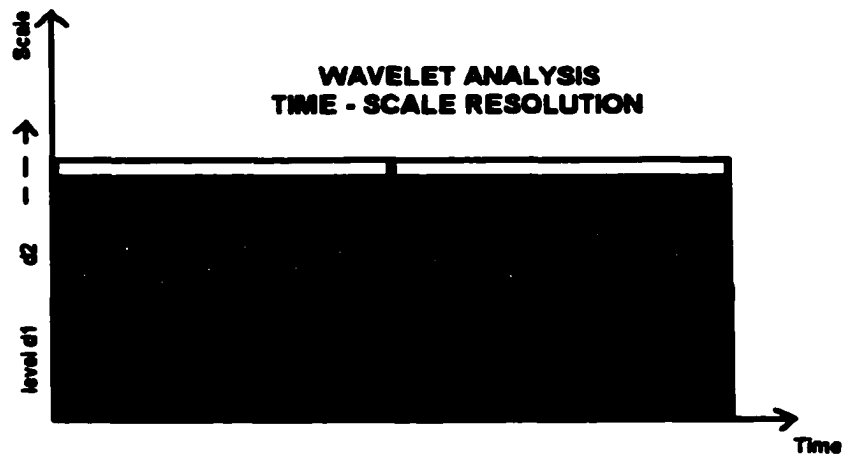

Figure 4: Pictorial Representation Of Wavelet Time – Scale Resolution.

Referring back to figure3. we can compute the frequency ranges for the 10 scales of wavelet decomposition using the equation (2) given below:

$$f = 2^{v}\left(f_s / N\right) \qquad -(3)$$

where f is the higher frequency limit of the frequency band represented by the level v. The f_s sampling frequency and N is the number of data points in the original input signal [8].

Table 1 shows the frequency to scale (level) relation for the different levels of Daubechies D4 wavelet decomposition shown in figure 3. The signal in figure 1 sampled at f_s = 1024 samples/sec and N = 1024.

Table 1: Frequency Band Information For The Daubechies D4 Wavelet For The Signal In Figure 1.

Level	Wavelet Scale	Frequency range (Hz)	Center Frequency (Hz)
0	a9	0 – 1.0	0.5
1	d9	1.0 – 2.0	1.5
2	d8	2.0 – 4.0	3.0
3	d7	4.0 – 8.0	6.0
4	d6	8.0 – 16	12
5	d5	16 – 32	24
6	d4	32 – 64	48
7	d3	64 – 128	96
8	d2	128 – 256	192
9	d1	256 - 512	384

Many books and papers have been written that explain and talk about wavelet decomposition of signals [19] – [22] and can be read for further understanding of the basics of wavelet theory. A short theory behind the wavelets is presented here for the sake of completeness.

WAVELET THEORY:

The wavelet transform moves a time domain signal into the wavelet domain. The basis functions of the wavelet transform are short waves of finite duration. Similar to the Fourier transform $F(\omega)$ which can be represented by:

$$F(w) = \int_{-\infty}^{\infty} f(t) e^{-j\cdot\omega\cdot t} dt \qquad -(4)$$

where $f(t)$ is the signal being transformed and the exponential $e^{-j\omega t}$ can be written in terms of the basis functions – sines and cosines as:

$$e^{j\omega t} = \cos\omega\cdot t + j\sin\omega\cdot t$$

the continuous wavelet transform (CWT) can be written as:

$$CWT(b,a) = \int_{-\infty}^{\infty} f(t) k_{b,a}(t) dt \qquad -(5)$$

where a is the scale variable of the wavelet (replaces the frequency variable ω of the Fourier transform), b the time shift variable of the wavelet (usually the time period variable τ), and the expression $k_{b,a}(t)$ can be written as the basis functions

$$k_{b,a}(t) = \frac{1}{\sqrt{a}} w^*\left(\frac{t-b}{a}\right) \qquad -(6)$$

where the right hand side of the equation (5) represents a weighted set of scaled wavelet functions of the mother wavelet $w(t)$ [7].

The mother wavelet basis function is a small wave with finite duration between time $t = 0$ and $t = N$ unlike the infinite time sines and cosines used for Fourier transform. This locality in time implies that most of the energy is restricted to a finite interval and function is ideally zero outside this interval. In general, we want fast, e.g. inverse polynomial or exponential, decay away from the center of mass of the function [6]. A typical wavelet $w(t)$ is compressed j times and shifted k times which is given by:

$$w_{jk}(t) = w(2^{j}t - k) \qquad -(7)$$

The remarkable property that is achieved by many wavelets is orthogonality [22]. That means the inner products of the wavelets are zero:

$$\int_{c} w_{jk}(t) w_{JK}(t) dt = 0 \qquad -(8)$$

except when $j = J$ and $k = K$.

In the discrete domain which is usually used in practice since the real world analog signals are sampled into discrete signals using an A/D converter and processed using computers, the above equation (4) can be for discrete wavelet transform (DWT) written as:

$$DWT[iT_s, a] = T_s \frac{1}{\sqrt{a}} \sum_{n} w^{*}\left(\frac{[n-i]Ts}{a}\right) s[nT_s] \qquad -(9)$$

where n is the number of samples in the signal, T_s is the sampling interval.

The discrete wavelet transform that is mostly used to reduce the computational expenditure is the dyadic wavelet transform which is dilated and scaled functions of the mother wavelet but uses the scales only in powers of two, where scale $a = 2^{j}$ [23].

Figure 5 shows the wavelets with dyadic shift of $k/2^{j}$ which is an integer multiple of the dyadic scale.

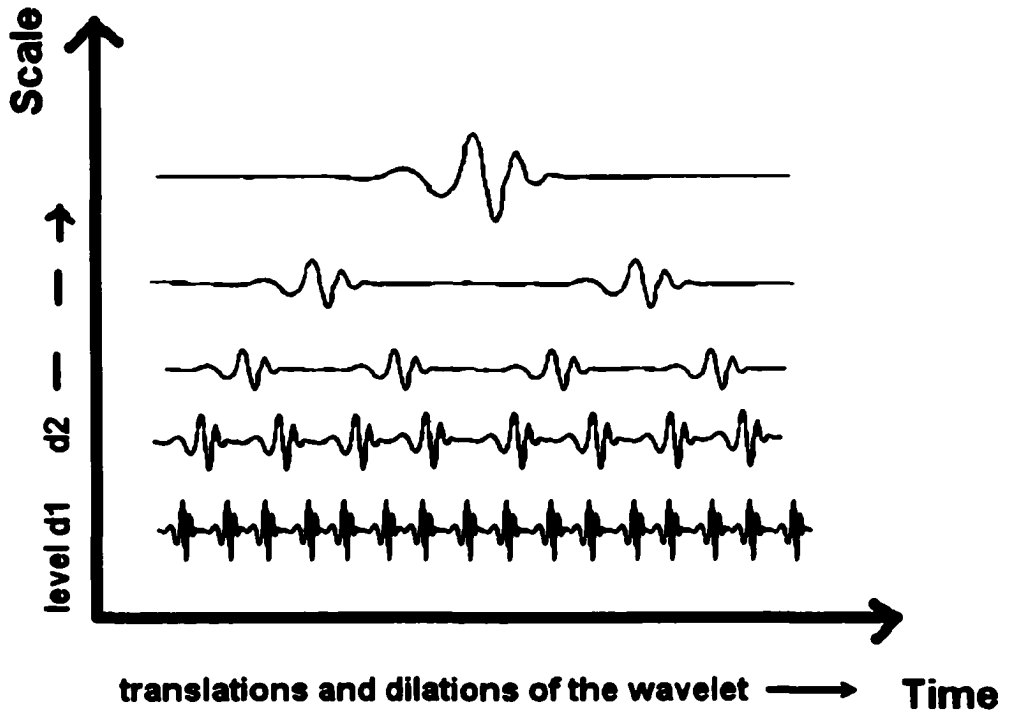

Figure 5: Wavelets At Dyadic Shifts And Scales.

In the figure (5), for the top most scale i.e., the approximation scale is only one shift and hence one inner product of the wavelet function with the input signal. As we go down the scales, i.e. towards detail level 1, the number of shifts increases and hence the inner products increase. For the scale level at the bottom in the figure, there are 16 shifts and hence 16 inner products. For a wavelet level decomposition more than five levels shown, the number of shifts and inner products are more than 16 and increase in multiples of 2. This method which is still computationally expensive for higher scales of decomposition is replaced by the Mallat's multiresolution analysis algorithm [24] referred to as the fast wavelet transform (FWT). For the signals of length n, the multiresolution

wavelet analysis has only $2n - 2$ calls to memory compared to $2n \cdot \log_2 n$ for a FFT computation. The transform is an $O(n)$ computation [22].

This fast wavelet transform is done through a process called "sub-band codification" which is done through digital filter techniques. The sub-band coding is achieved by passing the input signal through a filter bank having a low pass filter and a high pass filter which divide the whole frequency range (from zero to the Nyquist frequency) of the signal into half. Further down, the outputs of these filters are sampled in half to eliminate the even data points. Figure (6) shows the block diagram of the fast wavelet implementation by sub band coding. The rectangular block HPF represents the high pass filter and the LPF is the low pass filter. The circular block with a downward arrow and a number "2" next to it is for the down-sampling by 2.

The high pass filter leads to a wavelet function $w(t)$ while the low pass filter leads to a scaling function $\phi(t)$ [22]. The scaling function can further be scaled down to the next level of wavelet function and scaling function using the recursive filter bank of low pass filter - high pass filter and down sampling.

The wavelet $w(t)$ is the output of the high pass filtered scaling function. The last decomposition level produces a scaling function with one coefficient called the approximation wavelet level. Referring back to figure 3, it is the wavelet approximation level - a9.

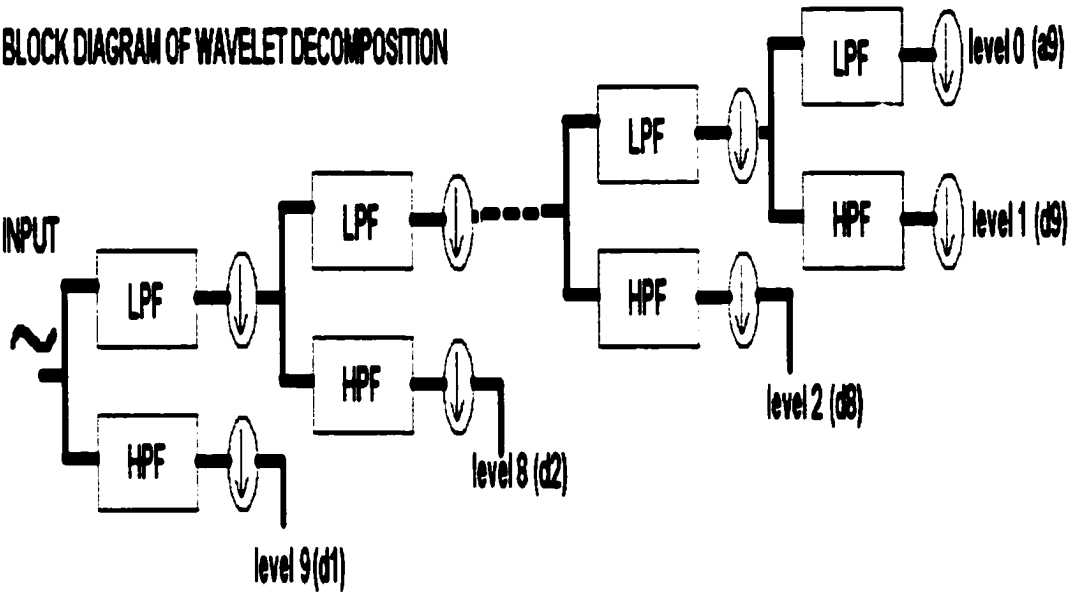

Figure 6: Block Diagram Of The Fast Wavelet Implementation Filter Tree.

The dilation equation for the scaling function $\phi(t)$ and wavelet equation for the wavelet function $w(t)$ in terms of the original filter coefficients [22] are given by:

$$\phi(t) = 2\sum_{k=0}^{N} h(k)\phi(2t-k) \qquad -(10)$$

$$w(t) = 2\sum_{k=0}^{N} g(k)\phi(2t-k) \qquad -(11)$$

where $h(k)$ are the low pass filter coefficients. $g(k)$ are the high pass filter coefficients. It is also interesting to note the presence of two time scales t and 2t in the above equations. The high pass filter coefficients $g(k)$ are related to the low pass filter coefficients $h(k)$ by:

$$g(k) = (-1)^k h(N-k) \qquad -(12)$$

where N is the total number of coefficients. These filters are known as quadrature mirror filters (QMF). Hence, for a given wavelet only the low pass filter coefficients (also known as wavelet coefficients) need to be known.

It is ideally required to have the bandwidths of the two filters in the filter bank to have a box function with perfect edges and no over-lap. However, this is not true in practice, and the selection of the wavelet coefficients that lead to good filters with good characteristics is important. The wavelet research community has presented several wavelet families with each mother wavelet having different shapes and different finite lengths leading to wavelet filter coefficients with different properties.

Though wavelets provide us with good localization of time, just being able to detect and locate an event is not sufficient for a complete analysis of a transient. For wavelet analysis to fully complement the popular Fourier analysis, it needs to address the issue of qualitatively quantifying the event. This research applies wavelets to identify and investigate certain properties of wavelets such as magnitude-phase characteristics, frequency bandwidth characteristics of wavelet components, energy distribution and leakage in these components, and dependence of sampling rate and number of data points of the signal. It is intended to motivate applications of wavelets to help in further the understanding of the wavelets by engineers in analysis of transient events. Applications of wavelets to signals obtained from sensors, motors, seismometers, and earthquakes are presented with detailed discussion of each and the effects of wavelet properties. Choosing the right wavelet for a specific application has been an open question due to lack of complete understanding of wavelets. Repeating the quotation from the previous chapter, " It is a misunderstanding that any wavelet is suitable for any signal and any applications.

Choosing or designing the right wavelet is crucial for a successful WT application" [18]. With this research we present some results that might help in selecting the right wavelet.

CHAPTER 3

WAVELET FILTER's MAGNITUDE – PHASE CHARACTERISITICS

As seen, discrete wavelet transform is equivalent to filtering it by a bank of constant-Q filters of non-overlapping bandwidths which differ by an octave [11]. The coefficients of these filter banks determined by the mother wavelet design will directly affect the wavelet decomposition outputs obtained. It is, therefore, important to know the behavior of these filters with these wavelet coefficients.

The normalized wavelet scaling function coefficients $c(k)$ of the mother wavelet related to the original low pass filter coefficients, by a factor of $\sqrt{2}$ and are given by

$$c(k) = \sqrt{2}h(k) \qquad -(13)$$

which corrects for the normalization due to losing half of the components by down sampling at the output of the filters. Similarly for the high pass filter we can write:

$$d(k) = \sqrt{2}g(k) \qquad -(14)$$

All information about the scaling function $\phi(t)$ and $w(t)$ - their support interval, their orthogonality, their smoothness, and their vanishing moments – will be determined by and from the c's and d's [22].

Most wavelets irrespective of their families of origin follow the same filter bank multiresolution analysis approach. Some of the more popular wavelet families are Haar Daubechies, Symlets, Coiflets, Meyer, Mexican hat, Morlet, B-Splines – to name a few. The wavelets are named after their inventor or after the properties and shapes they possess. Figure 7 shows some wavelets used in this research with their scaling function.

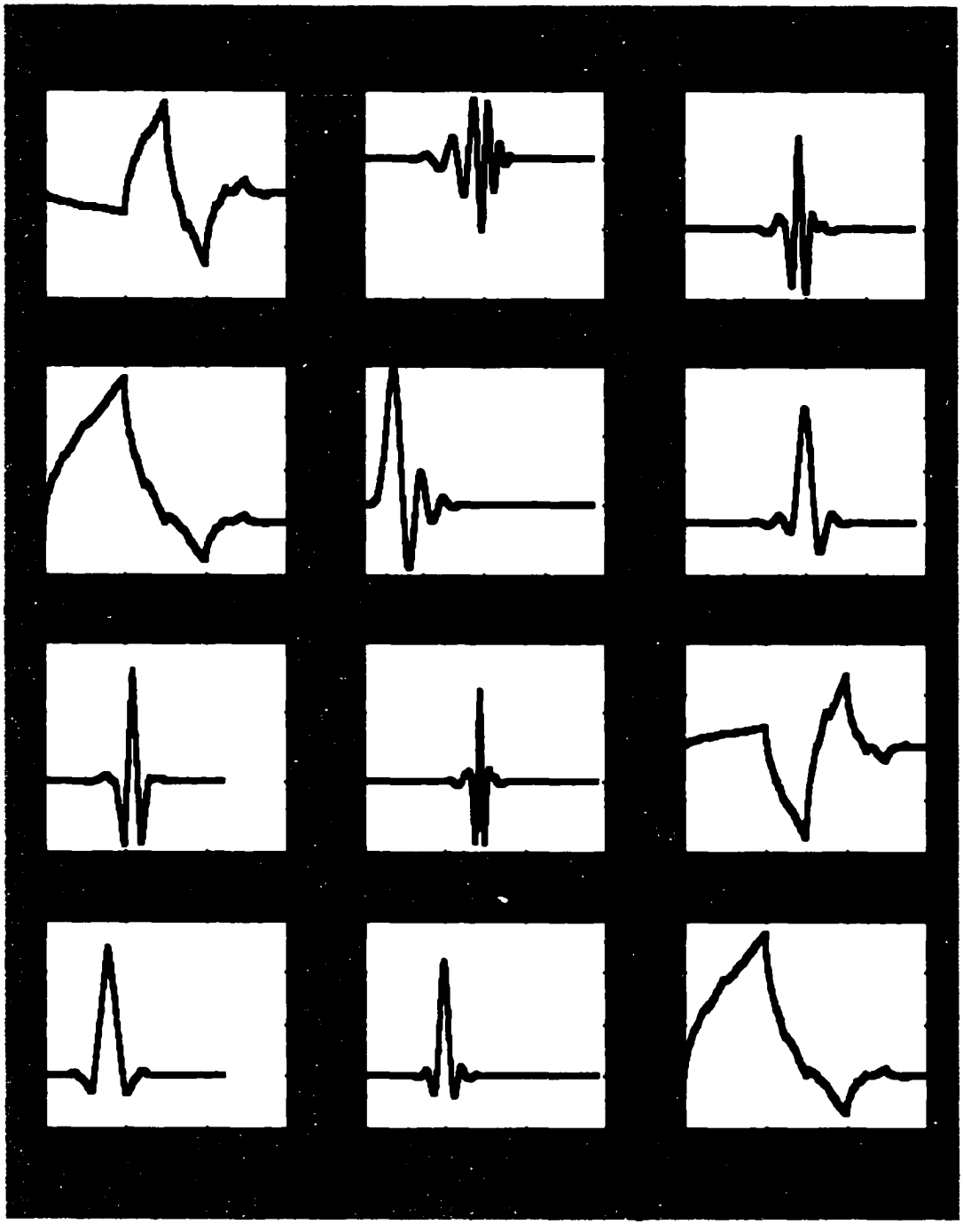

Figure 7: Wavelet Families

WAVELETS TO FILTERS:

The history of wavelets can be traced to the Haar function in 1910 (even though at that time the name wavelets didn't exist, but the connection of wavelets to filters wasn't recognized for a long time. Wavelets were constructed with great difficulty and were not compactly supported; i.e., they oscillated above and below zero along the whole line, decaying as $t \to \pm\infty$. The Morlet, Meyer and Mexican Hat wavelets created after Haar were found to show infinite impulse response (IIR). Daubechies in 1988 showed wavelets which were compactly supported and orthogonal. These wavelets were zero outside a bounded interval. Thus, these wavelet functions and their corresponding filters have finite impulse response (FIR). The Haar wavelet is a special case of Daubechies wavelets and is compactly supported, symmetric and orthogonal. Table 2 lists the wavelets with their filter types and other properties [14].

Table 2: Main Properties Of Some Popular Wavelet Functions

Type	Filter	Symmetry	Orthogonality
Haar	FIR	Symmetric	Orthogonal
Daubechies	FIR	Asymmetric	Orthogonal
Symlets	FIR	Near Symmetric	Orthogonal
Coiflets	FIR	Near Symmetric	Orthogonal
Spline	FIR	Symmetric	Bi-orthogonal
Morlet	IIR	Symmetric	No
Mexican Hat	IIR	Symmetric	No
Meyer	IIR	Symmetric	Orthogonal

Daubechies wavelets are the corner stone of modern wavelets, and their development was boosted by Mallat's pyramid algorithm that allowed for fast computation of wavelet transforms using compactly supported wavelets [9]. The words "*compact support*" mean that this closed set is bounded. The wavelet is zero outside a bounded interval: ***compact support means FIR*** [22]. The compactly supported Daubechies wavelets and their derivatives such as Symlets and Coiflets have coefficients that lead to finite impulse response (FIR) of the filters and are widely used. In practice, FIR Filters are simple to design and are guaranteed to be bounded input – bounded output stable. They have also have a very low sensitivity to filter coefficient quantization errors [24].

To understand what distinguishes these wavelet filters from the other FIR and IIR digital filters, as an engineer, it would be interesting to study the characteristics of the low pass and high pass filters in the wavelet filter bank in terms of the pole-zero location and the magnitude-phase characteristics.

In this study, I have first considered two wavelets D_4 and D_{20} of the same Daubechies family. In MATLAB, the Daubechies wavelets are represented by *dbN* with a filter length of 2N, i.e., for Daubechies D_4 wavelet is written as *db2* with the number of filter coefficients being 4. Some authors regularly use *db2N* instead, i.e., for the same Daubechies D_4, they write it as *db4* with the same 4 filter coefficients. The convention D_4 and D_{20} are used in this thesis to avoid confusion. Figure 8 shows the scaling function coefficients $C(k)$ for the two Daubechies wavelets D_4 and D_{20}. Note the length of the D_4 coefficients is 4 compared to D_{20}'s 20 coefficients.

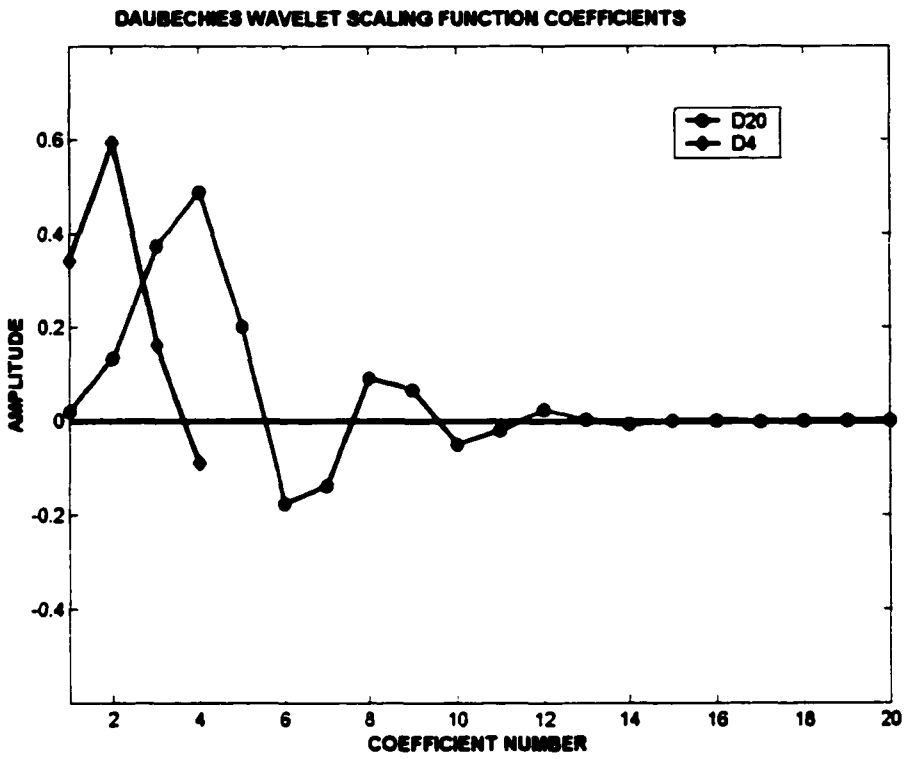

Figure 8: Daubechies Wavelet Scaling Function Coefficients – D_4 And D_{20}.

The Daubechies wavelet D_4 is more localized in time [8], [17]. The block diagram in figure 9 shows the order and the conversion of the scaling filter coefficients to the low pass and high pass filter coefficients for the Daubechies wavelet D_4. In Matlab, the scaling function coefficients are divided by their norm and then reversed in order to form the low pass decomposition filter coefficients. For the Daubechies D_4 wavelet, the scaling function coefficients are $c(1) = 0.3415$, $c(2) = 0.5915$, $c(3) = 0.1585$, $c(4) = -0.0915$. The norm of the four coefficients is calculated as:

$$\sqrt{c(1)^2 + c(2)^2 + c(3)^2 + c(4)^2} = \sqrt{0.3415^2 + 0.5915^2 + 0.1585^2 + (-0.0915)^2} = 0.7071 \quad \text{- (15)}$$

Therefore, the new normalized low pass filter coefficients are $c(1) = 0.4830$, $c(2) = 0.8365$, $c(3) = 0.2241$ and $c(4) = -0.1294$ and are implemented in the reversed order as shown in the block diagram.

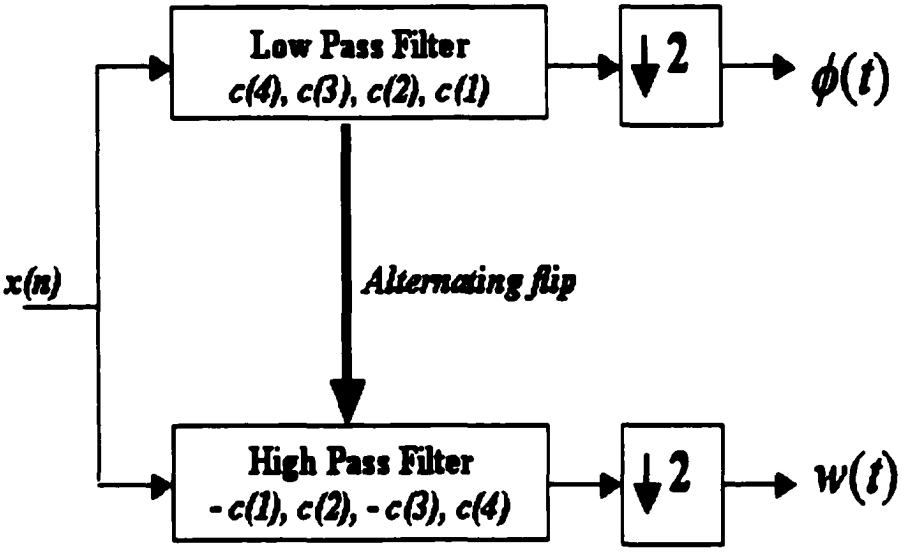

Figure 9: Block Diagram Of The Analysis Filter Bank For Daubechies Wavelet D_4.

The scaling function coefficients and the low pass decomposition filter coefficients for both the Daubechies wavelets D_4 and D_{20} are given in table 3. The coefficients for both the low pass and high pass filters for the two wavelets are plotted in figure 10.

Table 3: Filter Coefficients For Daubechies Wavelet D_4 And D_{20}

D_n	Scaling function coefficients *c(1), c(2),....,c(n)*	Normalized low pass filter coefficients *reverse(sqrt(2)*(c(1), c(2),...., c(n))*
D_4	0.3415, 0.5915, 0.1585, -0.0915	-0.1294, 0.2241, 0.8365, 0.4830
D_{20}	0.0189, 0.1331, 0.3728, 0.4868, 0.1988, 0.1767, -0.1386, 0.0901, 0.0658, -0.0505, -0.0208, 0.0235, 0.0026, -0.0076, 0.0010, 0.0014, -0.0005, -0.0001, 0.0001, -0.0000	-0.0000, -0.0001, -0.0001, 0.0007, 0.0020, -0.0014, -0.0107, -0.0036, 0.0332, 0.0295, -0.0714, -0.0931, 0.1274, 0.1959, -0.2498, -0.2812, 0.6885, -0.5272, 0.1882, -0.0267

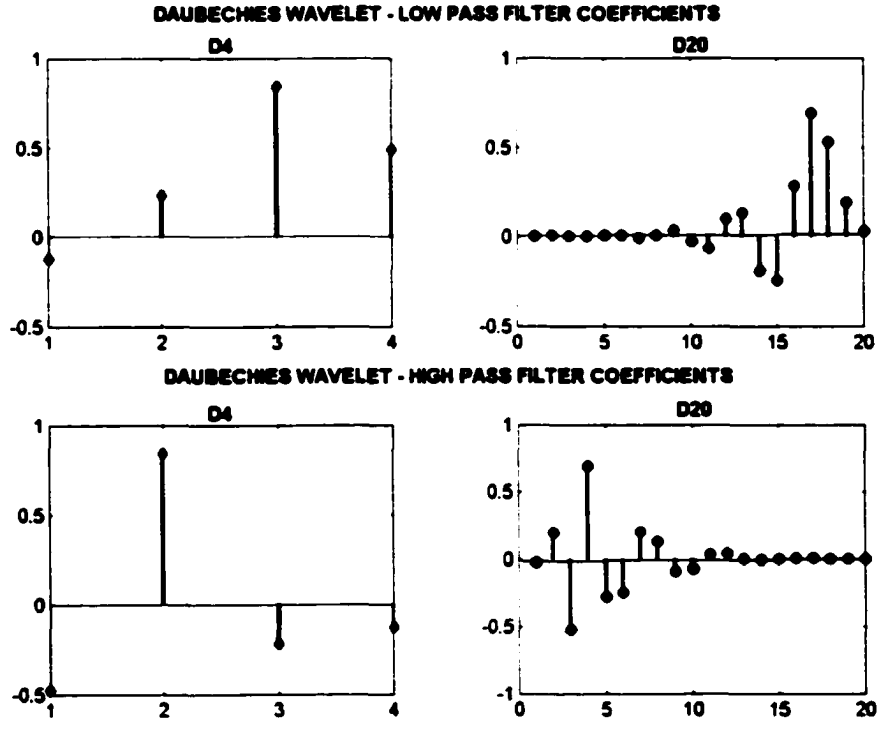

Figure 10: Plot Of The Low Pass And High Pass Filter Coefficients For Daubechies Wavelets.

The Daubechies wavelet filter coefficients have finite impulse response and have all zeros and no pole as seen in figure 11. The existence of only zeros and no pole makes the filter very stable. The pole – zero plot of the low pass filter for the two Daubechies wavelets D_4 and D_{20} filters are given in figure 11. The zeros at π ($z = -1$ in the figure 11) for the low pass decomposition filter are at the heart of wavelet theory and specify the accuracy of the approximation. For the filter to behave well in practice, when it is combined with the sub-sampling and repeated five times, it must have an extra property not built into earlier designs. This property expresses itself in the frequency domain by a sufficient number of "zeros at π" [22]. For Daubechies wavelets with $2p$ coefficients, we have p zeros at π. From figure 11, Daubechies D_4 wavelet with 4 coefficients has 2 zeros at π and Daubechies D_{20} with 20 coefficients has 10 zeros at π.

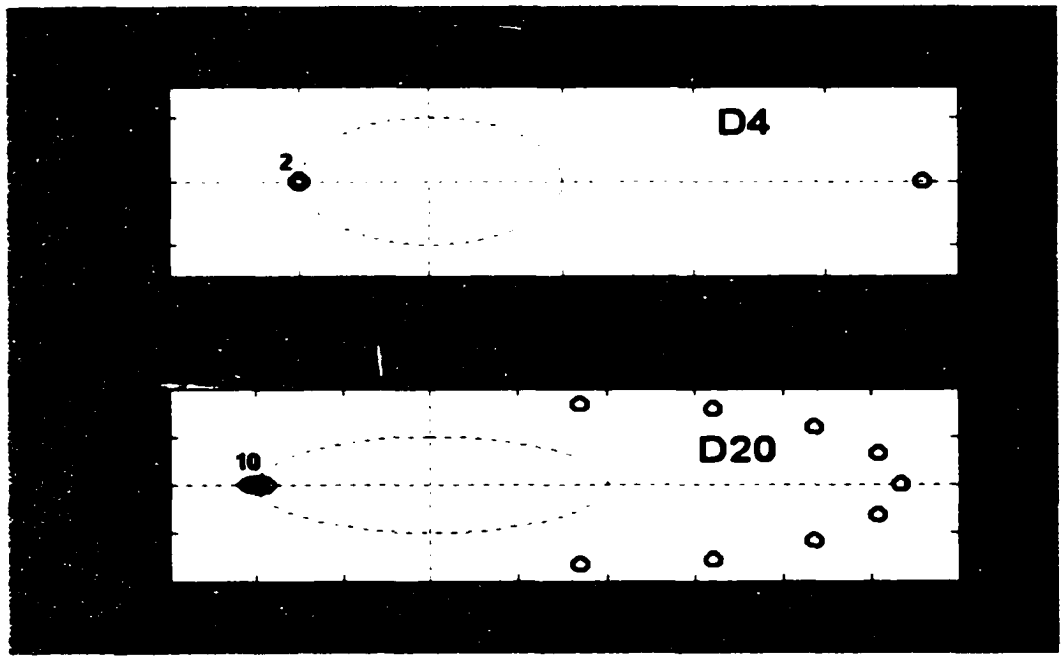

Figure 11: Pole – Zero Maps For Low Pass Filter – Daubechies Wavelets D_4 And D_{20}.

Equiripple filters are known to have the best practical design in terms having smallest maximum error in passband and stopband. Comparing the wavelet filters to the design of a equiripple 4-tap FIR filter with approximately similar magnitude response as D_4, we find that the equiripple filter has a one less zero at π than D_4 which has 2 zeros at π. Similar case holds for D_{20} where the equiripple filter comes close with 9 zeros at π compared to 10 for D_{20}. The equiripple filters are optimal in important respects but not optimal for iteration. The decimation by 2 sampling operators ($\downarrow 2$) will mix up the frequency bands that an equiripple filter carefully separates [22]. The Daubechies filter coefficients have no ripple and maximum flatness at $\omega = \pi$ and the iteration is very stable even after down sampling. Figure 12 shows the pole – zero plot and the coefficients of the equiripple low pass filter of 4 taps. The phase characteristics of the two filters equiripple and D_4 low pass were linear but different in terms of the slope of the phase lines. This is not plotted as only the magnitude similarity was considered to provide a comparison.

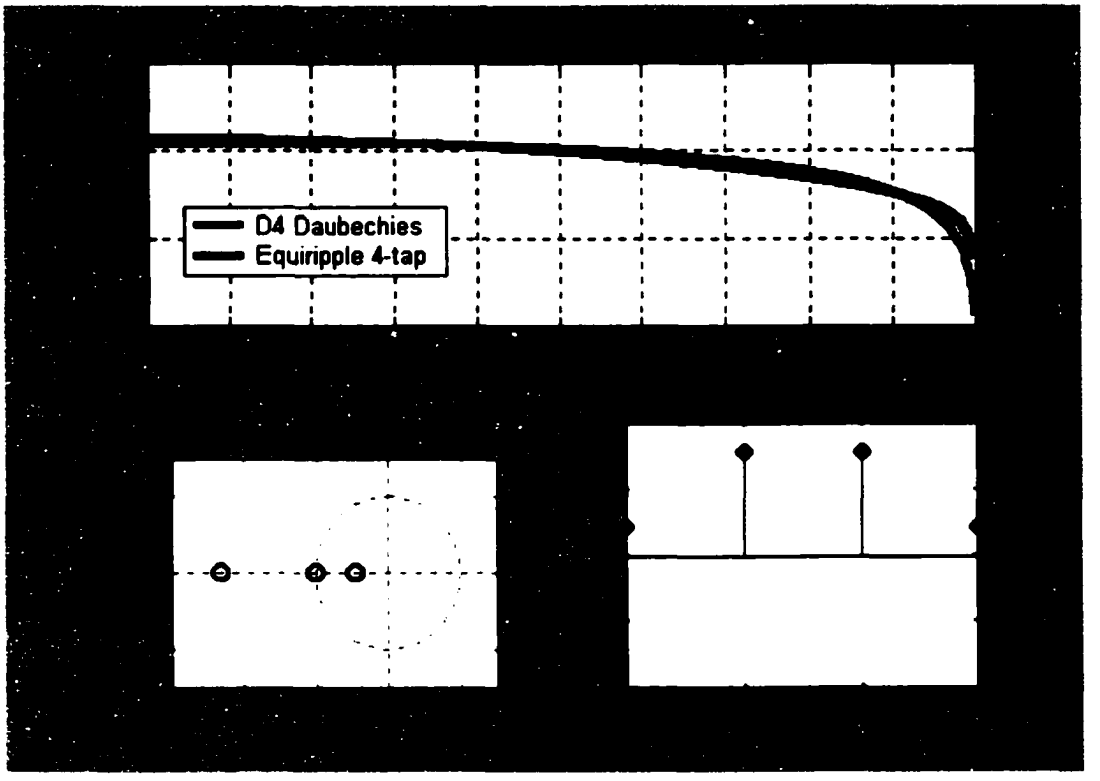

Figure 12: Equiripple FIR Low Pass Filter (Order 4) – Coefficients And The Pole Zero Map.

The requirement of sufficient zeros at π, i.e., p zeros for $2p$ coefficients of the filter is an important property of the wavelet filters. The double zero at $\omega = \pi$ produces two vanishing moments for the D_4 Daubechies filters. For every p^{th} zero in for the $H(\omega)$ of the low pass filter there exists a vanishing moment for the orthogonal wavelets. That means the high pass filters with regularity p will produce a zero output when convolved with a signal that can be exactly represented by a p-th order polynomial [26]. When this happens, the signal is exactly represented by its low pass approximation coefficients and hence the wavelet's order (accuracy) of approximation is p. The decay towards the low frequencies corresponds to the number of vanishing moments of the wavelet [22]. This is an important quantity for the high pass filter in the wavelet filter bank. There exists also a

term called the smoothness of the wavelet and is given by smoothness index s_{max} of the scaling function $\varphi(t)$ which is never greater than the number p of the vanishing moments. The smoothness of the function directly corresponds to the decay towards the high frequencies and is important for the low pass filter. The smoothness of a wavelet is given as the maximum s^{th} derivative (if the s derivatives exist) of the wavelet equation:

$$\phi^{(s)}(t) = 2^s \sum 2h(k)\phi^{(s)}(2t-k) \qquad \text{- (14)}$$

and s derivatives cannot exceed the order of the polynomial $p-1$.

The Daubechies D_4 and D_{20} wavelets, the high pass filter pole-zero maps are shown in figure 13.

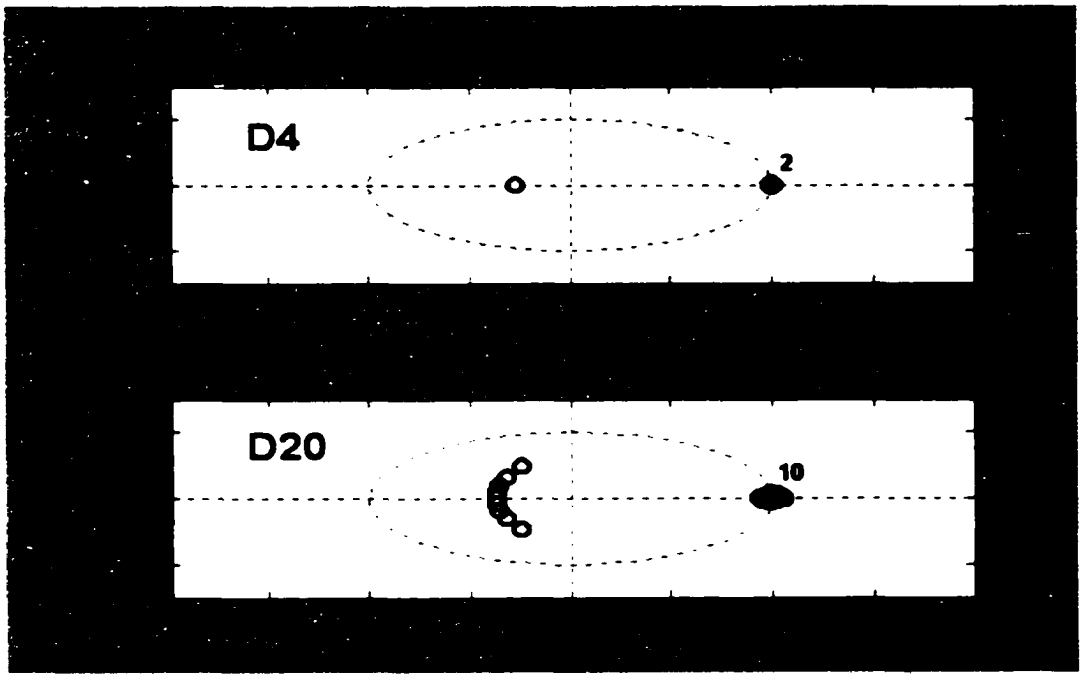

Figure 13: Pole – Zero Maps For High Pass Filter – Daubechies Wavelets D_4 And D_{20}.

The pole zero location of the high pass decomposition filter for Daubechies wavelets are opposite to the low pass with zeros at $\omega = 0$. This filter has a behavior opposite to the low pass filter and allows all signals in the upper half band to pass through

while attenuating the low frequency signals. The high pass filters are also known as quadrature mirror filters (QMF) as they are derived from the low pass filter coefficients by reversal of the coefficients and an alternating flip, i.e., negating the odd coefficients.

The magnitude phase plots for the low pass and high pass filters for the two Daubechies wavelets D_4 and D_{20} are plotted in the figure 18. The plots are plotted along with the magnitude and phase plots of other wavelets for comparison and study.

Two other wavelet families with finite impulse response (FIR) are considered for the study of magnitude and phase characteristics. These wavelets are Symlets wavelets and Coiflets wavelets.

Symlets wavelets are derived from the Daubechies wavelets and inherit most of their characteristics and properties. The Symlets wavelets Sym_4 and Sym_{20}'s scaling function coefficients are plotted in figure 14. The Symlets wavelets are more symmetric than the Daubechies wavelets and have the same number of vanishing moments for the given number of coefficients of the filters. As seen from figure 14, Sym_4 has 4 coefficients that are exactly equal to the Daubechies D_4 coefficients. Sym_{20} has 20 coefficients that are more symmetric than the Daubechies D_{20} coefficients. Figure 14 shows the symmetric Symlets wavelet scaling function but as you can see slight asymmetricity still exists in the wavelet filter. It is interesting to see the difference in magnitude and phase characteristics of the two wavelets Sym_{20} and D_{20} having known their differences in terms of the symmetry of the scaling function coefficients. So the question is, how does having more symmetry affect the characteristics? Figure 15 shows the low pass and high pass filter coefficients.

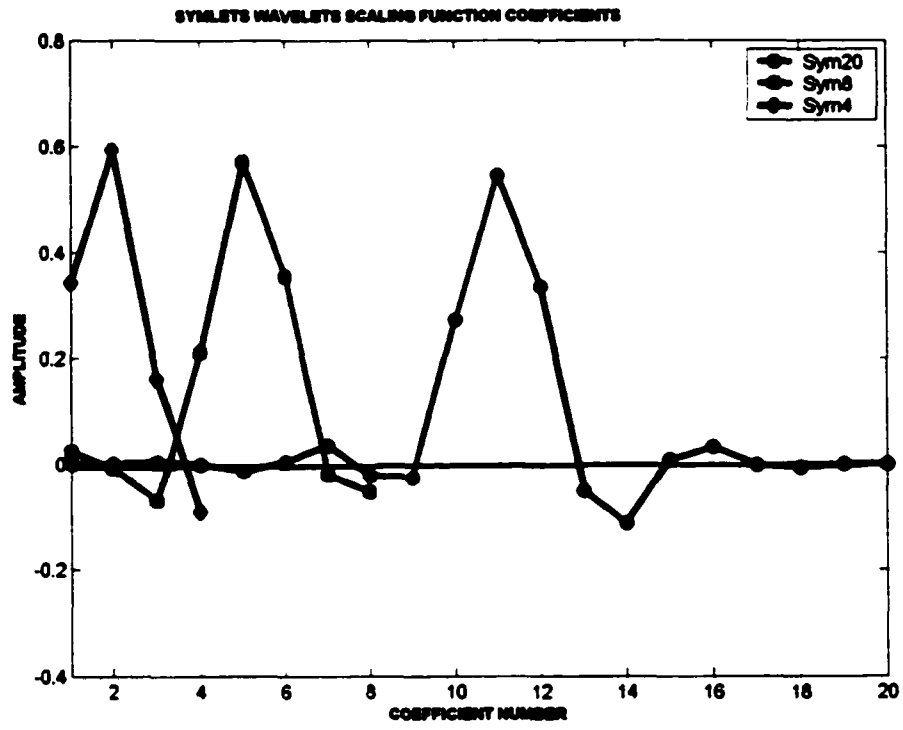

Figure 14: Symlets Wavelets Scaling Function Coefficients.

The low pass filter and high pass filter coefficients of the Sym_4 wavelet are also exactly equal to their Daubechies counterpart D_4. So, we can expect the same magnitude and phase characteristics for both Sym_4 and D_4 wavelets. A scaling function filter coefficients for Sym_8 is also included in the above figure 14 to show that the Symlets wavelets are increasingly symmetric with the increase in filter length. As Symlets wavelets are derived from Daubechies wavelets, they inherit most of its properties like the filter length and the number of vanishing moments, i.e., the number of zeros at π for a given wavelet length $2p$ coefficients.

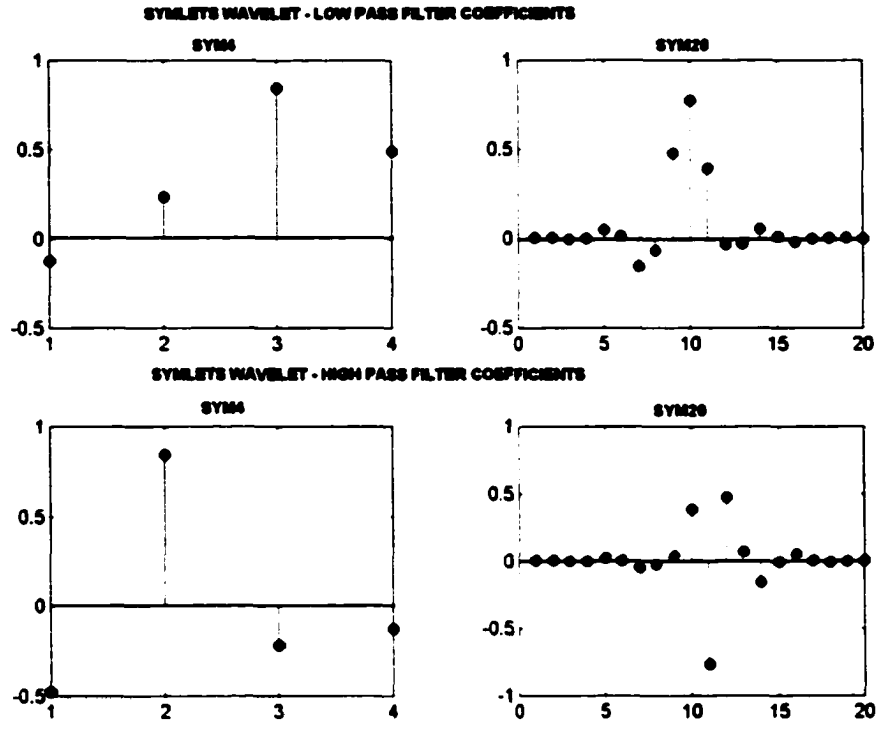

Figure 15: Plot Of The Low Pass High Pass Filter Coefficients For Symlets Wavelets.

The pole-zero map for the low pass and high pass filters of Symlets wavelets are shown in figure 16 and figure 17 respectively. The location of zeros for the Sym_4 wavelet is the same as D_4, but an interesting observation can be made for the higher order Symlets wavelet, Sym_{20}. The number of zeros at π "p" for "2p" coefficients of the Symlets wavelet filter is exactly same as for Daubechies wavelets, but the remaining zeros are distributed both inside and outside the unit circle. It will be interesting to see how the movement of some of these remaining zeros towards π for the low pass filter manifests itself in magnitude and phase characteristics of the Symlets wavelet compared to Daubechies wavelet. Similarly, the effect of change in the distribution of zeros in the high pass decomposition filter will be studied.

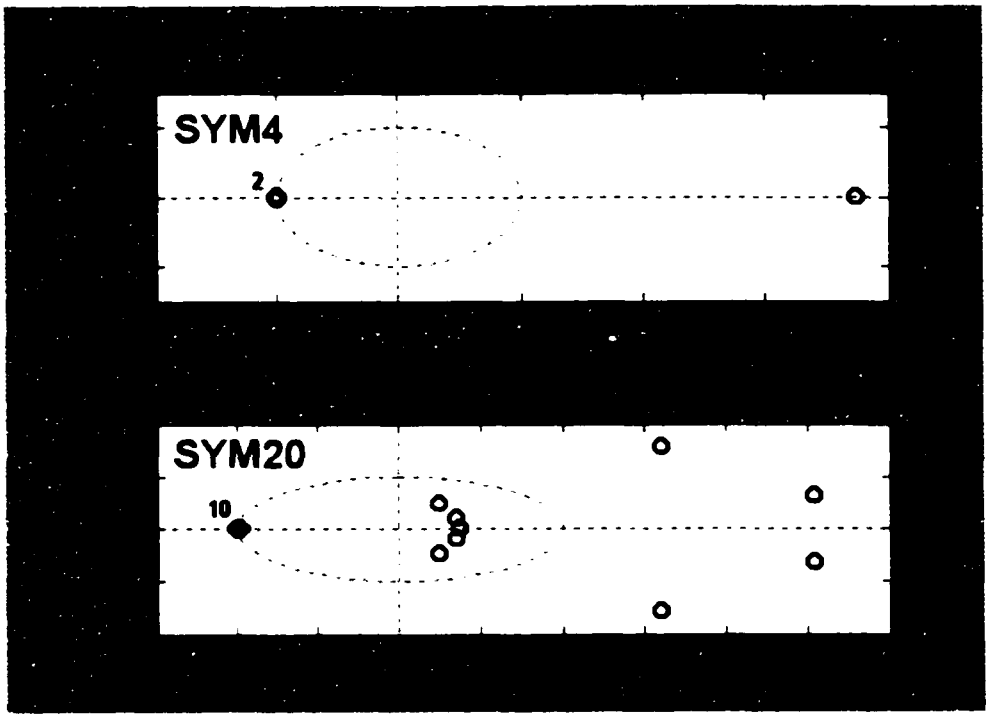

Figure 16: Pole – Zero Maps For Low Pass Filter – Symlets Wavelets Sym_4 And Sym_{20}.

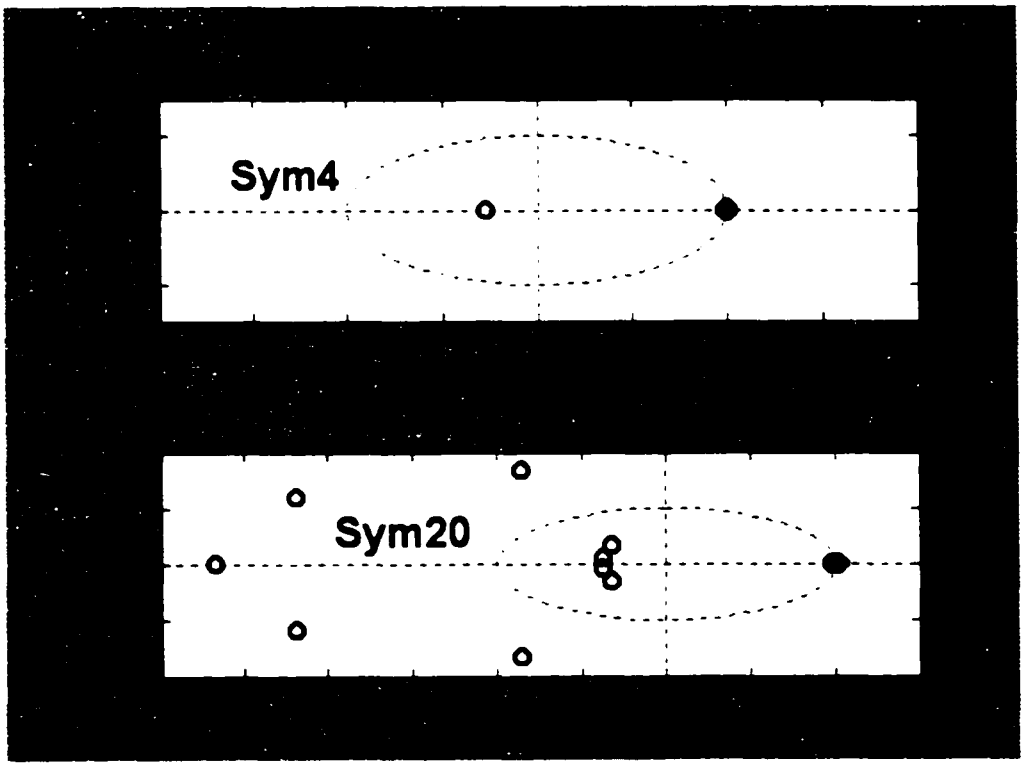

Figure 17: Pole – Zero Maps For High Pass Filter – Symlets Wavelets Sym_4 And Sym_{20}.

Before we go on to the Bode magnitude and phase characteristics plot to compare the FIR filters discussed above, we consider one more FIR wavelet family – Coiflets wavelets, which is related to the Daubechies family. Daubechies designed Coiflets wavelets for R. Coifman at his request with almost equally distributed vanishing moments for both the scaling and wavelet function. There are only five wavelets in the Coiflets family. These wavelets are derived from the Daubechies wavelets and have 3 times more coefficients for a given wavelet number than the Daubechies or Symlets. So for $Coif_2$ we have the number of coefficients $3(2p) = 12$ coefficients compared to 4 for D_2. Coiflets wavelets also have "$2p$" vanishing moments, i.e., "$2p$" zeros at π for the wavelet function ψ compared to "p" vanishing moments for the Daubechies and Symlets wavelets. The special property of Coiflets wavelets are the "$2p - 1$" vanishing moments for the scaling function ϕ which resolve the issue of good compression property for approximation. Daubechies wavelets have a good compression property for wavelet coefficients but not for approximation [27]. Figure 18 shows the scaling function coefficients for the Coiflets wavelets – $Coif_2$ and $Coif_5$. Comparing the Coiflets wavelet scaling function coefficients with the Daubechies and Symlets, the Coiflets scaling function is more symmetric and as indicated before, has more number of coefficients for the wavelet of the same number. The low pass filter and high pass filter decomposition filter coefficients are shown in figure 19 followed by their pole zero maps in figure 20 and figure 21 respectively.

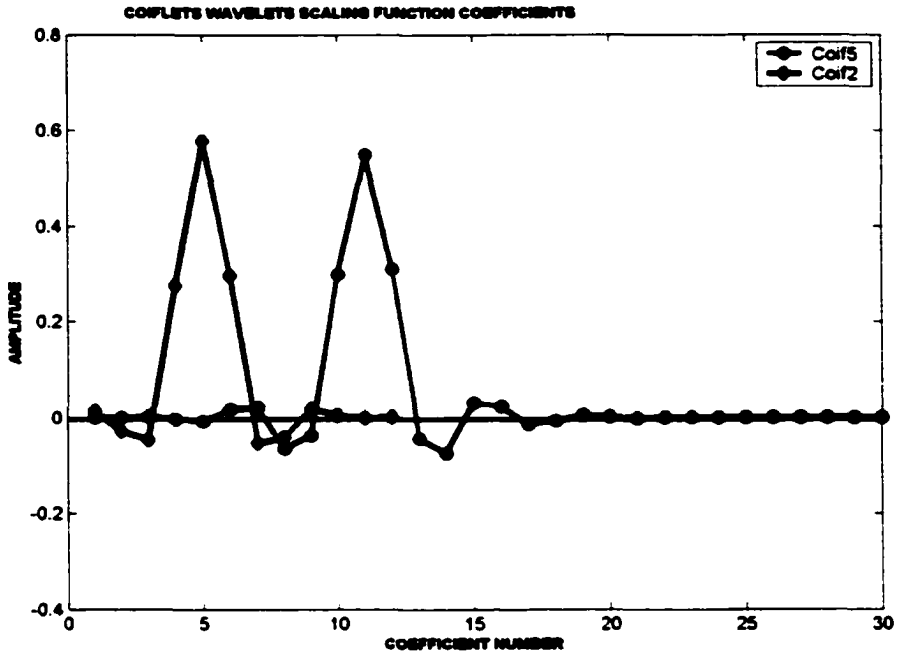

Figure 18: Coiflets Wavelets Scaling Function Coefficients.

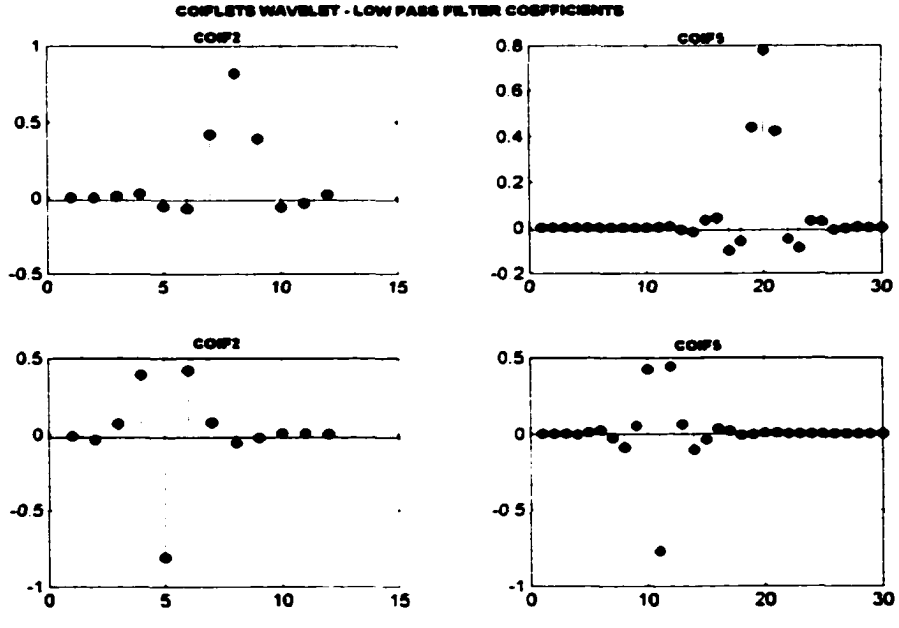

Figure 19: Plot Of The Low Pass And High Pass Filter Coefficients For Coiflets Wavelets

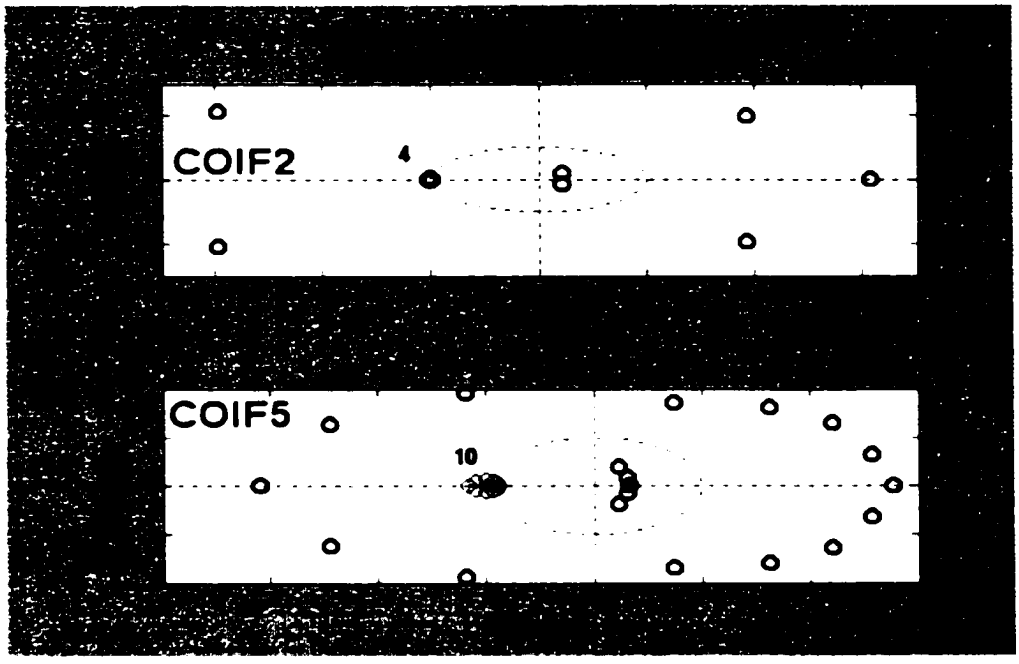

Figure 20: Pole – Zero Maps For Low Pass Filter – Coiflets Wavelets $Coif_2$ And $Coif_5$.

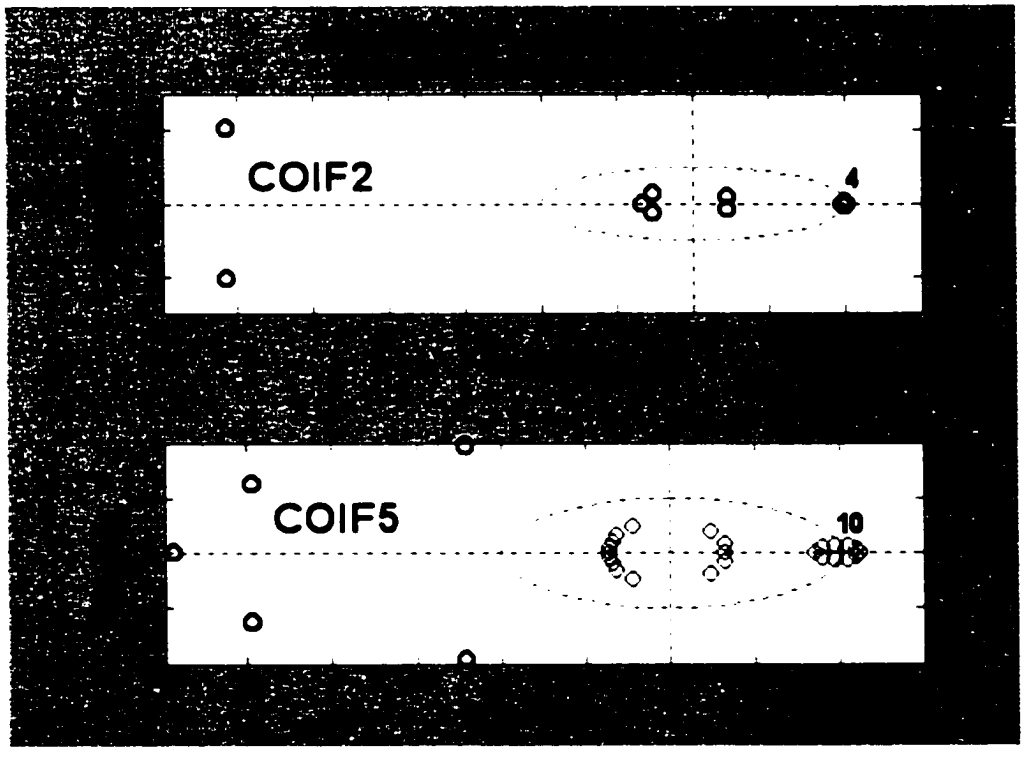

Figure 21: Pole – Zero Maps For High Pass Filter – Coiflets Wavelets $Coif_2$ And $Coif_5$.

The low pass and high pass filter coefficients are also more symmetric than Daubechies and Symlets wavelets. The pole zero maps show 4 zeros at π for the $Coif_2$ wavelet and 10 zeros at π for the $Coif_5$ wavelet.

The Bode plot – magnitude and phase characteristics of both the low pass filters and the high pass filters used in the above three wavelet families – Daubechies, Symlets and Coiflets are plotted. Figure 22 shows the magnitude characteristics in linear units and figure 23 has dB magnitude for the low pass decomposition filters. Phase characteristics for the same filters are plotted in figure 24.

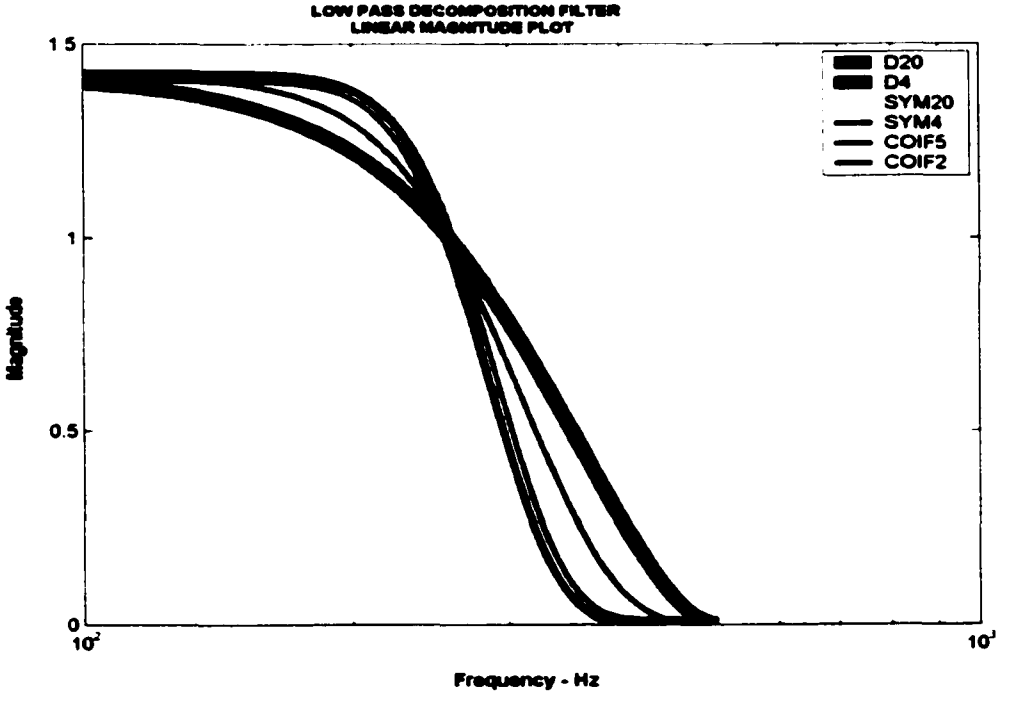

Figure 22: Linear Magnitude Plot – Low Pass Decomposition Filter – Daubechies, Symlets And Coiflets.

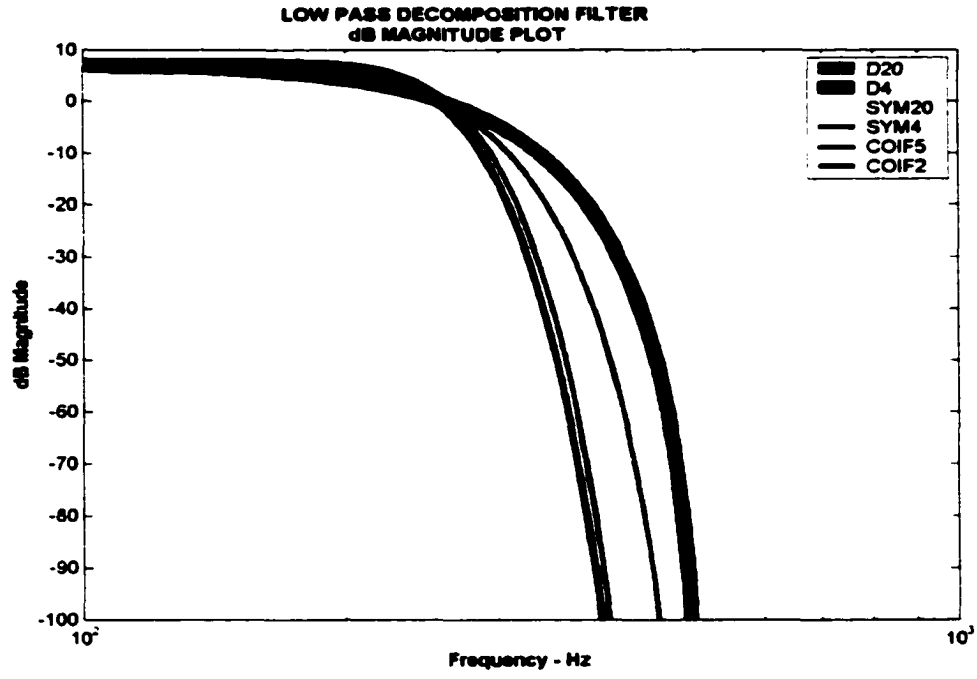

Figure 23: Db Magnitude Plot – Low Pass Decomposition Filter – Daubechies, Symlets And Coiflets.

The magnitude characteristics for the low pass decomposition filter in the two figures 22 and 23 exhibit exactly the same characteristics for some wavelets. As seen, Daubechies D20, Symlets SYM20 and Coiflets COIF5 have same magnitude characteristics with a steeper drop at the cut-off frequency than the wavelets Daubechies D4 and Symlets SYM4 which are both similar and have wider characteristics at the cut-off. COIF2 with 10 coefficients has a magnitude characteristic which falls between the above two. It was expected that the magnitude characteristics of D4 and SYM20 will be exactly same since their scaling function coefficients are also same; however, it is interesting that D20, SYM20 and COIF5 all have the same magnitude characteristics even though their scaling function coefficients and their filter coefficients were totally different.

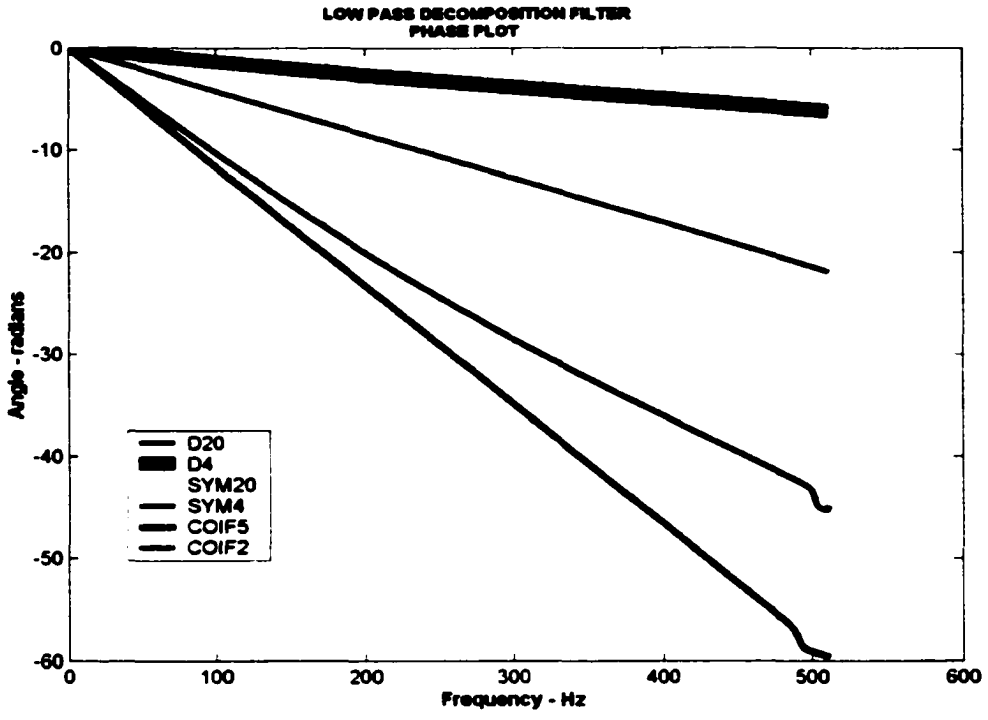

Figure 24: Phase Plot – Low Pass Decomposition Filter – Daubechies, Symlets And Coiflets.

The phase plot of the above wavelets is more interesting. The D4 and SYM4 have exact similar phase characteristics. Their phase change is linear but much smaller than the remaining wavelets. The phase characteristics for the D20, SYM20 and COIF5, which had the same magnitude characteristics, are different from each other. The phase characteristic of D20 has a slight non-linearity compared to both Symlets SYM20 and Coiflets COIF5. This can be attributed to the symmetry of the coefficients in the scaling function or the low pass filter. The slopes of the phase characteristics with respect to frequency are at varied steepness for the three wavelets. A variety of wavelets have the same magnitude spectrum but different phase spectrum [18]. This interesting property of wavelets can be used to choose wavelets for applications where the phase is a critical factor while still having the same magnitude response.

Figure 25 and figure 26 show the linear magnitude and dB magnitude characteristics for the high pass decomposition FIR filters of the three wavelet families.

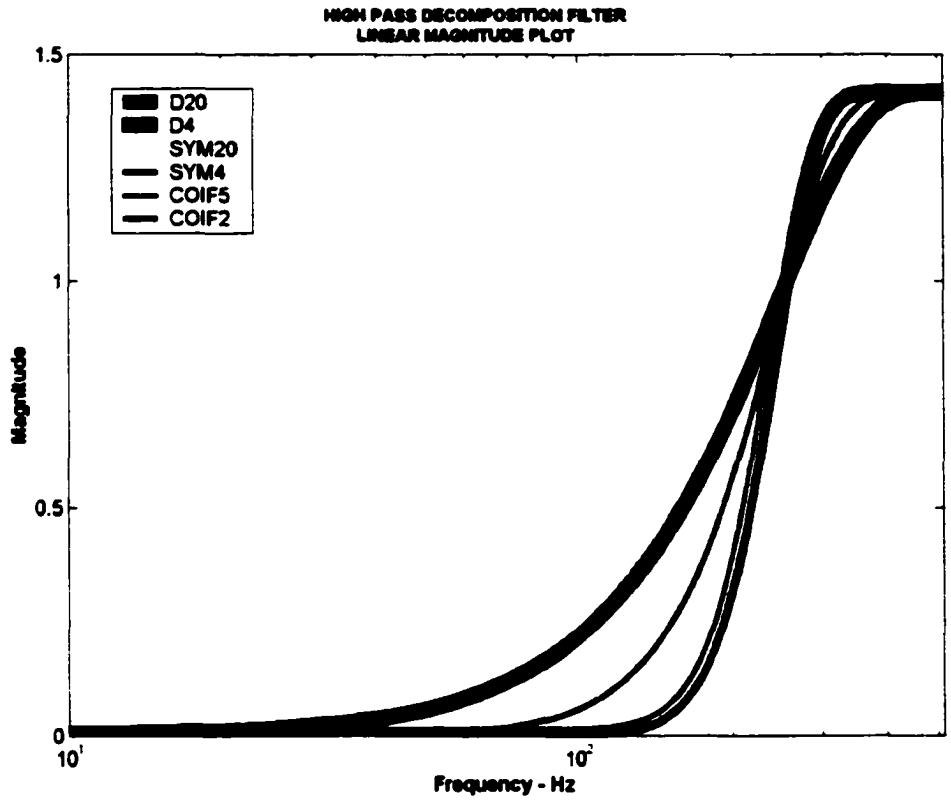

Figure 25: Linear Magnitude Plot – High Pass Decomposition Filter – Daubechies, Symlets And Coiflets.

The magnitude characteristics of the high pass filters for different wavelets behave as they did for the low pass filter. The wavelets with a higher number of coefficients decay faster and their slope approaches the vertical. The scaling function of these filters with more coefficients is smooth and has higher vanishing moments. The decay for the high pass filter is governed by the number of vanishing moments and hence D20, SYM20 and COIF5 decay faster. It is also seen that the decay is different for both the low pass filter and the high pass filter. The number for smoothness of the scaling function governs the decay for the low pass filter. The number for smoothness is never greater than the

number for the vanishing moments [14] and hence the difference in the decay of the low pass and high pass filters.

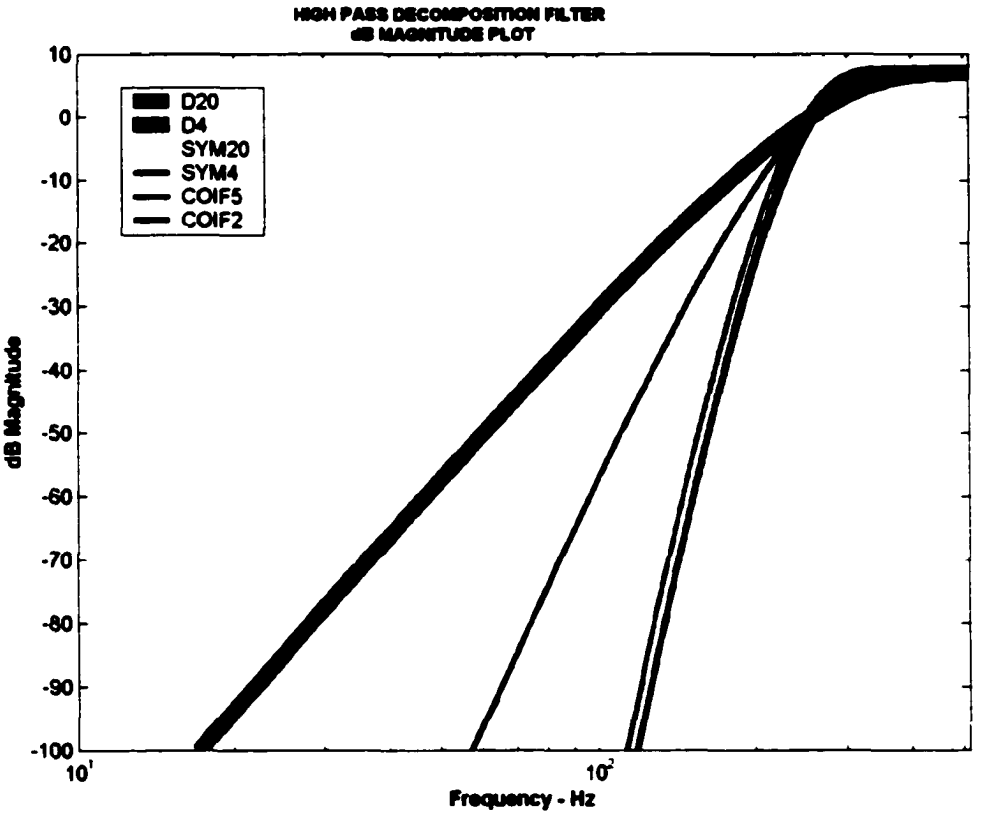

Figure 26: Db Magnitude Plot – High Pass Decomposition Filter – Daubechies, Symlets And Coiflets.

This difference in decay can be clearly seen by comparing the dB magnitude plots for both the low pass and high pass filters. Figure 27 shows the phase plot of the high pass decomposition filters for the three wavelet families. The phase characteristics of both the SYM20 and COIF5 are exactly similar and can be seen lying on top of each other in the figure.

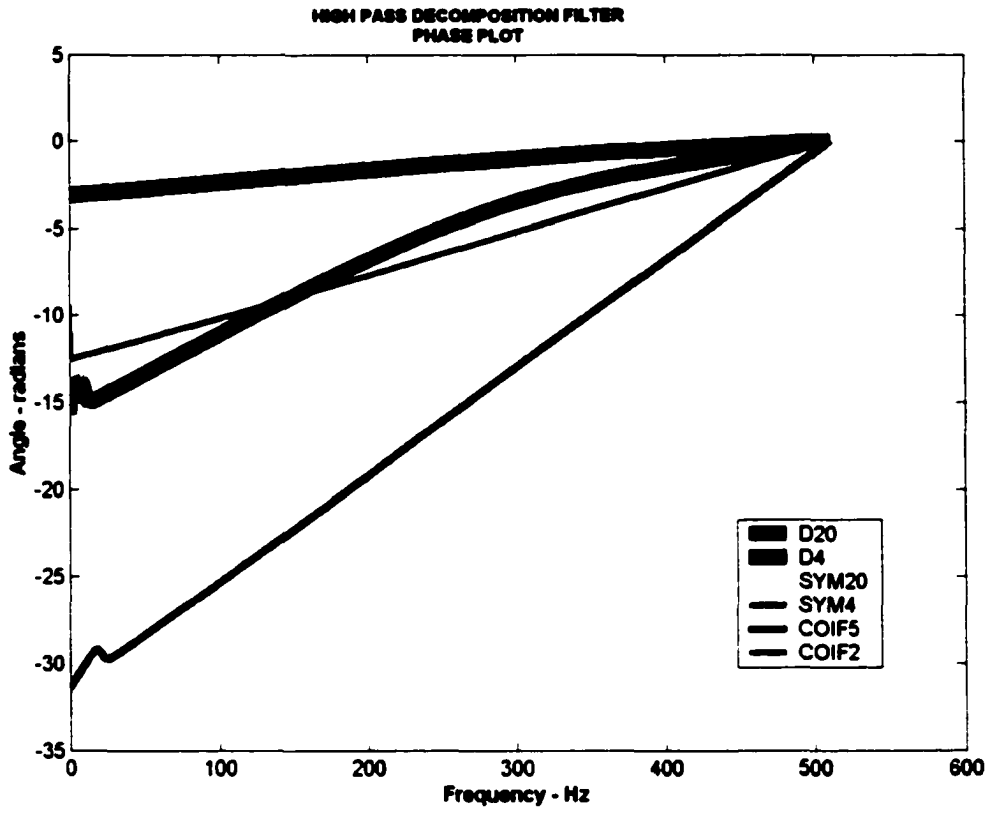

Figure 27: Phase Plot – High Pass Decomposition Filter – Daubechies, Symlets And Coiflets.

This is in contrast to the phase characteristics of the low pass filters. The non-linearity of the D20 wavelet phase is more pronounced in the high pass filter. The steepness of the slopes is more for the low pass filters than the high pass filters. The phase characteristics of SYM20, COIF5 and COIF2 are exactly linear which can be attributed to the symmetricity of the filter coefficients.

It is observed that the for the low pass wavelets filters, movement of zeros towards π for the Symlets and Coiflets wavelets compared to the Daubechies wavelets does not affect the magnitude characteristics but changes the phase characteristics by increasing the slope. Note that equally there are 10 zeros at π for all the three wavelets - Daubechies D20, Symlets SYM20 and COIF5.

For the use of wavelets in signal processing, knowledge of magnitude and phase characteristics of the wavelet filters are important. The above information obtained by comparing the three FIR wavelets is one of the properties which might be useful in choosing the right wavelet. So, it is just not enough to know the wavelet's scaling function coefficients or its filter coefficients but the actual magnitude and phase response. Two wavelet filters have the same magnitude response, but one has a much greater slope in its phase response than the other. If both have essentially a linear phase response, then you would choose the filter having a lesser slope in phase response because it would have a smaller time delay for time critical applications.

In the next chapter, an application of wavelets to fast detection of fault current in a transformer is shown which clearly shows the advantages of D4 over Daubechies D20.

CHAPTER 4

INNOVATIVE METHODS OF INRUSH AND FAULT CURRENT IDENTIFICATION/ PROTECTION USING WAVELETS

Transformers are used in every aspects of everyday life from households to industries, from low power lighting to power large refineries, in equipments from electrical engineering to trenchless technology, etc. Research is being carried out in the area of detection and identification of inrush current and distinguishing it from the fault current.

Let us consider an application and use wavelets for analyzing and identifying of the inrush current and the fault current of a transformer. The inrush current is a transient signal in the transformer which occurs when the input to the transformer is turned on. The amplitude of this inrush current is often much higher than the rated full load current [28], [29] and is one of the grave concerns for engineers. The transient magnetizing inrush current causes false tripping of differential relays used for transformer protection [30].

The inrush current obtained from a single-phase 5 KVA transformer is shown in figure 28. Only 2048 data points of the inrush current are shown and considered for our wavelet analysis. The inrush current waveform shape is easily distinguished by the human eye when compared to the fault current shown in figure 29. The fault is generated by sudden short at the output of the secondary of the transformer.

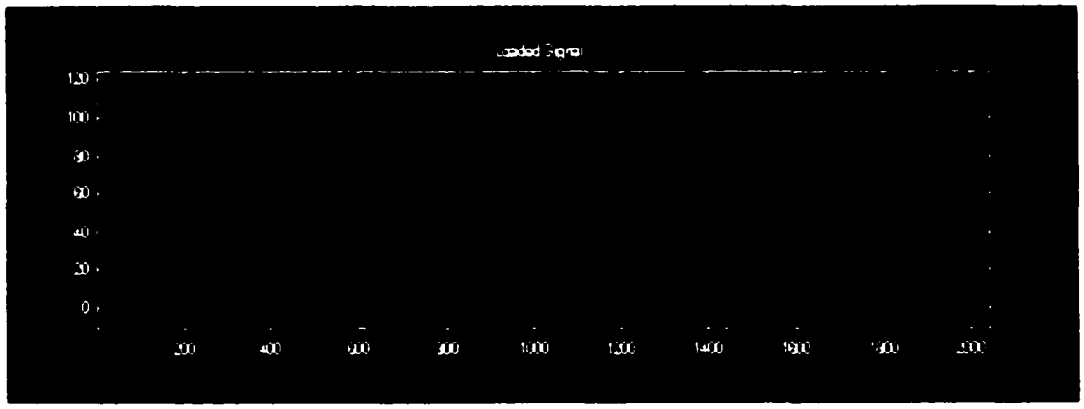

Figure 28: Transformer Inrush Current

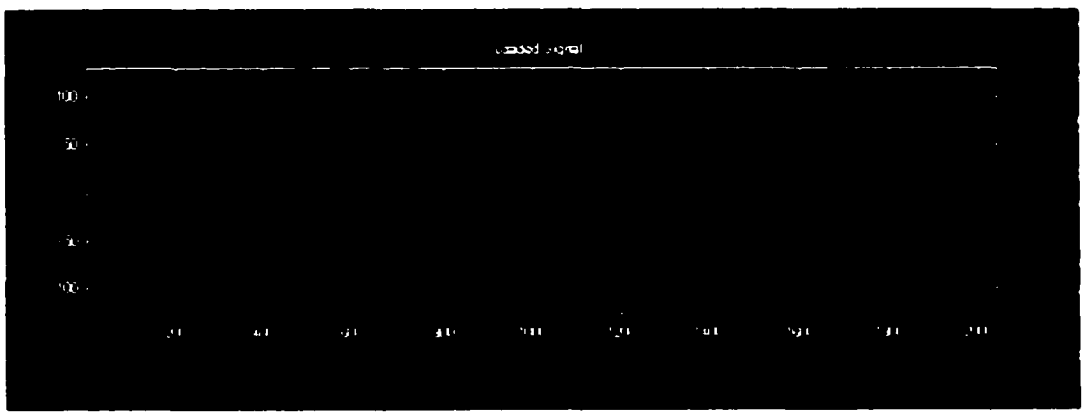

Figure 29: Transformer Fault Current

The fault current also has 2048 data points chosen to show the occurrence of fault. The inrush current has intermittent peaks with valleys in between them. The fault current,

on the other hand, is perfectly symmetric (assuming the dc offset is removed) and has equal positive and negative half cycles.

Applying Daubechies D4 and D20 wavelets to the two signals, the wavelet decomposition signals are shown in figures 30 through 33. For 2048 data points, there are 11 levels of full wavelet decomposition. The figures 30 and 31 show the original signal and the 11 level wavelet decomposition of the transformer inrush current for Daubechies D4 and D20 respectively.

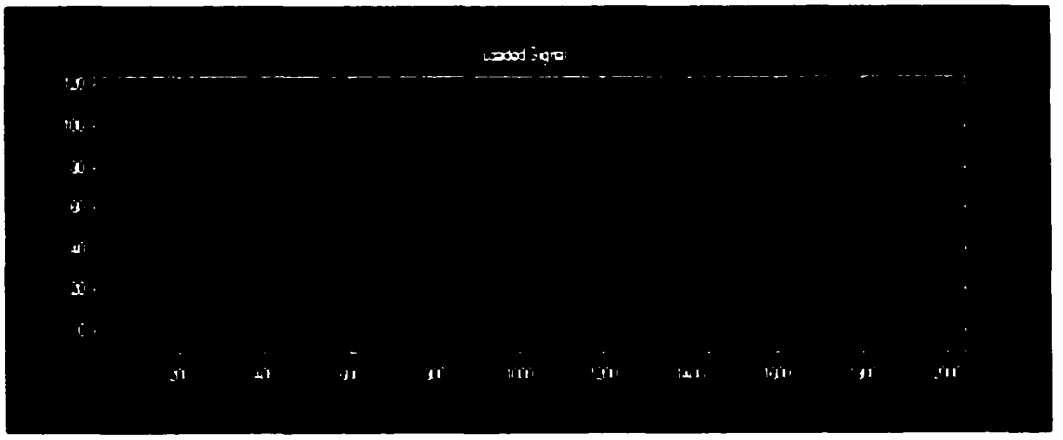

Figure 30 (a): Original Input Signal - Transformer inrush current.

Figure 30(b): Approximation a10 (Level 0)

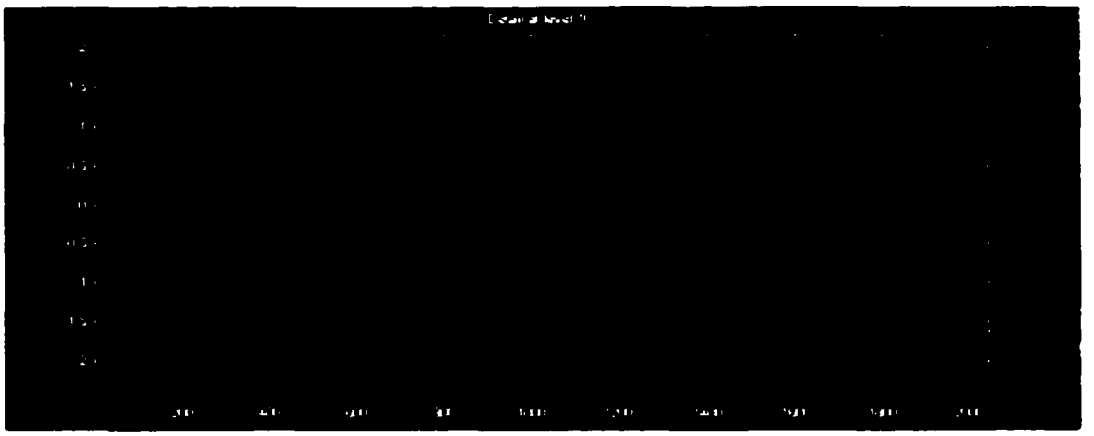

Figure 30(c): Detail d 10 (Level 1)

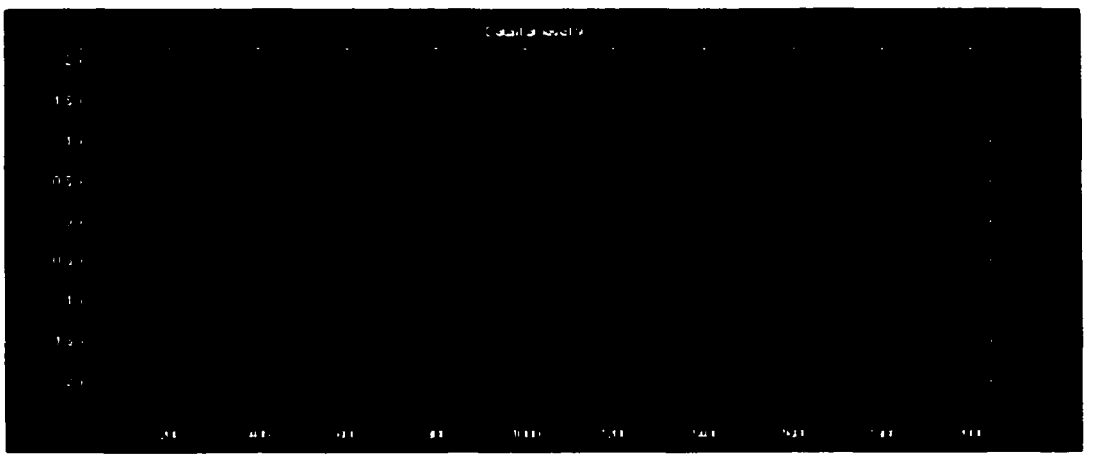

Figure 30(d): Detail d 9 (Level 2)

Figure 30(e): Detail d 8 (Level 3)

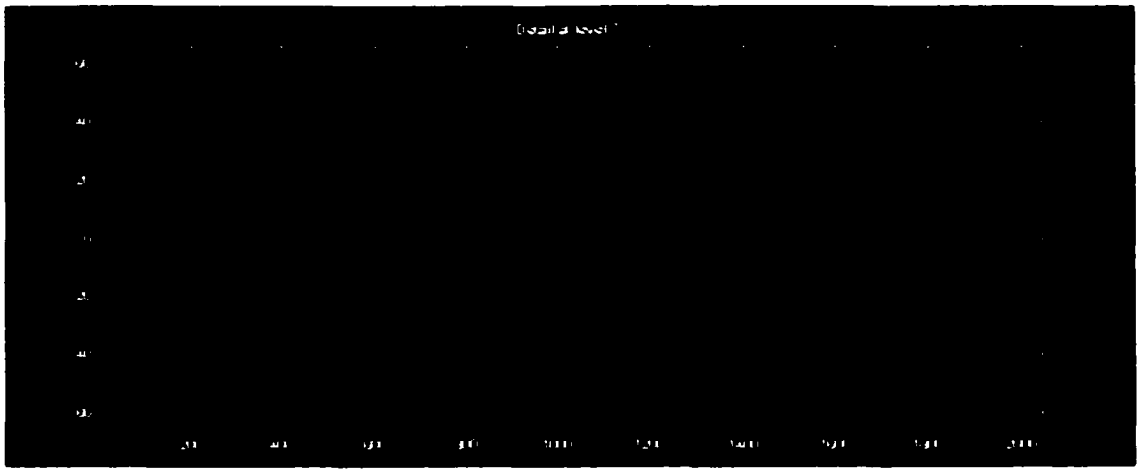

Figure 30(f): Detail d 7 (Level 4)

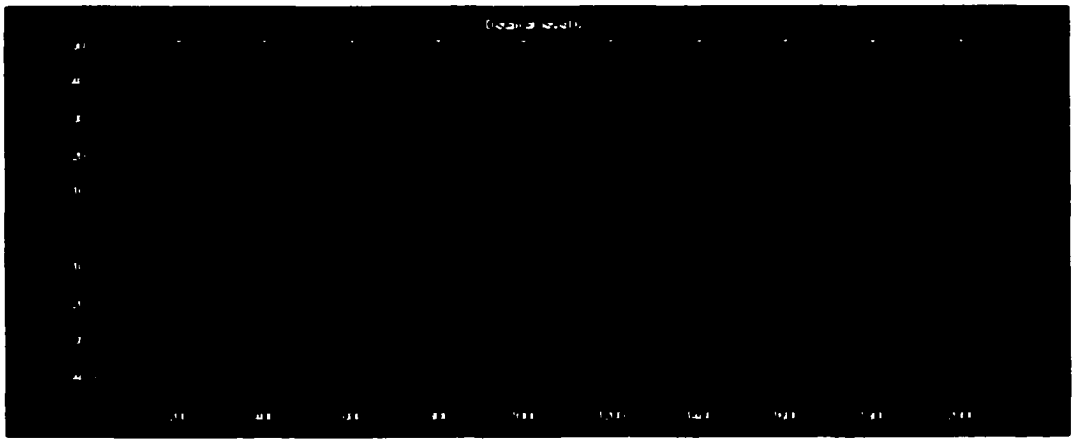

Figure 30(g): Detail d 6 (Level 5)

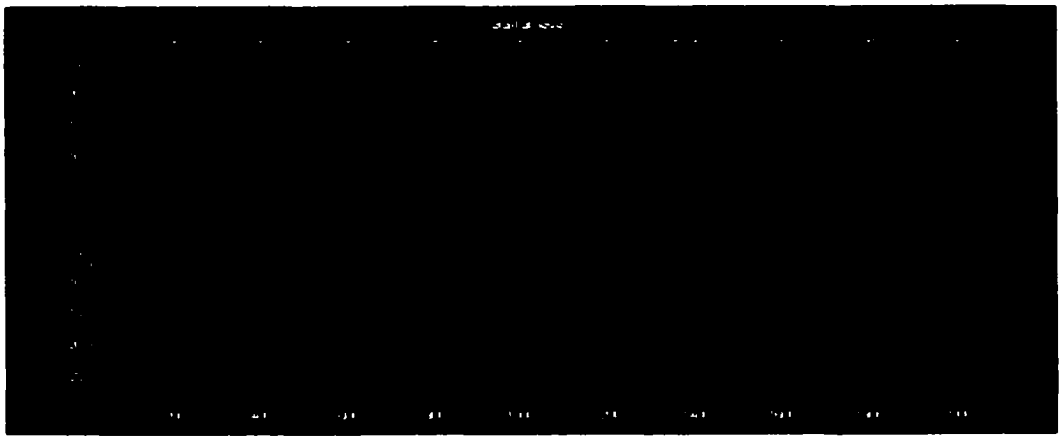

Figure 30(h): Detail d 5 (Level 6)

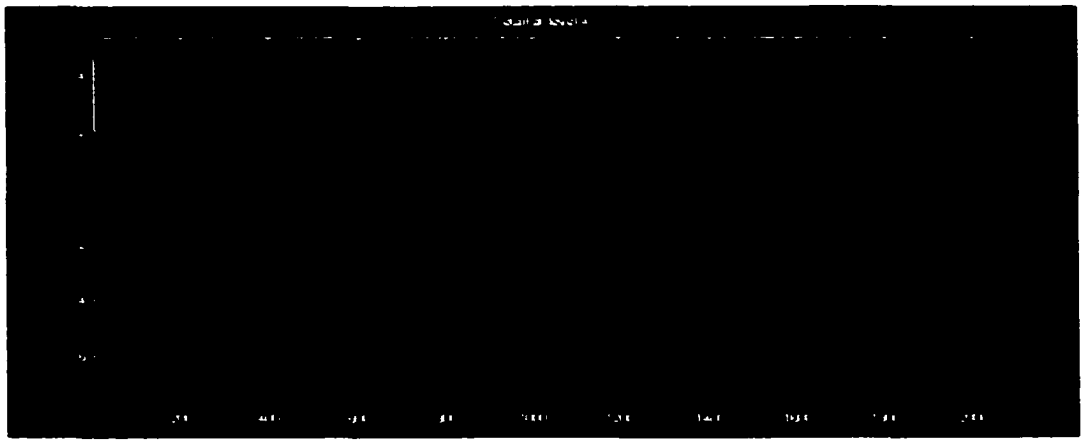

Figure 30(i): Detail d 4 (Level 7)

Figure 30(j): Detail d 3 (Level 8)

Figure 30(k): Detail d 2 (Level 9)

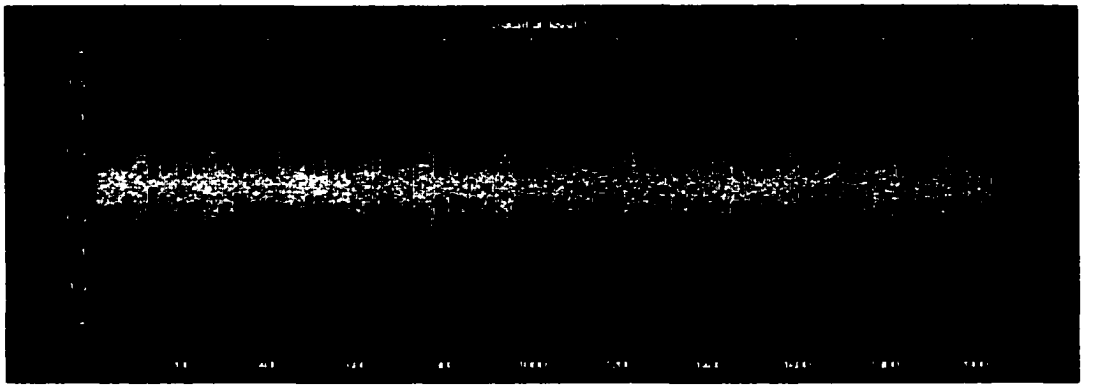

Figure 30(l): Detail d 1 (Level 10)

Figure 30: Wavelet Decomposition Of The Signal Using Daubechies D4 Wavelet Function

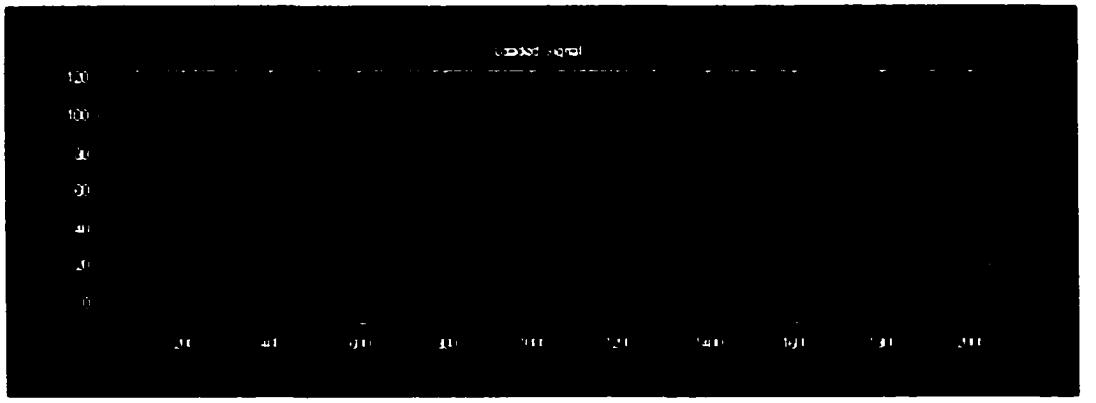

Figure 31 (a): Original Input Signal - Transformer inrush current.

Figure 31 (b): Approximation a 10 (Level 0)

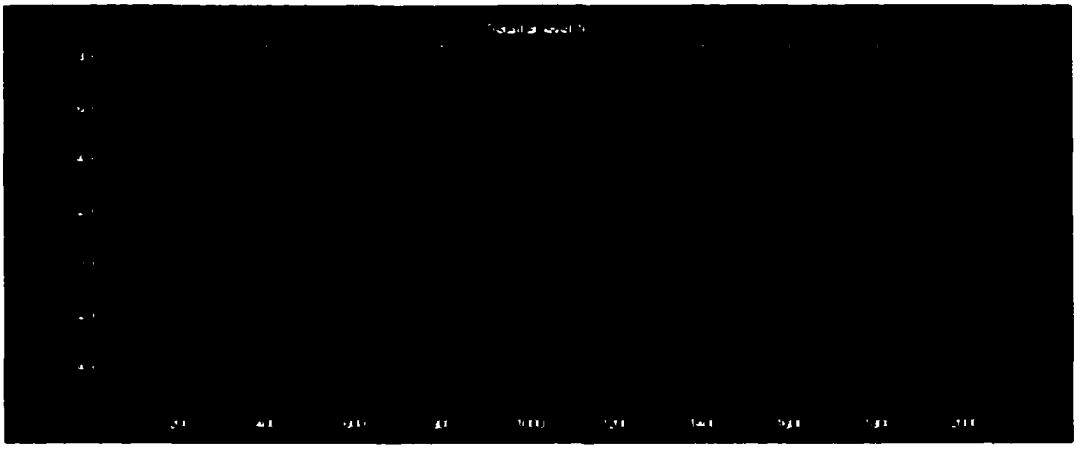

Figure 31 (c): Detail d 10 (Level 1)

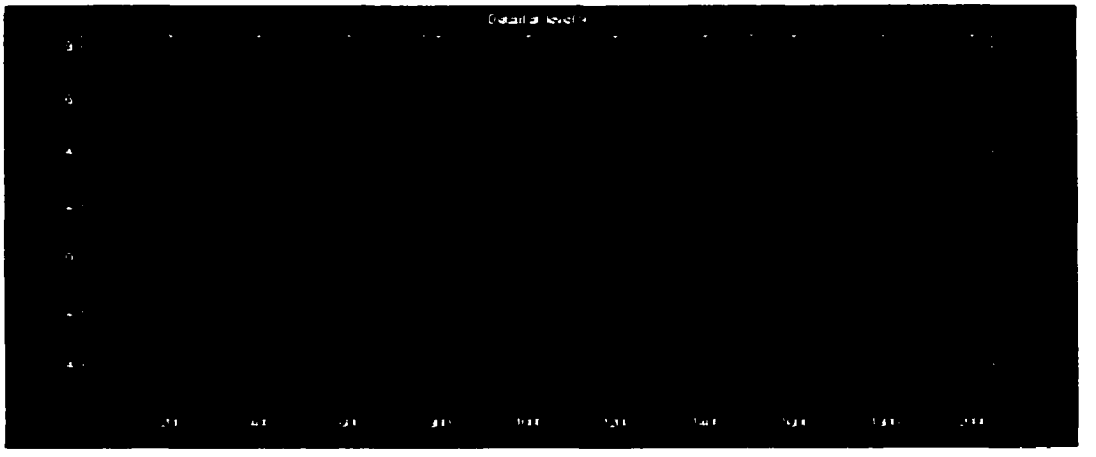

Figure 31 (d): Detail d 9 (Level 2)

Figure 31 (e): Detail d 8 (Level 3)

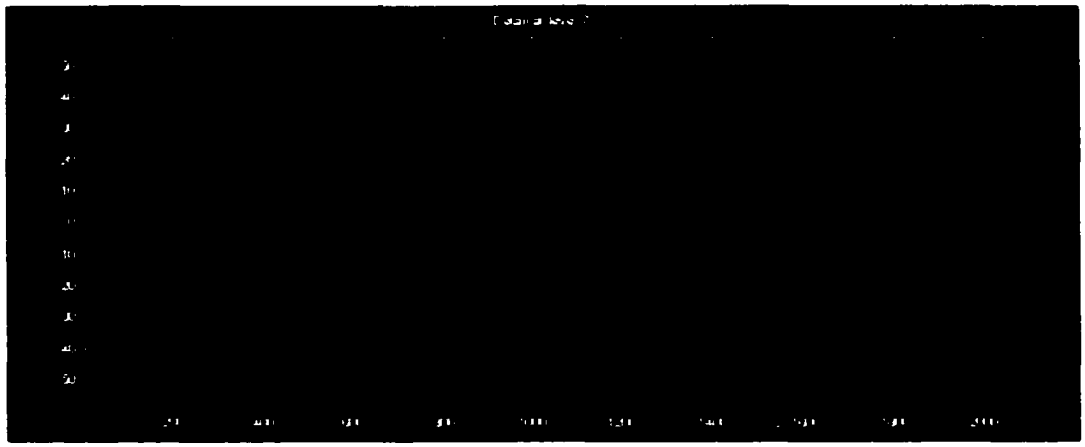

Figure 31 (f): Detail d 7 (Level 4)

Figure 31 (g): Detail d 6 (Level 5)

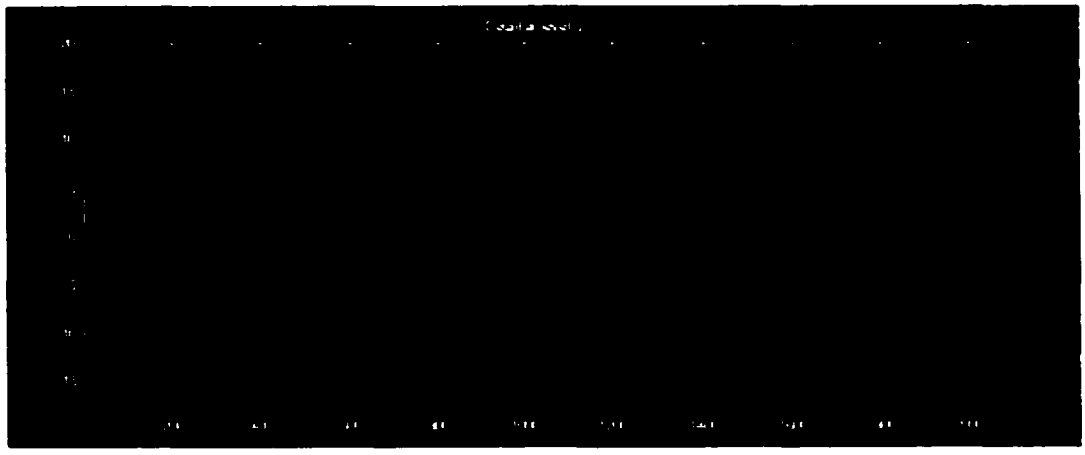

Figure 31 (h): Detail d 5 (Level 6)

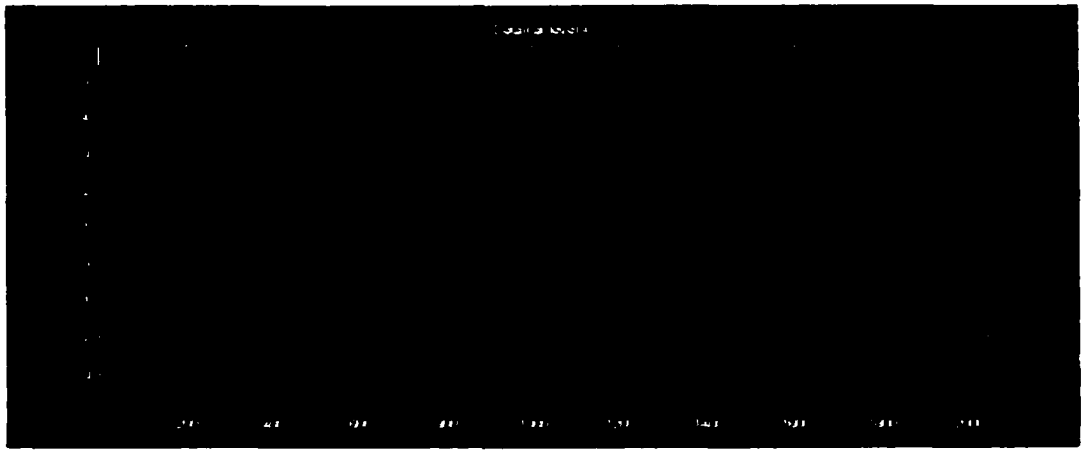

Figure 31 (i): Detail d 4 (Level 7)

Figure 31 (j): Detail d 3 (Level 8)

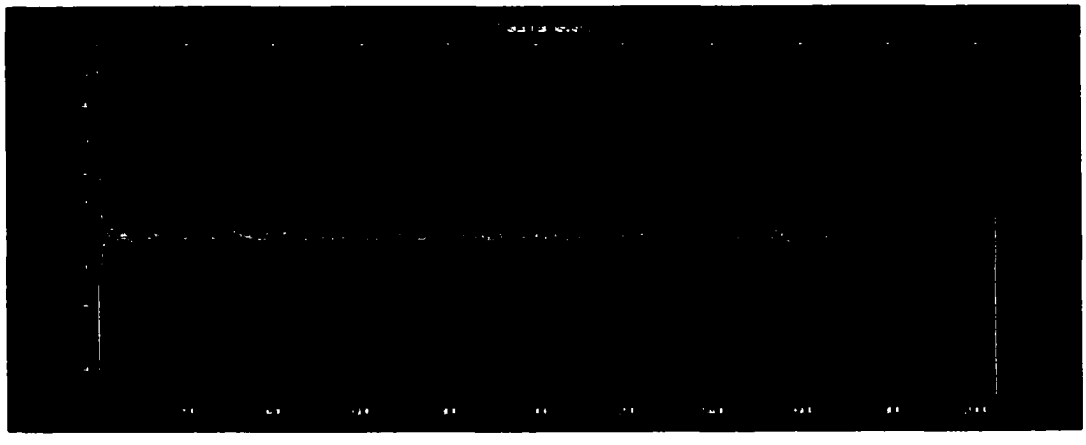

Figure 31 (k): Detail d 2 (Level 9)

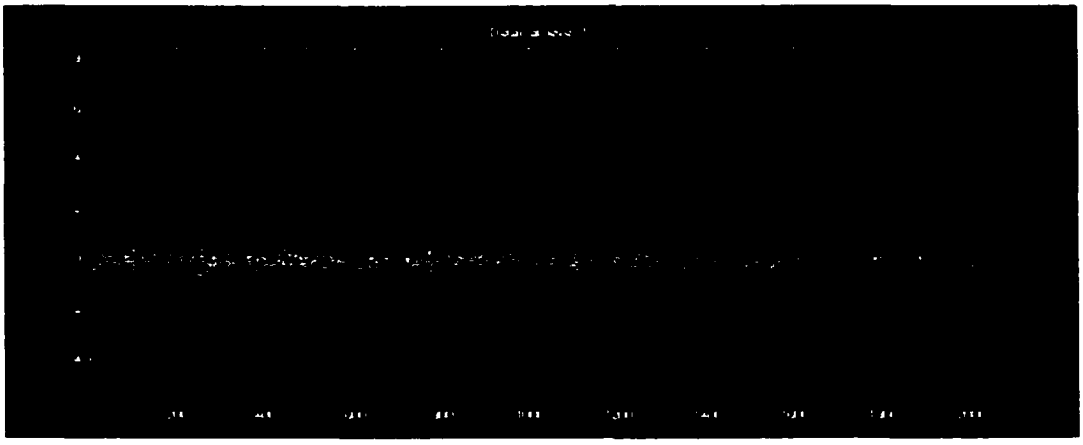

Figure 31 (l): Detail d 1 (Level 10)

Figure 31: Wavelet Decomposition of the signal using Daubechies D20 wavelet function.

The wavelet decompositions of the transformer inrush current using Daubechies D4 in figure 30 are compared with those obtained using Daubechies D20 in figure 31. For the Daubechies D4 wavelet, detail output d 4 (level 7) (See figure 30(i)) has an output that has large amplitude peaks corresponding to the peaks of the inrush current and smaller amplitude signal almost closer to a value of zero corresponding to the valleys (null period) in between the peaks. For the same transformer inrush signal, the Daubechies D20 wavelet decomposition doesn't have any clearly distinguishable characteristics for any output decomposition level as in Daubechies D4. The Daubechies D20 wavelet's detail output d 4 (level 7) (See figure 3 1(i)) has an output that appears to be more averaged from the longer scaling function with more coefficients. The higher the number of coefficients of the wavelet, it tends to smooth out the output decomposition. So for a transient signal with varying amplitudes and short duration, Daubechies D4, a wavelet with fewer coefficients is a good choice.

Similarly, to compare with the decomposition of the fault current, its wavelet decompositions using both the Daubechies D4 and D20 are plotted in figures 32 and 33 respectively. The fault current signal shows the fault occurs at the 450th data point in the time period considered. For the transformer short fault, the signal saturates at both positive and negative peaks at the time of the fault. Circuit breakers are used to detect this sudden increase in current due to fault and turn off the input to the transformer thereby reducing the damage. Clearly distinguishing this fault current from the inrush current is critical in ensuring the circuit breaker doesn't fail for the inrush current. This transient magnetizing inrush current causes false tripping of the differential relay and hence shutting the power circuit off [30].

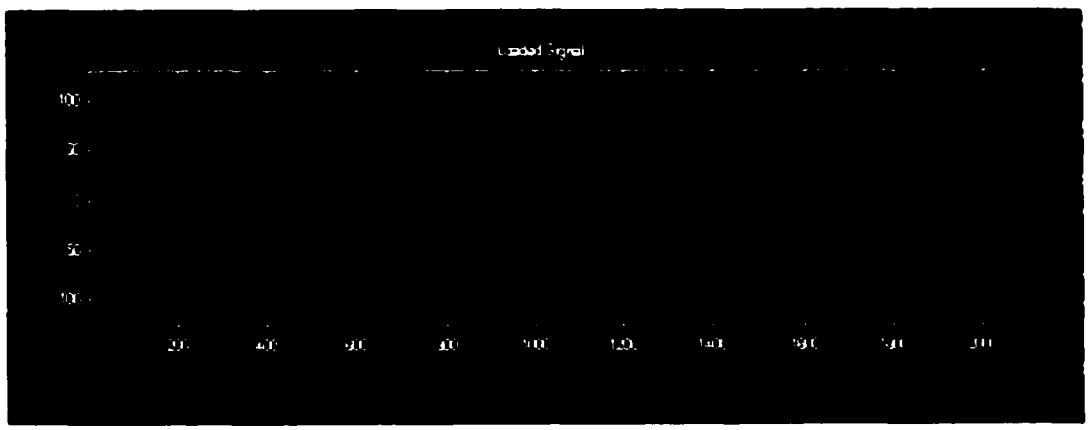

Figure 32 (a): Transformer fault current signal

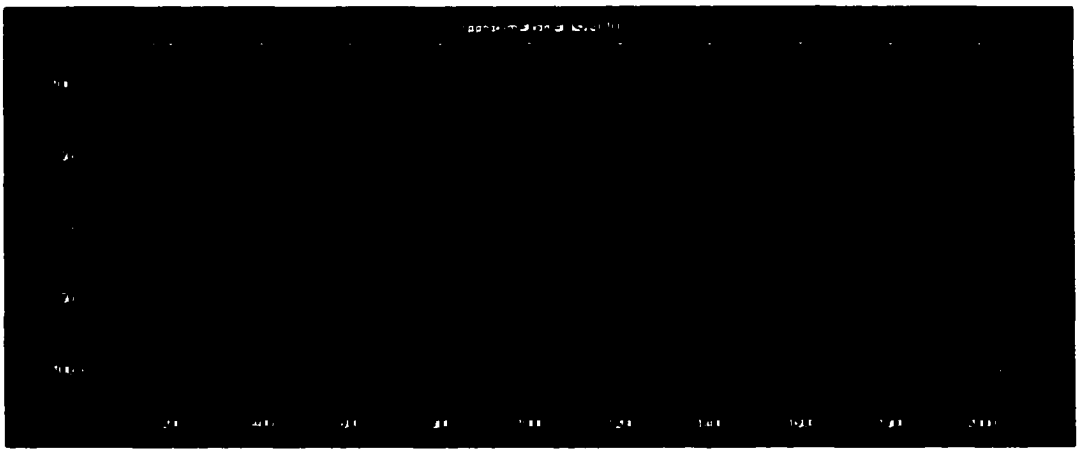

Figure 32 (b): Approximation a 10 (Level 0)

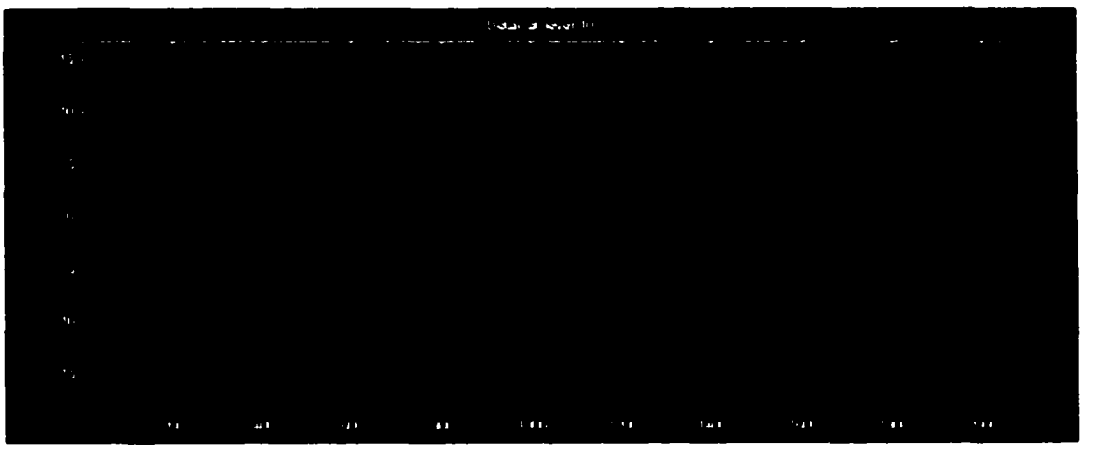

Figure 32 (c): Detail d 10 (Level 1)

Figure 32 (d): Detail d 9 (Level 2)

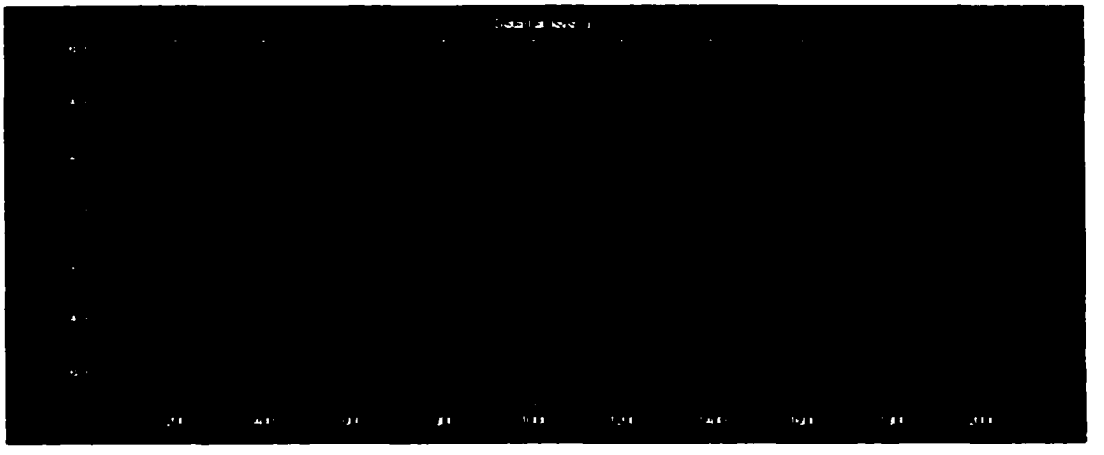

Figure 32 (e): Detail d 8 (Level 3)

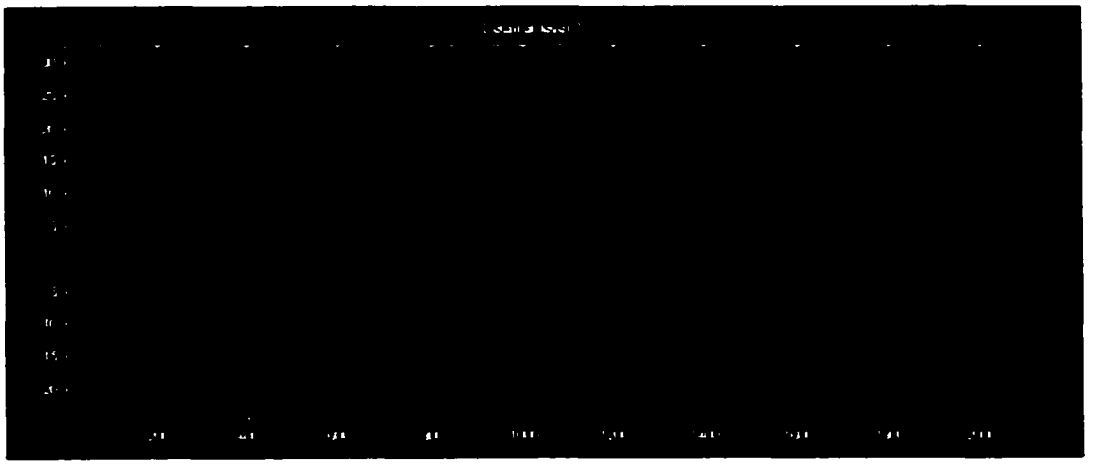

Figure 32 (f): Detail d 7 (Level 4)

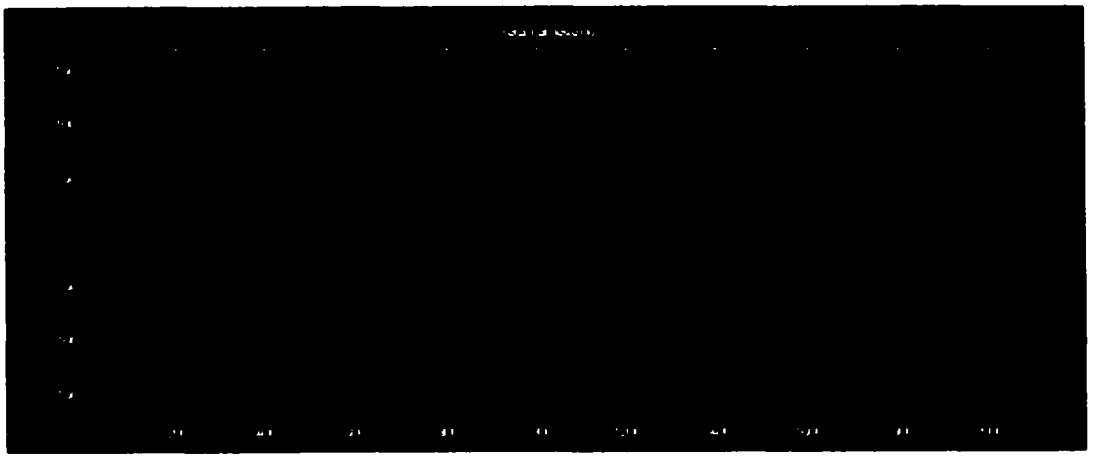

Figure 32 (g): Detail d 6 (Level 5)

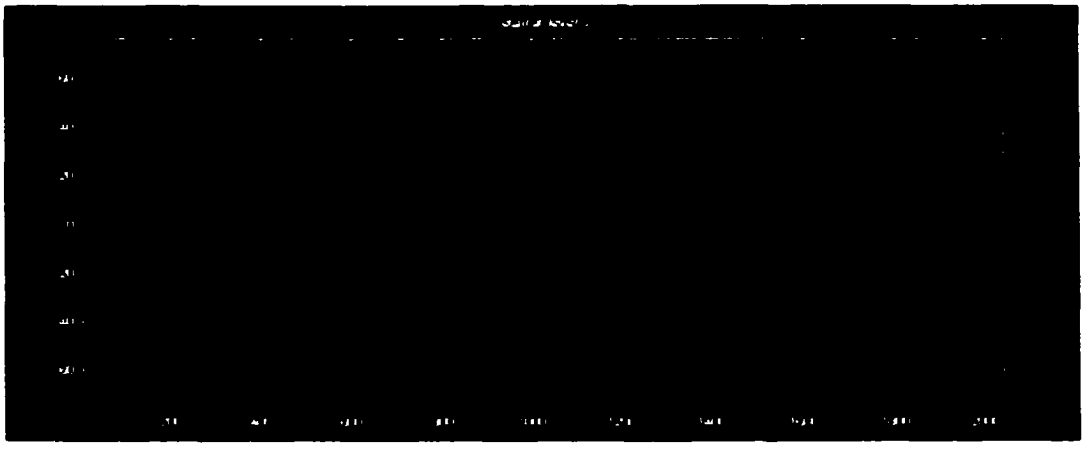

Figure 32 (h): Detail d 5 (Level 6)

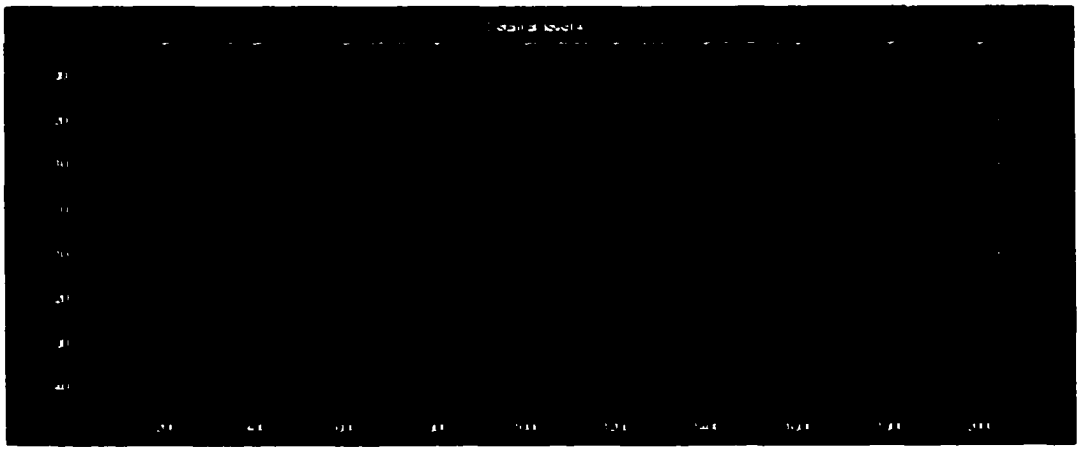

Figure 32 (i): Detail d 4 (Level 7)

Figure 32 (j): Detail d 3 (Level 8)

Figure 32 (k): Detail d 2 (Level 9)

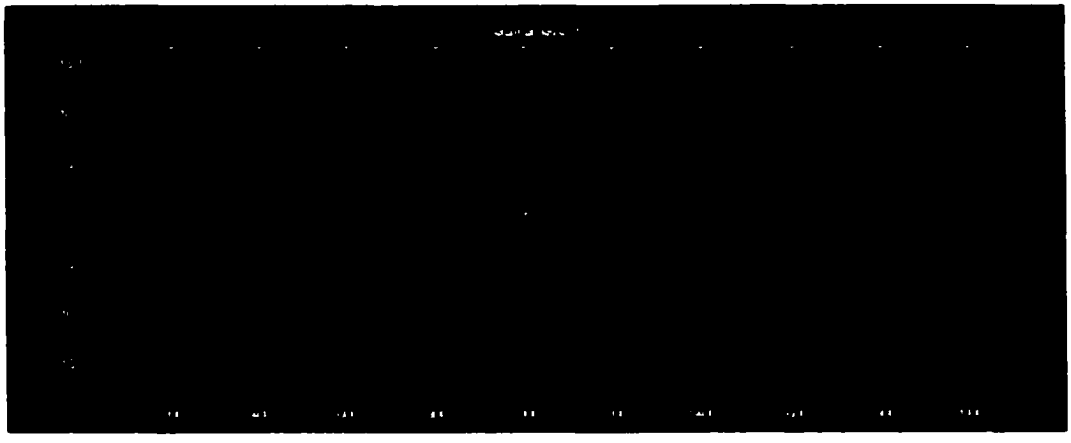

Figure 32 (l): Detail d 1 (Level 10)

Figure 32: Wavelet Decomposition Of The Fault Current Signal Using Daubechies D4

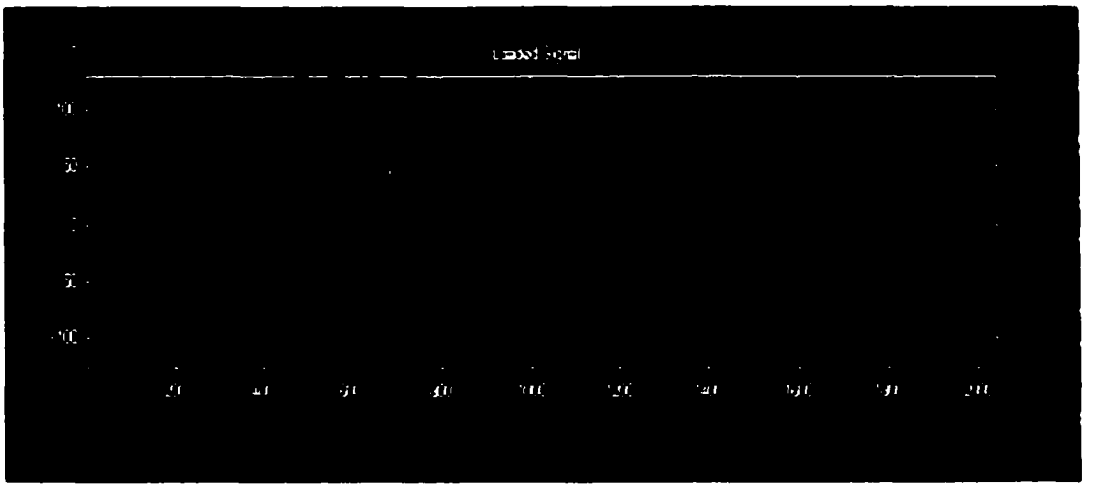

Figure 33 (a): Transformer fault current signal

Figure 33 (b): Approximation a 10 (Level 0)

Figure 33 (c): Detail d 10 (Level 1)

Figure 33 (d): Detail d 9 (Level 2)

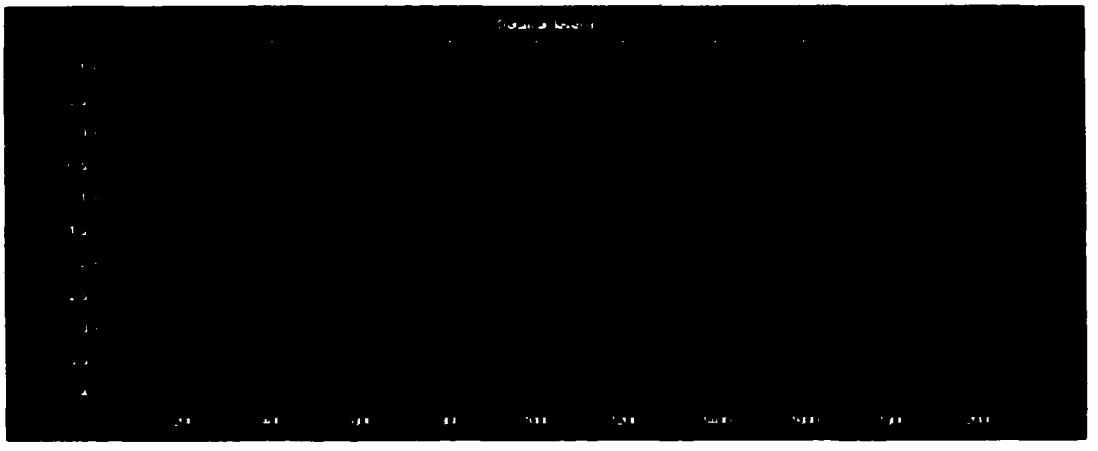

Figure 33 (e): Detail d 8 (Level 3)

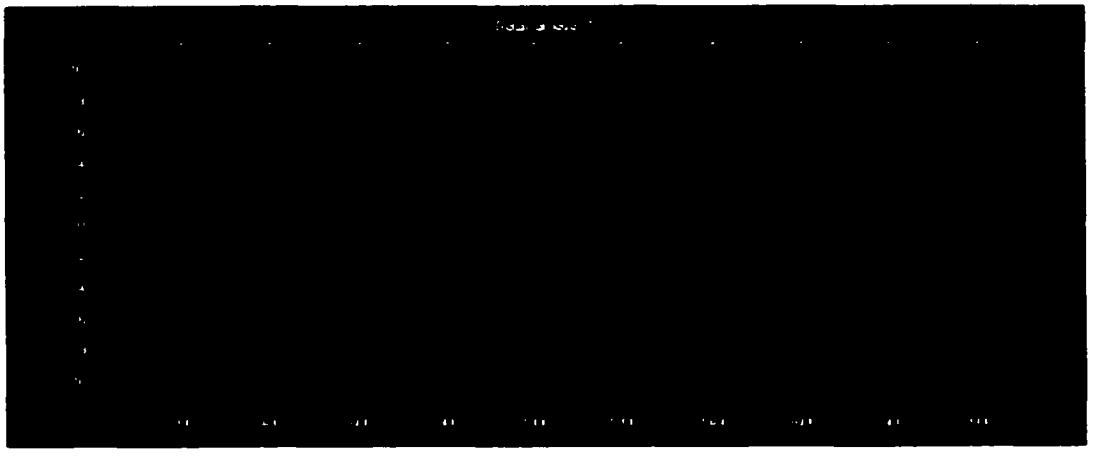

Figure 33 (f): Detail d 7 (Level 4)

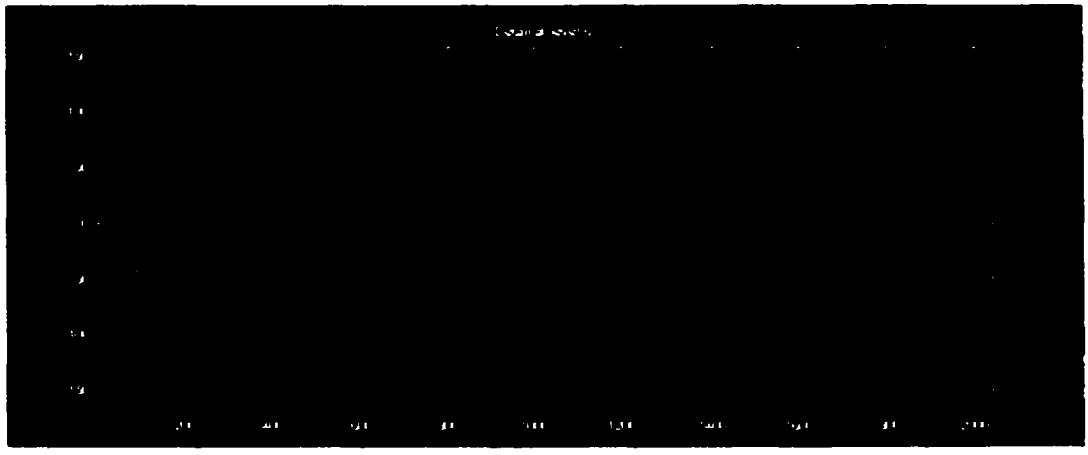

Figure 33 (g): Detail d 6 (Level 5)

Figure 33 (h): Detail d 5 (Level 6)

Figure 33 (i): Detail d 4 (Level 7)

Figure 33 (j): Detail d 3 (Level 8)

Figure 33 (k): Detail d 2 (Level 9)

Figure 33 (l): Detail d 1 (Level 10)

Figure 33: Wavelet Decomposition Of The Fault Current Signal Using Daubechies D20.

The Daubechies wavelet decomposition for the fault current doesn't display the same kind of behavior the wavelet decomposition of the magnetizing current shows. As seen in the wavelet decompositions for both the D4 and D20 of the fault current, they do not show any distinctive behavior except for a few large spikes at the state of transition from the normal current to the fault current. The output decomposition after the initial spurt decays and remains the same for all periods of time. This method of discriminating the magnetizing inrush current from the transformer fault current is better than the existing second harmonic component method used for most of the differential protective schemes [28], [29]. In the wavelet transform, the detection principle is based on the null period that exists in the inrush current. A paper describing the above research for identification of inrush current along with other research done, authored by Dr. Mickey Cox and me, has been accepted for publication in the IEEE transaction for Power Systems [17]. A copy of the paper is attached in Appendix B.

Hence, for applications where the information at a specific instance of time or for a very short period of time is to be retrieved the wavelets with less number of coefficients is a better choice. In our application to distinguish between inrush and fault currents, Daubechies D4 is a better choice. D4 wavelet's detail d4 (level 7) for the inrush current and D4 wavelet's detail d4 (level 7) for the fault current show how clearly the inrush and fault current are distinguished.

For information spread over long period of time or for signals with constant behavior over time, wavelet decomposition with D20, a wavelet with more number of coefficients is a good choice, as it tends to give a smoother output. The wavelet decomposition can be used to identify the frequencies (though not exactly, but within

specific frequency bands) of the event. Compare the D4 and D20 output wavelet decompositions of the fault current. The D20 wavelet decompositions are smoother than the D4 wavelet decompositions. The D4 wavelet with 4 coefficients tends to introduce discontinuities and breaks due to its wavelet function characteristic shape. For the D4 wavelet decomposition of the fault signal, the output amplitude is maximum in the detail d6 (level 5) with the detail d5 (level 6) having approximately 1/2 the maximum amplitude in the region after the transition from normal to fault state. For the D20 wavelet decomposition of the same fault signal, the output amplitude is maximum in the detail d6 (level 5) with the detail d5 (level 6) having less than $1/5^{th}$ of the maximum amplitude. For the above wavelet decomposition, detail d6 and detail d5 correspond to two different frequency bands separated by an octave. This shows that for the same fault signal, the amplitude in the detail d5 is different for different wavelets D4 and D20. The energy of the output wavelet decomposition using D4 is more spread out between two frequency bands compared to output wavelet decomposition using D20. So if we assume that D20 with more number of coefficients identifies the signal lies in one frequency band, D4 with less number of coefficients has very bad frequency localization. D4 shows the signal has frequencies with higher amplitudes in the next octave band.

The number of coefficients in the wavelet is shown to affect both the time localization and the frequency localization. Wavelets with fewer coefficients are better in detecting localized events but are not better tool for qualitatively quantifying the energy and frequency of wavelet decomposition. The next chapter is dedicated to the research done on quantifying the energy distribution and leakage in wavelet decompositions.

PROTECTIVE RELAYING TECHNIQUES FOR FAULTS:

The phase difference in the wavelet filter characteristics is a very important feature when used for applications with time as the critical factor. Identification of the fault current in the power system and shutting down the power to the system immediately is one of the important research studies in power system protection. The proper use of protective relay devices can substantially reduce the impact of faults and other disturbances on the operation of the power system [48].

Fuses were the earliest power protection devices which, though still being used widely, have been replaced in major circuits by circuit breakers to protect motors, generators, transformers etc. The circuit breaker's trip coils were controlled originally by electromechanical relays. Attempts to replace these by electronic solid state relays were hard at the beginning due to failures and bad designs, but with the advancement of digital technology and modifications to designs, they are being used in most circuit breakers and have found wide-spread acceptance. Current developments in micro-controller based electronics and miniaturization, these microprocessor based relays [49] are now incorporated with intelligence to be able to identify and classify faults in a timely manner before shutting down the circuit or raising alarms as appropriate depending on the type of fault.

The new microprocessor based relaying techniques call for improved software algorithms that are competent to perform different functions based on the outcome of detecting varying parameters of fault such as the type of fault, the fault location, fault impedance and the fault incident time that determine the corresponding transient current and voltage waveforms [50]. The new detection and classification approach has to reliably

conclude, in a very short time (1 – 2 cycles), whether and which type of fault occurs under a variety of time-changing operating conditions [51]. Several new methods and algorithms such as neural networks, fuzzy logic, and wavelet transforms for detecting of fault parameters are being researched.

One of the important characteristics of a good relaying system is its short time response. This has been given utmost importance in terms of being able to detect the fault early and provide a response within the least amount of time possible. Design optimization and performance evaluation of relaying algorithms, relays and protective systems is ongoing research [52]. For a good algorithm, it should trace the feature of the signal (for example, the amplitude after the occurrence of fault), reflecting the changes instantaneously. Due to well know trade-off between speed and accuracy, the time responses between the ideal and practical measuring algorithms differ [52].

Choosing the best algorithm to minimize this trade-off is an important part of the protective relaying research. Wavelets have very interesting characteristics that can provide answers to the time response of the relay algorithm. In the last example, we clearly saw the advantages of using the wavelets to identify and classify the inrush and fault currents. Once this classification has been done and the fault current identified, the wavelet algorithm can be used to shutdown power circuits or raise alarms for action. The wavelets' phase characteristics seen in the previous chapter can be used as an important tool in choosing the appropriate wavelet that will help in designing faster response relays.

From the phase characteristics of the wavelet filters, the D4 and D20 Daubechies wavelets have varying slopes of the phase response. D4 with a few coefficients has a smaller slope compared to the D20 with a greater number of coefficients. D4 was found

suitable for discriminating between the inrush and fault currents of the previous example. Applying the same two Daubechies wavelet decompositions to the fault currents, we obtain the wavelet decompositions shown in figures 32 and 33. The wavelet level d6 has the frequency band of 40 to 80 Hz, which is the frequency of our interest.

Figure 34 shows the 2048 data points of the transformer fault signal obtained in the lab. Figures 35 and 36 show the wavelet level d6 of the Daubechies decompositions of the fault signal for the two wavelets D4 and D20 respectively.

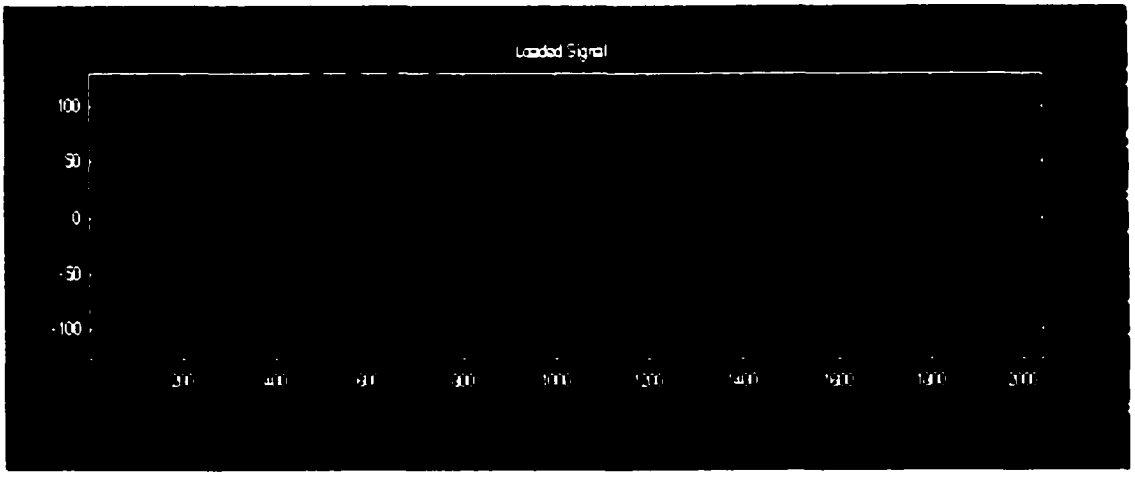

Figure 34: Transformer fault current signal

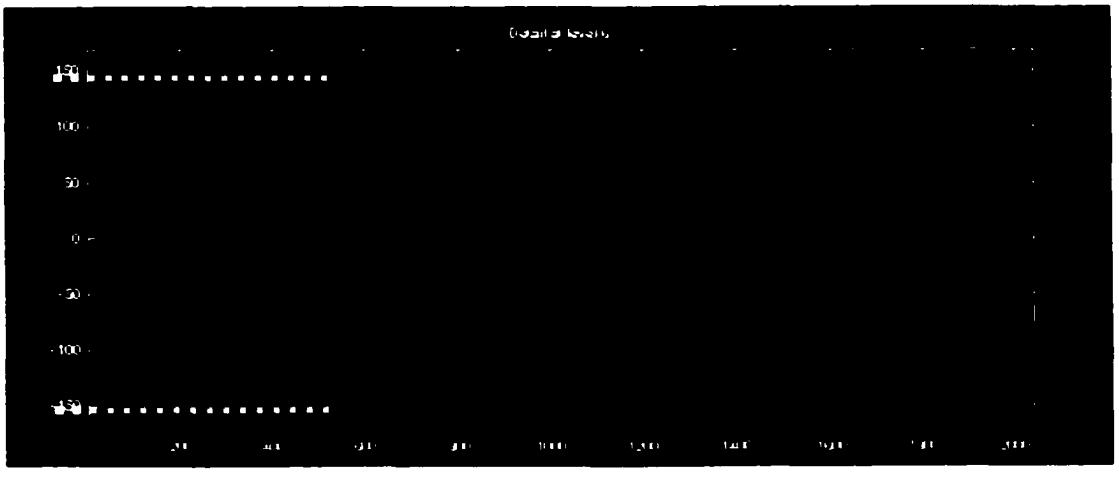

Figure 35: Wavelet level d6 – Daubechies D4 decomposition of the fault signal.

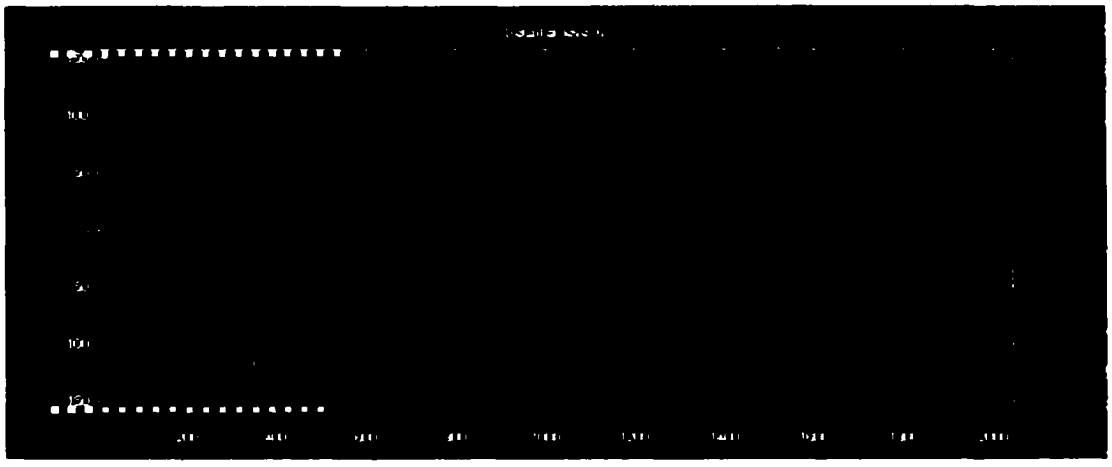

Figure 36: Wavelet level d6 – Daubechies D4 decomposition of the fault signal

The above plots are plotted with the fault current threshold cut-off lines at 150. The higher thresholds are to avoid false triggers by high amplitude inrush currents or transients. It can be seen that the D4 with a smaller phase slope has a smaller delay and follows the fault current signal. The D20 on the other hand, has more delay for the same 60 Hz signal due to the higher slope phase characteristics. The wavelet level d6 for the Daubechies D4 crosses the threshold value at around the 500^{th} data point about 100 points earlier than D20's 600^{th} point.

D4 with fewer number of coefficients which was found suitable for clearly classifying the inrush and fault currents can be further used as a trip algorithm to identify the fault incident time early and to shutdown the circuit breakers with in the first two cycles. A paper outlining the phase characteristics of wavelets and its applications as a tool for protective relaying techniques is in progress for publishing in the IEEE journal.

Wavelets as seen in the above research, show potential as a promising tool for further study towards applying them to the area of protective power systems. Practical

applications such as the ones mentioned above will aid in popularizing the wavelet tool for signal processing applications.

CHAPTER 5

ENERGY DISTRIBUTION OF WAVELET DECOMPOSITIONS

As seen in the previous chapter, for detecting the frequency composition of the signal being analyzed, we get different results with energy distributed in the wavelet decompositions of the same signal using D4 and D20. To further analyze this, we consider a sinusoidal signal simulated with MATLAB(R) having the fundamental frequency combined with its seventh harmonic frequency component at half amplitude. This signal is given by:

$$f(t) = \sqrt{2}\sin(2\pi 60t) + 0.5 \times \sqrt{2}\sin(2\pi 420t) \qquad -(16)$$

Three cycles of the signal at 60 Hz with 512 data points and sampled at a 10,240 Hz are considered as shown in figure 37. The fundamental frequency 60 Hz and the seventh harmonic 420 Hz are considered for our example. This signal is wavelet transformed to obtain the approximation and the details of the signal. For this signal with $N = 512$ data points, there are 9 wavelet levels, i.e., 8 detail levels and 1 approximation level.

The octave bands of frequency range from DC to 5120 Hz, half sampling frequency 10,240 Hz. The rms value of the signal decomposition in each level is calculated and studied to understand the wavelet energy distribution and leakage. Daubechies D20 wavelet decomposition of the above signal is shown in figure 38.

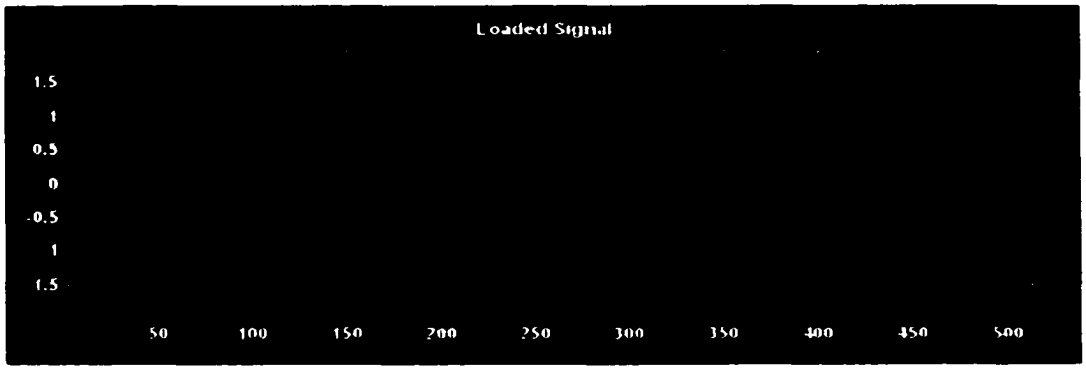

Figure 37: Simulated Signal Using Matlab.

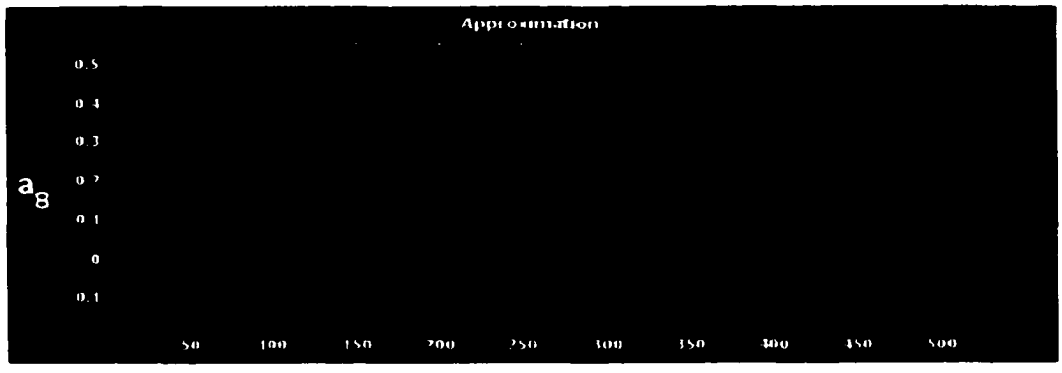

Figure 38(a): Approximation a8 (Level 0)

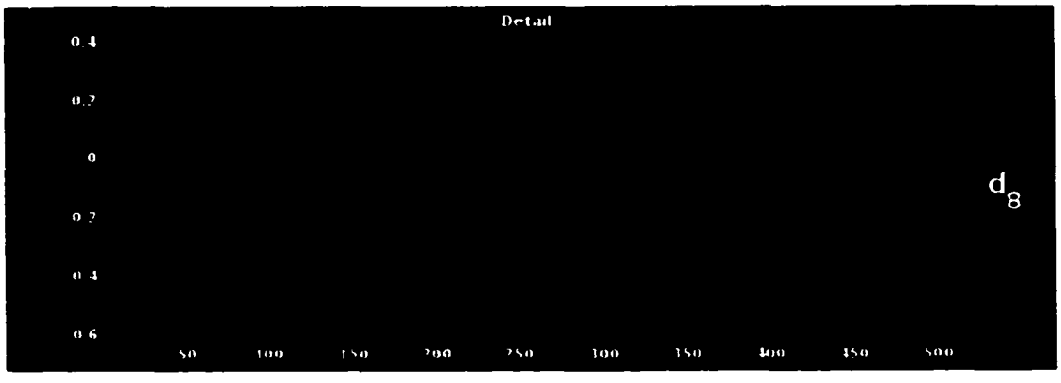

Figure 38(b): Detail d8 (Level 1)

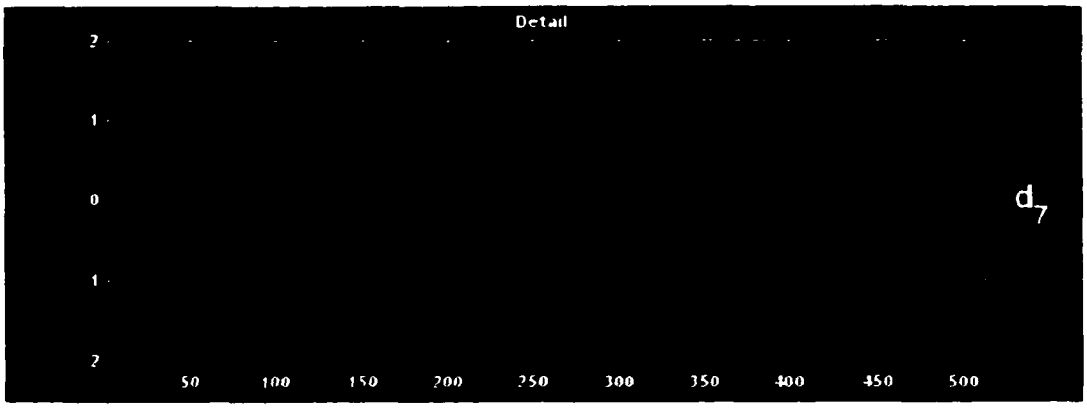

Figure 38(c): Detail d7 (Level 2)

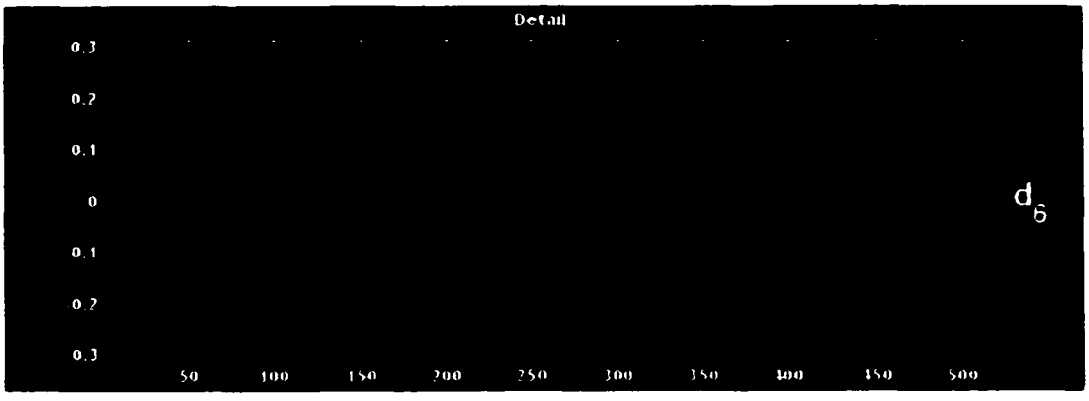

Figure 38(d): Detail d6 (Level 3)

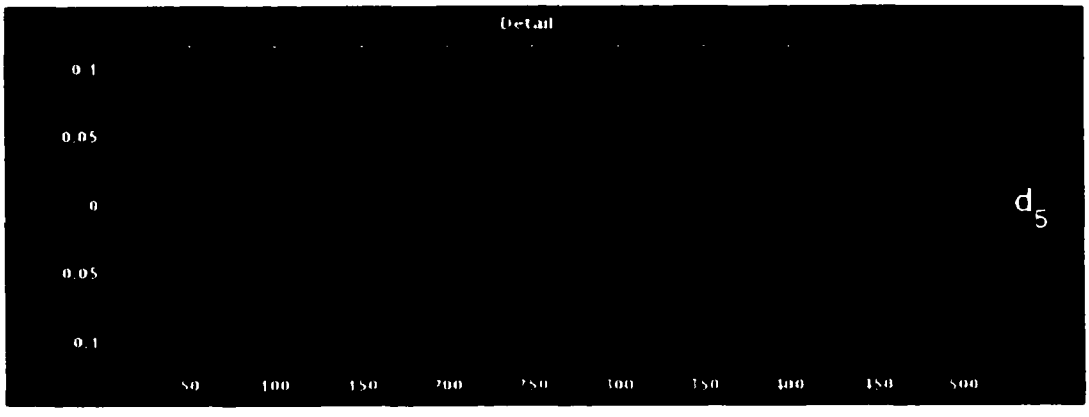

Figure 38(e): Detail d5 (Level 4)

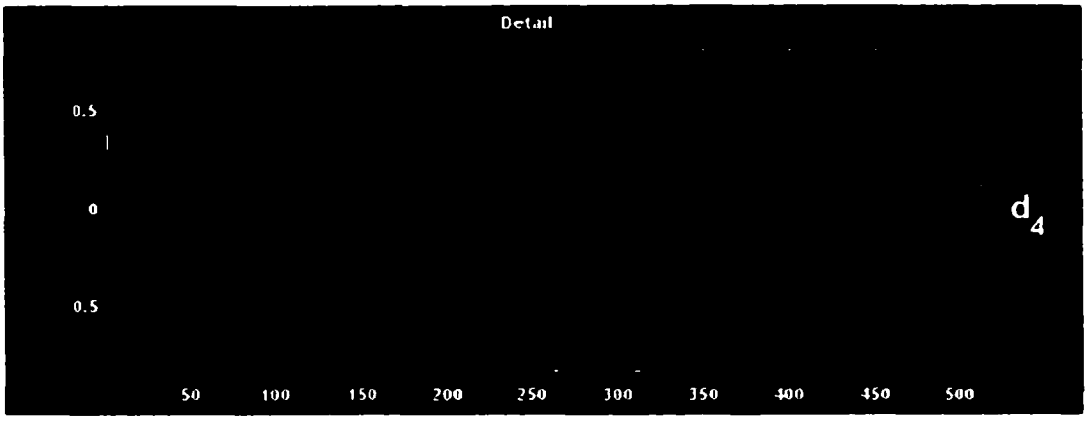

Figure 38(f): Detail d4 (Level 5)

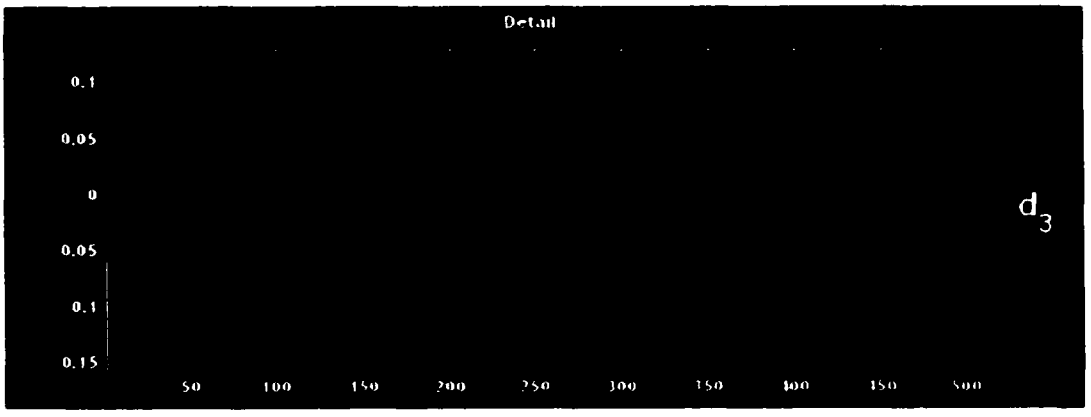

Figure 38(g): Detail d3 (Level 6)

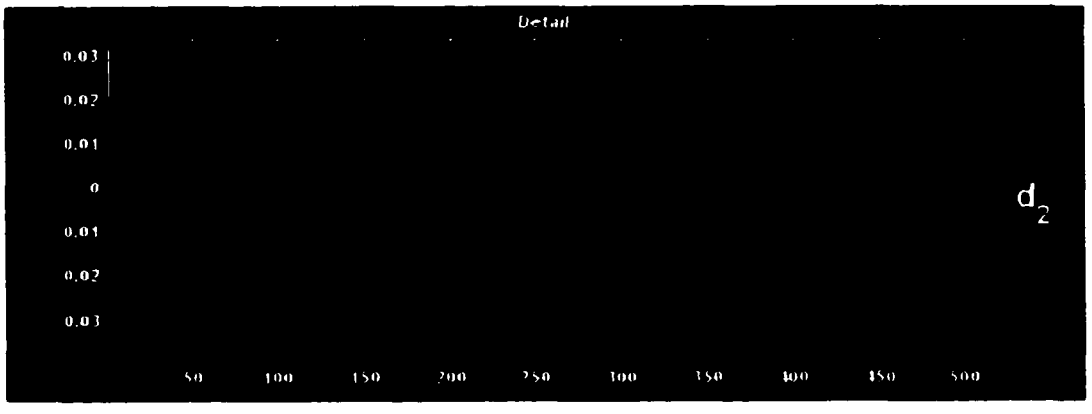

Figure 38(h): Detail d2 (Level 7)

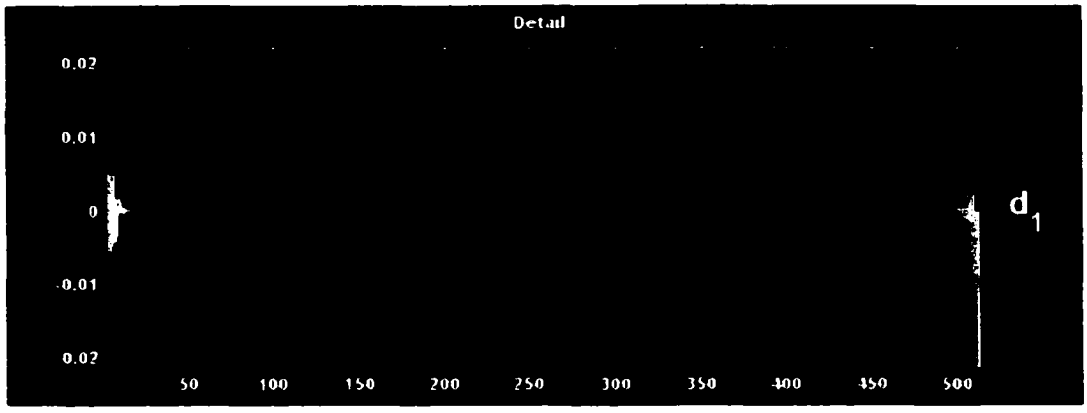

Figure 38(i): Detail d1 (Level 8)

Figure 38: Wavelet Decomposition Of Simulated Signal Using Daubechies D20 Wavelet Function.

The rms amplitude value and the energy of the simulated signal is calculated as:

$$f(t) = \sqrt{2}\sin(2\pi 60t) + 0.5 \times \sqrt{2}\sin(2\pi 420t)$$

$$rms(f(t)) = \sqrt{(1)^2 + (0.5)^2}$$

$$rms(f(t)) = \sqrt{1.25} = 1.118 \qquad -(17)$$

Energy of the signal = $(rms(f(t)))^2 = 1.25$

The rms amplitude value and energy of the individual wavelet decompositions is calculated. The "energy" mentioned above is based on the *Parseval's theorem*: "the energy that a time domain function contains is equal to the sum of all energy concentrated in the different resolution levels of the corresponding wavelet transformed signal"[31]. The rms value and energy of the individual wavelet level L is given by:

$$rms(levelL) = sqrt(\tfrac{1}{512} \times sum(A(L,:)^2) \qquad -(18)$$

where $A(L,:)$ is the coefficients of the wavelet decomposition level L signal.

The total energy of the signal can be mathematically expressed as [32], [33]:

$$\sum_{n=1}^{N}|f(n)|^2 = \sum_{n=1}^{N}|a_j(n)|^2 + \sum_{j=1}^{l}\sum_{n=1}^{N}|d_j(n)|^2 \qquad -(19)$$

where N is the number of data points, l is the total number of wavelet decomposition levels. The above expression shows that the total signal energy is the sum of the j^{th} level approximation signal and the sum of all the detail level signals from 1^{st} detail to j^{th} detail.

Table 4 shows the details of the wavelet decomposition in terms of frequency bands, center frequency, rms and energy values of the individual levels for wavelet transform of the simulated signal using Daubechies D20.

Table 4: Rms Value Of The Daubechies D20 Wavelet Levels For The Simulated Signal.

Wavelet Level	Frequency band	Center frequency	Rms value	Energy
0 (a8)	0-20 Hz	10 Hz	0.1981	0.0392
1 (d8)	20 Hz – 40 Hz	30 Hz	0.2827	0.0799
2(d7)	40 Hz – 80 Hz	60 Hz	0.8779	0.7706
3(d6)	80 Hz – 160 Hz	120 Hz	0.1777	0.0316
4(d5)	160 Hz – 320 Hz	240 Hz	0.0775	0.0060
5(d4)	320 Hz – 640 Hz	480 Hz	0.4831	0.2334
6(d3)	640 Hz – 1280 Hz	960 Hz	0.0596	0.0035
7(d2)	1280 Hz – 2560 Hz	1920 Hz	0.0074	0.0001
8(d1)	2560 Hz – 5120 Hz	3840 Hz	0.0021	0.0000

The square root of the sum total of all the rms values is

Rms value = Square Root [(square of rms value of approximation level) + (sum of squares of rms values of all detail levels)].

$$\sqrt{\sum (rmsvalue)^2} = \sqrt{\begin{matrix}(0.1981)^2 + (0.2827)^2 + (0.8779)^2 + (0.1777)^2 \\ + (0.0775)^2 + (0.4831)^2 + (0.0596)^2 + (0.0074)^2 \\ + (0.0021)^2\end{matrix}}$$

$$rms(f(t)) = \sqrt{1.16} = 1.08$$

Energy = energy of approximation level + sum of energies of all details

$$Energy = \begin{pmatrix} 0.0392 + 0.0799 + 0.7706 \\ + 0.0316 + 0.0060 + 0.2334 \\ + 0.0035 + 0.0001 + 0.0000 \end{pmatrix}$$

$$Energy = 1.16$$

This value determined by the wavelet decomposition is approximately in good agreement with the rms value of the simulated signal calculated earlier in equation 16. This shows that the total energy of the signal is distributed among the wavelet levels and no energy or very little energy is lost in the decomposition. Figure 39 shows the histogram of the rms and the energy values in table 4. It can be seen from the histogram plots, the energy is concentrated in a few wavelet decomposition levels, i.e., wavelet level 2 (d7), wavelet level 5 (d4). These levels correspond to frequency bands – 40 Hz to 80 Hz and 320 Hz to 640 Hz respectively. The signal is made of 60 Hz and 420 Hz frequencies which should lie only in level d7 and d4. The wavelet decomposition of the signal shows the signal has some frequency components lying in the bands around these two bands but with smaller amplitude. Since the total energy calculated is shown to be the same, then there exists energy leakage between the bands.

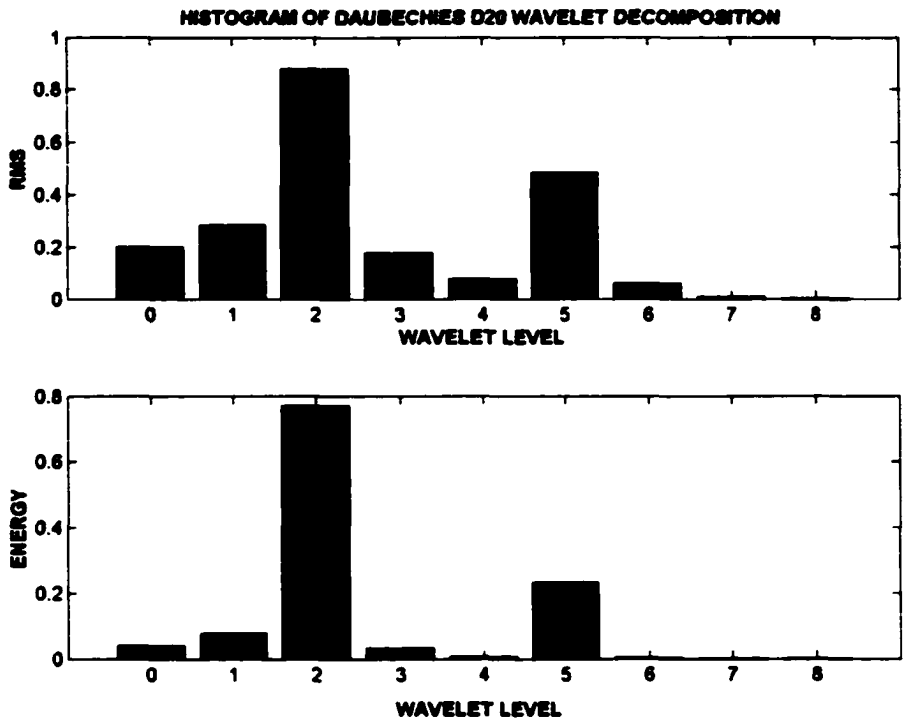

Figure 39: Histogram of the Daubechies D20 wavelet decomposition of the simulated signal.

To understand the energy leakage further, let us consider the Daubechies wavelet D4 wavelet decomposition of the same simulated signal $f(t)$ and calculate the rms and energy values of the decomposition. Figure 40 shows the 9 level wavelet decomposition of the simulated signal using Daubechies D4 wavelet. The rms and energy values of the wavelet levels are calculated using the same method described earlier and are tabulated in table 5. These values of Daubechies wavelet in table 5 are compared to values of Daubechies wavelet D20 in table 4.

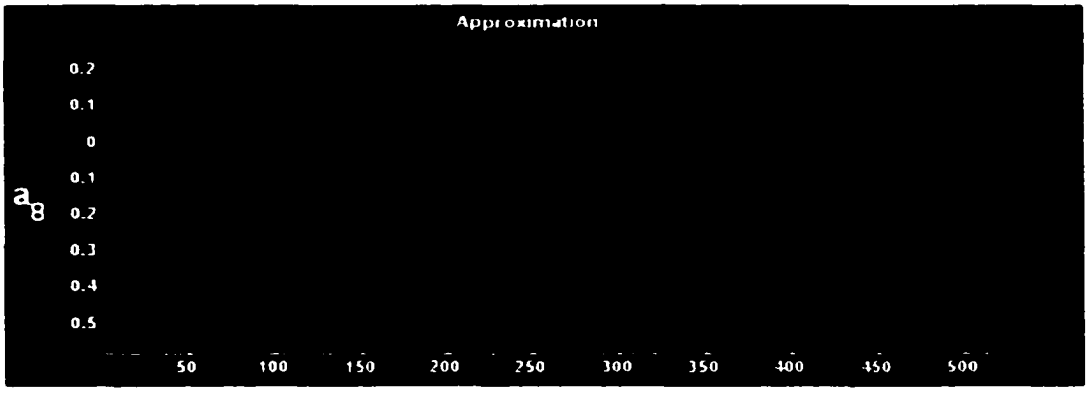

Figure 40(a): Approximation a8 (Level 0)

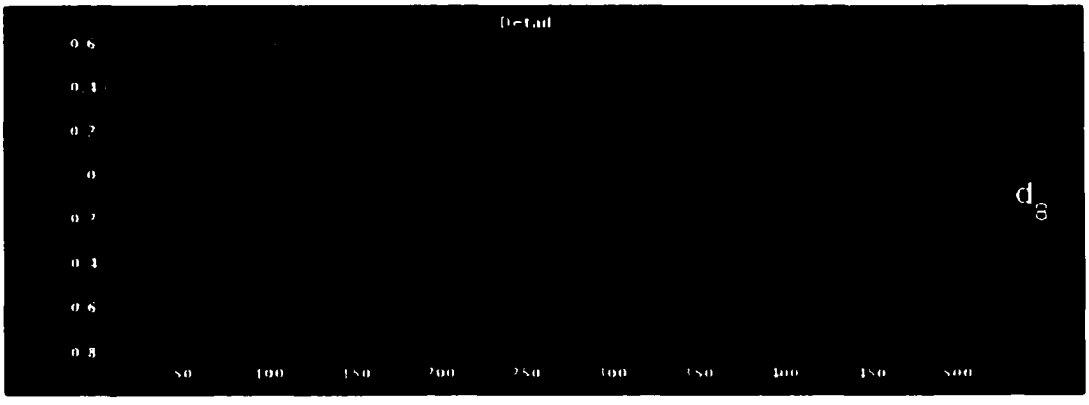

Figure 40(b): Detail d8 (Level 1)

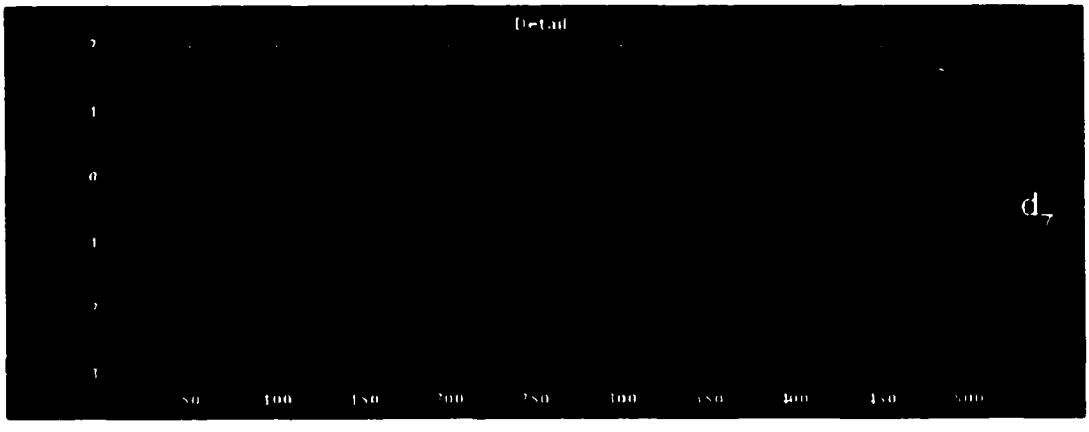

Figure 40(c): Detail d7 (Level 2)

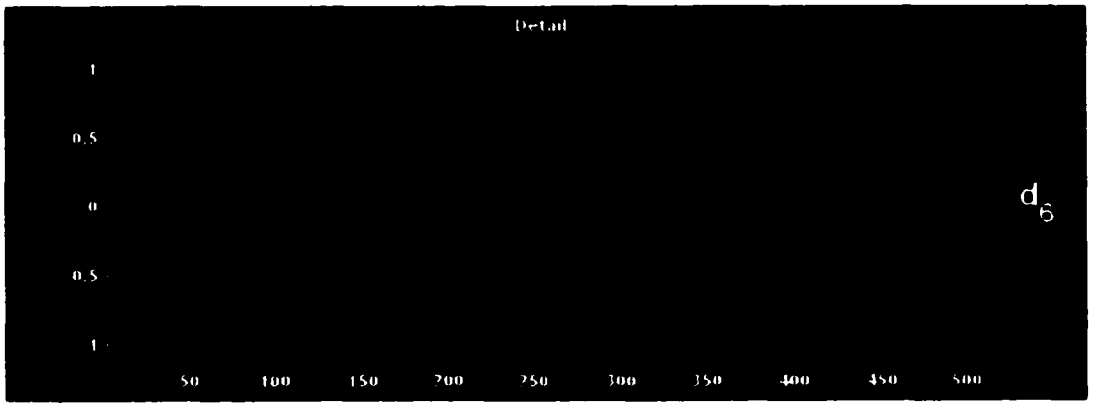

Figure 40(d): Detail d6 (Level 3)

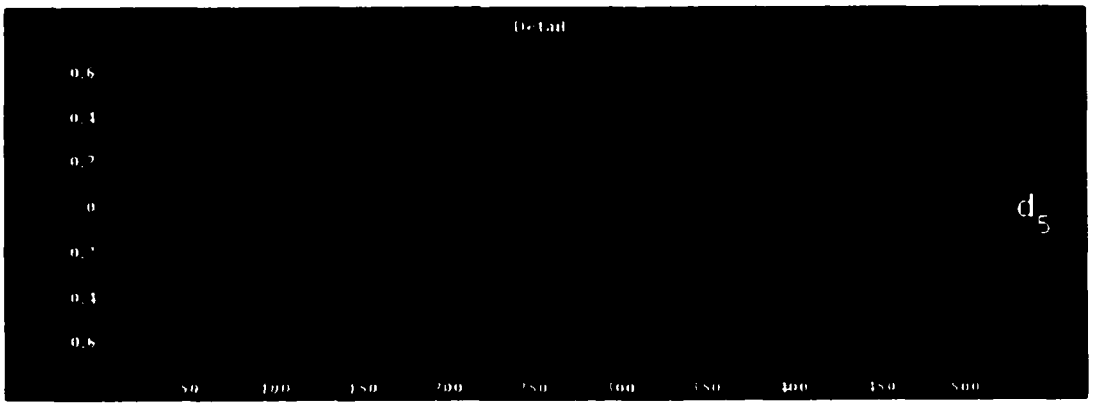

Figure 40(e): Detail d5 (Level 4)

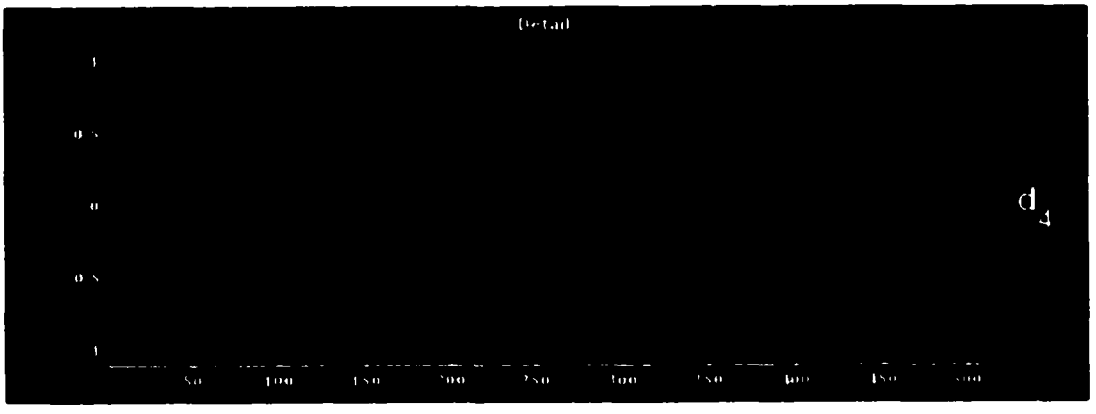

Figure 40(f): Detail d4 (Level 5)

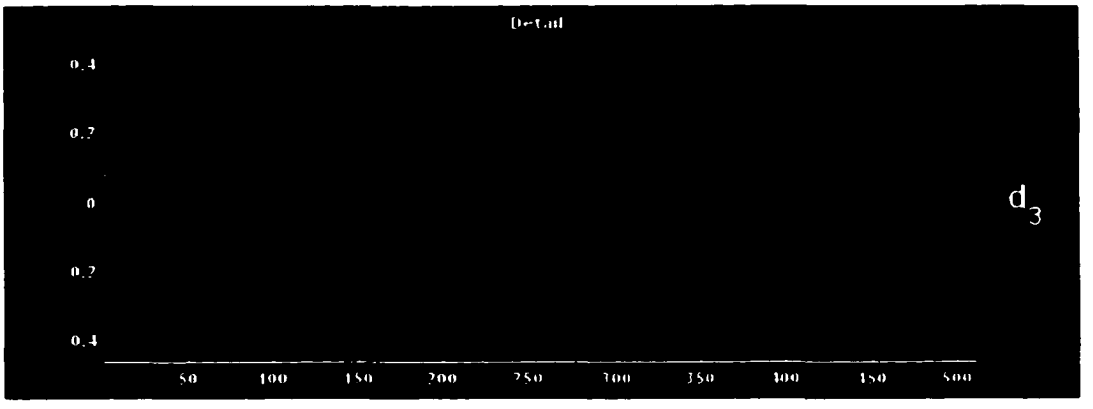

Figure 40(g): Detail d3 (Level 6)

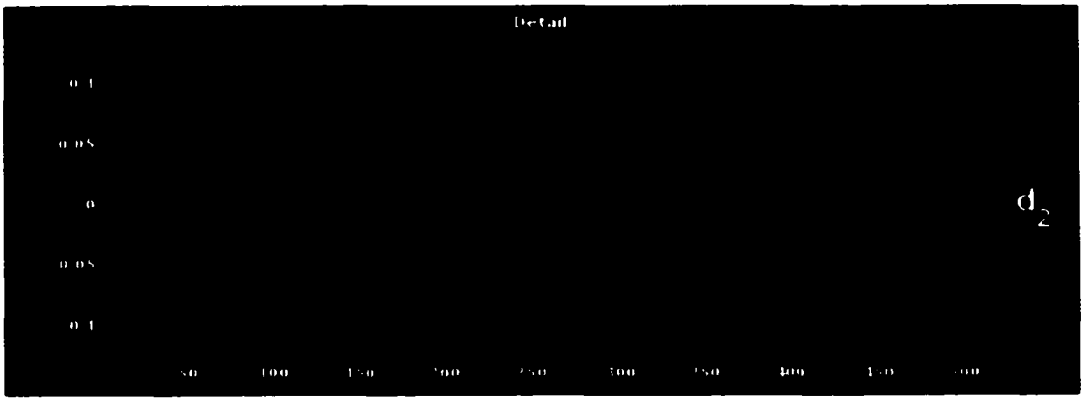

Figure 40(h): Detail d2 (Level 7)

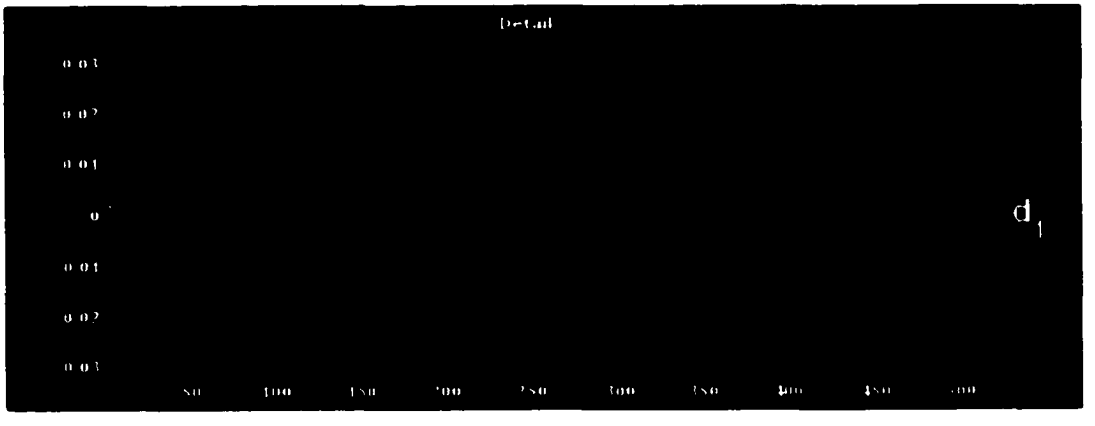

Figure 40(i): Detail d1 (Level 8)

Figure 40: Wavelet Decomposition Of Simulated Signal Using Daubechies D4 Wavelet Function

Table 5: Rms Value Of The Daubechies D4 Wavelet Levels For The Simulated Signal.

Wavelet Level	Frequency band	Center frequency	Rms value	Energy
0 (a8)	0-20 Hz	10 Hz	0.2704	0.0731
1 (d8)	20 Hz – 40 Hz	30 Hz	0.2909	0.0846
2(d7)	40 Hz – 80 Hz	60 Hz	0.7603	0.5780
3(d6)	80 Hz – 160 Hz	120 Hz	0.4817	0.2320
4(d5)	160 Hz – 320 Hz	240 Hz	0.2342	0.0548
5(d4)	320 Hz – 640 Hz	480 Hz	0.4111	0.1690
6(d3)	640 Hz – 1280 Hz	960 Hz	0.1890	0.0357
7(d2)	1280 Hz – 2560 Hz	1920 Hz	0.0562	0.0032
8(d1)	2560 Hz – 5120 Hz	3840 Hz	0.0156	0.0002

The total rms value and the energy of D4 output calculated from the above table is:

Rms value = Square Root [(square of rms value of approximation level) + (sum of squares of rms values of all detail levels)].

$$\sqrt{\sum (rmsvalue)^2} = \sqrt{\begin{matrix}(0.2704)^2 + (0.2909)^2 + (0.7603)^2 + (0.4817)^2 \\ + (0.2342)^2 + (0.4111)^2 + (0.1890)^2 + (0.0562)^2 \\ + (0.0156)^2\end{matrix}}$$

$$rms(f(t)) = \sqrt{1.23} = 1.11$$

Energy = energy of approximation level + sum of energies of all details

$$Energy = \begin{pmatrix}0.0731 + 0.0846 + 0.5780 \\ + 0.2320 + 0.0548 + 0.1690 \\ + 0.0357 + 0.0032 + 0.0002\end{pmatrix} = 1.23$$

The histogram of the rms and energy values for Daubechies D4 wavelet decomposition for the simulated signal is shown in figure 41. Comparing the histograms of the two wavelet decompositions of D4 and D20, we see the total energy is the same for both cases, but an interesting observation can be made with regards to the energy distribution.

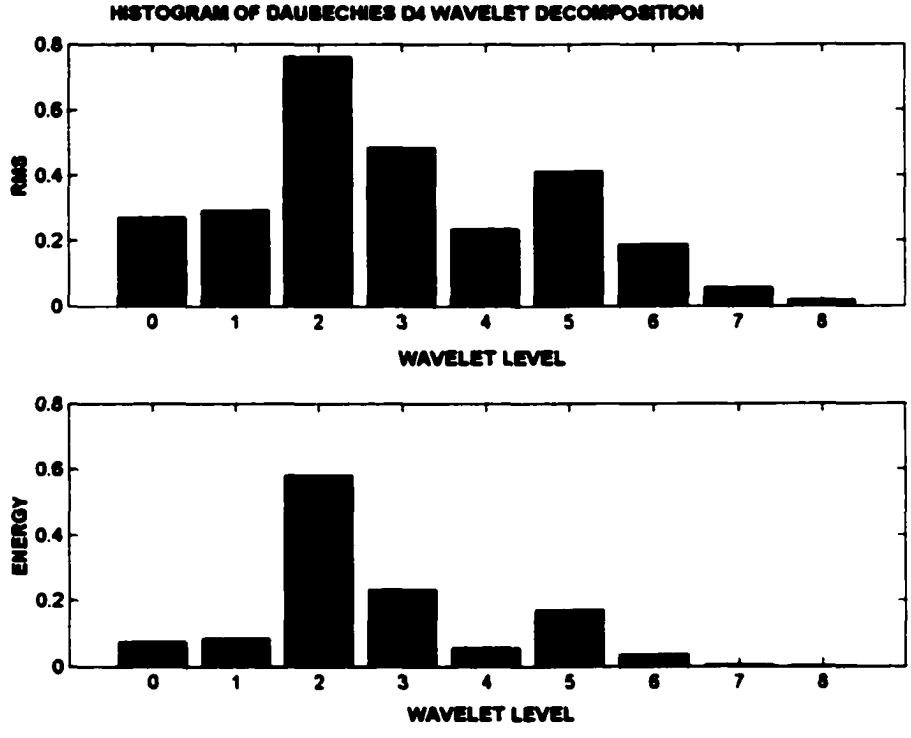

Figure 41: Histogram Of The Daubechies D4 Wavelet Decomposition Of The Simulated Signal.

For the ideal decomposition of our simulated signal, the energy should be concentrated only in the two wavelet levels – d7 (40 Hz to 80 Hz) and d4 (320 Hz to 640 Hz). However, for the Daubechies wavelet, we see the energy is still concentrated in levels 2 (d7) and 5 (d4), but there exists energies at other levels too. For Daubechies D4, the energy is also considerably high in level 3 (d6: 80 Hz to 160 Hz), while for both the Daubechies D4 and D20, it can be seen there is also more leakage into level 0 (a8: 0 Hz to

20 Hz), level 1 (d8: 20 Hz to 40 Hz), level 4 (d5: 160 Hz to 320 Hz) and level 6 (d2: 640 Hz to 1280 Hz). This leakage is significantly larger than that of the Daubechies D20 wavelet decomposition.

This analysis shows that even when the total energy is the same in both cases, the energy distribution varies within wavelet levels. This brings us to the next question, what are the frequency bandwidth characteristics of the wavelet levels. The above research was published in the paper authored by Dr. Cox and myself in the IEEE transactions of Power Systems [17].

Before we go on to the next chapter, let us study the energy distribution behavior for the wavelet decomposition of same signal using Symlets wavelet SYM20 and Coiflets wavelets COIF2 and COIF5. The procedure used above is repeated, and the rms values calculated. Only the final histogram plots of the rms and energy of the wavelet decompositions are plotted for clarity. The Symlets SYM4 wavelet with the exact same coefficients and magnitude phase response as Daubechies D4 has an energy distribution which matches to the D4 characteristics described earlier. Figure 42 shows the histogram of the energy distribution for SYM20 wavelet decomposition. It is appropriate to again mention that the Symlets and Coiflets wavelets are more symmetric than the Daubechies wavelets.

Seen from figure 42, the Symlets SYM20 when compared to its Daubechies counterpart D20, show a small increase in the rms and the energy for the levels other than the main frequency bands of 40 Hz to 80 Hz and 320 Hz to 640 Hz. The energy increase in some of the levels is significant. The rms value of the level 0 is 0.3027 for SYM20 but only 0.1981 for D20. This shows an increase of at least 50 % more in the SYM20 wavelet

decomposition in the 0 Hz to 20 Hz band. With the improvement in the symmetricity of the SYM20 wavelet coefficients, an increase in this level is usually not expected. Instead, we would have thought to see a decrease.

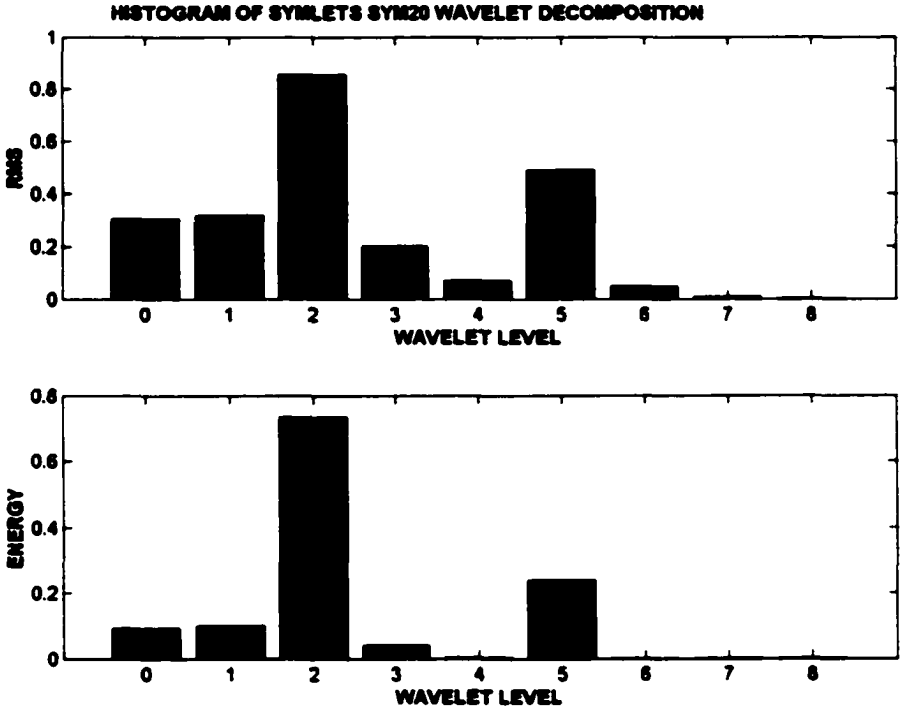

Figure 42: Histogram Of The Symlets SYM20 Wavelet Decomposition Of The Simulated Signal

Even though this increase is very small, it is clear that the energy distribution is affected by the difference in phase characteristics even though the magnitude characteristics were the same as discussed in chapter 3. The histogram plot of the wavelet decomposition of the simulated signal using Coiflets COIF2 is shown in figure 43.

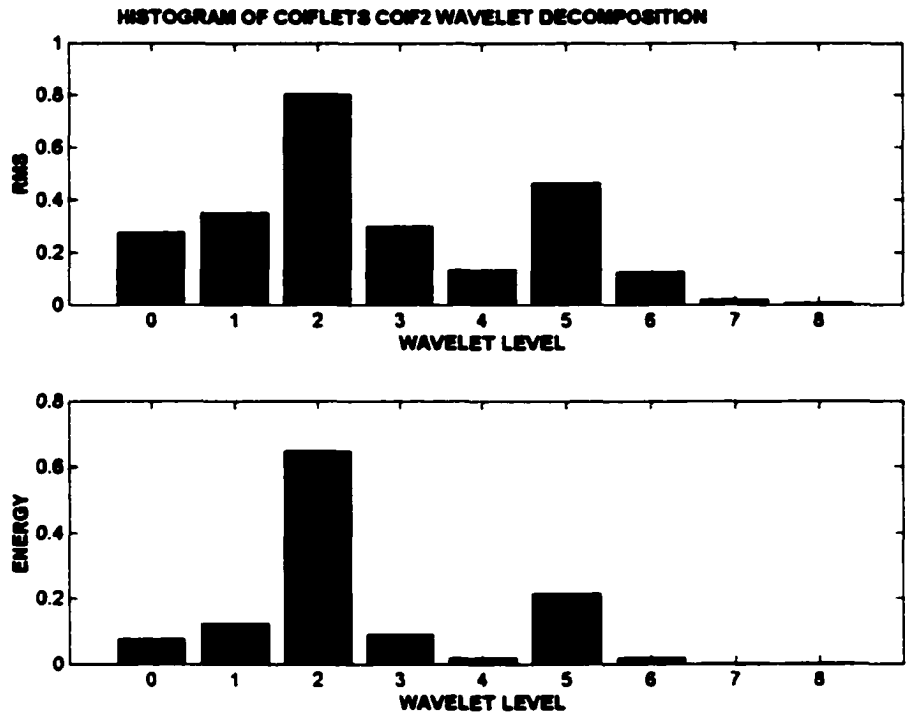

Figure 43: Histogram of the Coiflets COIF2 wavelet decomposition of the simulated signal.

The Coiflets COIF2 wavelet has only 12 coefficients compared to 20 coefficients for SYM20 or D20. As seen for Daubechies D4, the energy leakage is more for the COIF2 wavelet decomposition than the Daubechies 20 or SYM20, but it is still better than D4. The histogram plot of the wavelet decomposition using Coiflets COIF5 wavelet with 30 coefficients is shown in figure 44. The COIF5 wavelet exhibits exactly same magnitude characteristics as the D20 or SYM20 wavelets, but its phase characteristics are different for both low pass and high pass filters. Just looking at the histogram plots of the SYM20 and COIF5 wavelet decompositions, they seem to possess similar characteristics. It is interesting to compare them in detail and to see the change the in the energy distribution.

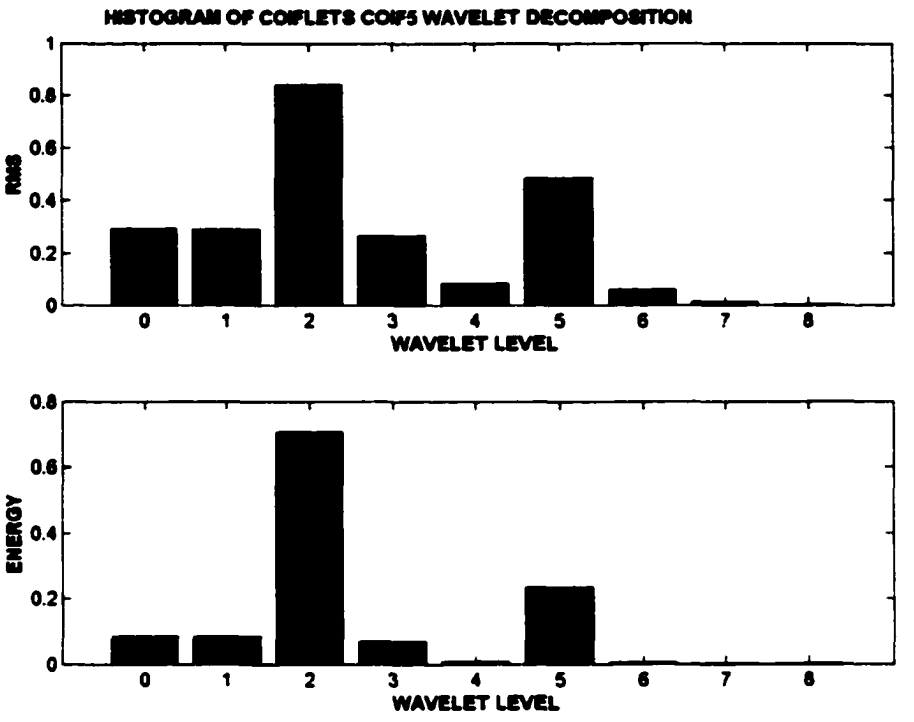

Figure 44: Histogram of the Symlets COIF5 wavelet decomposition of the simulated signal.

Even though the differences are not very large, for the COIF5 wavelet the energy level is less than the SYM20 wavelet for all levels below the 40 to 60 Hz band but the energy level is more than the SYM20 above this band with an exception of the second frequency band 320 Hz to 640 Hz. Looking back at the phase characteristics for the SYM20 and COIF5, the high pass decomposition phase plot shows the two wavelets have the same phase slope. For the low pass the slope of SYM20 is less than the slope of COIF5 and the difference is significant. This manifests itself in the energy distribution of the wavelet decomposition with SYM0 having higher energy leakage for the higher frequencies than the COIF5 wavelet decomposition.

Figure 45 shows the comparison of the rms value distributions of all the wavelet decompositions described above.

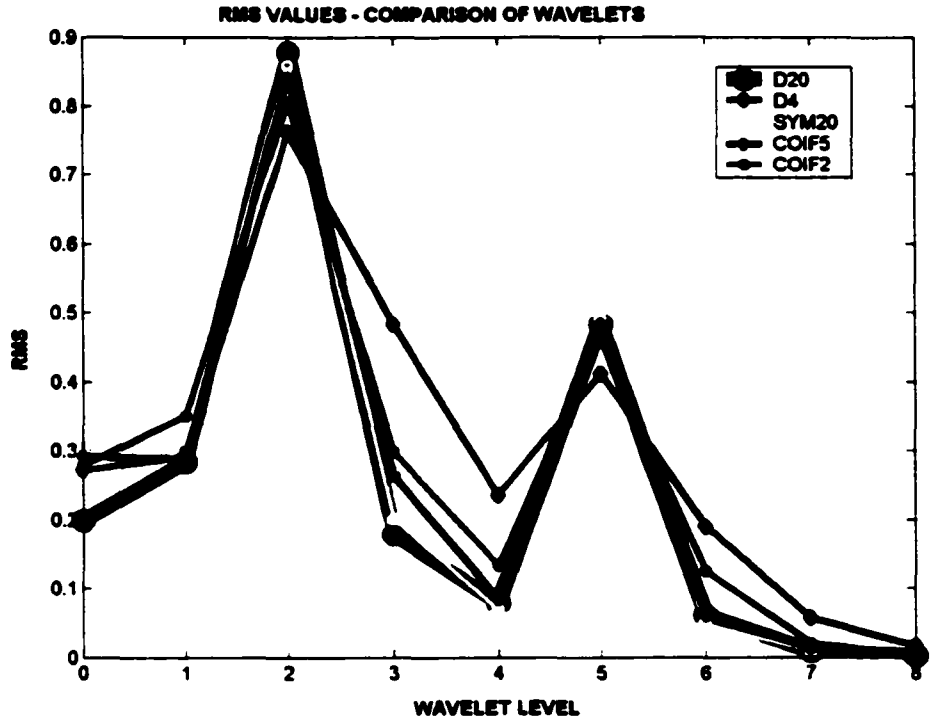

Figure 45: Comparison Of Energy Distributions Between Wavelet Decompositions

This shows the energy distributions are almost similar with minute differences for the Daubechies D20, Symlets SYM20 and Coiflets COIF5. Daubechies D4 is the worst with more energy in the adjacent bands. Also interestingly for the SYM20 and COIF5 wavelets, the lower level's energies are higher and some of them are comparable to the Daubechies D4.

To understand the distribution further, a signal with single frequency is wavelet transformed. The next few plots are the histograms of the rms values for decomposition of a simulated signal with single frequency 240 Hz which is in the middle of the nine frequency bands. Figure 46 shows the rms distribution histograms for the four wavelet decompositions D4, D20, SYM20 and COIF5.

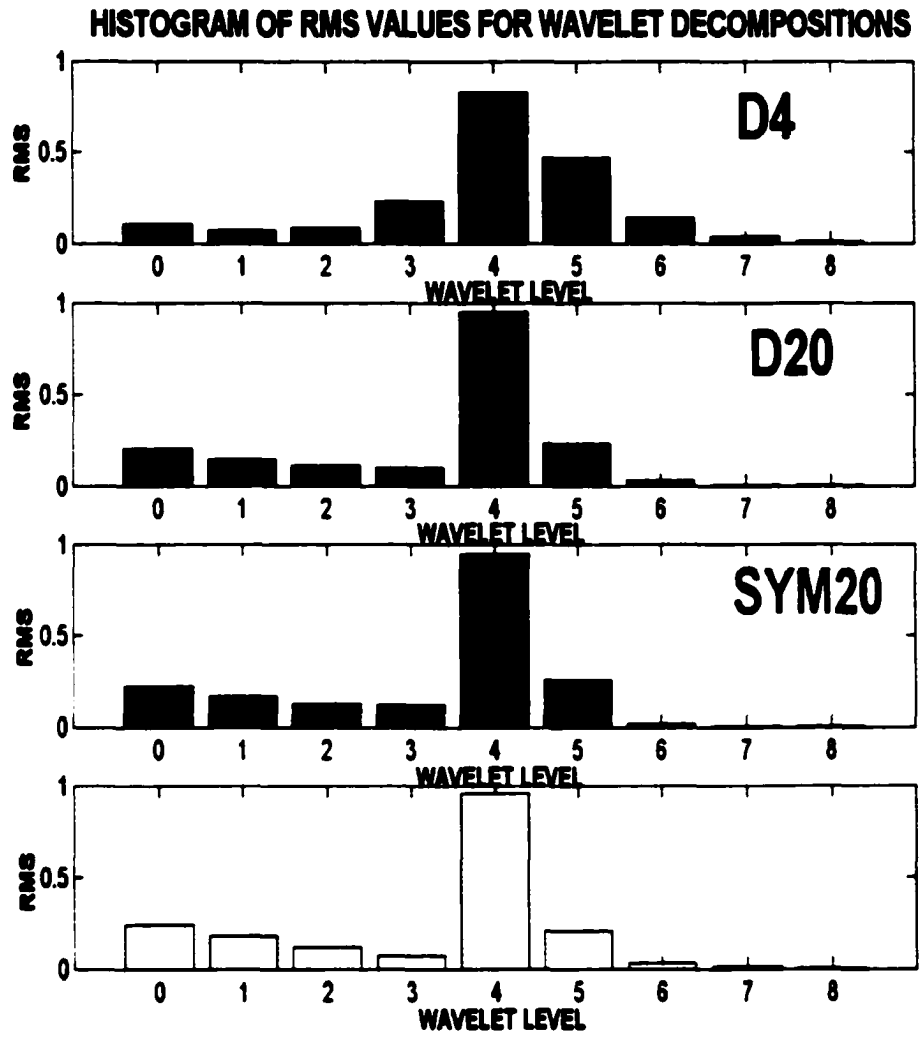

Figure 46: Histogram Of Rms Distributions For D4, D20, SYM20 And COIF5 Wavelets.

The above figures show that for wavelets with higher coefficients, the energy is concentrated in the frequency band 160 Hz to 320 Hz., i.e., it has slightly higher energy compared to D4. Away from this center frequency, the energy distribution is different for different wavelets. The comparisons of the above wavelet decomposition distributions for different wavelets can be clearly seen in the 3D histogram plots of figures 47 and 48. The

plots show the differences in height for the rms values of the different wavelet decompositions.

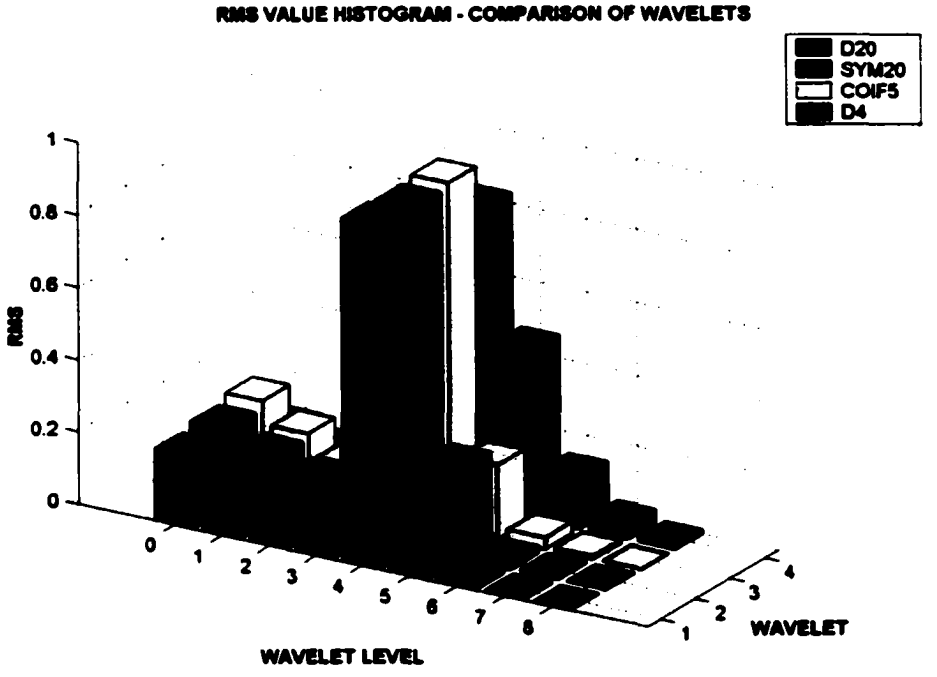

Figure 47: Comparison Of Wavelet Decompositions – Looking From The Right.

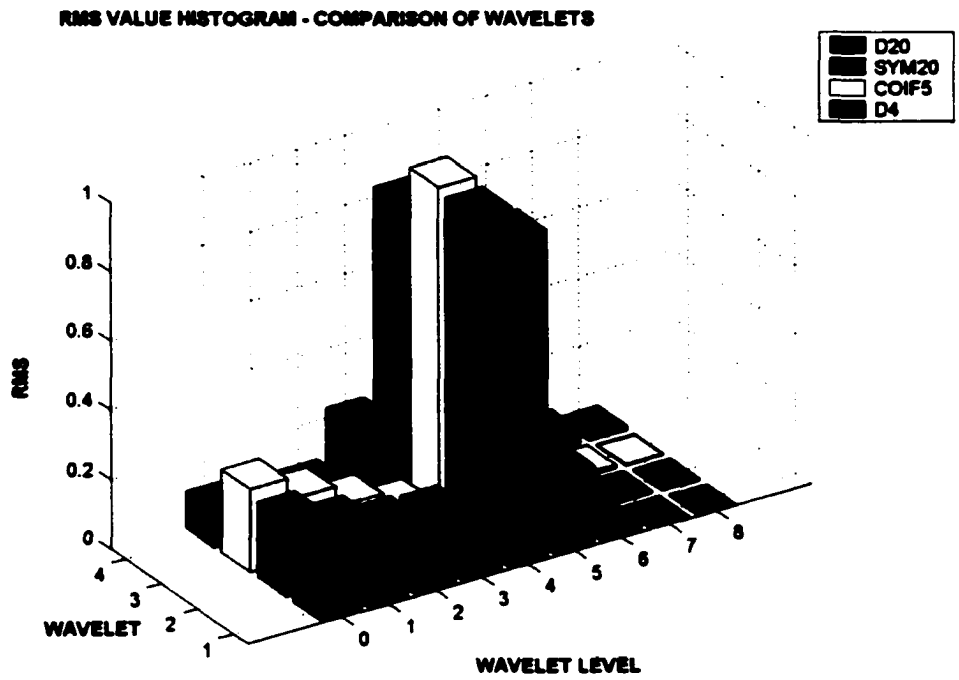

Figure 48: Comparison Of Wavelet Decompositions – Looking From The Left.

The study of frequency bandwidth characteristics in the next chapter might throw some light into the behavior of the wavelet decompositions and energy distributions.

CHAPTER 6

FREQUENCY BANDWIDTH CHARACTERISTICS

To find the frequency bandwidth characteristics of the wavelet decomposition, a sinusoidal signal is chosen and its frequency is swept between the minimum and maximum frequency of the chosen wavelet level. With the amplitude of the selected frequency component kept constant over the entire sweep range, the energy distributed in the wavelet level under consideration must remain constant with sharp edges. This is true in ideal conditions, but for the non-ideal filters used for wavelet decomposition, the energy distribution amplitude doesn't remain constant and at the edges rolls over to the next frequency level.

Let us select a sinusoidal signal of 512 data points which provides us with 9 wavelet levels as in the previous chapter. Selecting wavelet level 2 (d7: 40 Hz to 80 Hz) we can sweep the sinusoidal signal's frequency from 40 Hz to 80 Hz and calculate the rms value of the wavelet level at different frequency points along the sweep. This can be graphically represented as in figure 49.

The block diagram shows the input signal is applied at the left most filter bank and the multiresolution wavelet analysis continues using similar low pass and high pass filter banks. The output of the high pass filter is the details and the level 2 (d7) is shown where the output is measured. So, before the signal is measured at the output level 2 (d7), it passes through a few low pass filters and one high pass filter with down-sampling in between each filter.

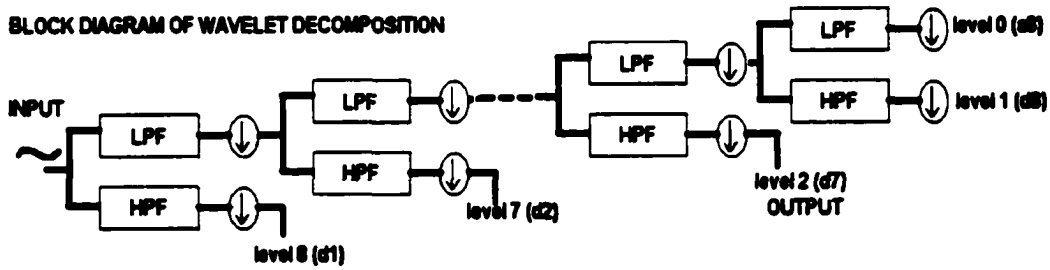

Figure 49: Block Diagram Of Wavelet Decomposition

Figure 50 shows the sinusoidal signal with 512 data points at frequency 60 Hz, the center frequency between the 40 Hz and 80 Hz. This sinusoidal signal's frequency is swept from 20 Hz to 100 Hz in steps, and then at each step it is decomposed into different levels by wavelet transform. The rms value of the wavelet decomposition level 2 is calculated for each step of the frequency sweep. The frequency characteristics are plotted with the rms value in dB on the y-axis and the frequency on the x-axis.

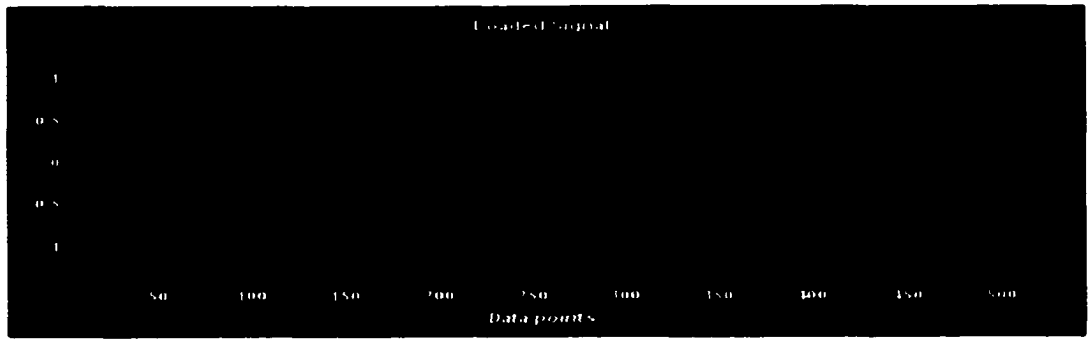

Figure 50: 60 Hz sinusoidal signal – 512 data points.

The above signal is decomposed using Daubechies wavelet D4 at each frequency step of the sweep range and at each step the rms value of detail level 2 is calculated. The results obtained are shown in table 6 along with the calculated dB values.

Table 6: Frequency Sweep And Its Corresponding Energy Amplitudes Both In Rms And In Decibel Values For The Wavelet Level D2 Of The Daubechies D4 Decomposition

Freq in Hz	RMS value	decibel value (dB)
20	0.2489	-26.7633
21	0.2609	-25.8221
22	0.2671	-25.3493
23	0.2709	-25.0644
24	0.2779	-24.5555
25	0.2939	-23.4407
26	0.3214	-21.6459
27	0.3583	-19.4763
28	0.3979	-17.3782
29	0.4324	-15.7179
30	0.4540	-14.7393
31	0.4570	-14.6103
32	0.4377	-15.4715
33	0.3966	-17.4463
34	0.3400	-20.5223
35	0.2866	-23.9441
36	0.2727	-24.9346
37	0.3276	-21.2649
38	0.4341	-15.6374
39	0.5605	-10.5261
40	0.6852	-6.5088
41	0.7941	-3.5593
42	0.8776	-1.5595
43	0.9298	-0.4028
44	0.9487	0
45	0.9364	-0.2624
46	0.8992	-1.0716
47	0.8484	-2.2355
48	0.7986	-3.4452
49	0.7654	-4.2948
50	0.7592	-4.4564
51	0.7799	-3.9182
52	0.8170	-2.9896
53	0.8558	-2.0616
54	0.8837	-1.4192
55	0.8933	-1.2044
56	0.8829	-1.4390
57	0.8567	-2.0403
58	0.8240	-2.8189
59	0.7967	-3.4926
60	0.7855	-3.7757
61	0.7948	-3.5414
62	0.8200	-2.9166
63	0.8504	-2.1894
64	0.8738	-1.6459
65	0.8811	-1.4788
66	0.8683	-1.7716
67	0.8375	-2.4952
68	0.7970	-3.4868
69	0.7606	-4.4218
70	0.7437	-4.8708
71	0.7561	-4.5386
72	0.7957	-3.5176
73	0.8493	-2.2153
74	0.8994	-1.0676
75	0.9307	-0.3845
76	0.9319	-0.3587
77	0.8969	-1.1236
78	0.8246	-2.8044
79	0.7186	-5.5576
80	0.5871	-9.5972
81	0.4448	-15.1489
82	0.3180	-21.8644
83	0.2572	-26.1025
84	0.2984	-23.1321
85	0.3902	-17.7685
86	0.4805	-13.6079
87	0.5476	-10.9917
88	0.5842	-9.6967
89	0.5900	-9.4985
90	0.5698	-10.1972
91	0.5324	-11.5540
92	0.4903	-13.2042
93	0.4568	-14.6163
94	0.4422	-15.2676
95	0.4473	-15.0380
96	0.4638	-14.3151
97	0.4798	-13.6351
98	0.4859	-13.3815
99	0.4772	-13.7455
100	0.4533	-14.7734

Figure 51 shows the plot of frequency bandwidth characteristics. The plot of the frequency bandwidth characteristics in dB for level 2 (40 Hz to 80 Hz) of the Daubechies D4 shows a clear good roll off at both the end frequencies 40 Hz and 80 Hz. The two vertical lines indicate the boundary for the wavelet level d2.

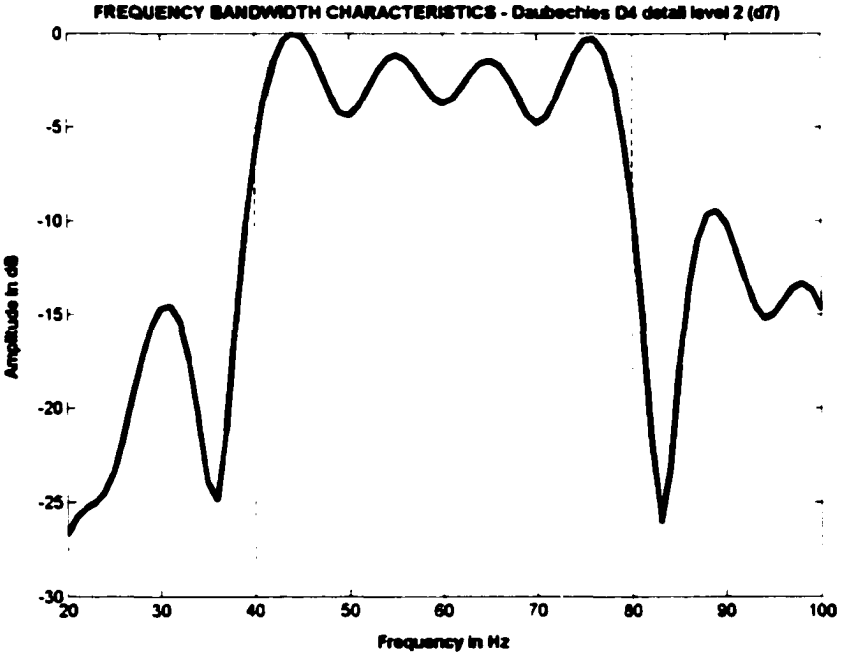

Figure 51: Frequency Bandwidth Characteristics For Daubechies D4 - Wavelet Level d2.

The passband for D4 is not flat but has significant ripple as seen in the plot. This ripple has an average variation of more than 3 dB, as opposed to the flat magnitude characteristics of the individual low pass and high pass filter seen earlier. The first side lobes that are on either side in the stop bands are significantly high, especially the one towards the higher frequency. Table 7 shows the frequency bandwidth values for the Daubechies D20 for the same wavelet level.

Table 7: Frequency Sweep And Its Corresponding Energy Amplitudes Both In Rms And In Decibel Values For The Wavelet Level D2 Of The Daubechies D20 Decomposition.

Freq in Hz	RMS value	decibel value (dB)
20	0.0659	-52.4409
21	0.0630	-53.3332
22	0.0594	-54.5011
23	0.0638	-53.0709
24	0.0833	-47.7443
25	0.1152	-41.2637
26	0.1529	-35.5995
27	0.1904	-31.2079
28	0.2225	-28.0998
29	0.2441	-26.2465
30	0.2510	-25.6867
31	0.2400	-26.5807
32	0.2095	-29.2953
33	0.1610	-34.5610
34	0.1056	-43.0023
35	0.0964	-44.8221
36	0.1739	-33.0292
37	0.2851	-23.1365
38	0.4061	-16.0642
39	0.5263	-10.8758
40	0.6382	-7.0202
41	0.7354	-4.1856
42	0.8129	-2.1814
43	0.8676	-0.8795
44	0.8984	-0.1819
45	0.9066	0
46	0.8959	-0.2373
47	0.8722	-0.7745
48	0.8428	-1.4600
49	0.8156	-2.1164
50	0.7971	-2.5754
51	0.7908	-2.7333
52	0.7965	-2.5909
53	0.8106	-2.2385
54	0.8286	-1.7990
55	0.8464	-1.3747
56	0.8614	-1.0235
57	0.8728	-0.7604
58	0.8810	-0.5736
59	0.8867	-0.4437
60	0.8904	-0.3605
61	0.8917	-0.3309
62	0.8897	-0.3763
63	0.8834	-0.5197
64	0.8725	-0.7683
65	0.8582	-1.0967
66	0.8438	-1.4370
67	0.8333	-1.6864
68	0.8311	-1.7391
69	0.8395	-1.5395
70	0.8571	-1.1243
71	0.8789	-0.6204
72	0.8975	-0.2019
73	0.9046	-0.0453
74	0.8927	-0.3085
75	0.8567	-1.1328
76	0.7937	-2.6609
77	0.7038	-5.0651
78	0.5900	-8.5931
79	0.4582	-13.6499
80	0.3182	-20.9391
81	0.1908	-31.1704
82	0.1422	-37.0470
83	0.2179	-28.5142
84	0.3233	-20.6237
85	0.4161	-15.5778
86	0.4849	-12.5148
87	0.5262	-10.8807
88	0.5401	-10.3607
89	0.5296	-10.7522
90	0.5004	-11.8857
91	0.4602	-13.5594
92	0.4182	-15.4772
93	0.3831	-17.2284
94	0.3612	-18.4082
95	0.3528	-18.8767
96	0.3529	-18.8686
97	0.3543	-18.7896
98	0.3511	-18.9724
99	0.3403	-19.5953
100	0.3222	-20.6934

The frequency bandwidth characteristics for the same wavelet level using Daubechies D20 decomposition is plotted in figure 52.

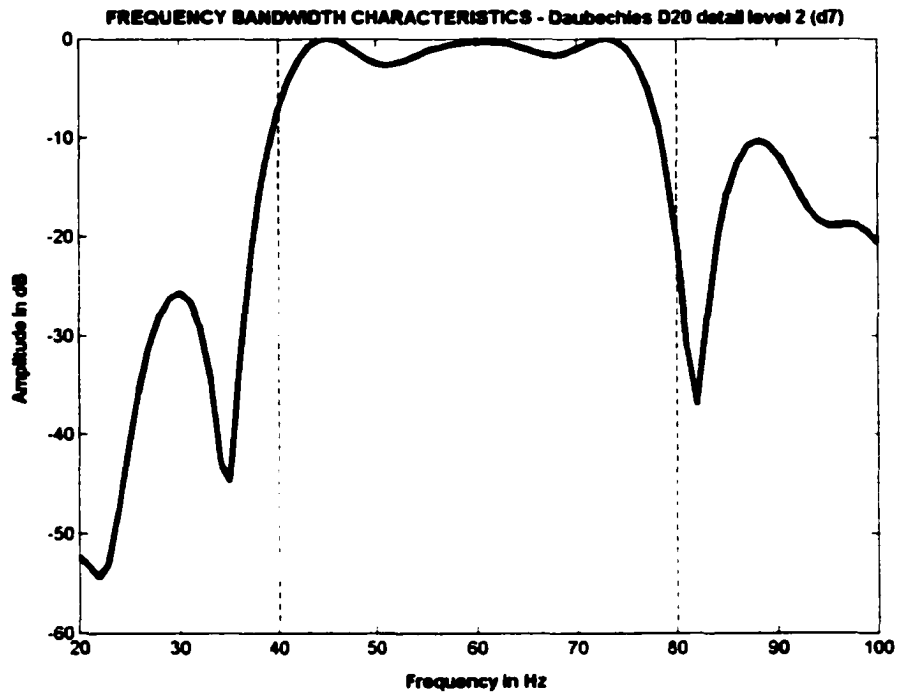

Figure 52: Frequency Bandwidth Characteristics For Daubechies D20 – Wavelet Level D2.

Daubechies D20 wavelet decomposition is more flat in the passband compared to the Daubechies D4 decomposition. The lower frequency side lobe is better in the D20 compared to the D4, but the higher frequency side lobe has the same magnitude. This shows Daubechies D20 with higher number of coefficients is a better wavelet for quantifying the signal frequencies in the passband. We can make the filter's transition region more narrow using additional h(k) filter coefficients, but we cannot eliminate the passband ripple [33]. This ripple known as Gibbs' phenomenon, is due to the instantaneous discontinuities demanded by the wavelet decomposition at the edges and no matter how wide we make this window, we will always have ripples. Hence, both

Daubechies D4 and dD20 have a poor rollover and adjacent frequency rejections but the transition region for the D20 with 20 coefficients is slightly better by an Hz compared to the D4 with 4 coefficients. The next two figures show the energy of the next wavelet level – level 3 (d6) for the same frequency sweep of 20 Hz to 100 Hz. These two figures show how the energy shows up in the next level for the signal that has frequencies pertaining to the previous level. Figure 53 is the frequency bandwidth characteristics of the wavelet level 3 (d6) for the Daubechies D4 wavelet decomposition of the signal whose frequency is swept between 20 Hz to 100 Hz.

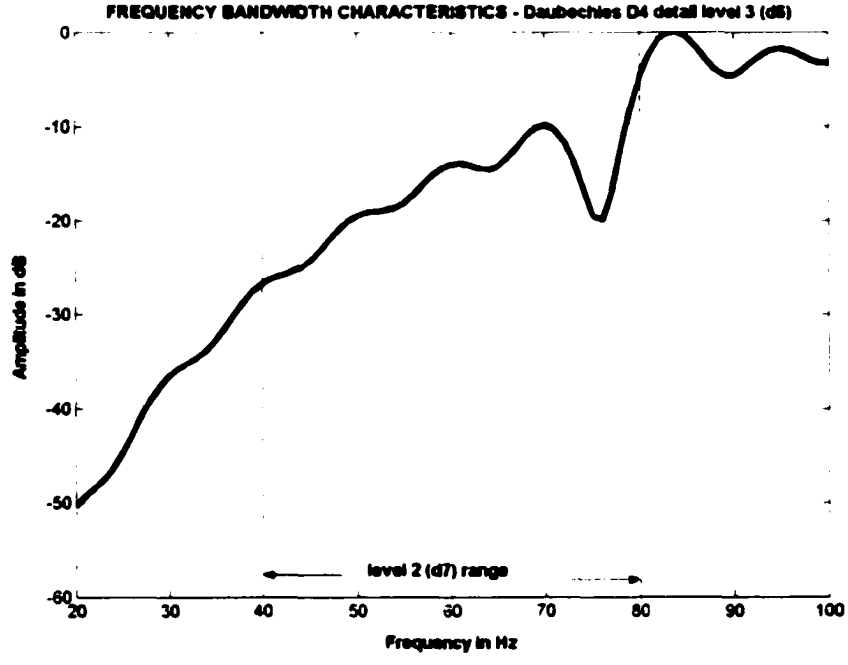

Figure 53: Frequency Bandwidth Characteristics Of Wavelet Level 3 (D6) For Daubechies D4 Wavelet Decomposition – Frequency Sweep 20 Hz To 100 Hz.

It can be seen that the signal with a frequency very close to the end regions but lying in the next frequency band or level will show up with a considerable amplitude in the current frequency band under consideration. Say for example, as seen in figure 53 and 54, a signal with frequency 90 Hz shows up with an amplitude of approximately negative

10 dB in the detail level 2 (d7). The same holds for a signal with frequency of 70 Hz which not only shows up in the level 2 (d7) but also has significant negative 15 dB amplitude in the next level 3 (d6).

Figure 55 and figure 56 show the lower frequency level 1 (d8)'s bandwidth characteristics for the same frequency sweep of 20 Hz to 100 Hz for the D4 and D20.

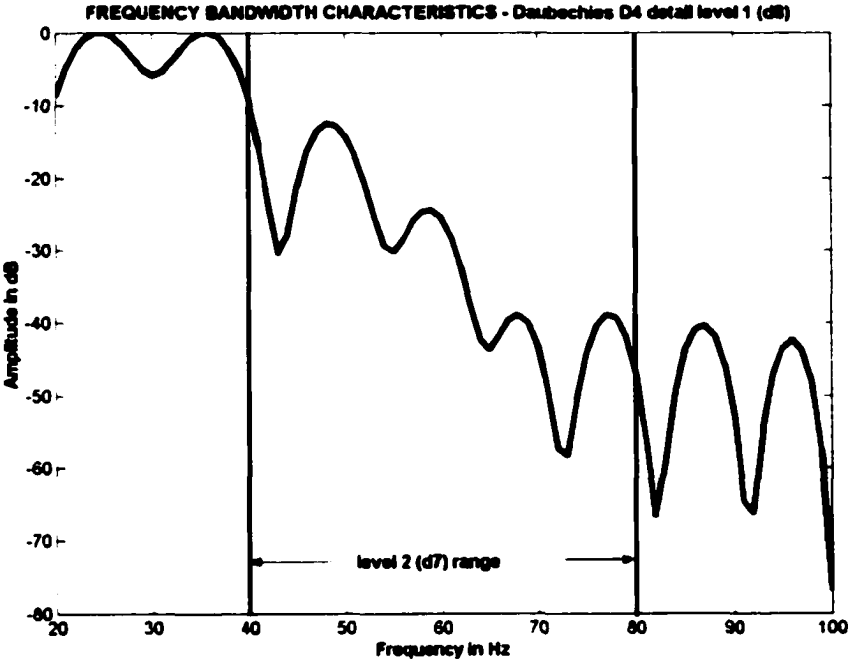

Figure 54: Frequency Bandwidth Characteristics Of Wavelet Level 1 (D8) For Daubechies D4 Wavelet Decomposition – Frequency Sweep 20 Hz To 100 Hz.

D20 characteristics in figure 56 show a sharper cut off at the higher frequency 40 Hz of wavelet level 1. However, the side lobes for both D4 and D20 are at the same slope unlike the characteristics we saw for wavelet level 3.

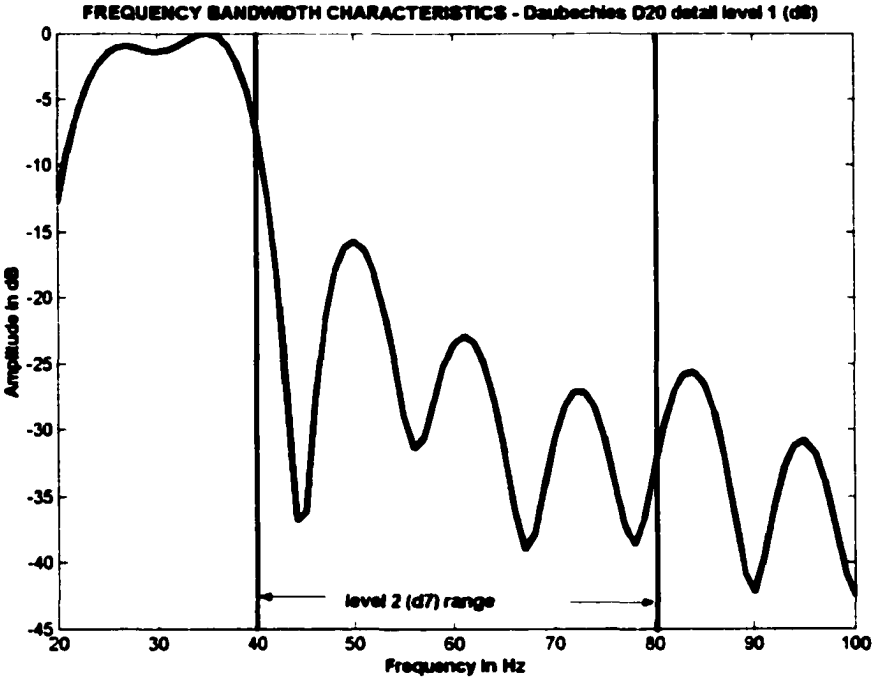

Figure 55: Frequency Bandwidth Characteristics Of Wavelet Level 1 (D8) For Daubechies D4 Wavelet Decomposition – Frequency Sweep 20 Hz To 100 Hz.

The above frequency band characteristics are repeated for the next level with the frequency swept from 80 Hz to 160 Hz. The results of this experiment are presented in the next six figures.

Figure 57 and figure 58 show the frequency wavelet characteristics for the wavelet level d3 for the D4 and D20 respectively for the frequency sweep from 60 to 180 Hz. Figures 59 and 60 show the corresponding frequency bandwidth characteristics for the wavelet decomposition level 2 (d7).

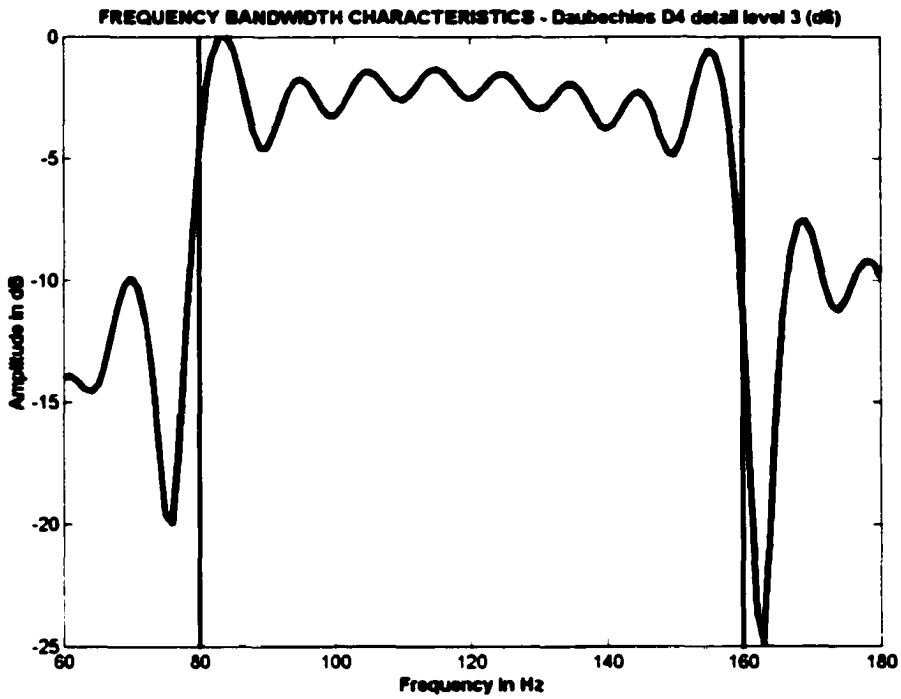

Figure 56: Frequency Bandwidth Characteristics For Daubechies D4 – Wavelet Level D3.

Figure 56 again confirms D20 has more flat passband characteristics with lesser amplitude ripples than D4. Also seen is an increase in amplitude in the regions near the edges due to the characteristics of the filters which is more prominent in the D4 decomposition.

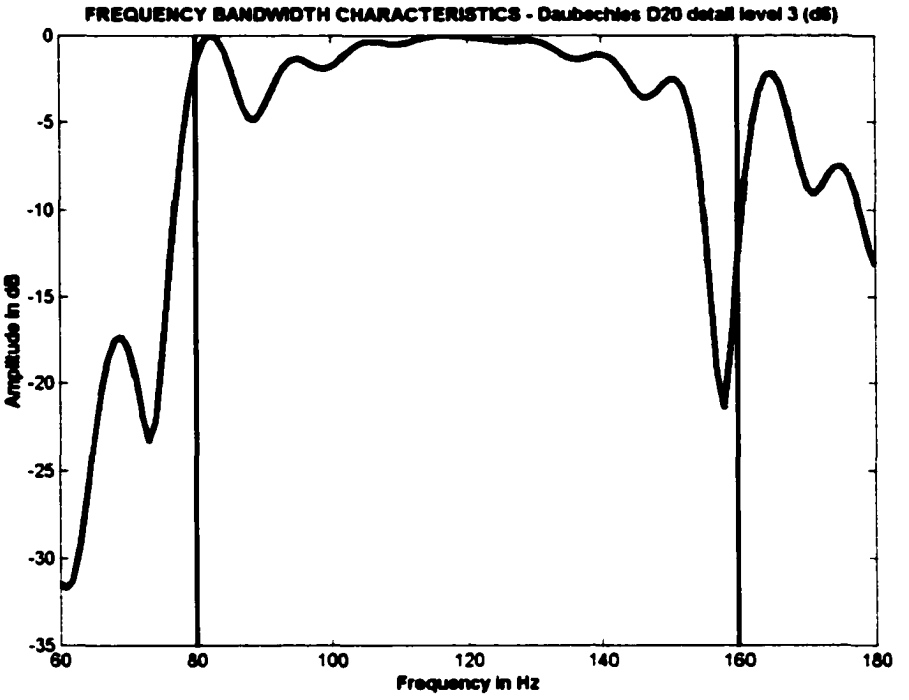

Figure 57: Frequency Bandwidth Characteristics For Daubechies D20 – Wavelet Level D3.

The figure 59 and 60 show the higher frequency energies that present in the current band are almost similar for both the Daubechies D4 and D20 wavelet decomposition. This higher frequency component in the current band is due to the non-ideal characteristics of the low pass filter. An ideal low pass filter would have cut off any frequencies above 80 Hz for this wavelet level 2 (d7). This type of behavior may be attributed to the presence of vanishing moments only for the high pass wavelet function and not for the low pass filter scaling function as seen earlier. There is only one high pass wavelet function filter in the decomposition of each wavelet level but more number of low pass filters in the chain. This high pass filter with a greater number of coefficients for D20 has more vanishing moments which are responsible for the better slope in the lower frequency end as seen in figure 54.

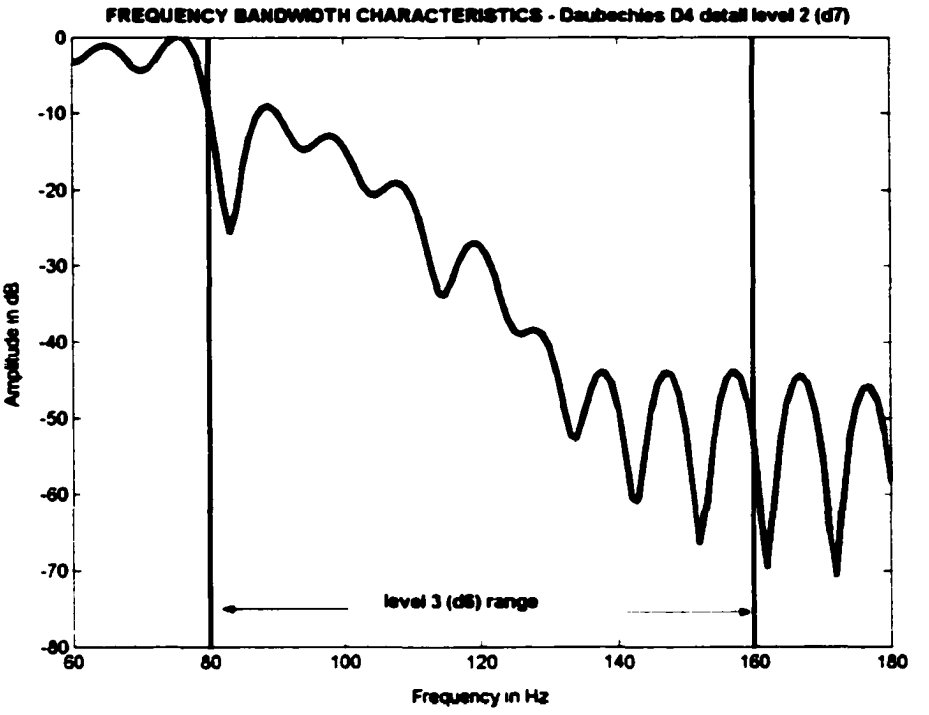

Figure 58: Frequency Bandwidth Characteristics Of Wavelet Level 2 (D7) For Daubechies D4 Wavelet Decomposition – Frequency Sweep 60 Hz To 180 Hz.

On the other hand, the low pass filters of both the Daubechies D4 and D20 behave similarly as seen in figures 59 and 60 without any vanishing moments for the Daubechies scaling functions. The low pass filter also known as the "*averaging filter*" averages the frequency components of the signal and finally displays this low frequency average at the approximation level. Figure 60 shows the ripple in the stop band for Daubechies D20 is better than for the D4 decomposition in figure 59.

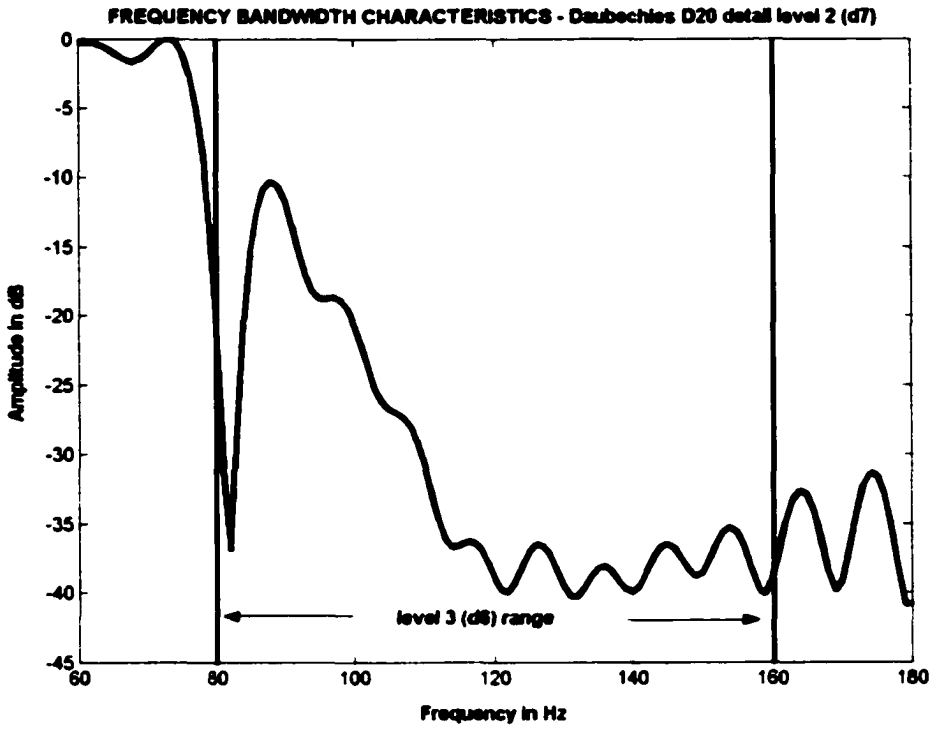

Figure 59: Frequency Bandwidth Characteristics Of Wavelet Level 2 (D7) For Daubechies D20 Wavelet Decomposition – Frequency Sweep 60 Hz To 180 Hz.

Figures 61 and 62 show the frequency bandwidth characteristics for the higher frequency wavelet level 4 (d5: 160 Hz to 320 Hz) for a frequency sweep of the signal in the range 80 Hz to 160 Hz. These figures show the response for the high pass filter for the next band which has a cut-off frequency at 160 Hz. The slope of D20 wavelet in figure 62 is better than the D4 of figure 61, for frequencies below the high frequency cut-off of the wavelet level 4.

The above study shows the that D20 is a better wavelet in terms of the passband flatness, and it also has a good high pass filter characteristics that has low energy leakage to the next lower frequency level.

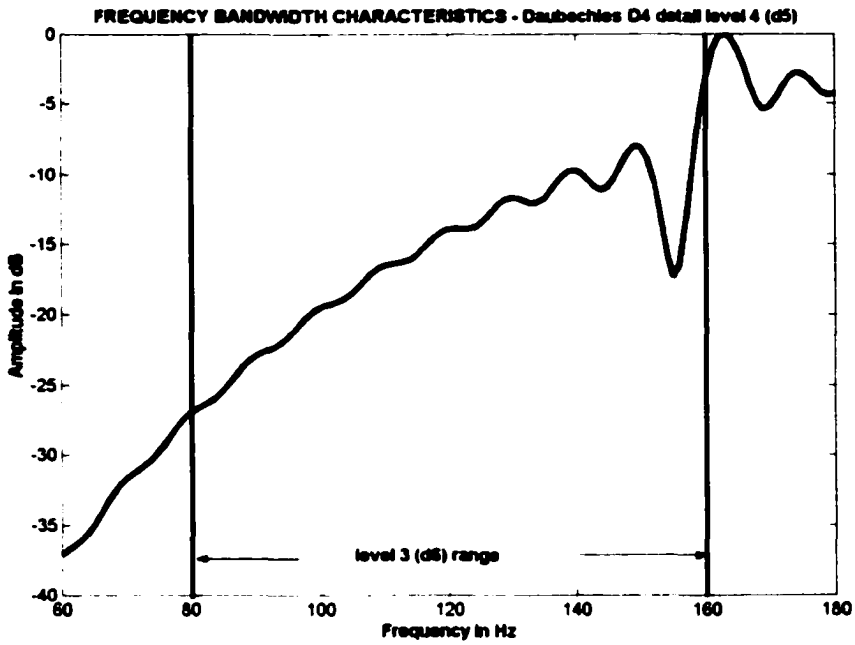

Figure 60: Frequency bandwidth characteristics of wavelet level 4 (d5) for Daubechies D4 wavelet decomposition – Frequency sweep 20 Hz to 100 Hz.

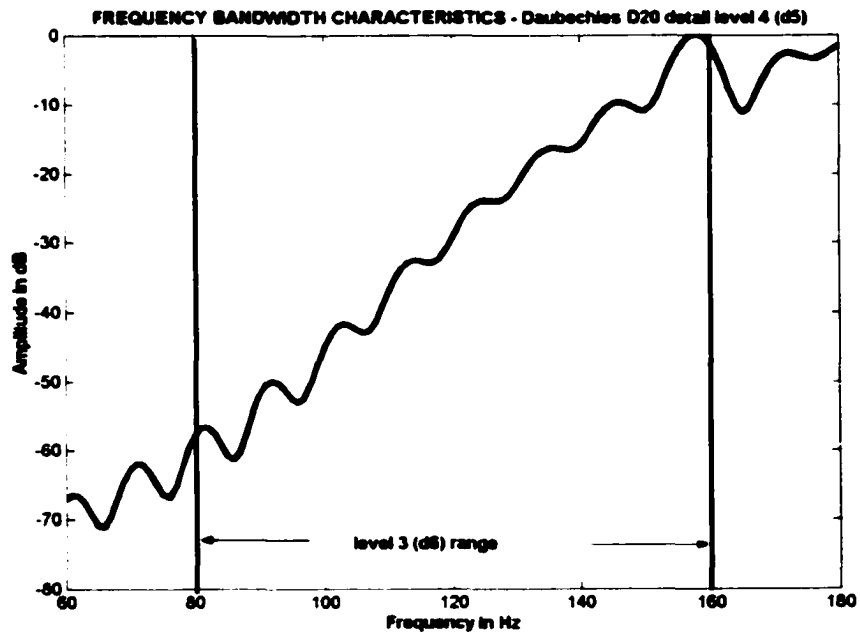

Figure 61: Frequency bandwidth characteristics of wavelet level 4 (d5) for Daubechies D20 wavelet decomposition – Frequency sweep 20 Hz to 100 Hz.

The frequency bandwidth characteristics are further studied for the Symlets and Coiflets wavelets for comparison. Figures 63 through 65 show the Symlets wavelet SYM20 wavelet decomposition of the signal whose frequency sweep range is between 20 Hz to 100 Hz.

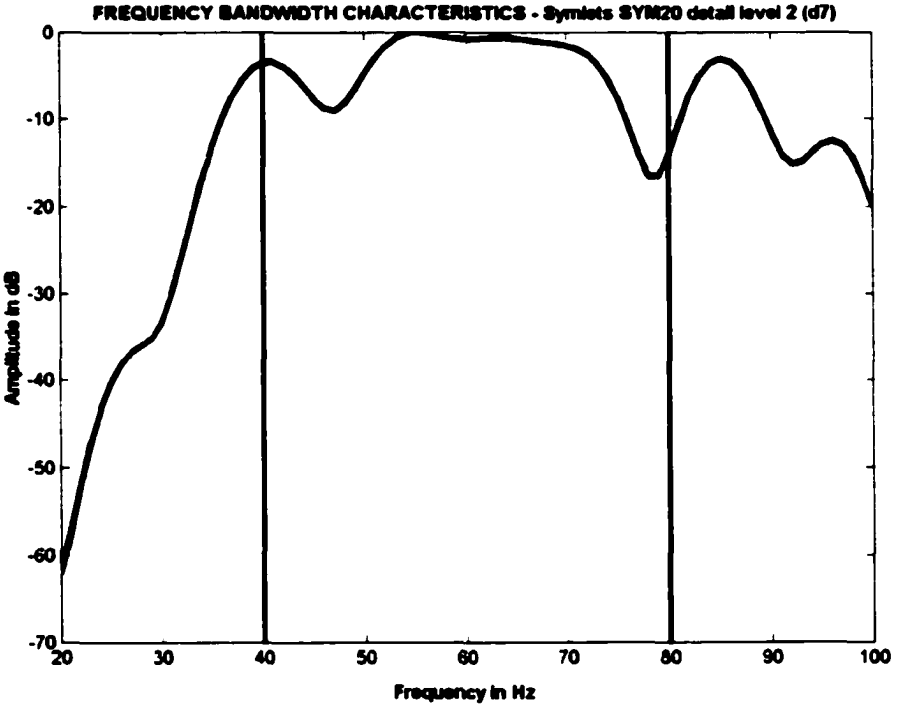

Figure 62: Frequency bandwidth characteristics of wavelet level 2 (d7) for Symlets SYM20 wavelet decomposition – Frequency sweep 20 Hz to 100 Hz.

Symlets wavelets have more symmetric coefficients than Daubechies wavelets which manifest in the good flatness with minimum ripple at a very narrow set of frequencies near the center of the wavelet level. But this symmetry of the Symlets coefficients affects the transition region near the ends by not having sharper cut-offs.

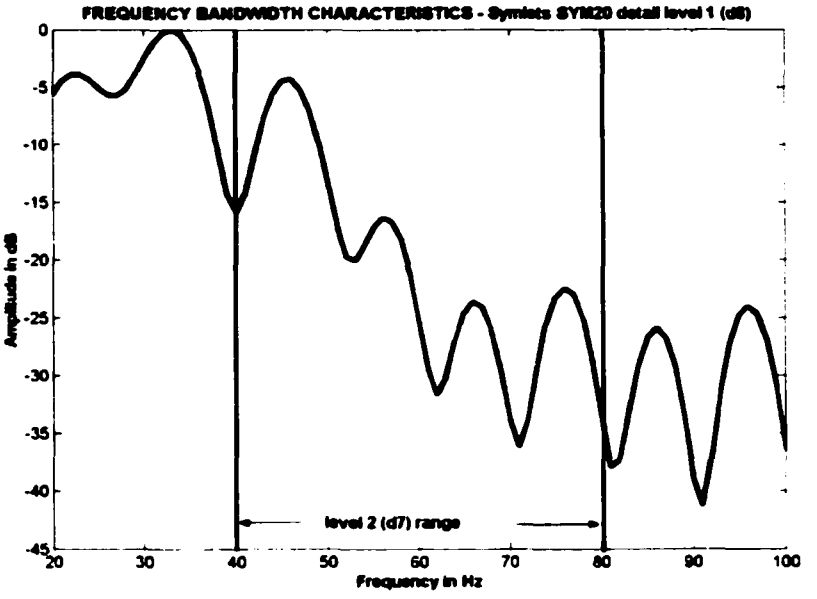

Figure 63: Frequency Bandwidth Characteristics Of Wavelet Level 1 (D8) For Symlets SYM20 Wavelet Decomposition – Frequency Sweep 20 Hz To 100 Hz.

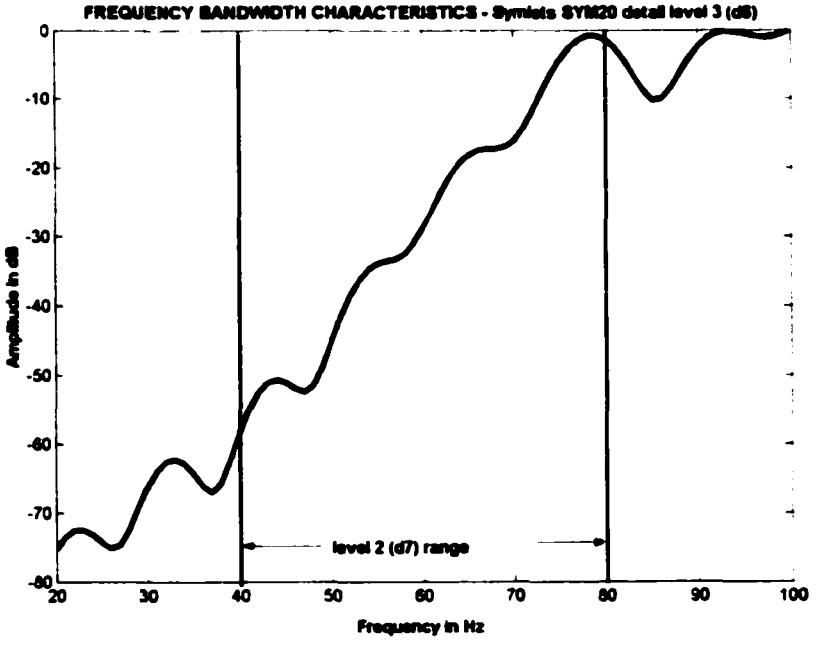

Figure 64: Frequency Bandwidth Characteristics Of Wavelet Level 3 (D6) For Symlets SYM20 Wavelet Decomposition – Frequency Sweep 20 Hz To 100 Hz.

Similarly for COIF5, the frequency bandwidth characteristics are plotted in figures 66 through 68.

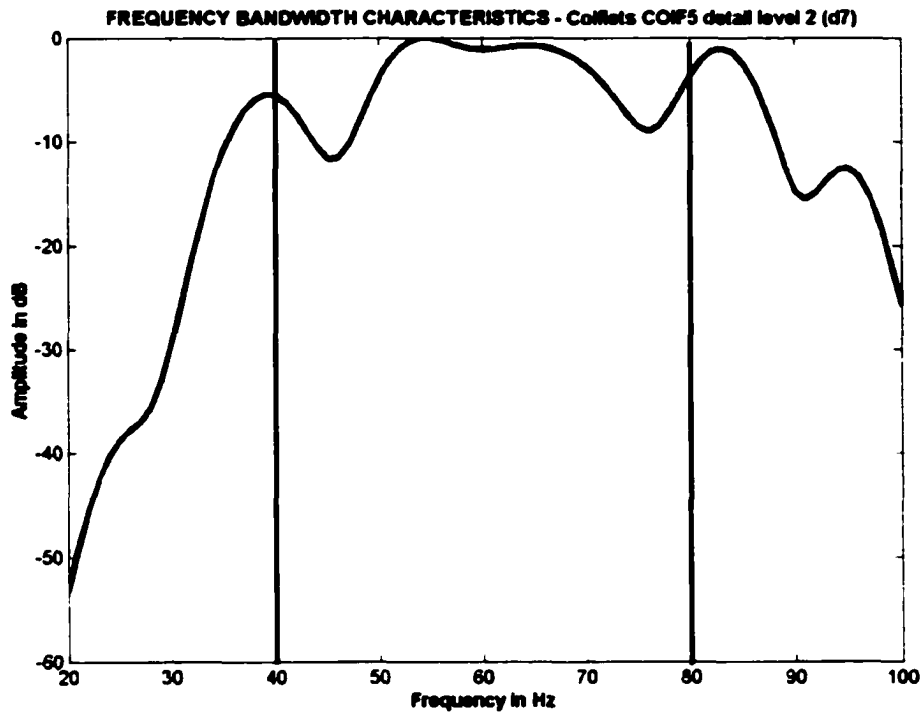

Figure 65: Frequency Bandwidth Characteristics Of Wavelet Level 2 (D7) For Coiflets Wavelet Decomposition – Frequency Sweep 20 Hz To 100 Hz.

Coiflets also have symmetric coefficients and display similar frequency bandwidth characteristics as Symlets wavelets. The end regions near the transition band are worse as in the Symlets characteristics with significant ripple. Figure 67 and 68 of the Coiflets show comparable characteristics with figures 64 and 65 of the Symlets.

Both Symlets and Coiflets have similar flat amplitude characteristics in the middle of the wavelet band which make them suitable for analyzing a signal with frequencies in the center of the band.

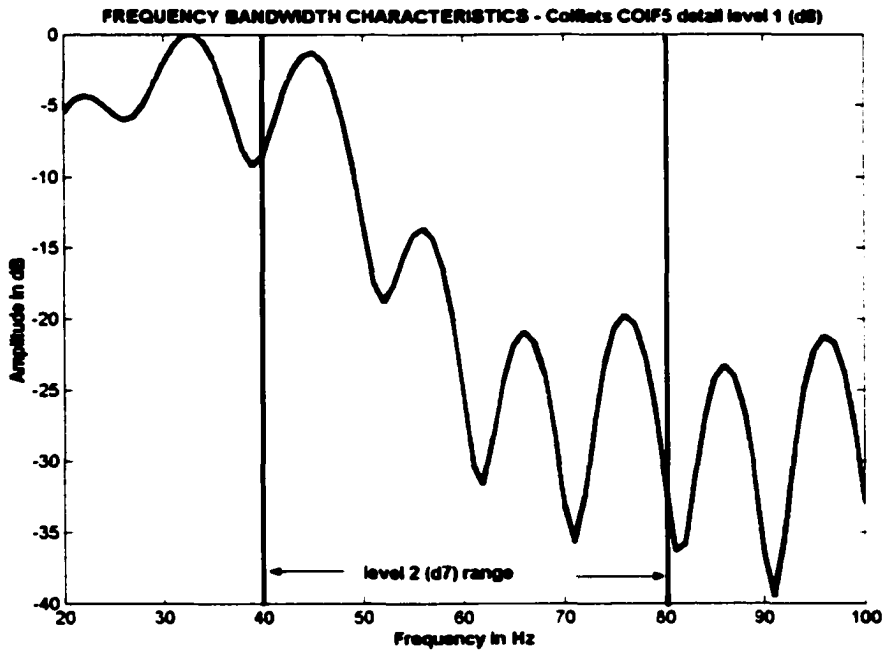

Figure 66: Frequency Bandwidth Characteristics Of Wavelet Level 1 (D8) For Coiflets COIF5 Wavelet Decomposition – Frequency Sweep 20 Hz To 100 Hz.

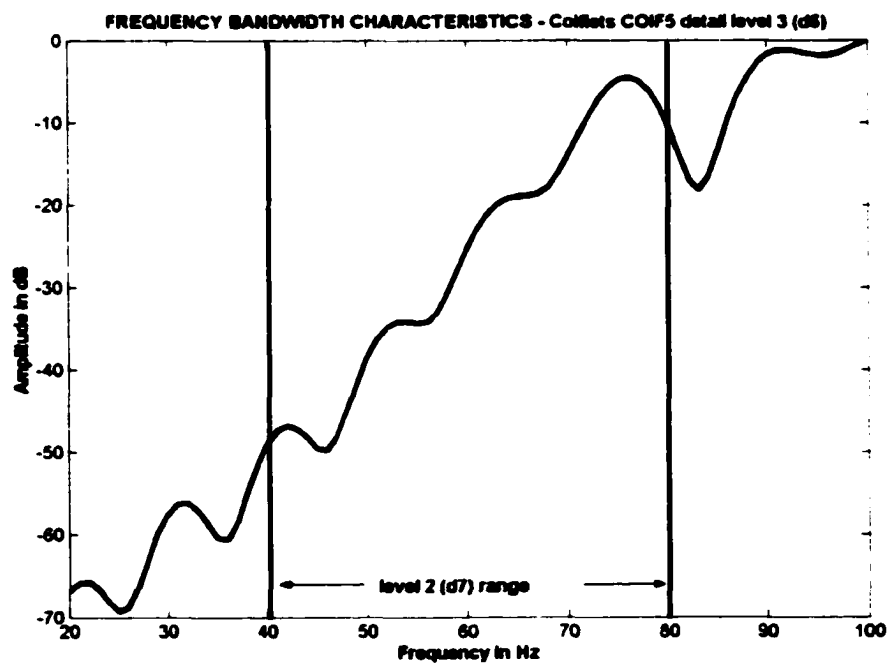

Figure 67: Frequency Bandwidth Characteristics Of Wavelet Level 3 (D6) For Coiflets COIF5 Wavelet Decomposition – Frequency Sweep 20 Hz To 100 Hz.

In conclusion, the above frequency bandwidth characteristics show wavelets do not exhibit the ideal non-overlapping bandwidths but have a small rollover to the next band. For the Daubechies D4 wavelet, the bandwidth characteristics are poorer, and hence a lot of leakage can be seen between the bands. The characteristics of Daubechies D20 wavelet is better than D4 and also has sharper cut off with narrower transition regions. D20 still has ripples in both the pass band and the stop band due to the sharp discontinuities of the rectangular window of the wavelet levels. Symlets and Coiflets have maximum flatness for a set of few frequencies near the middle of the wavelet level. However, the end transition region is very poor with wider transition regions, even when compared with the Daubechies wavelets.

These results indicate that a careful selection of the number of data points and the sampling frequency have to be made to avoid the frequency of interest from falling on the edges of the band. It is better for the frequency to be at the center of the band to avoid loss of information.

For example, consider the same simulated signal of chapter 5 with the fundamental frequency of 60 Hz and the seventh harmonic 420 Hz having 512 data points. If the fundamental frequency of interest is 60 Hz and the sampling frequency is 1024 Hz, then for the $N = 512$ we have 9 levels of wavelet decomposition. Table 8 shows the frequency bands for the different levels of the wavelet decomposition. Similarly, the frequency bands of the wavelet levels for the sampling frequency 10240 Hz is also shown in table 8. For the 1024 Hz sampling frequency, the d4 wavelet level has a frequency range from 32 Hz to 64 Hz as seen in the center column of the table 8.

Table 8: Wavelet Decomposition Frequency Bands.

Wavelet level	Frequency bands for sampling frequency 1024 Hz	Frequency bands for sampling frequency 10240 Hz
d1	512 Hz to 256 Hz	5120 Hz to 2560 Hz
d2	256 Hz to 128 Hz	2560 Hz to 1280 Hz
d3	128 Hz to 64 Hz	1280 Hz to 640 Hz
d4	64 Hz to 32 Hz	640 Hz to 320 Hz
d5	32 Hz to 16 Hz	160 Hz to 80 Hz
d6	16 Hz to 8 Hz	80 Hz to 40 Hz
d7	8 Hz to 4 Hz	40 Hz to 20 Hz
d8	4 Hz to 2 Hz	20 Hz to 10 Hz
a8	DC to 2 Hz	DC to 10 Hz

But for the 10240 Hz sampling frequency, 60 Hz lies in the d6 wavelet level which has a frequency range of 40 Hz to 80 Hz. The frequency of interest 60 Hz is very close to the 64 Hz edge of the wavelet level frequency band for the 1024 Hz sampling frequency case while for the 10240 Hz sampling frequency case, it is at the center of the 40 Hz to 80 Hz band. Hence, from the above research, we know the measurements made may not be accurate using the former sampling frequency due to the frequency characteristics of the wavelet. Since the number of wavelet levels and their frequency band ranges are dependent on the two parameters (number of data points and the sampling frequency), the selection of these is critical in qualitative and quantitative analysis of signals. If the frequency of interest, 60 Hz in this case, lies at the center of the bandwidth, the amplitude

is maximum at the center as seen in the frequency characteristic plots, and hence the accuracy is improved.

For some applications, the sampling frequency is decided by the hardware, i.e., the A/D converter or by the frequency of interest. If the frequency we are interested in a signal is 1000 Hz, then the minimum sampling frequency given by the Nyquist frequency is 2 KHz. So, we are left to carefully select the number of data points N considering the component of the signal we are interested in analyzing.

A similar argument holds good for the selection of sampling frequency when the number of data points are fixed due to the time period of the events in the signal. In this case, the sampling frequency is carefully chosen to obtain the right frequency ranges for the wavelet levels.

CHAPTER 7

WAVELET SEISMIC EVENT DETECTION

Seismic data is being collected all around the world to study the behavior of the earth and to better understand the natural events that occur frequently. The data monitored these days, thanks to technology, is collected in large volumes and stored digitally on computers. These current advances in technology have made it impractical to parse through this data manually and analyze them effectively in a cost-worthy and timely manner by human analysts. Automation of analyzing these large volumes of data and detection of important and critical events is very important. Research in this field of automatic seismic event identification and detection is of greatest interest in the seismic community.

Several automatic seismic event detection methods have been proposed based on various methods of analysis and events of interest that need to be identified and detected. Some of these methods have made a profound impact among analysts and are being used for routine monitoring.

Some of the automatic seismic event detection techniques that have been proposed are based on an off-line analysis method. The STA/LTA (Short Time Average/Long Time Average) phase picker method [34, 35] is one of the commonly used methods for marking the occurrence of a seismic event. Once the occurrence of the event is marked, human analysts are called in to classify the event or off-line softwares are used to identify the event. This method of identification and reporting of the seismic event is time efficient and has implicit latency problems. As the data becomes extensive with numerous events that constantly occur at a more frequent rate, it becomes unwieldy to use to detect the events manually from data obtained at seismic stations all over the world.

Some innovative approaches that address the issue of automatic detection are also proposed. For example, a method that uses the time-frequency bases of Walsh transform to detect the seismic event automatically was proposed in 1981 [36]. A new event detector by Murdock and Hutt was designed to use with the Seismic Research Observatories [53]. These tested and tried methods that have already been used for decades are harder to replace or complement with other methods unless the new method does prove that the change is worth the effort. A human seismic analyst with routine monitoring is more proficient and reliable in identifying seismic events and becomes indispensable, as it is easier to recognize patterns in different events by human eye. These reasons have always posed a challenge to new methods being developed.

To develop automated event identification and detection methods, there have also been efforts to understand the seismic event by looking at signals and characterizing them for different behaviors before, during and after the event. Pattern recognition techniques [37] have also been considered to detect and classify seismic events such as earthquakes.

Neural network algorithms [38] are also being studied for detecting the P and S waves of an earthquake. In short, there is ongoing research to successfully automate the role of human analysts [39]. The idea of using wavelets to identify and classify the seismic events has been floated around and has caused interest among the seismic community. The properties of wavelet transforms and their promising potential for use in signal processing of short time transient events is driving the research towards using then for automated real-time detection and reporting of seismic events.

Wavelets provide a good time-frequency localization of seismic signals. Hence, the time of occurrence of an event is not lost in the analysis and can complement or augment other methods presently in use. Seismic signals for earthquake events have two important properties, the P phase (wave) and the S phase (wave). Figure 69 shows a typical seismic signal with an earthquake event. The P and the S phases along with their arrival times are marked.

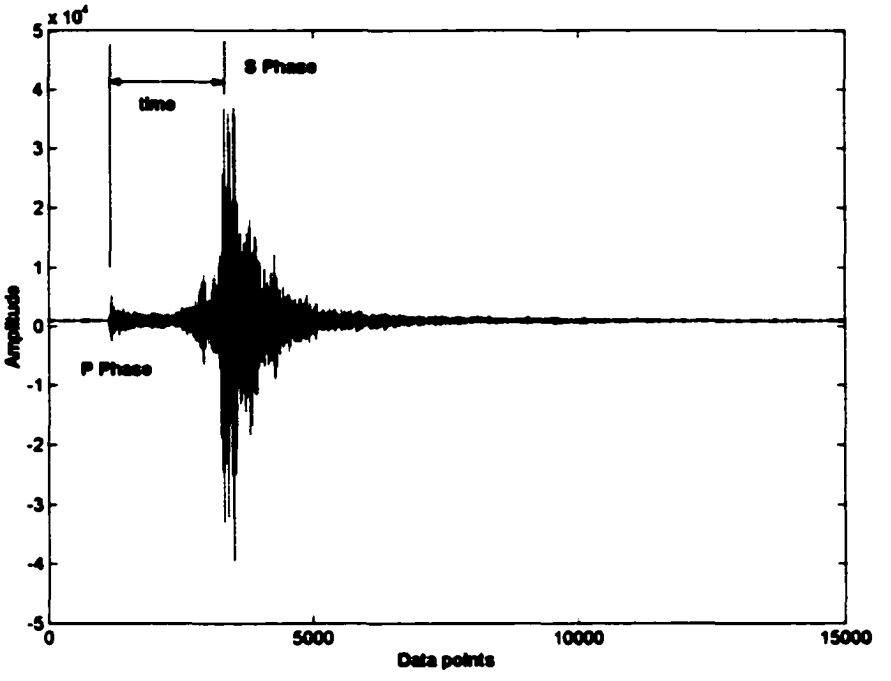

Figure 68: Seismic Signal With An Earthquake Event.

The occurrence of these waves and their time of arrival in the seismic signals are important for classifying earthquakes. For example, the ability to detect the arrival time of P phase and S phase and their amplitudes correctly is one of the key factors in determining the distance and magnitude of earthquakes. The wavelets, which have good time localization, possess the ability to detect the time of arrival correctly compared to other methods that rely on various statistical trigger processes or the human eye. The frequency bands of the wavelet decompositions provide the frequency information of these components of the event. Research to understand the time-frequency decomposition of the wavelets when applied to seismic signals has been in the forefront in the last few years [40].

This research is to study how effectively the wavelet transform can be used to detect the important features of the earthquake in a seismic signal and classify it. One

important feature is to detect the arrival time of the first wave – the P phase. The commonly used STA/LTA method mentioned earlier is a continuous comparison of 'rectified' or RMS trace power in two windows of short (STA) and long (LTA) durations [35]. This method has an inherent delay due to the averaging method used for signal analysis. The benefits of using the wavelet transform can be seen in early detection of this P phase arrival. This is possible due to the characteristics of the wavelets which help us to look for amplitudes of predominant frequency components of the P wave in the seismic signal. Ability to identify this P phase early and fast gives us a little extra time to take remedial measures to prevent damage to life and property. Any amount of time gained is a valuable asset to disaster management and emergency response teams. Identification and classification of earthquakes with an ability to pinpoint the magnitude and location of the origin of the earthquake is important in taking remedial measures and resource management. Wavelets have a potential to be used in analysis of events in seismic signals that pose a threat to our resources like gas and water pipelines, roads, electric networks, buildings and infrastructure. For example, the recent earthquake in the western United States with a magnitude of 7.9 cracked highways, damaged supports to the Trans-Alaska pipeline and sent ripples throughout the country [41]. The possibility of saving money and life during unpredictable natural events is driving the research on using various techniques for detection of seismic signal events including wavelets.

Signals obtained from various sensors or instruments always have two components into which they can be divided – one, the noise and the other, the actual information. Each sensor or instrument has its own noise floor that is not a just a constant but a randomly varying component. This noise is sometimes modeled by statistical methods to a Gaussian

noise, white noise, colored noise etc., The ability to be able to separate out this noise component is important in positive detection of the disturbance or information caused by an event. The signal $s(t)$ can be represented as:

$$s(t) = n(t) + e(t) \qquad \text{- (20)}$$

The noise $n(t)$ is sometimes similar but mostly different between different sensors and also at different times due to various circumstances. This changing noise has to be modeled correctly in order to avoid confusion and false identification. In this research, a seismic signal obtained from a seismometer, the noise is modeled during the quiet time continuously till an event is detected. Thus discriminating the noise and the event is simplified to a hypothesis test between the two models based on multiscale threshold test.

The seismic signal can be represented in its wavelet bases as [42]:

$$s(t) = \sum_{j,n} d_{j,n}(s)\psi_{j,n}(t) \qquad \text{for } j > 0 \text{ and } n \in I \qquad \text{- (21)}$$

where $d_{j,n}(s) = d_{j,n}(n) + d_{j,n}(e)$ and $\psi_{j,n}(t)$ is the dilated and translated bases of the mother wavelet.

The noise $n(t)$ or $d_{j,n}(n)$ is modeled as for each wavelet level as a Gaussian noise with a mean of zero and a standard deviation of σ_j^2 and can be written as:

$$d_{j,n}(n) = N(0, \sigma_j^2) \qquad \text{- (22)}$$

The figure 67 below shows the empirical pdf histogram of noise for the quiet period for the decomposed signals of two wavelet levels 2 and 3 [42]. A Gaussian approximation is superimposed on the histogram plot to emphasize the Gaussian nature of the decomposed signals for the quiet period.

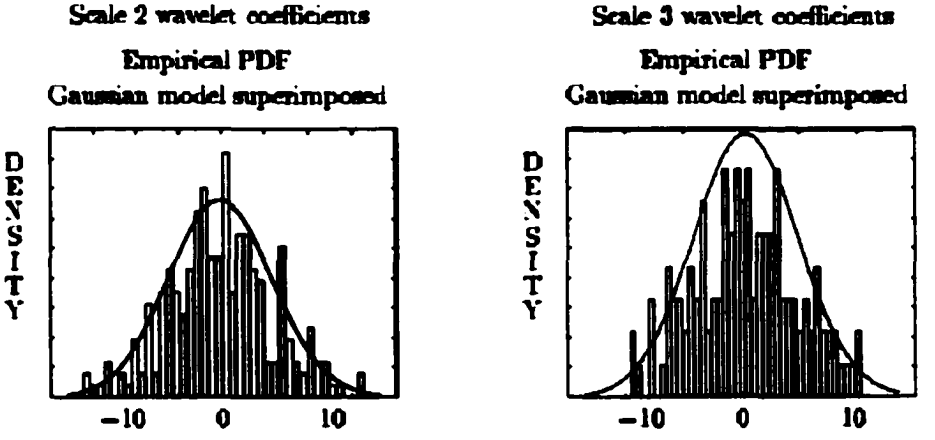

Figure 69: The pdf Of The Decomposition Signals Of The Wavelet Levels 2 And 3 For The Quiet Period.

For the multiscale threshold test we hypothesize that for any event to be detected in the seismic signal $s(t)$,

$$\left|d_{j,n}(s)\right| > 4\sigma_j \qquad -(22)$$

i.e., the occurrence of an event in the signal is true if any of the wavelet level amplitude falls outside the 4σ boundary of the noise model.

In this research we considered a few prominent earthquakes that occurred within the last year both in the US and around the world. The data for these earthquakes are available from the IRIS Consortium [43], a seismic database center which catalogs and makes data available for researchers through its web site. The data is stored in full sampling rate of 40 samples/sec obtained from seismometers at different seismic monitoring stations around the world. Data from the IRIS consortium can be obtained with the P phase arrival time as the reference point, and going up to 5 minutes before P and up to more than 50 minutes after P.

This method of data retrieval is good for our research as we propose to apply wavelets to detect the P phase arrival much before the arrival time specified by the current methods.

The earthquake events whose data are used in this research are listed below in table 9 below. The magnitude, time and date of occurrence of the events are also shown.

Table 9: Earthquake Events

Earthquake Event	Magnitude	Time in UTC	Date
Central Alaska	7.9	22:12:40	Nov 3, 2002
Southern Indiana	5.0	17:37:13	Jun 18, 2002
New York	5.1	10:50:44	Apr 20, 2002
Washington	6.8	18:54:32	Feb 28, 2001
South India	7.7	03:16:40	Jan 26, 2001

Starting off with the New York earthquake in April 2002 since it caused much concern around the northeast due to the density of population in the area, the seismic plot for the earthquake event is shown in figure 71. The data for this earthquake were obtained from two seismic stations with Streckeisen seismometers having 40 Hz sampling rate. The plot shows 55 minutes of seismic data with 127050 data points for the earthquake event seen at the Oxford, Mississippi seismic station.

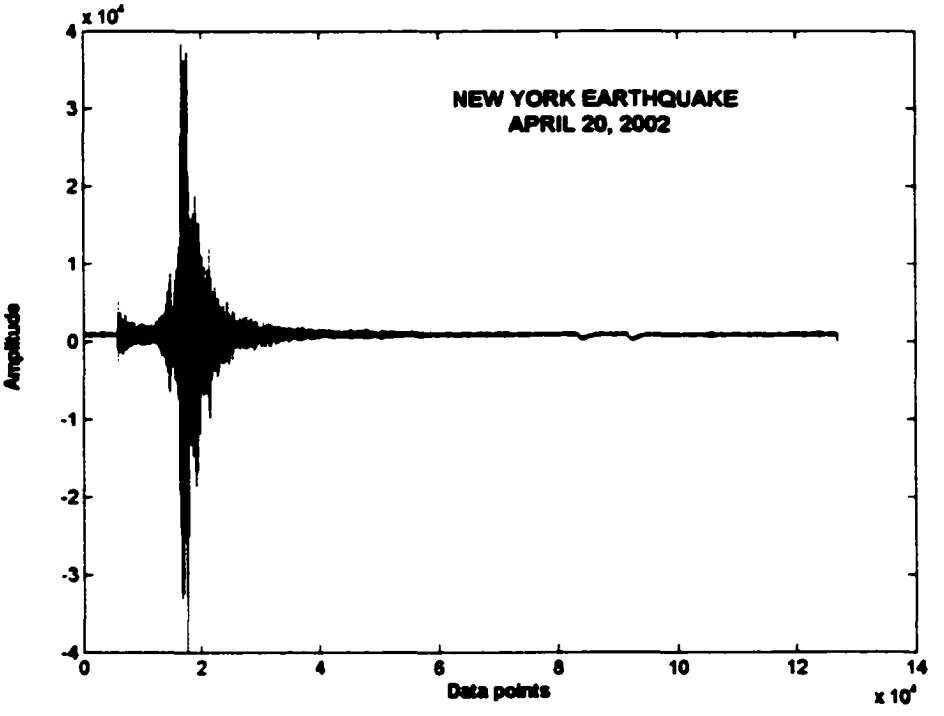

Figure 70: New York Earthquake Event Seismic Signal.

This data shows the quiet period at the beginning of the plot, the P phase, the S phase and the final ring down of the sensor signal after the earthquake. This data is downloaded as indicated earlier with 5 minutes before P and 50 minutes after P. Therefore at 40 samples/sec, the P phase arrival time according to the method used by the seismic station is:

$$\textit{sample rate x time till P phase in seconds} = 40 \times 5 \times 60 = 12000. \qquad -(23)$$

Wavelet analysis is applied to this seismic signal for every 1024 data points, i.e, a non overlapping moving window of 1024 points, from the beginning of the signal as shown in figure 72. The wavelet analysis is continued with time along the length of the signal.

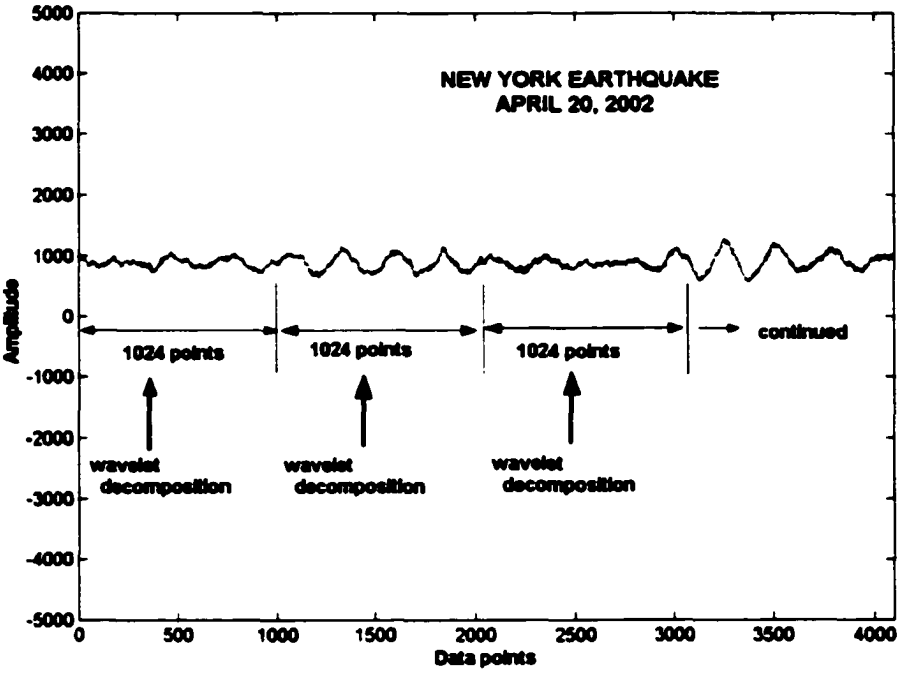

Figure 71: Wavelet Analysis Of The Seismic Signal For First 4096 Data Points.

The DC offset of the signal is approximately reduced to zero to avoid large DC signals in the wavelet decomposition which tend to shadow the other frequency bands. This can be achieved in practice by sending the signal from the seismometer through a pre-amp or zeroing this offset digitally before performing a wavelet analysis. This offset may be different for each seismometer and hence reducing this offset helps to compare wavelet decompositions of seismic signals from two or more stations by eliminating the differences in analysis due to DC offsets.

Given the sampling rate of the seismometer signal, it is important, as seen in the previous chapter, to select the number of data points for the wavelet decomposition and the level of wavelet decomposition. The maximum frequency of the wavelet decomposition is given by the Nyquist frequency of 20 Hz.

Considering a Fourier transform of a seismic signal at quiet time, we can observe that the seismic signal peaks at a frequency between 0.1 to 0.3 Hz. This frequency band is called the microseism band and is due to the effects of motion of the earth due to ocean tides [44]. Figure 73 shows the Fourier transform of the seismic signal during quiet period (period where no significant earthquake was recorded).

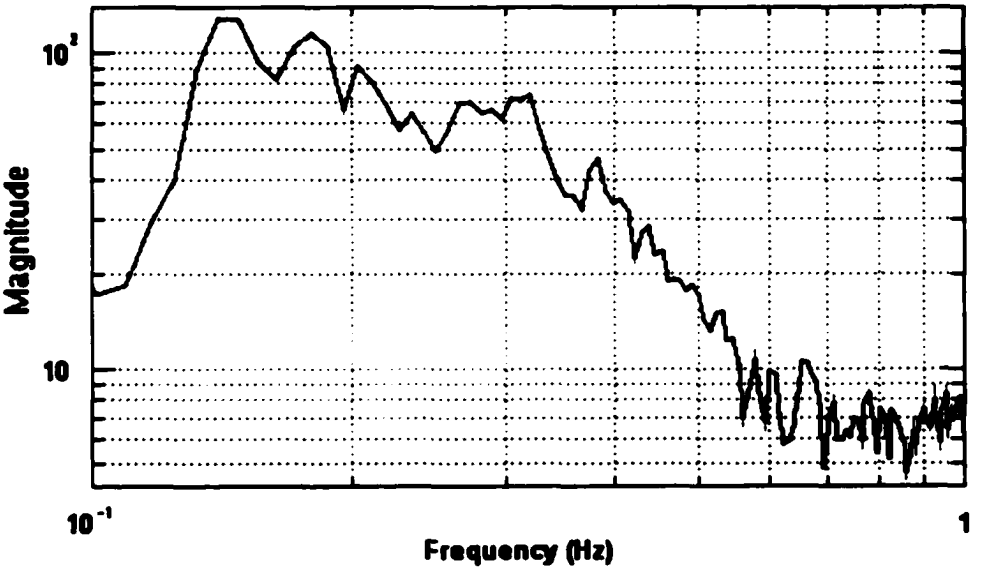

Figure 72: Fourier Transform Of The Seismic Signal Showing The Microseism Peak.

To contain most of this frequency range to a single wavelet level and also to meet the criteria for number of data points to be in powers of two, we select $N = 1024$ data points with 10 levels of wavelet decomposition as shown in table 10. This provides us with two wavelet levels 2 and 3, whose frequency ranges from 0.075 to 0.31 Hz, which is where mostly the microseism peak lies. The above selection helps to notice any microseism changes in the wavelet levels 2 and 3, and also to eliminate the microseism changes from appearing in any other bands used for earthquake analysis, thus preventing false alarms.

Table 10: Wavelet Decomposition Frequency Bands Of The Seismic Signal
N = 1024 Data Points, F_{max} = 20 Hz

Level	Wavelet Scale	Frequency range (Hz)	Center Frequency (Hz)
0	a9	0 – 0.037	0.018
1	d9	0.037 – 0.075	0.058
2	d8	0.075 – 0.15	0.117
3	d7	0.15 – 0.31	0.234
4	d6	0.31 – 0.62	0.468
5	d5	0.625 – 1.25	0.937
6	d4	1.25 – 2.50	1.875
7	d3	2.5 – 5.0	3.75
8	d2	5 - 10	7.5
9	d1	10 - 20	15

Each 1024 data point's section of the seismic signal, which corresponds to 25.6 seconds in length of time, is processed by wavelet analysis and the corresponding decompositions are obtained. The rms values of the decomposed wavelet decompositions are calculated. Appendix A has the Matlab program "seisrmscalc.m" which was written to automate this process of performing the wavelet analysis to obtain wavelet decompositions and calculating the rms and energy values of each level the wavelet decomposition. The rms values obtained are then compared with the threshold level set by the quiet (only noise) part of the signal.

For the seismic signal of the New York earthquake obtained from the Oxford, MS seismic station, the wavelet decomposition of the first 1024 data points of the signal using the Daubechies D20 wavelet is shown in figure 74.

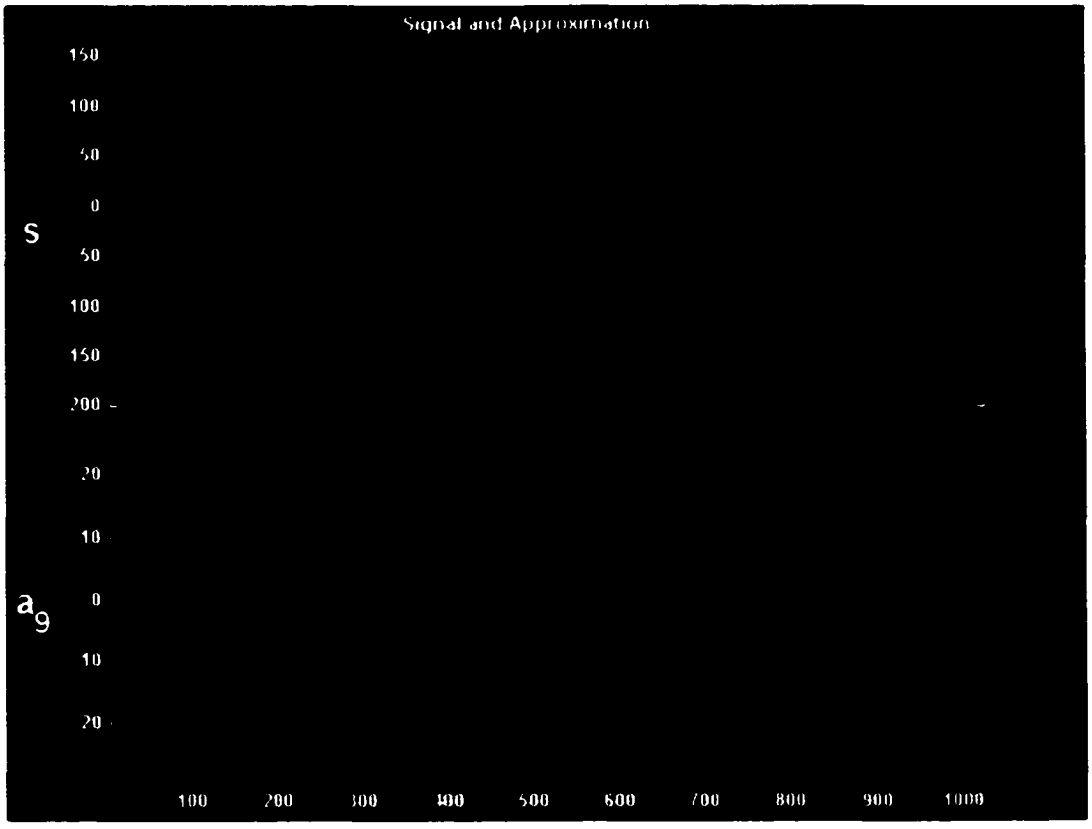

Figure 73: D20 Wavelet Decomposition Of The First 1024 Data Points Of The New York Earthquake Seismic Signal.

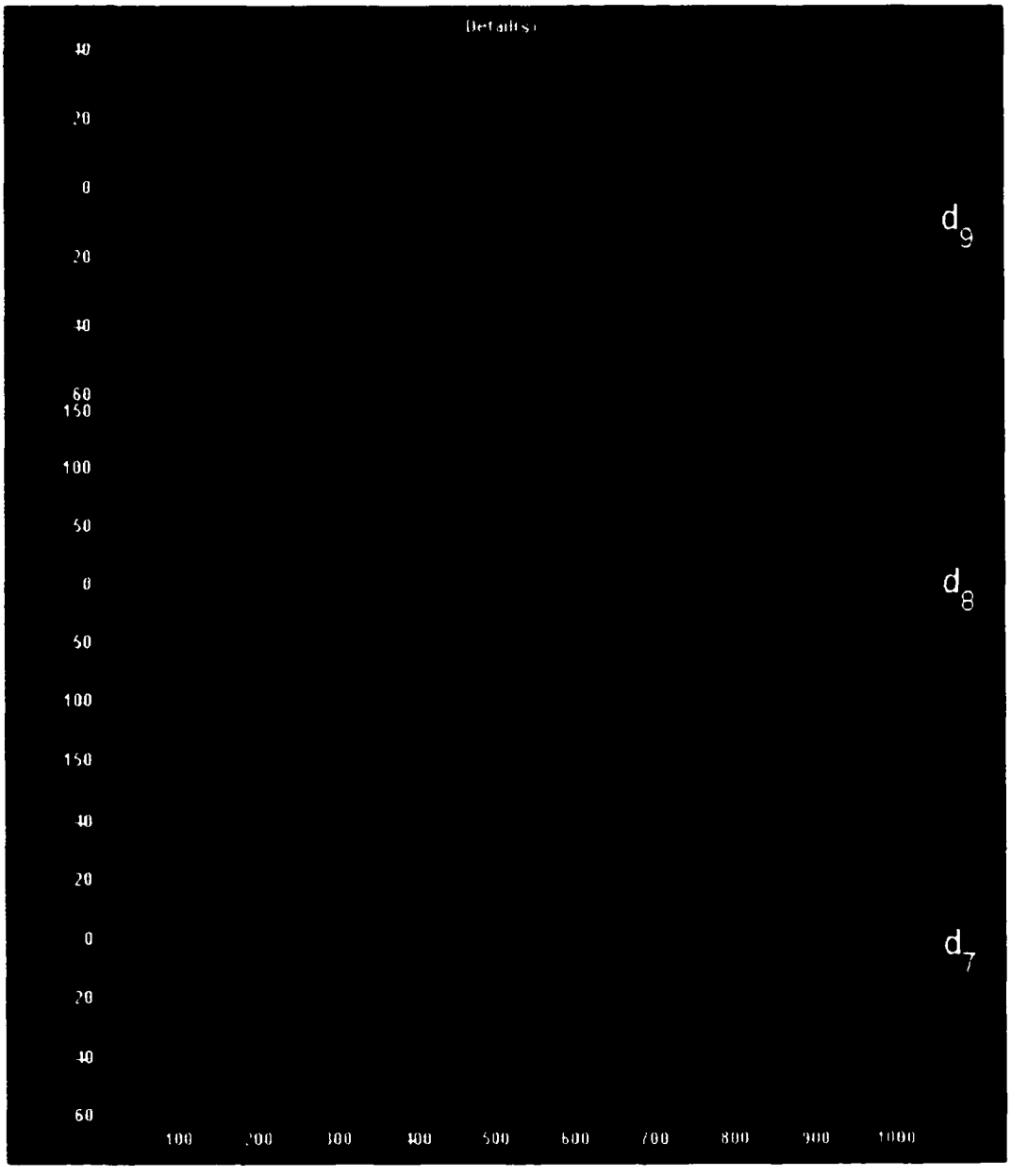

Figure 74 (Continued): D20 Wavelet Decomposition Of The First 1024 Data Points Of The New York Earthquake Seismic Signal.

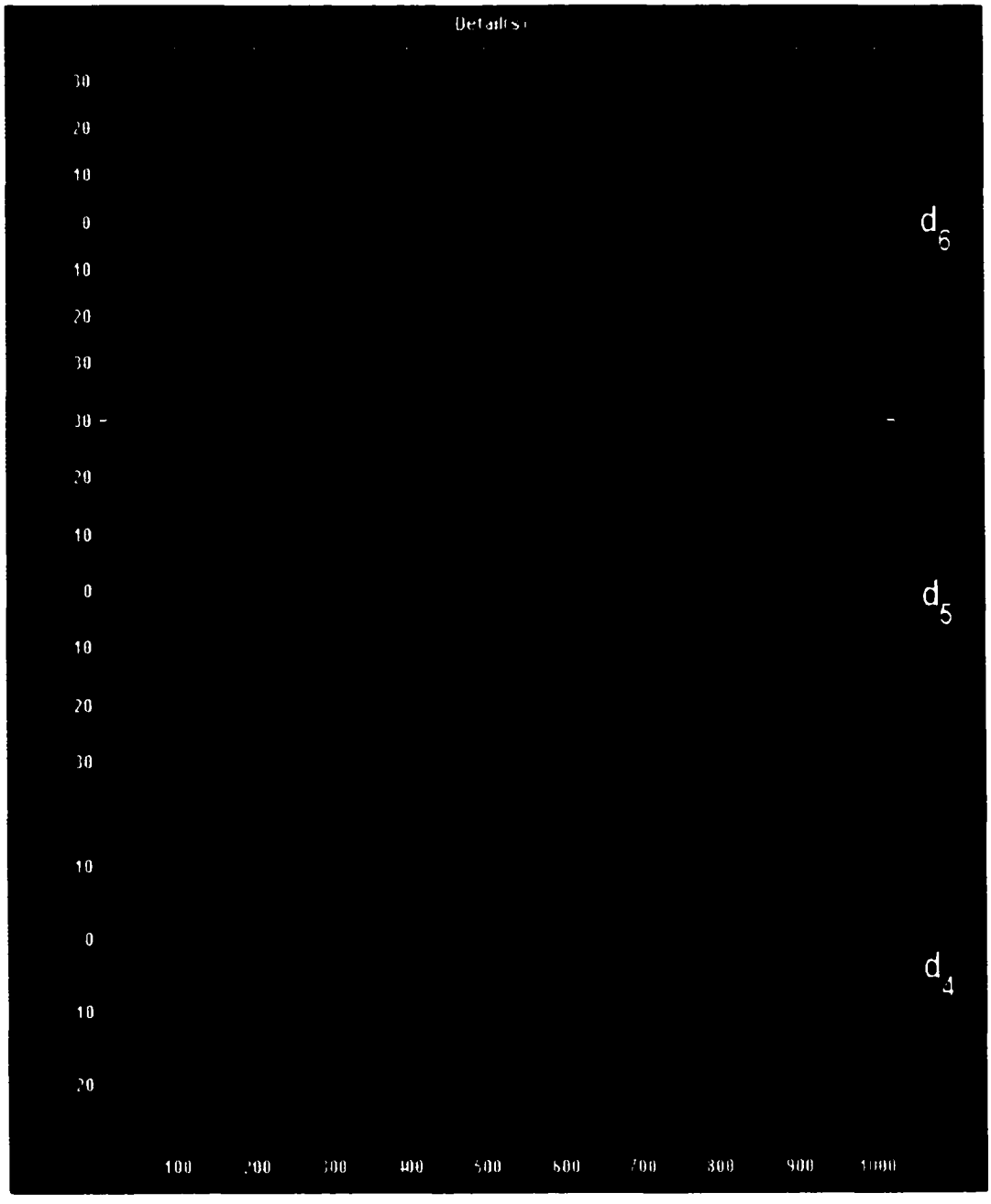

Figure 74 (Continued): D20 Wavelet Decomposition Of The First 1024 Data Points Of The New York Earthquake Seismic Signal.

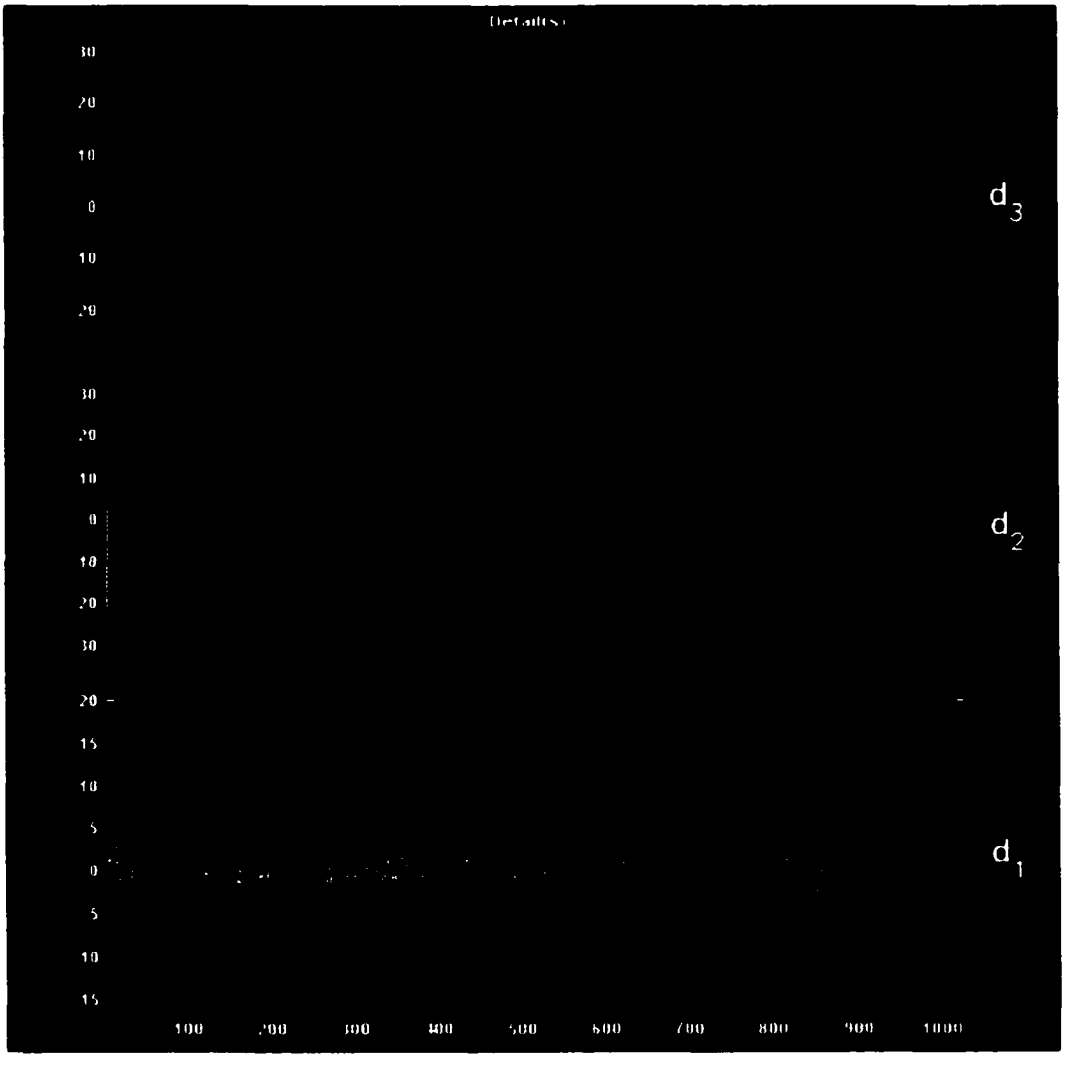

Figure 74 (Continued): D20 Wavelet Decomposition Of The First 1024 Data Points Of The New York Earthquake Seismic Signal Recorded At Oxford, MS.

The rms and energy values calculated for the above wavelet decomposition are shown in the histogram plot of figure 75. Note the signal's dc offset has been reduced to near zero, and hence a small rms value is seen in the level 0 of the plot. As expected the wavelet level 2 shows higher rms value due to the microseism peak present in the seismic signal. This microseism peak is around 0.15 Hz during quiet times, and the peak tends to shift right towards 0.3 Hz with increase in storm activity.

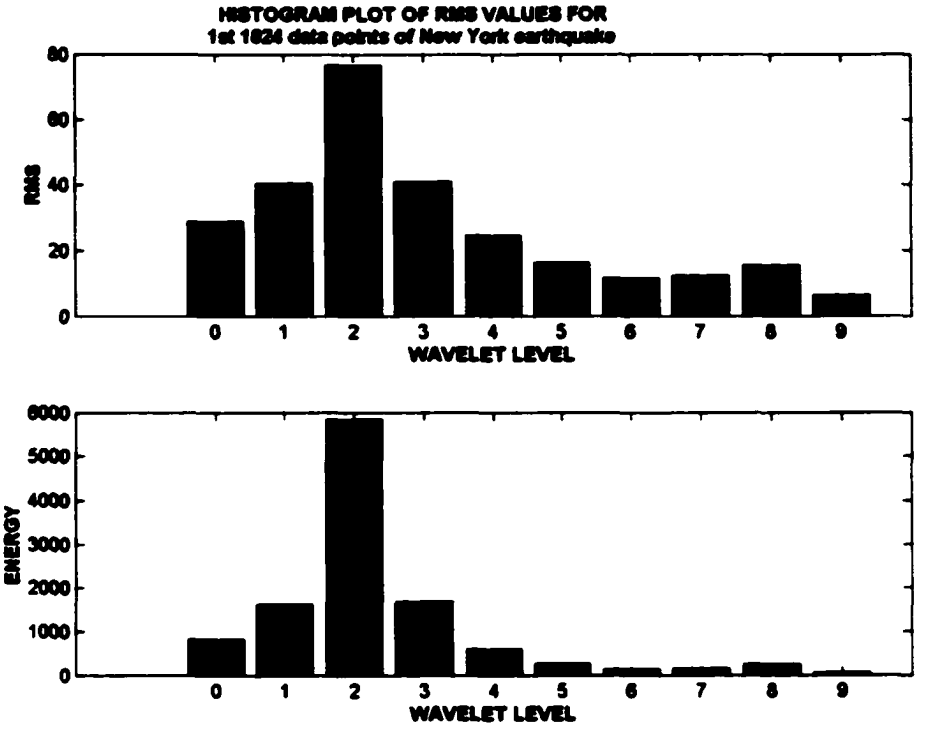

Figure 74: Histogram Plot Of The Rms And Energy Values For The 1st 1024 Data Points' Wavelet Decomposition In Figure 71.

The wavelet decomposition is repeated continuously for every 1 024 data points using the non-overlapping moving window and the rms values calculated. The histograms of the next few windows are shown in the following figures which are named accordingly. Only the rms values histogram is plotted for clarity and convenience. Figure 76 shows the histogram plot of the rms values for the wavelet decompositions of the seismic signal from 1024 to 5120 data points in steps of 1024 data points. Continuing for the next four windows of wavelet decomposition, figure 77 shows the histogram plots.

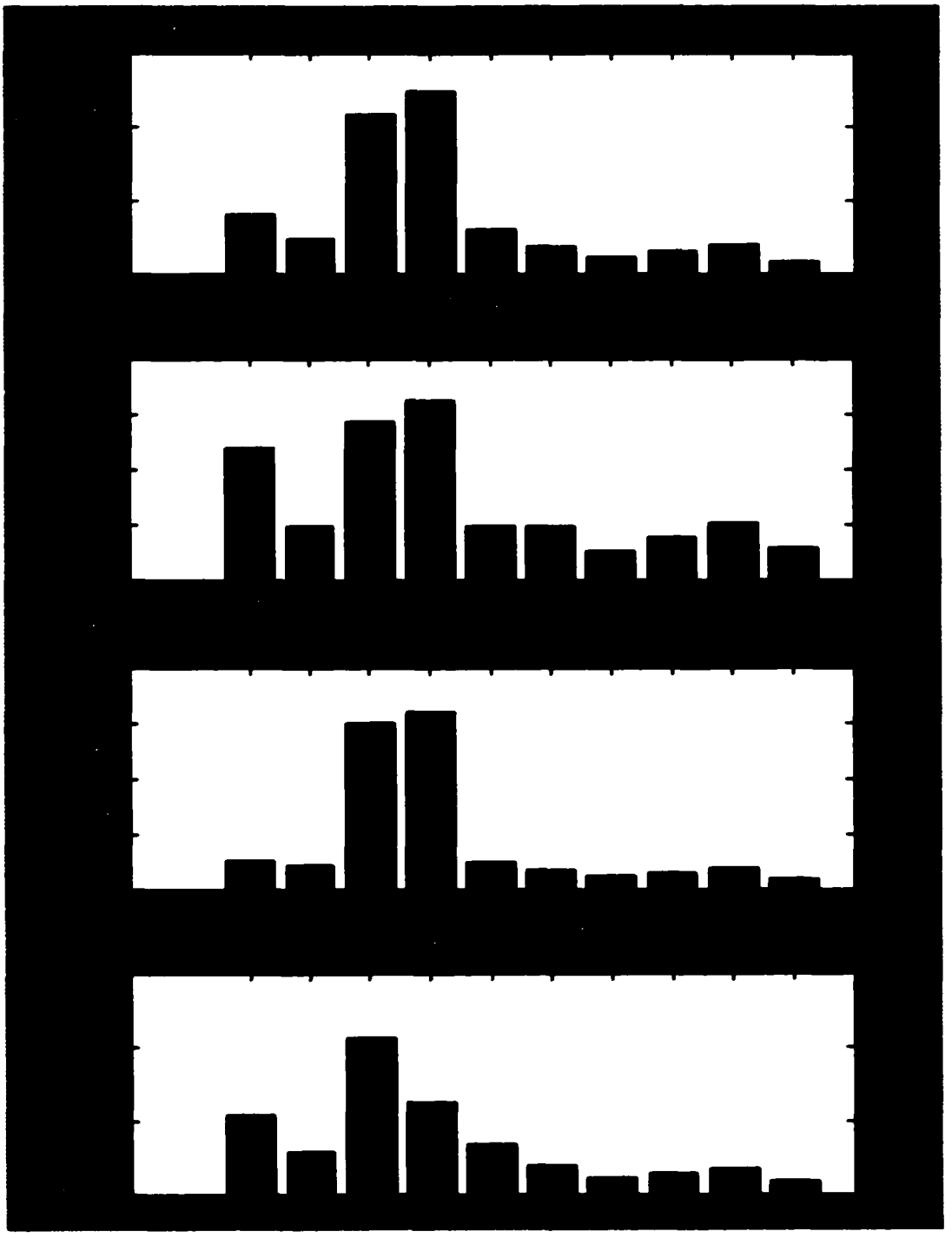

Figure 75: Histogram Plots Of Rms Values For D20 Wavelet Decompositions Of The New York Earthquake Seismic Signal Recorded At Oxford, MS.

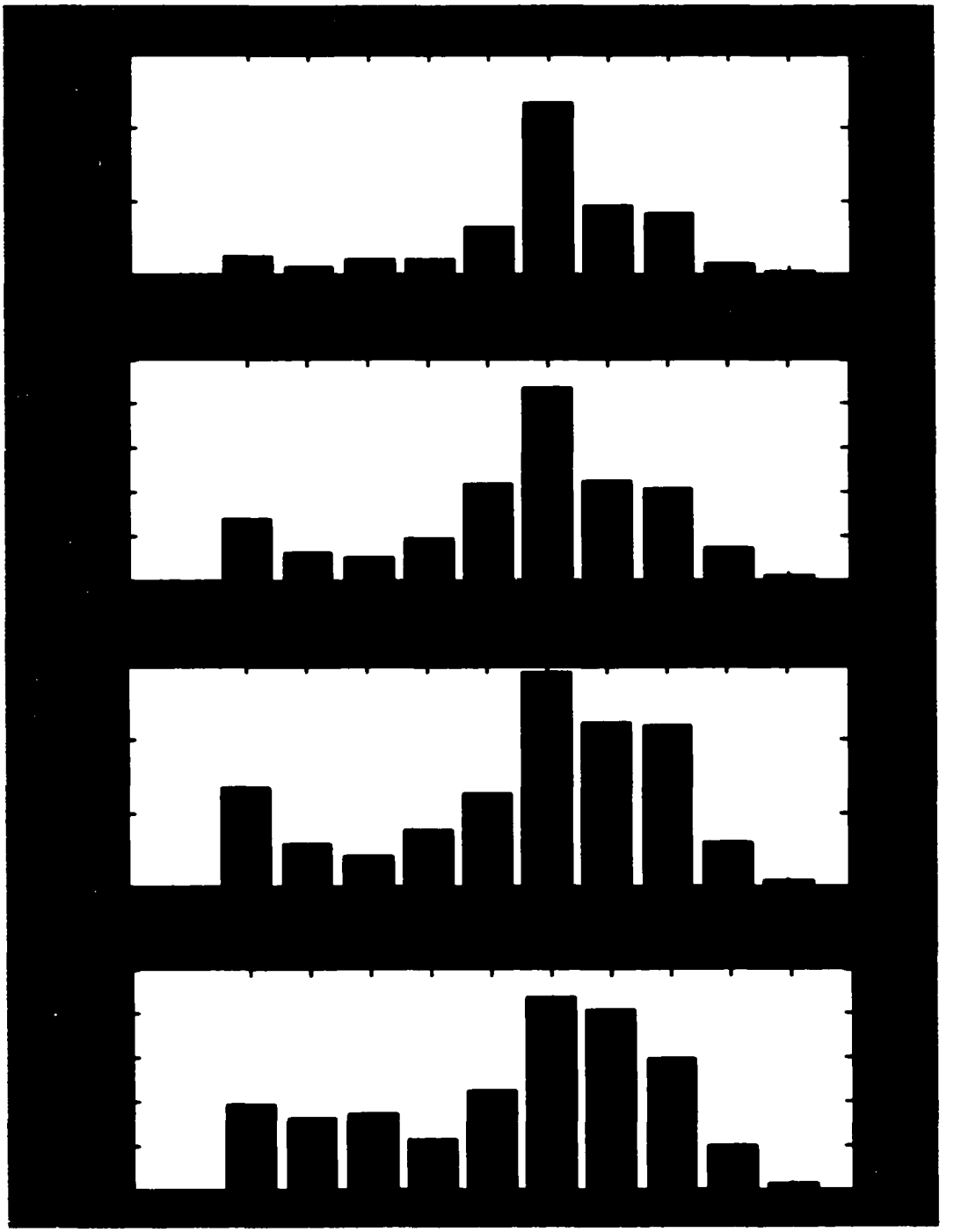

Figure 76: Histogram Plots Of Rms Values For D20 Wavelet Decompositions Of The New York Earthquake Seismic Signal Recorded At Oxford, MS.

We can clearly see that there is a sudden change in the histogram plot of 5120 – 6144 points compared to its predecessors. Plotting the time series between the points 5120 to 6144 in figure 78, we clearly see that the wavelet decomposition has clearly identified the arrival of the P phase of the earthquake event.

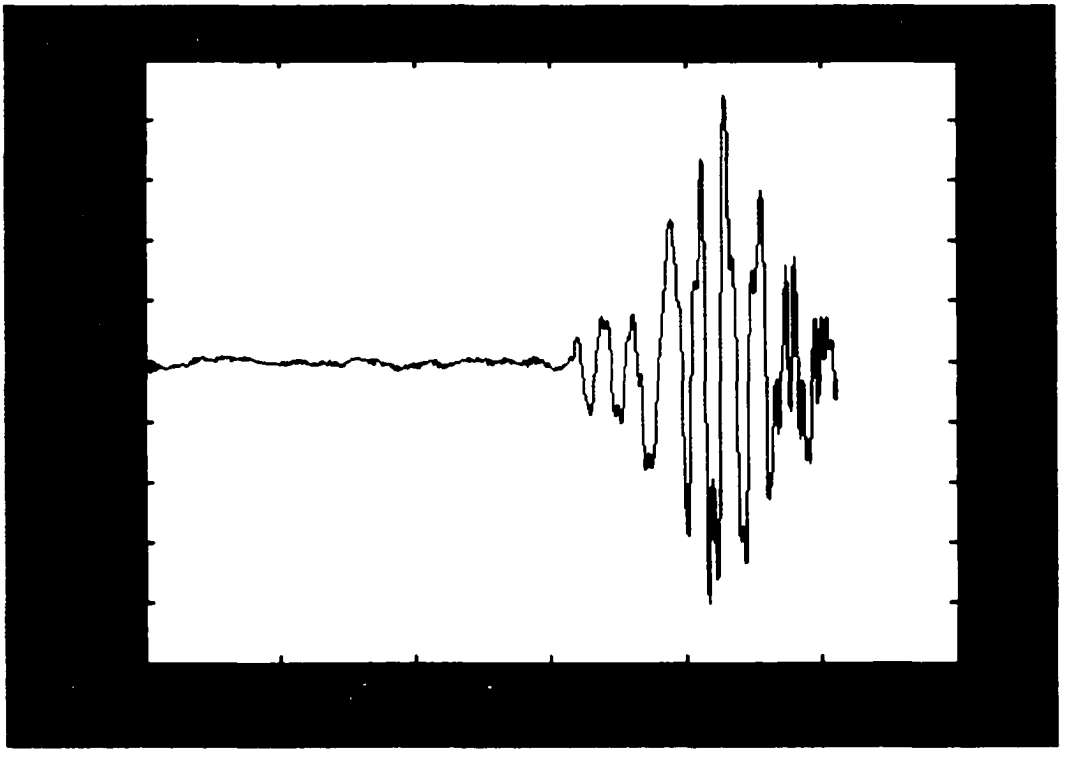

Figure 77: Time Series Plot Of The New York Earthquake Between 5120 And 6144 Points.

. The quiet period (the only noise period) of the seismic signal's histogram plots in figure 76 show that the maximum rms value is less than 200 counts for any wavelet level. The wavelet level 2 and wavelet level 3 are the only two wavelet levels that have considerable amplitude due to the microseism.

A simple amplitude threshold trigger which simply detects any wavelet level amplitude of the decomposed seismic signal exceeding the pre-set threshold can be employed for detection. The amplitude threshold can be pre-set to a fixed value or can be

adaptive by looking at a set past windows and obtaining an optimum threshold. If we select a pre-set threshold of 200 counts, we see from figure 77, the wavelet level 5 (0.62 Hz to 1.25 Hz) shoots up very high, clearly exceeding the threshold value. Also seen is that some of the other wavelet levels have also exceeded the 200 count threshold. This event when detected can be flagged as true for detection of the event, in this case a P phase. Once the event is detected, the wavelet decomposition of the seismic is continued to check for the existence of S phase whose amplitude is much more than the P phase. The rms values are calculated, and the values are compared with the new amplitude threshold set after the detection of the first event.

For our test with the New York earthquake, the P phase was detected at the sixth wavelet decomposition of the seismic signal which gives us a time of arrival of 153.6 seconds. This is much earlier than 5 minutes or 300 seconds as detected by the algorithm used by the seismic station. This is a good 150 seconds earlier time of detection, a long time in terms of time gained for emergency response.

The STA/LTA trigger method which is the most broadly used algorithm in weak-motion seismology, calculates the average values of the absolute amplitude of the seismic signal in two consecutive moving-time windows. The short time window (STA) is sensitive to seismic events while the long time window (LTA) provides information about the temporal amplitude of seismic noise at the site. When the ratio of both exceeds a pre-set value, an event is declared and the data starts being recorded to a file [45]. The STA/LTA ratio trigger method's successful detection of seismic events depends on the proper settings of the trigger parameters such as the length of the windows and the threshold values used. Reference 45 clearly shows the effects of the variations in the

window length and threshold parameters on the detection of seismic events. Figure 79 shows how the reduction in the length of the LTA window from 100 seconds to 45 seconds misses the P phase wave while detecting the S phase. Once the event is detected, a length of the pre-event and post-event signal is also recorded along with the triggered time for retrospective analysis and correction by seismologists.

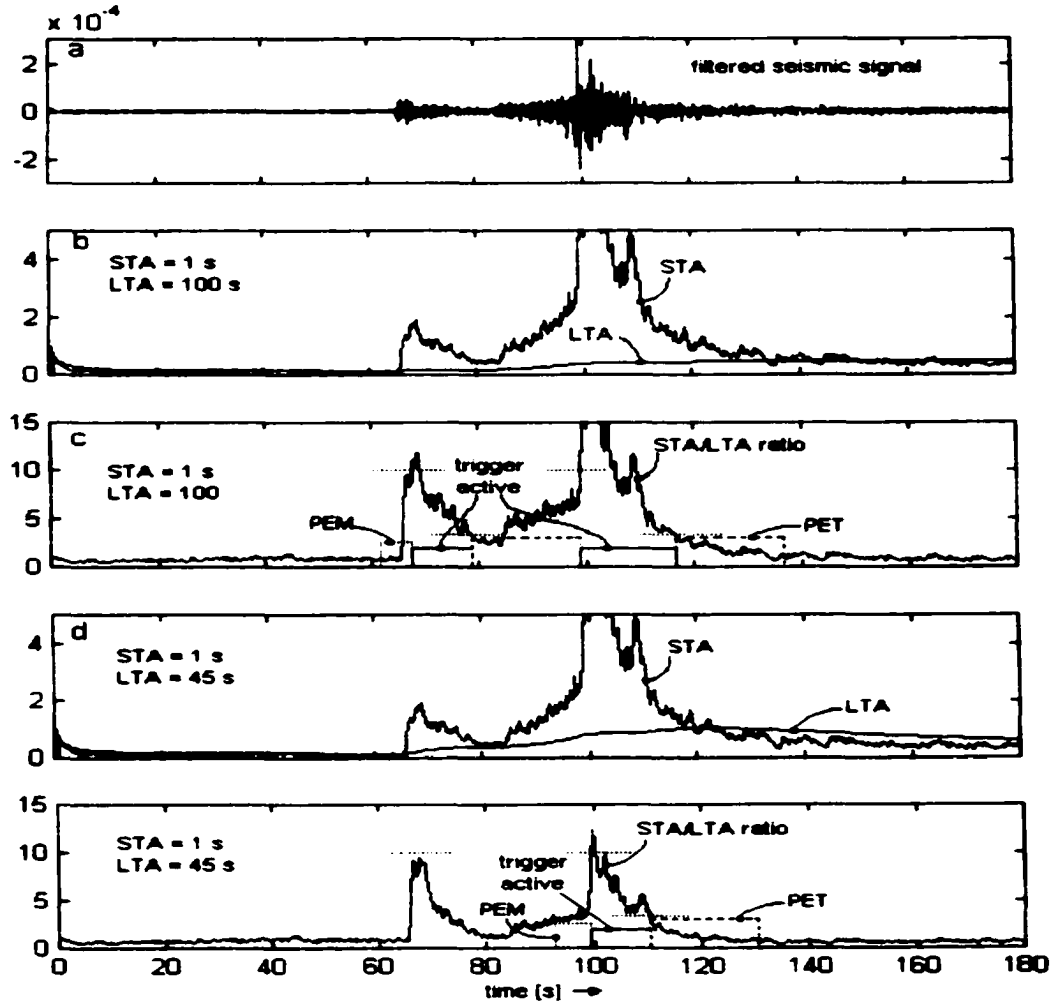

Figure 78: Influence Of LTA Duration On The Trigger Algorithm Sensitivity To Earthquakes.

Similar observations can be made for changes in the STA time window and also the threshold levels used to trigger active and inactive levels. More sophisticated

algorithms are known from literature, but they are rarely used in seismic data loggers currently in the market. However, the sophisticated adjustments of operational parameters to actual signals and seismic noise conditions at each seismic site that these triggers require has proven unwieldy and subject to error in practice. This is probably the main reason why the STA/LTA trigger algorithm still remains the most popular [45].

The wavelet method above uses a fixed non-overlapping moving window which is 1024 data points of a seismic signal sampled at 40 samples/second. There is an inherent 25.6 seconds delay due to the windowing nature. This can be drastically reduced by using over-lapping windows with a shift of 256 points (6.4 seconds delay) or, even better, 128 points (3.2 seconds delay) but with a computational overload.

Figures 80, 81 and 82 show the histogram plots of the rms values for the next eleven windows. We can observe as we move along the signal, the amplitude of the wavelet level 5 increases sharply to 15000 counts at the 17^{th} wavelet decomposition from the beginning, i.e., the lowest plot in figure 81. The next plot (first in figure 82) of the 18^{th} wavelet decomposition shows almost similar amplitude at 15000 compared to the current plot, but it is still less than the current plot's wavelet level 5 amplitude. This maximum at the 17^{th} wavelet decomposition corresponds to the S phase of the earthquake. The plot of the time series for the period between 16384 to 17408 points is shown in figure 83. The maximum amplitude of the time series is at 35000 counts at a few points in the signal where the S phase is maximum.

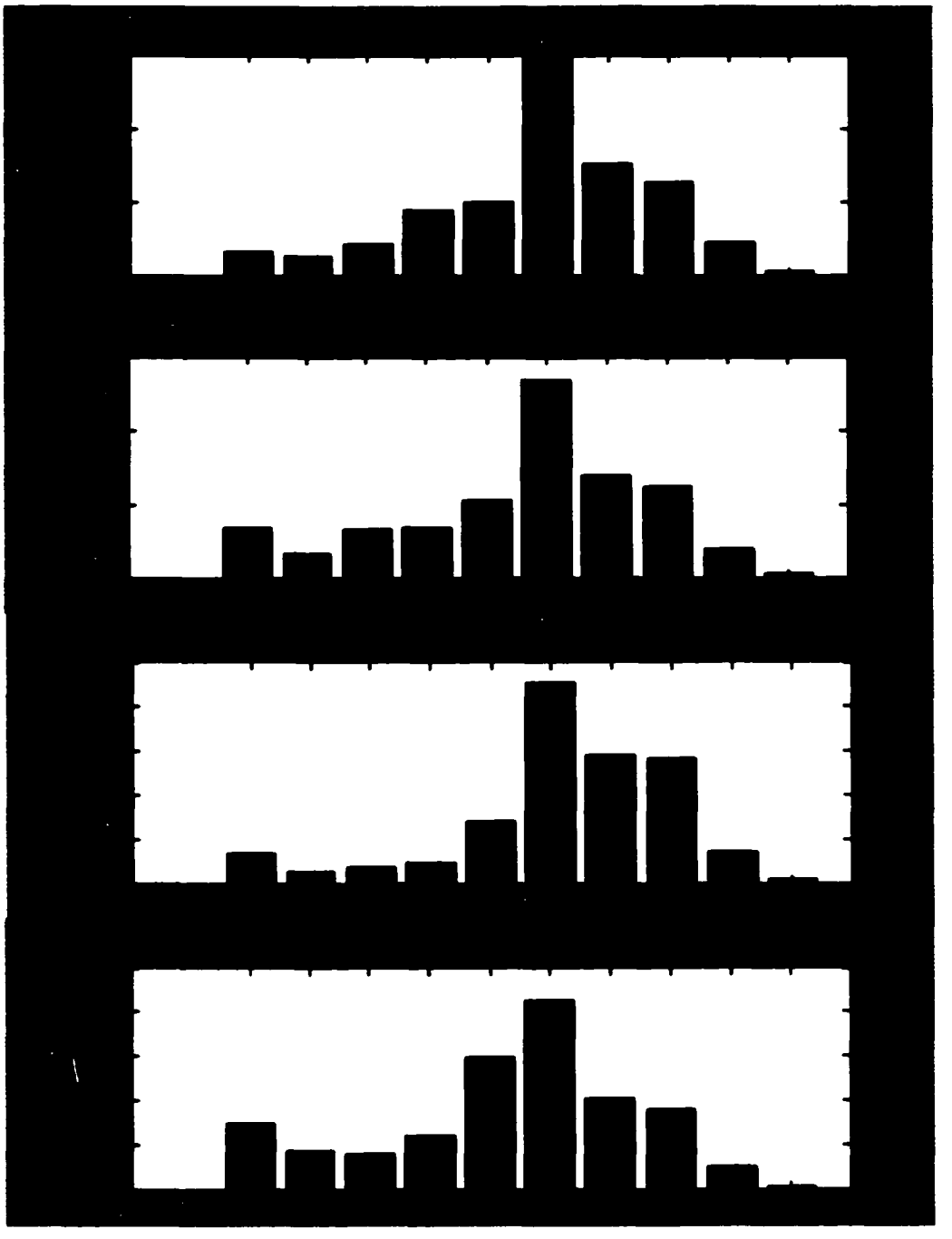

Figure 79: Histogram plots of rms values for D20 wavelet decompositions of the New York earth quake seismic signal.

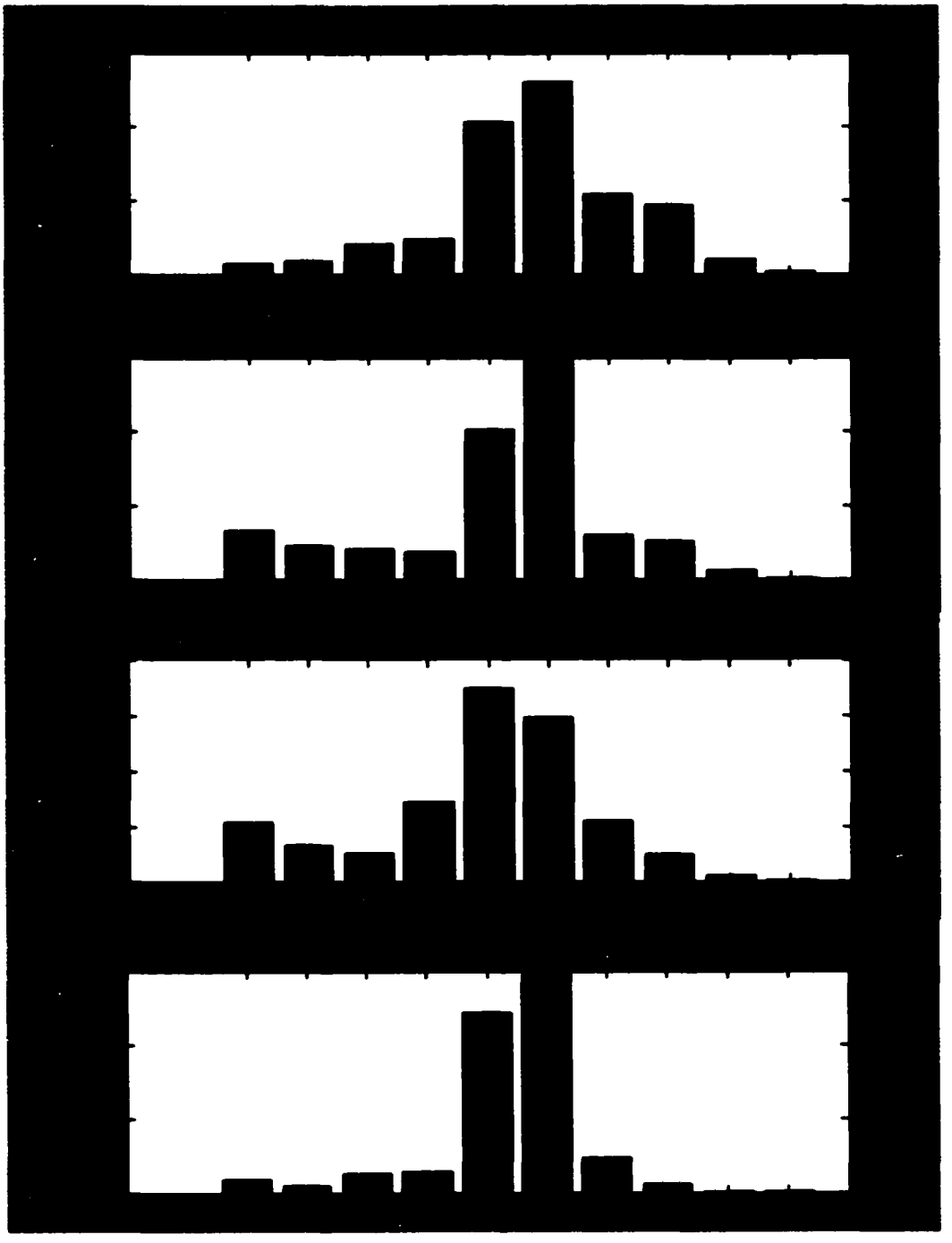

Figure 80: Histogram plots of rms values for D20 wavelet decompositions of the New York earth quake seismic signal.

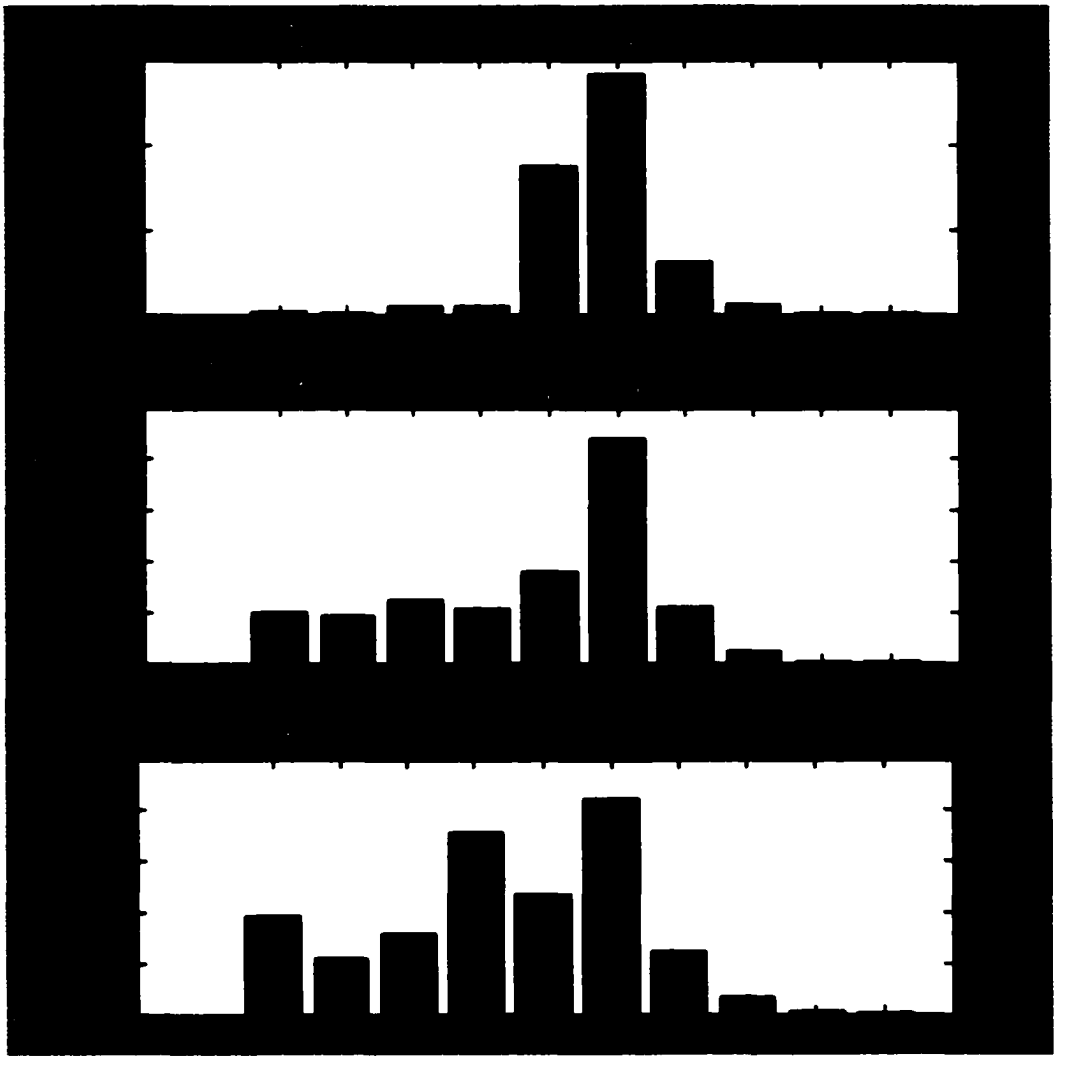

Figure 81: Histogram plots of rms values for D20 wavelet decompositions of the New York earth quake seismic signal.

The time series shows the occurrence of the peak of the waveform at around 16750th data point, which can be more accurately detected with the over-lapping moving window.

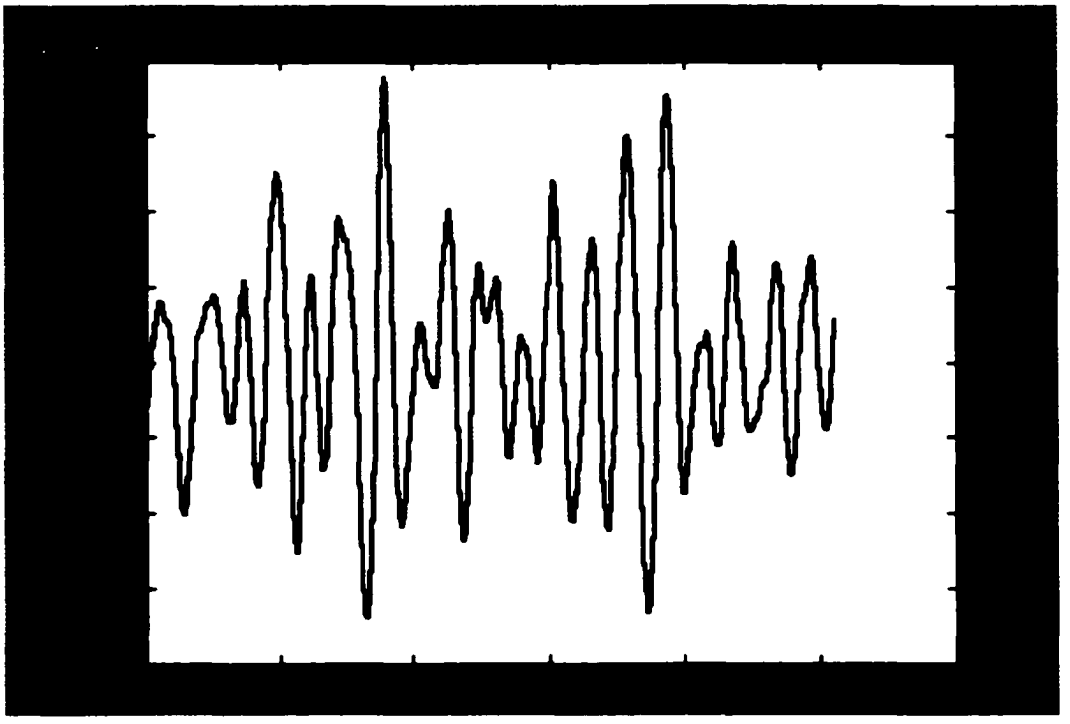

Figure 82: Time series plot of the New York earthquake between 16384 and 17408 points.

As explained earlier, the time of arrival of the S phase can be calculated using the length of wavelet decomposition window. For the S phase detected in the 17^{th} wavelet decomposition window, the time of arrival is 435.2 seconds. This measurement can be made more accurate using the overlapping moving window as explained previously. The difference between the S phase arrival time and the P phase arrival time is:

435.2 (7.25 min) – 153.6 (2.56 min) = 281.6 seconds (4.69 min)

From the P and S phase arrival time diagram [46] shown in figure 84 below, the distance of the earthquake epicenter can be calculated. From the figure, the relation between the arrival time difference S-P and the distance in kilometers is a factor of 10.

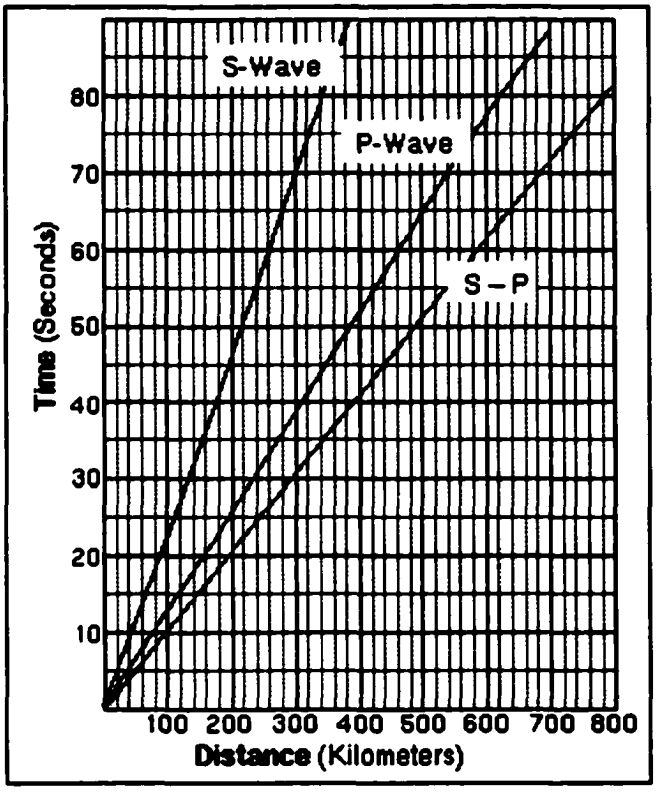

Figure 83: P And S Phase Arrival Time Diagram.

The epicenter of the earthquake is approximately calculated by multiplying the difference of S phase and P phase arrival time in seconds by 10 km/sec, giving us 2816 kms (1748 miles). This is approximately equal to the distance between the actual epicenter of the earthquake at Plattsburg, New York and the Oxford, Mississippi seismic station which is 1583 miles. However, for accurate measurement of the distance, the use of an overlapping window is suggested with optimized lower threshold trigger levels.

The wavelet transform method can be successfully applied to the analysis of seismic signals for identification and classification of the earthquake features. This method finally reduces to a simple amplitude threshold trigger mechanism similar to the simple STA/LTA trigger method commonly used. This provides the wavelet method an

upper hand as a potential future tool to replace or augment the existing techniques for better performance.

Continuing our study of the New York earthquake, we apply the above wavelet amplitude trigger mechanism to a signal recorded at the Junction City, Texas seismic station (JCT). Figure 85 shows the 55 minutes of New York earthquake event recorded at the above station.

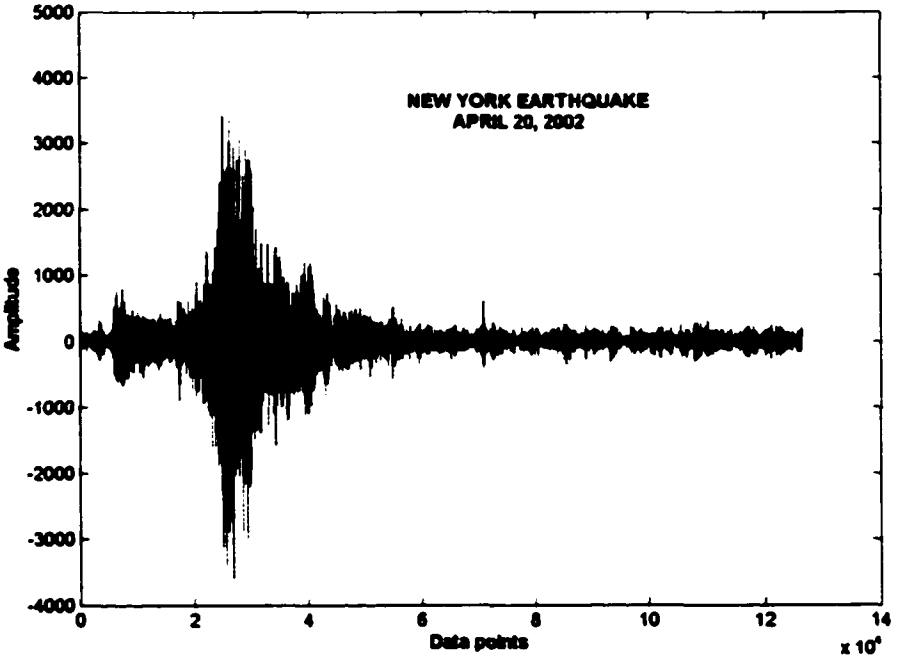

Figure 84: New York earthquake event seismic signal recorded at seismic station JCT.

The wavelet transform of the seismic signal is performed for every 1024 data points and the rms values calculated as in our previous example. The histograms of the rms values for the windows of wavelet decomposition of the signal in figure 85 are shown in figure 86. The data point numbers of the window are indicated on top of each histogram plot.

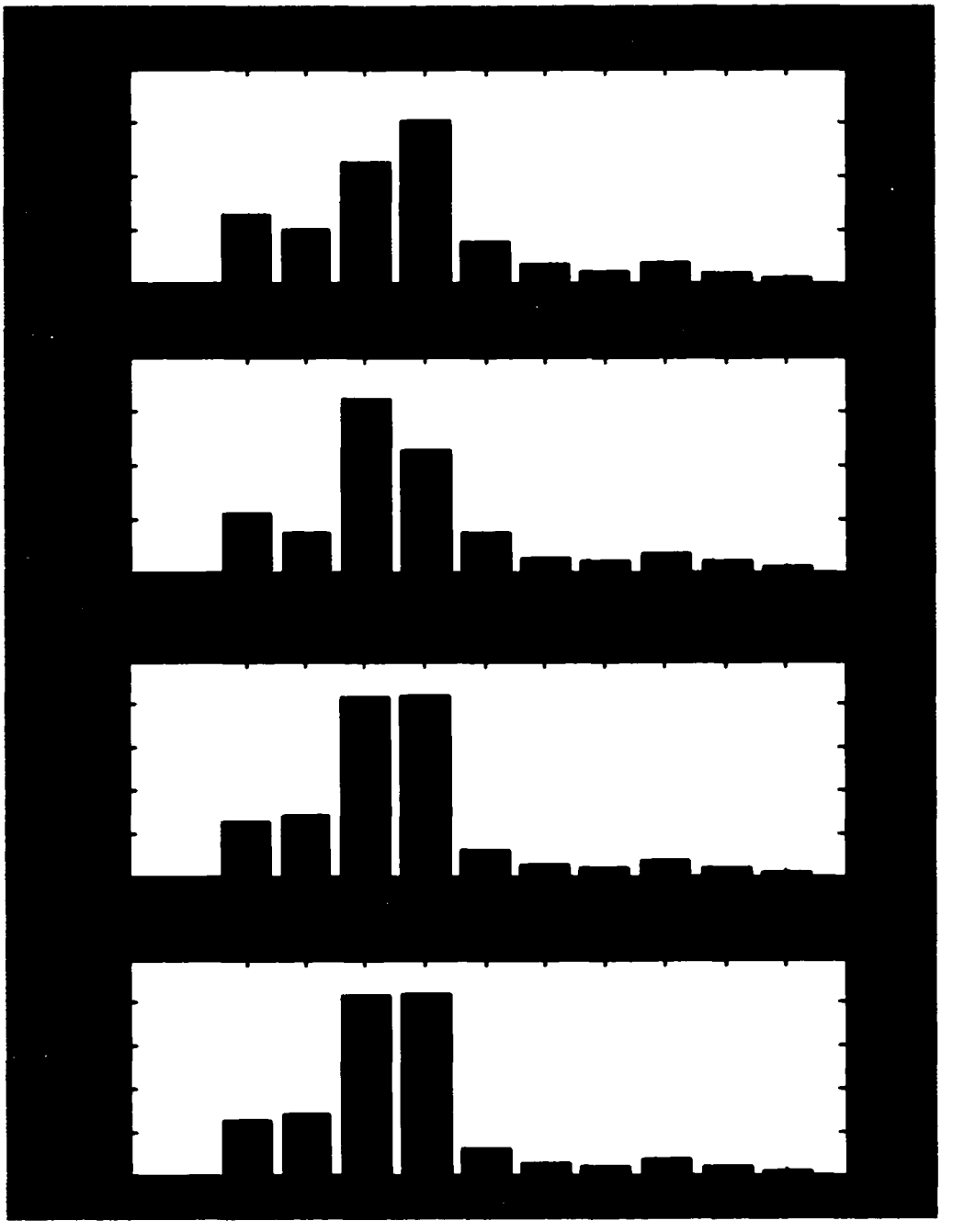

Figure 85: Histogram Plots Of Rms Values For D20 Wavelet Decompositions Of The New York Earth Quake Seismic Signal.

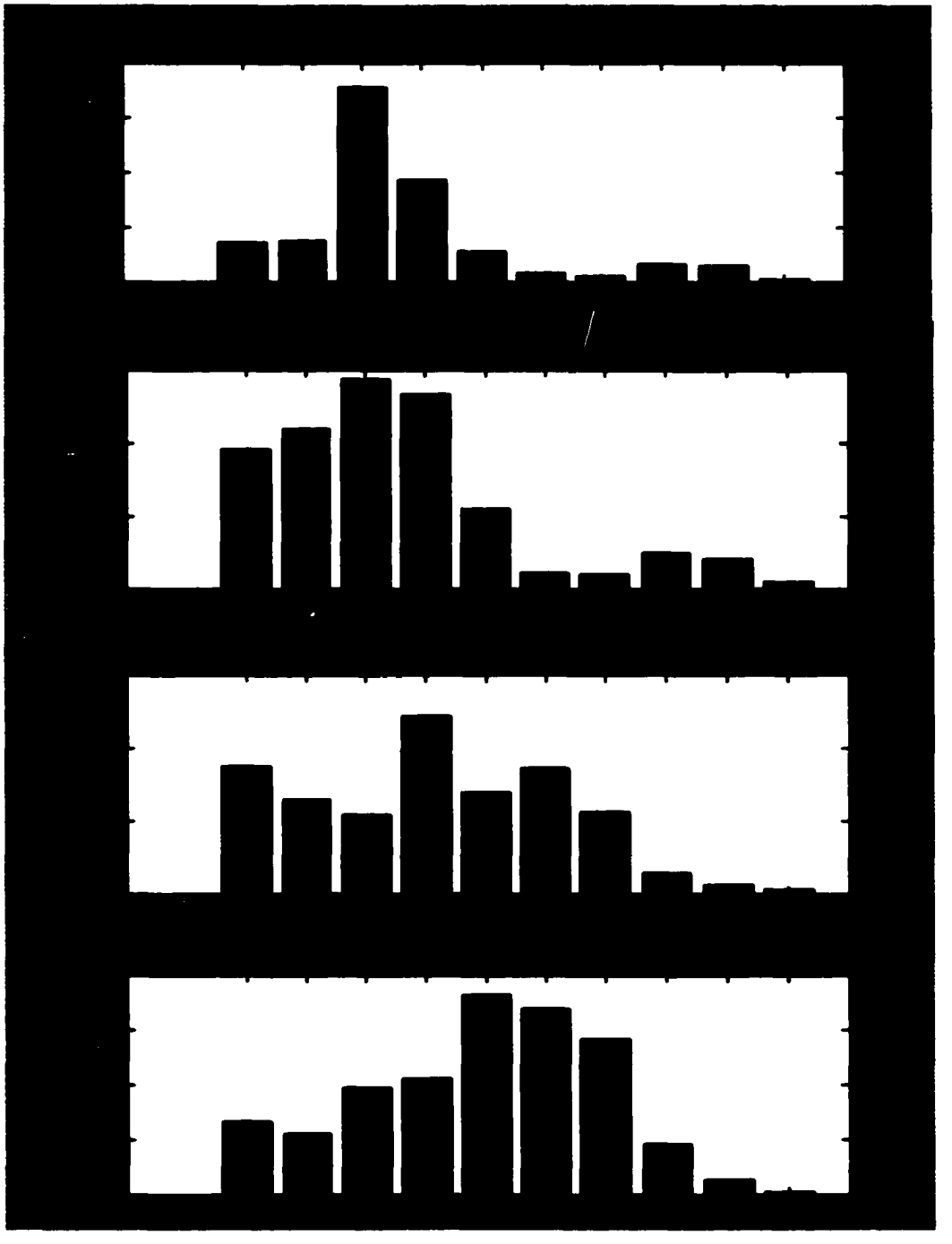

Figure 86: Histogram Plots Of Rms Values For D20 Wavelet Decompositions Of The New York Earth Quake Seismic Signal.

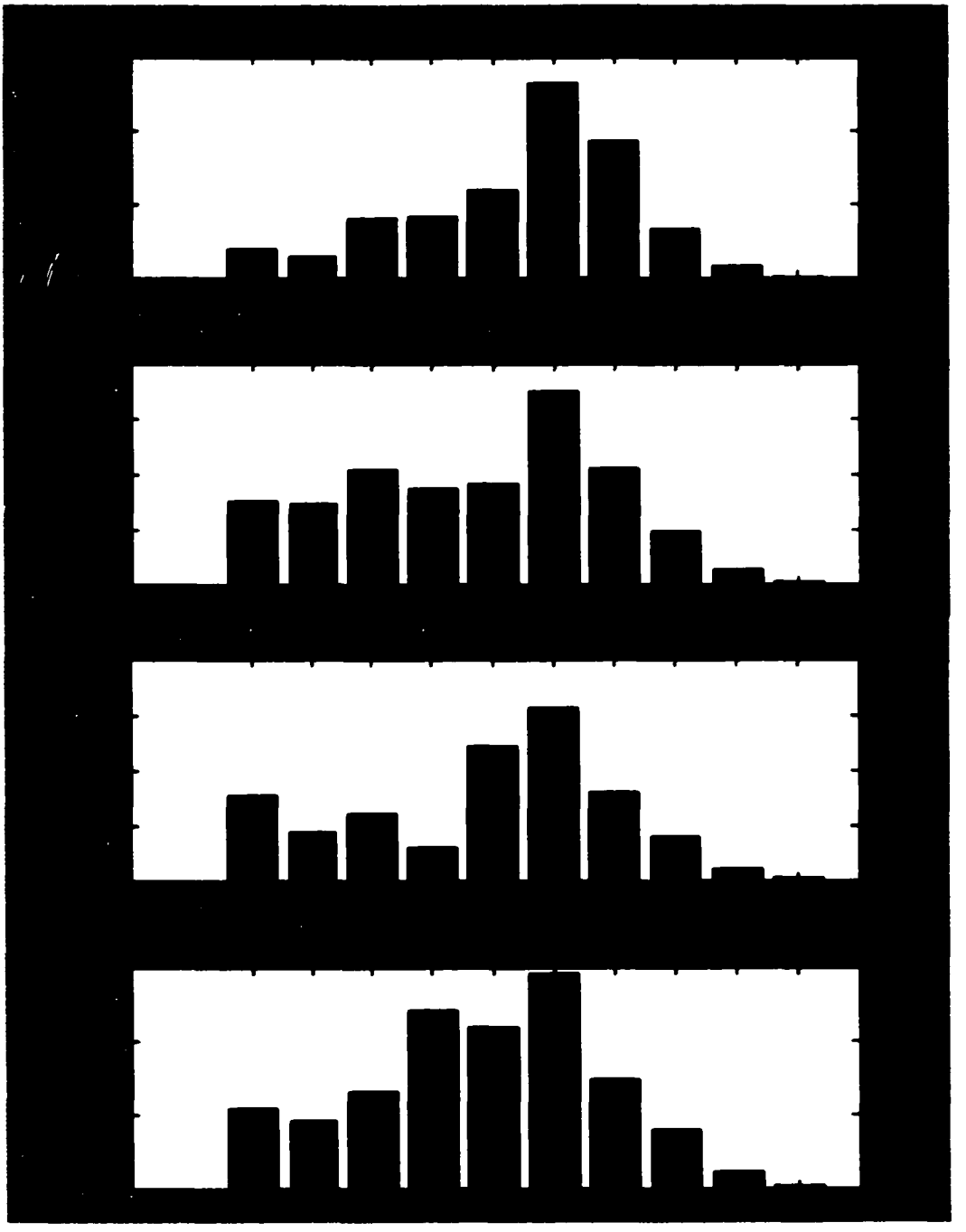

Figure 87: Histogram Plots Of Rms Values For D20 Wavelet Decompositions Of The New York Earthquake Seismic Signal.

The P phase of the New York earthquake is detected in the range of 8192 – 9216 points of the wavelet decomposition of the seismic signal obtained at the Junction City, Texas location, when it crosses the 200 count amplitude in the level 5 of the histogram

plot of rms values. This point of detection is much later than the similar detection by wavelet decomposition at Oxford, MS. This was expected and now confirmed, due to the extra distance the P phase wave has to travel from the point of origin of the earthquake - New York. Continuing the analysis to detect the S phase signal, the plots of histograms of rms values are plotted in the following figures 89 through 92.

The P phase is detected in the 9^{th} wavelet decomposition window giving us a time of arrival of 230.4 seconds. The S phase is detected in the 25^{th} wavelet decomposition window and the time of arrival is 640 seconds. This measurement can be made more accurate using the overlapping moving window as explained previously. The difference between the S phase arrival time and the P phase arrival time is:

640 (10.67 min) – 230.4 (3.84 min) = 409.6 seconds (6.83 min)

The epicenter of the earthquake is approximately calculated by multiplying the difference of S phase and P phase arrival time in seconds by 10 km/sec, giving us 4096 kms (2545 miles). This is approximately equal to the distance between the actual epicenter of the earthquake at Plattsburg, New York and the Junction City, Texas, seismic station which is 2142 miles.

This is one more example of the wavelet transform method which can be successfully applied to the analysis of seismic signals for identification and classification of the earthquake features.

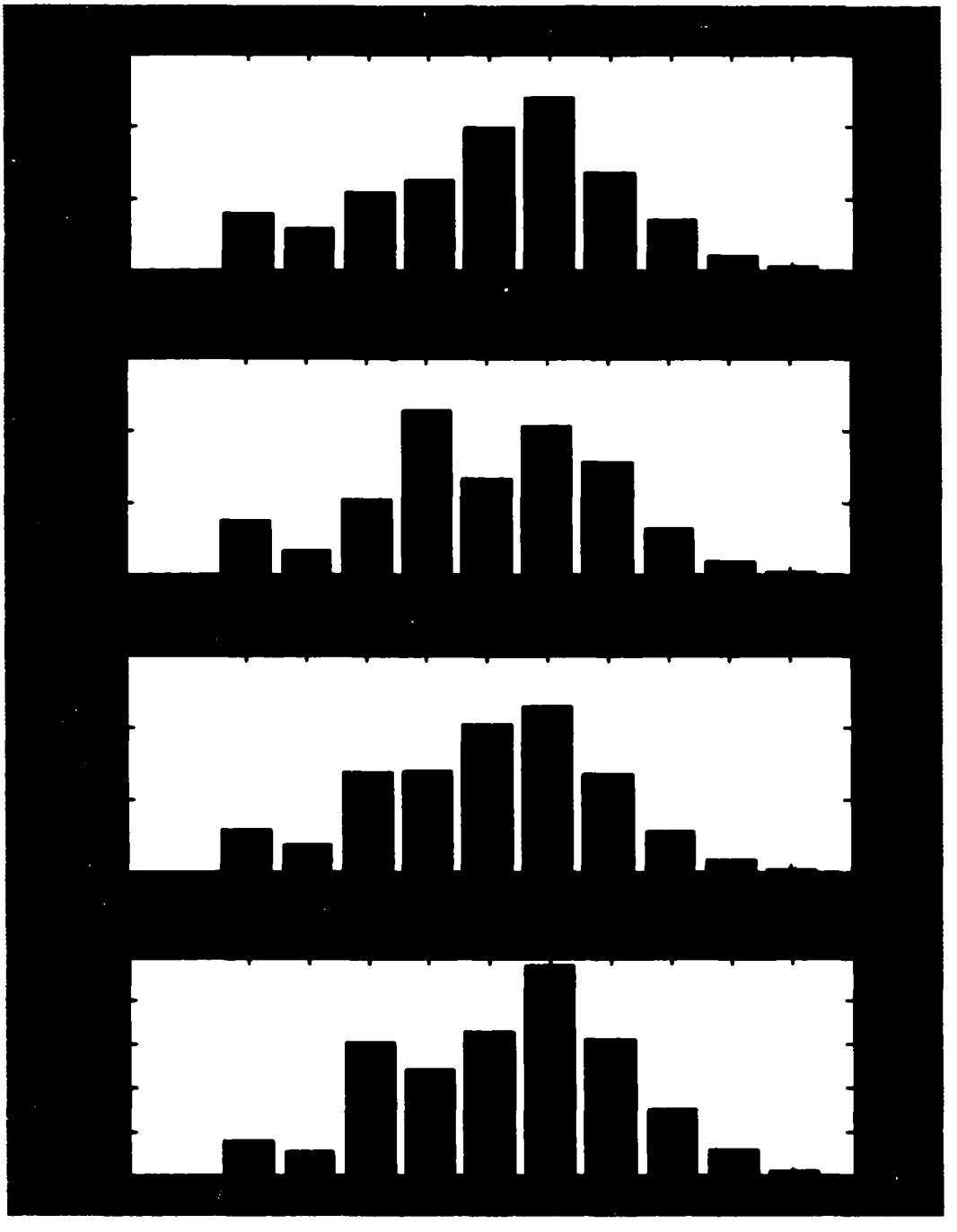

Figure 88: Histogram Plots Of Rms Values For D20 Wavelet Decompositions Of The New York Earth Quake Seismic Signal.

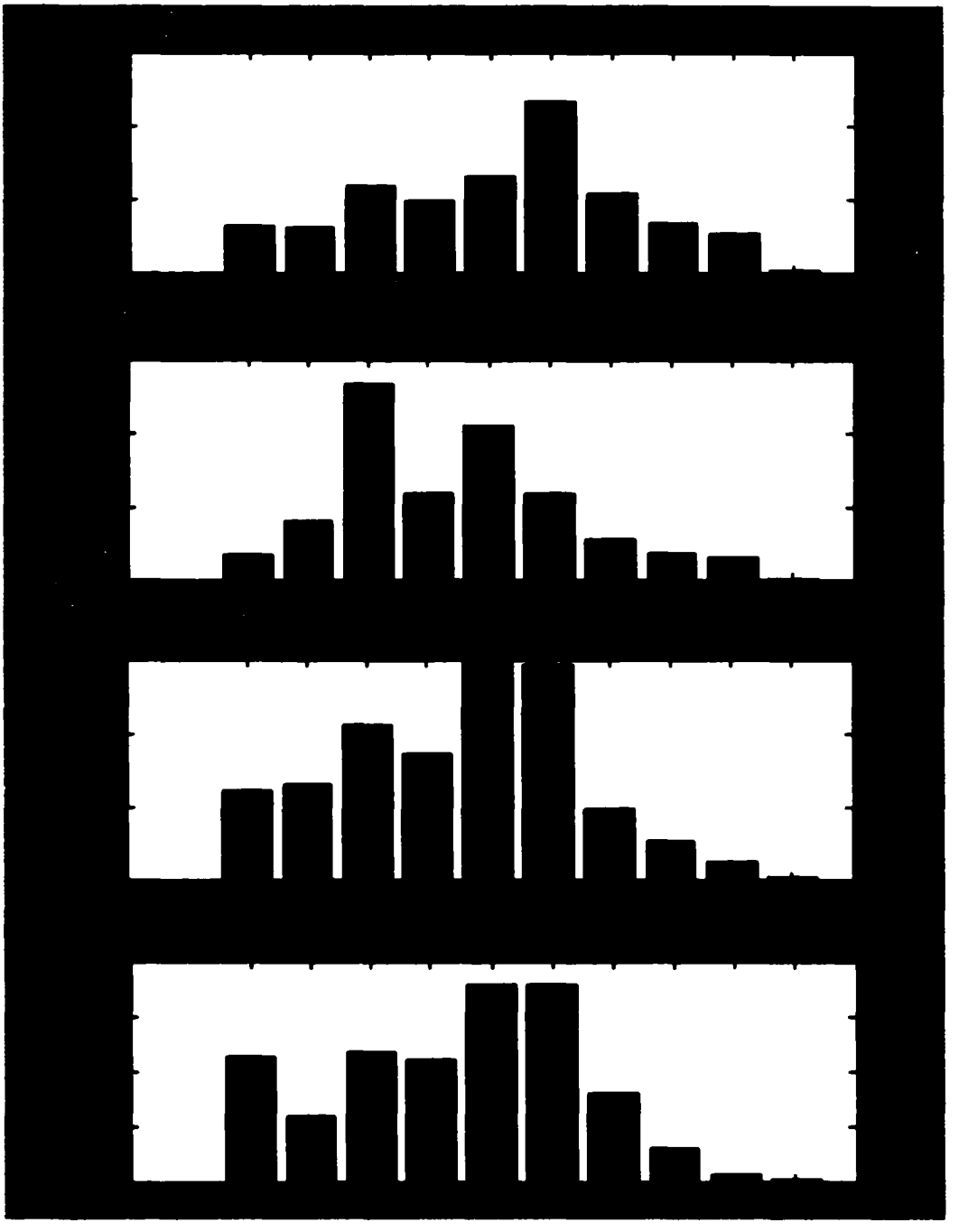

Figure 89: Histogram Plots Of Rms Values For D20 Wavelet Decompositions Of The New York Earth Quake Seismic Signal.

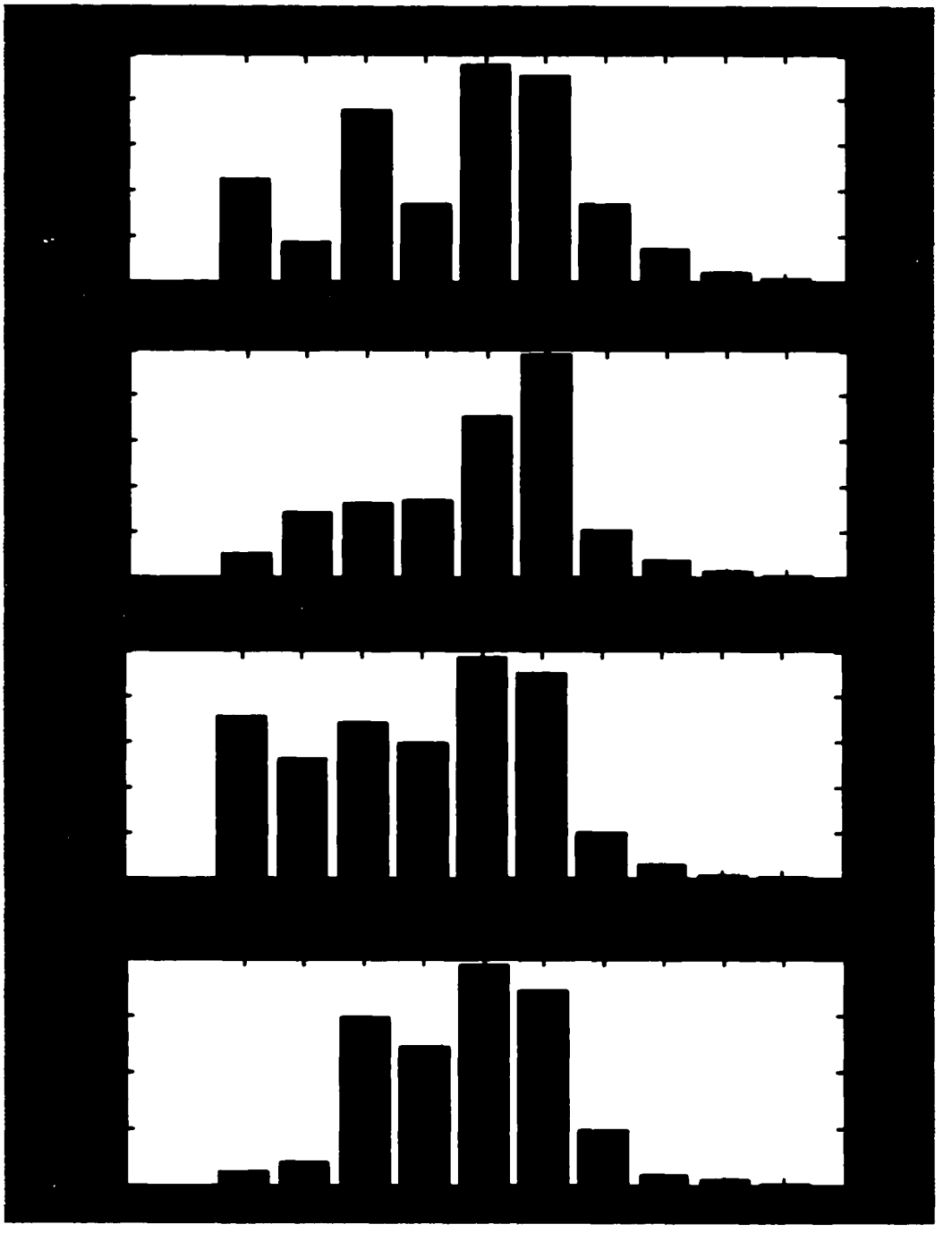

Figure 90: Histogram Plots Of Rms Values For D20 Wavelet Decompositions Of The New York Earth Quake Seismic Signal.

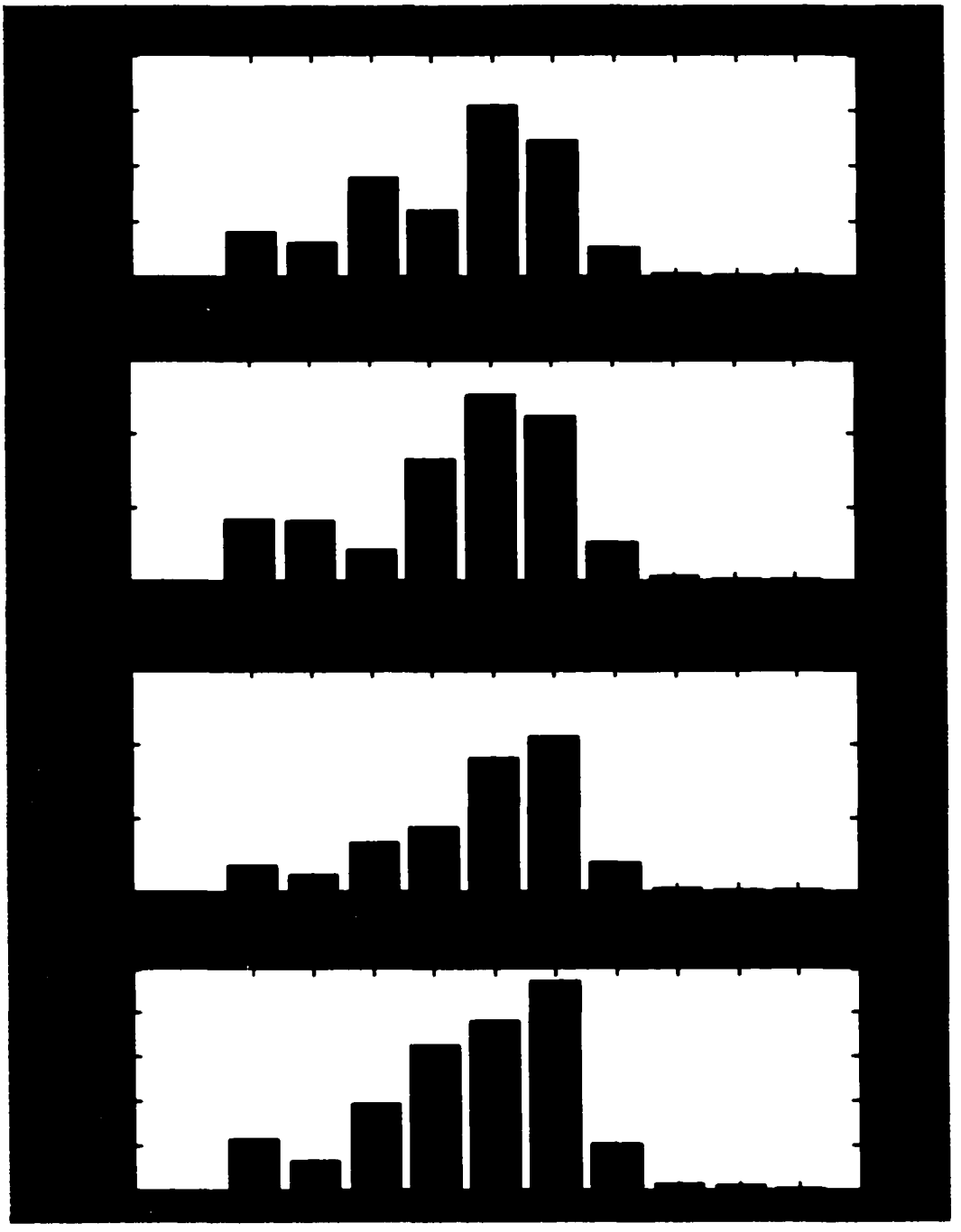

Figure 91: Histogram Plots Of Rms Values For D20 Wavelet Decompositions Of The New York Earth Quake Seismic Signal.

The inherent known margin of error in measurement is the time of detection of the P phase and the S phase wave which is 25.6 seconds, i.e., the window length of the

wavelet transform. Hence, a total of 51.2 seconds or 500 kms (310.7 miles) measurement error due to the window length of the measurement technique can be reduced by overlapping windows, enhancing resolution and accuracy.

Using a moving window of length 1024 data points and sliding it by 128 data points each time, we can compute the wavelet transform of the signal. Plot 93 shows the output of the Daubechies D_{20} wavelet level 5 for the New York seismic signal for both fixed non-overlapping window and the 128-point shift over-lapping window of length 1024.

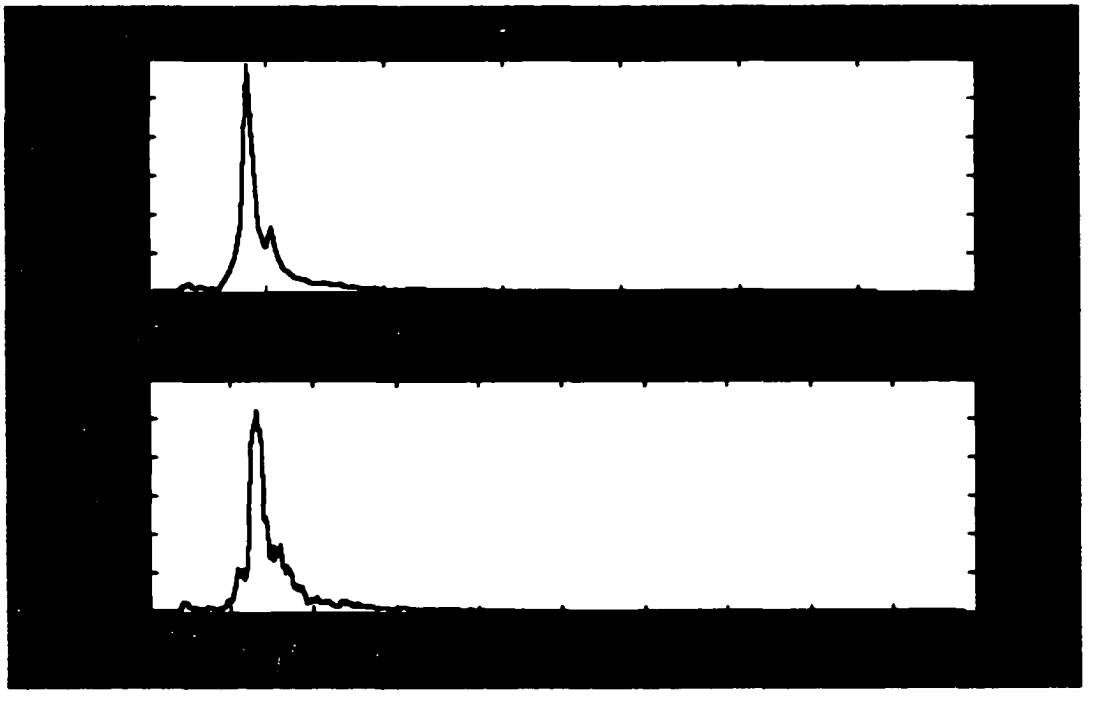

Figure 92: Daubechies D_{20} Wavelet Level 5 For The New York Seismic Signal For Both Fixed Non-Overlapping Window And The 128- Point Shift Over-Lapping Window Of Length 1024.

In figure 93 the overlapping window plot shows a few more fine features than the fixed non-overlapping window. Zooming in on the P phase section of the plots, we can clearly

see as shown in Figure 94, the output signal crosses the 200 counts amplitude threshold much earlier for the former.

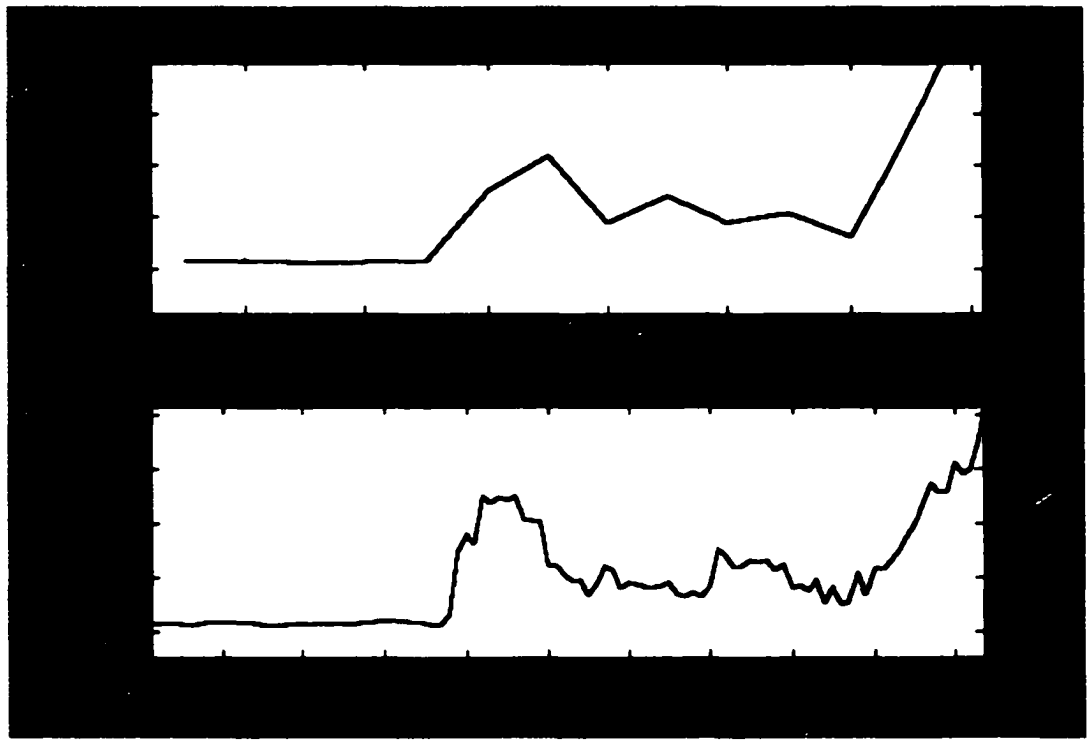

Figure 93: Zoomed In Plot Of Figure 89 Showing The P-Phase Section.

As shown earlier in the discussion of the New York earthquake signal measured at Oxford, MS, for the non-overlapping window the P-phase wave is detected at the 6^{th} window for a threshold of 200 counts amplitude, corresponding to an arrival time of 153.6 seconds. For the 128-point shift over-lapping window, the P-phase wave is detected at the 39^{th} window, corresponding to a time of 124.8 seconds. The change in time of the measurement can be attributed to the better measurement accuracy of the overlapping window technique.

Applying the above wavelet method to other earthquake signals recorded at different stations, we can show that the wavelet method has a promising potential in detecting the P

phase and S phase waves of earthquakes accurately. Table 11 shows the times of detection of both the P phase and S phase waves and the estimated distance for the respective earthquakes.

Table 11: Earthquake phase detection times and calculated distance using wavelets for various earthquakes at different stations.

Earthquakes recorded at given stations	P Phase arrival time (seconds)	S Phase arrival time (seconds)	Estimated time difference seconds (distance in kms)
New York (20 Apr 2002 – Plattsburg, NY)			
- Oxford, MS	124.8	422.4	297.6 (2976)
- Junction, TX	156.8	614.4	457.6 (4576)
Southern Indiana (18 June 2002 - Evansville, IN)			
- Oxford, MS	153.6	220.8	67.2 (672)
- Junction, TX	192.0	428.8	236.8 (2368)
Washington (28 Feb 2001 – Nisqually, WA)			
- Pine, OR	60.8	192	131.2 (1312)
- Longmire, WA	3.2	38.2	35.2 (352)
South India (26 Jan 2001 – Gujarat, India)			
- Kislovodsk, Ru	230.4	723.2	492.8 (4928)
- Ala Archa, Ky	204.8	556.8	352 (3520)
Central Alaska (3 Nov 2002 – Cantwell, AK)			
- Oxford, MS	297.6	1562.4	1264(12640)
- Junction, TX	297.6	1562.4	1264(12640)

CHAPTER 8

CONCLUSION

This researched reviewed the basics of wavelet analysis, and an effort was made to understand the wavelet filters and characteristics and apply wavelets to real world engineering applications. Wavelets are becoming popular and are being used widely, generating an interest in the research of wavelet analysis. Clear understanding of wavelets and their characteristics are a key to successful applications. Many theoretical and application-oriented papers have already been written that address the application of wavelets to signal processing, data compression, image processing and other applications. Yet some fundamental questions such as the wavelet filters and characteristics and the one addressed in this research have not been completely answered. The choice of a right wavelet for a given application is an ongoing quest which has not been satisfactorily solved. This research has successfully identified certain issues, and an effort has been made to provide solutions.

The wavelet transform is a powerful analysis tool used in detection of localized signal disturbances and transient signals. The wavelet family is

exhaustive and the use of the right wavelet is important in signal analysis to effectively identify, classify and quantify the signal's events. This research looks towards understanding wavelet filters which are the basis of dyadic wavelet transform using multiresolution analysis. It is shown that the individual low pass and high pass wavelet filters have very good magnitude and almost linear phase characteristics, with maximum flatness both in the passband and stop band. This research also compares the magnitude and phase characteristics wavelet filters of different wavelet families such as Daubechies, Coiflets, Symlets and shows how some wavelets have exactly the same magnitude characteristics but different phase characteristics that differ in the linear slope of the response. The pole zero locations of these wavelet filters are also studied to understand how wavelet filters differ from the usual filter such as an elliptical filter. It is observed that for the low pass wavelet filters, movement of zeros towards π for the Symlets and Coiflets wavelets compared to the Daubechies wavelets does not affect the magnitude characteristics but changes the phase characteristics by increasing the slope. The difference in decay characteristics of the low pass and the high pass filters is observed to be due to the difference in the number for smoothness which governs the decay for the low pass filter and the number for vanishing moments which governs the decay for the high pass filter.

The above information obtained about the magnitude and phase characteristics of the wavelet filters is one of the properties which might be useful in choosing the right wavelet. So, it is not just enough to know the wavelet's scaling function coefficients or its filter coefficients but the actual magnitude and phase response. Two wavelet filters may have the same magnitude, but one has a much greater slope in its phase response than the

other. If both essentially have a linear phase response, then you would choose the filter having a lesser slope in phase response because it would have smaller time delay.

An application of wavelets to fast detection of fault current in a motor is shown which clearly shows the advantages of Daubechies D4 over Daubechies D20. Chapter 4 shows some innovative methods of inrush and fault current identification/protection using wavelets. D4 with fewer coefficients has been shown to clearly distinguish between the inrush current and the fault current. In the wavelet transform, the detection principle is based on the null period that exists in the inrush current. This part of the research has been published in a paper accepted by the IEEE transactions for Power Systems. D4 is found to be a good choice for applications with short period events.

The wavelets are further studied as an alternative to protective relaying techniques in existence at present. For protective relaying, one of the important characteristics of a good relaying system is its short time response, i.e., the fault must be detected early and a response provided with the least amount of time possible, preferably within 1-2 cycles. From the phase characteristics of wavelets with varying phase response slopes, D4 with a smaller slope is shown to detect the fault current earlier than D20.

For detecting the frequency composition of the signal being analyzed, an understanding of the energy distribution in the output wavelet decompositions is required. This research shows how total energy of the wavelet decompositions between two wavelets is the same, but the energy distributed in the individual wavelet levels is different. A comparison of energy distributions for different wavelet families is done and tabulated. Wavelets with fewer coefficients are found to have more energy leakage into adjacent bands.

When the filters are used in the wavelet filter bank, the frequency bandwidth characteristics of the different levels of the wavelet transform do not show the same flatness both in the passband and the stopband. It is shown that the wavelet levels have ripple both in the passband and the stopband. Also, these frequency bands do not have sharp cutoff at the ends but some of the energy is seen in the adjacent bands. The characteristics display flatness at the middle of the frequency band clearly confirming that the frequency of interest should be in the middle of the frequency band when performing a wavelet transform. Symlets wavelets with more symmetric coefficients than Daubechies exhibit good flatness with minimum ripple at the very narrow set of frequencies near the center of the frequency band, but the transition region near the ends do not have sharper cut off.

Since the number of wavelet levels and their frequency band ranges are dependent on the two parameters (number of data points and the sampling frequency), the selection of these is critical in qualitative and quantitative analysis of signals. This research shows why a careful selection of the sampling frequency and the number of data points for analyzing a signal is important. Care has to be taken to ensure the frequency of interest is in the center of the band in the wavelet level.

With more understanding of wavelet characteristics, a wavelet seismic event detection method is proposed. This research shows how wavelets can be applied to detect the P phase and S phase waves of earthquakes successfully. This wavelet method uses the classification of the seismic signal into different wavelets each pertaining to a frequency band. These individual bands can then be used to separate out the seismic signal and as in this research: only one of the bands (wavelet level 5) containing the information can be

used to detect the P phase and the S phase of wavelets by a simple amplitude threshold trigger method. This method can be a potential tool for detection of earthquakes since it possesses the same simplicity of detection present in the currently used methods but with a better performance as shown in this research.

The field of wavelets is wide open to research and exploration for applications in engineering and technology. It is intended that with this research, future research will help us to understand the fundamentals of wavelet better to make well-qualified decisions in choosing a right wavelet for an application. Wavelets are a promising tool that will complement the existing signal processing methods available and can be used widely if its advantages and limitations are understood.

In summation, the contributions of this research can be listed as:

1) Presenting the basics of wavelets with an engineering perspective.
2) Understanding of wavelet filters in terms of their pole – zero locations and their magnitude and phase characteristics.
3) Showing that some of the wavelet filters have exactly the same magnitude characteristics but differ in the phase characteristics by their linear slopes.
4) Presenting innovative methods in identification and detection of inrush and fault currents, and proposing a wavelet method of protective relaying technique.
5) Research on energy distribution and leakage in output wavelet decompositions among different wavelet families.
6) Presenting the study of frequency bandwidth characteristics of wavelet levels and a comparison between different wavelet families.

7) Showing the importance of careful selection of sampling frequency and number of data points to ensure frequency of interest lies in the middle of the band.

8) Proposing a wavelet method for detection of P-phase and S-phase waves in earthquakes and applying it to recent earthquakes in the past to show its better performance.

REFERENCES

1. Mackenzie. D.. "Wavelets: Seeing the Forest and the Trees." National Academy of Sciences. December 2001.

2. Qian. S.. "Introduction to Time-Frequency and Wavelet Transforms " National Instruments Corp. Prentice Hall. Inc.. 2002.

3. Aki. K. and Richards. P.G.. " Quantitative Seismology " first edition (1980). Freeman and Company. CA and second edition (2002). University Science Books. CA.

4. Jepsen. D. C.. and Kennett. B.L. N.. " Three-component analysis of regional seismograms ". Bulletin of Seismological Society of America. 80. 2032-2052. 1990.

5. Bear. M.. and Kradolfer. U.. " An automatic phase picker for local and teleseismic events ". Bulletin of Seismological Society of America. 77(4). 1437-1445. 1987

6. Sweldens. W.. " Wavelets: What Next? ". AT & T Bell Laboratories. Murray Hill. NJ 07974.

7. Bentley. P. M.. and McDonnell. J.T.E.. " Wavelet Transforms: An Introduction. " Electronics and Communication Engineering. Vol 6. No. 4. August 1994.

8. Wilkinson. W. A. and Cox. M. D.. " Discrete Wavelet Analysis of Power System Transients." IEEE Transactions on Power Systems. 1996.

9. Galli. A.W. and O.M.Nielsen. "Wavelet Analysis for Power System Transients." IEEE Computer Applications in Power. Vol. 12. No. 1. January 1999.

10. Bruce. A. D. Donoho. H. Gao. "Wavelet Analysis." IEEE Spectrum. October 1996.

11. Sarkar. T.K. C. Su. R. Adve. M. Salazar-Palma. L. Garcia-Castillo. R. R. Boix. "A Tutorial on Wavelets from and Electrical Engineering Perspective. Part 1: Discrete Wavelet Techniques." IEEE Antennas and Propagation Magazine. Vol. 40. No. 5. October 1998

12. Resende, J.W., Chaves, M.L.R., and Penna, C., " Identification of power quality disturbances using the MATLAB wavelet transform toolbox " Universidade Federal de Uberlandia (MG) – Brazil.

13. Ezekiel, S., Hovis, R. A., Kramer, J. M., and Aisheri, A. A., " Seismic signal Processing by Wavelet Based Multifractal Analysis ". Ohio Northern University, Ohio and Mine Safety and Health Administration, PA.

14. Fu, S., Liu, X., Muralikrishnan, B., and Raja, J. " Wavelet Analysis with Different Wavelet Bases for Engineering Surfaces " Center for Precision Meterology, The University of North Carolina at Charlotte, NC.

15. Yoon, W. and M.J. Devaney. " Power Measurement Using the Wavelet Transform." IEEE Transactions on Instrumentation and Measurement, Vol. 47, No. 5, October 1998.

16. Rao, N., " Speech Compression Using Wavelets ", Thesis, University of Queensland, QLD, UK, October 2001.

17. Parameswariah, C., and Cox, M. D., " Frequency Characteristics of Wavelets " IEEE Transactions on Power Systems, PE-618PRD, October 2001.

18. Xiangxun, C., "Discussion of Frequency Characteristics of Wavelets." IEEE Journal of Power Systems, PE-618PRD (10-2001).

19. Misiti, M., Y. Misiti, G. Oppenheim and J. Poggi., Wavelet Toolbox – User's Guide, Natick, MA: The MathWorks, Inc., 1984-1997.

20. NewLand, D.E., An Introduction to Random Vibrations, Spectral and Wavelet Analysis, 3rd ed. New York: John Wiley and Sons, Inc., 1993.

21. Daubechies, I., "The Wavelet Transform, Time-Frequency Localization and Signal Analysis." IEEE Transactions on Information Theory, Vol. 36, No. 5, September 1990.

22. Nguyen, T. Strang, G. "Wavelets and Filter Banks.." Wellesley – Cambridge Press, Massachusetts, USA, (1996).

23. Bruce, L. M., Li, J., and Burns, M., " Wavelets: Seeing the Forest and the Trees ". University of Nevada, Las Vegas, NV.

24. Mallat, S., " A Theory For Multiresolution Signal Decomposition: The wavelet Representation ". IEEE Transactions on Pattern Analysis and Machine Intelligence, Vol 11, pp. 674-693, July 1989.

25. Litwin, L., "FIR and IIR digital filters", IEEE Potentials, October/November 2000.

26. Ridsdill-Smith, T. A., "The Application of the Wavelet Transform to the Processing of Aeromagnetic Data", Ph.D Thesis, Department of Geology and Geophysics, The University of Western Australia.

27. Reza, A. M., "Wavelet Characteristics, What Wavelet Should I use?", White Paper, Spire Lab, University of Wisconsin, Milwaukee, October 1999.

28. Wai, C.T and Li, Q "A Dyadic Wavelet Method for Transformer Inrush Current Detection", NTU EEE Review.

29. Wai, C.T, Li, Q, and Keerthipala, K.K.L, "Transformer Inrush current Investigation based on Wavelet Analysis." AUPEC, September 1998.

30. Gomez-Morante, M. and Nicoletti, D.W, "A Wavelet-based Differential Transformer Protection." IEEE Transactions on Power Delivery, Vol.14, No. 4, October 1999.

31. Resende, J.W., Chaves, M.L.R., and Penna, C., "Identification of power quality disturbances using the MATLAB wavelet transform toolbox", Universidade Federal de Uberlandia (MG) –Brazil.

32. Angrisani, L., P. Daponte, M. D'Apuzzo and A. Testa, "A Measurement Method Based On The Wavelet Transform For Power Quality Analysis." IEEE Transactions on Power Delivery, Vol. 13, No. 4, October 1998.

33. Lyons, R. G., "Understanding Digital Signal Processing", Addison Wesley Longman Inc., 1999.

34. Allen, R., "Automatic Phase Pickers: Their Present use and Future Prospects", Bulletin of the Seismological Society of America, Vol 72, No. 6, December 1982.

35. Fedorenko, Y. V., and Husebye, E. S., "Simulating Seismic Signal Detectors", 21st Seismic Research Symposium, September 1999.

36. Herrin, E. and Goforth, T., "An Automatic Seismic Signal Detection Algorithm based on Walsh transform", Bulletin of Seismological Society of America, Vol 71, No 4, August 1981.

37. Joswig, M., "Pattern Recognition for Earthquake Detection", Bulletin of Seismological Society of America, Vol 80, No. 1, February 1990.

38. Dowla, F. and Taylor, S., "Seismic Discrimination with Artificial Neural Networks: Preliminary Results with Regional Spectral Data", Bulletin of Seismological Society of America, Vol 80, No. 5, October 1990.

39. Murdock, J. and Hutt, C., "A New Event Detector Designed for the Seismic Research Laboratories", United States Department of the Interior Geological Survey, Open File Report 83-785, October 1983.

40. Chakraborty, A. and Okaya, D., "Frequency – time decomposition of seismic data using wavelet-based methods", Geophyics, Vol 60, No. 6, 1906-1916, December 1995.

41. Regan, T. L., "Quake Ripples Felt", The Times, www.nj.com/news/times, Nov 13, 2002.

42. Oonincx, P. J., "Automatic phase detection in seismic data using the discrete wavelet transform", Probability, Networks and Algorithms, CWI, PNA-R9811, October 1998

43. IRIS Consortium, http://www.iris.washington.edu

44. Melchior, P. "The tides of Planet Earth", Pergamon Press, Oxford, 1978.

45. Tmkoczy, A., "Understanding and parameter setting of STA/LTA trigger algorithm", Manual of Seismological Observatory Practices, http://www.seismo.com/msop

46. Brearley, A., "How the earth works", 2001.

47. Gendron, P., Ebel, J., and Manolakis, D., "Automatic Seismic Event Detection, Characterization and Classification: A Probabilistic Approach", September 1998.

48. Sidhu, T. S., and Sachdev, M. S., "Use of EMTP for Designing and Testing Protective Relays", http://www.electricityforum.com/et

49. Kezunovic, M., and Russell, B. D., "Microprocessor Applications to substation control and protection", IEEE Computer Applications in Power, Vol 1, No. 4, pages 16 – 20, October 1988.

50. Vasilic, S., and Kezunovic, M., "New Design of a Neural Network Algorithm for Detecting and Classifying Transmission Line Faults", Texas A&M University, College Station, TX.

51. Power System Relaying Committee, Working Group D5 of the Line Protection Subcommittee, "Proposed statistical performance measures for microprocessor-

based transmission line protective relays. Part I and II". IEEE transactions in Power Delivery. Vol 12. No. 1. pages 134 –156. January 1997.

52. Kezunovic. M.. and Kaztenny. B.. "Design Optimization and Performance Evaluation of the Relaying Algorithms. Relays and Protective Systems Using Advanced Testing Tools". Texas A&M University. College Station. TX.

53. Mudock. J. N.. and Hutt. C. R.. " A New Event Detector Designed for the Seismic Research Observatories". Open File Report 83 – 785. US Department of the Interior Geological Survey. Albuquerque. New Mexico. October 1993.

APPENDIX A

MATLAB PROGRAMS

1) EnergyDistribution.m

```
% EnergyDistribution.m
%
% A matlab program that sweeps the frequency between two frequency limits in steps of 1 Hz and
% calculates the wavelet transform at each step. Then it plots the values for two wavelet levels
% as frequency bandwith characteristics both in linear magnitude and dB.
%
Set number of data points and time.
t = 0:0.1/511:0.1
z = 1
% Set frequency limits and step (lower_limit:step:upper_limit)
for f = 120:1:360
   f
   freq(z) = f;
   s = sqrt(2)*sin(1*pi*t*f);
   % Which wavelet transform
   w = 'db10';
   lvl = 8;
   % Perform the wavelet transform
   [C,L] = WAVEDEC(s,lvl,w);
      for i = 1:lvl
         A(i,:) = wrcoef('a',C,L,w,i);
         D(i,:) = wrcoef('d',C,L,w,i);
      end
      % Calculate the rms values
      for i = 1:lvl
         Alvlrms(i) = sqrt((1/512)*sum(prod([A(i,:);A(i,:)])));
         Dlvlrms(i) = sqrt((1/512)*sum(prod([D(i,:);D(i,:)])));
      end
      for i = 1:lvl+1
         binlvl(i) = i - 1;
      end
   % Arrange the rms values and get the last approximation
   rmslvl = [Dlvlrms Alvlrms(lvl)];
   rmslvl = wrev(rmslvl);
   % Put the rms values for level 5 and 6 into arrays
   rmsvald5(z) = rmslvl(5);
   rmsvald6(z) = rmslvl(6);
   z = z+1
end
rmsvald5
rmsvald6
% Plot all figures and name them correctly.
plot(freq,rmsvald5)
TITLE('FREQUENCY BANDWIDTH CHARACTERISTICS - Daubechies D20 detail level d5')
XLABEL('Frequency in Hz')
YLABEL('Amplitude')
figure:plot(freq,rmsvald6)
TITLE('FREQUENCY BANDWIDTH CHARACTERISTICS - Daubechies D20 detail level d6')
XLABEL('Frequency in Hz')
YLABEL('Amplitude')
rmsvald5db = 20*log(rmsvald5/max(rmsvald5))
figure:plot(freq,rmsvald5db)
TITLE('FREQUENCY BANDWIDTH CHARACTERISTICS - Daubechies D20 detail level d5')
```

```
XLABEL('Frequency in Hz')
YLABEL('Amplitude in dB')
rmsvald6db = 20*log(rmsvald6/max(rmsvald6))
figure;plot(freq,rmsvald6db)
TITLE('FREQUENCY BANDWIDTH CHARACTERISTICS - Daubechies D20 detail level d6')
XLABEL('Frequency in Hz')
YLABEL('Amplitude in dB')
```

2) Hist_of_rmsenergy.m

```
% Hist_of_rmsenergy.m
% This program calculates the wavelet transform of a input signal s and plots the histogram of
% the wavelet levels both in rms and energy.
%
% load the simulated signal
load signal60420
t=0:0.1/511:0.1;
s = signal60420;
% Plot the signal time series
plot(s)
figure
% Choose the wavelet
w = 'db10';
lvl = 8;
% Do the wavelet transform
[C,L] = WAVEDEC(s,lvl,w);
for i = 1:lvl
   A(i,:) = wrcoef('a',C,L,w,i);
   D(i,:) = wrcoef('d',C,L,w,i);
end
% Calculate the rms values for each level
for i = 1:lvl
   Alvlrms(i) = sqrt((1/512)*sum(prod([A(i,:);A(i,:)])));
   Dlvlrms(i) = sqrt((1/512)*sum(prod([D(i,:);D(i,:)])));
end
for i = 1:lvl+1
   binlvl(i) = i - 1;
end
% Arrange the rms values into an array
rmslvl = [Dlvlrms Alvlrms(lvl)];
rmslvl = wrev(rmslvl)
% Plot the rms values
subplot(2,1,1)
bar(binlvl, rmslvl)
% Calculate the Energy values
rmslvlsq = prod([rmslvl;rmslvl]);
rmsenergy = sum(rmslvlsq);
rmstotal=sqrt(rmsenergy);
% Plot the energy values
subplot(2,1,2)
bar(binlvl,rmslvlsq)
```

3) Seisrmscalc.m

```
% seisrmscalc.m
%
% This program reads in the seismic data obtained from iris consortium which is in array
% of 5 columns and converts it into a column array. This is then windowed and wavelet %transformed.
% The rms and energy values at each window are calulated and plotted. These plots are saved.
%
% Load the data
[data] = textread('C:\MATLAB6p1\chethan\Dissertation\seismic\ny_oxf.txt','','delimiter',' ');
[m, n] = size(data);
% set y such that the number of rows selected gives us 1024 data points
y = 1; z = y + 205;
% Start loop to conver data to single column array
while z < 12411
k = 1
   for i = y:1:z
      for j = 1:1:n
         fulldata(k) = data(i,j);
         k = k+1;
      end
   end
fulldata1 = fulldata;
fulldata_1 = fulldata1-900;
% Get only 1023 data points
fulldata_1 = fulldata_1(1:1023);
length(fulldata_1);
s = fulldata_1;
% Plot and save the time series
h = plot(s);
saveas(h,num2str(z),'fig')
saveas(h,num2str(z),'jpg')
h1 = figure;
% Choose the wavelet
w = 'db10';
lvl = 9;
% Perform wavelet transform
[C,L] = WAVEDEC(s,lvl,w);
for i = 1:lvl
   A(i,:) = wrcoef('a',C,L,w,i);
   D(i,:) = wrcoef('d',C,L,w,i);
end
% Calcualte the rms values
for i = 1:lvl
   Alvlrms(i) = sqrt((1/512)*sum(prod([A(i,:);A(i,:)])));
   Dlvlrms(i) = sqrt((1/512)*sum(prod([D(i,:);D(i,:)])));
end
% Arrange number of bins
for i = 1:lvl+1
   binlvl(i) = i - 1;
end
% Arrange the rms values
rmslvl = [Dlvlrms Alvlrms(lvl)];
rmslvl = wrev(rmslvl);
% Plot rms values
```

```
subplot(2,1,1)
bar(binlvl, rmslvl)
% Calculate Energy
rmslvlsq = prod([rmslvl:rmslvl]);
rmsenergy = sum(rmslvlsq);
rmstotal=sqrt(rmsenergy);
% Plot energy
subplot(2,1,2)
bar(binlvl,rmslvlsq)
% Finally save one plot for every window.
saveas(h1,num2str(z+1),'fig')
saveas(h1,num2str(z+1),'jpg')
% increment both y and z
y = z; z = z + 205;
figure
% Clear the variables
clear fulldata1 fulldata_1;
end
```

4) eventdetect_mw.m

```
% eventdetect_mw.m
%
% This program detects the P phase and S phase waves of the seismic earthquake event.
% Load the seismic signal data into an array
[data] = textread('C:\MATLAB6p1\chethan\Dissertation\seismic\ny_oxf.txt','','delimiter',' ');
[m, n] = size(data);
cnt = 1
k = 1;
% Convert the whole data into a column array
   for i = 1:1:25410
      for j = 1:1:n
         fulldata(k) = data(i,j);
         k = k+1;
      end
      k
   end
fulldata1 = fulldata;
fulldata_1 = fulldata1-900;
% set initial window parameters
r = 1; p = 1023;
% Start loop
while p <= k
fulldata_2 = fulldata_1(r:p);
s = fulldata_2;
% Choose wavelet
w = 'db10';
lvl = 9;
% Perform wavelet transform
[C,L] = WAVEDEC(s,lvl,w);
for i = 1:lvl
   A(i,:) = wrcoef('a',C,L,w,i);
   D(i,:) = wrcoef('d',C,L,w,i);
end
% Calculate the rms values
```

```
for i = 1:lvl
   Alvlrms(i) = sqrt((1/512)*sum(prod([A(i,:);A(i,:)])));
   Dlvlrms(i) = sqrt((1/512)*sum(prod([D(i,:);D(i,:)])));
end
for i = 1:lvl+1
   binlvl(i) = i - 1;
end
% Arrange the rms values
rmslvl = [Dlvlrms Alvlrms(lvl)];
rmslvl = wrev(rmslvl);
% Put the rmsvalues for level 5 into an array
eventdetect_mw(cnt) = rmslvl(5);
cnt = cnt + 1;
% Slide window
r = r + 128; p = p + 128;
% Clear variables
clear s fulldata_2;
end
% Finally save when done looping over all data.
save eventdetect_mw
save fulldata
```

APPENDIX B

COPY OF PUBLISHED PAPER

FREQUENCY CHARACTERISTICS OF WAVELETS

Chethan Parameswariah, Student Member, IEEE Mickey Cox, Senior Member, IEEE
Department of Electrical Engineering
Louisiana Tech University
Ruston, LA 71272 USA

Abstract: Wavelets detect and locate time of disturbances successfully, but for measurement of power/energy they also have to estimate and classify them accurately. This paper investigates the factors on choice of a certain wavelet function and qualitatively shows how the number of coefficients of the wavelets is an important number that affects output decomposition and energy distribution leakage. Wavelets provide an output in terms of the time – frequency scale. The frequency bandwidth characteristics of these individual wavelet levels provide better understanding of the wavelets. The sampling frequency and the number of data points are important parameters and must be carefully selected to avoid the frequency of interest falling into the end regions.

Keyword: wavelet transforms, transforms, frequency response, power quality, frequency.

I. INTRODUCTION

The Fourier transform (FFT) and the Short Time Fourier transform (STFT) have been often used to measure transient phenomena. These techniques yield good information on the frequency content of the transient, but the time at which a particular disturbance in the signal occurred is lost [5],[12].

Wavelets are relatively new analysis tools that are widely being used in signal analysis. In wavelet analysis, the transients are decomposed into a series of wavelet components, each of which is a time-domain signal that covers a specific octave band of frequency. These bands of frequency are non-overlapping bands with constant-Q characteristics [13]. Wavelets do a very good job in detecting the time of the signal, but they give the frequency information in terms of frequency band regions or scales.

Tutorial and theoretical papers have been published that address the issue of time localization [1]-[4]. This paper primarily focuses on the frequency characteristics of wavelets.

II. REVIEW OF WAVELET ANALYSIS

A typical transformer inrush current and several of its decomposed components are shown in figure 1. The MATLAB® wavelet toolbox was used in this study to generate the Daubechies D4 wavelet components for the inrush current waveform [6],[7],[14]. To conserve space, only three of the eleven wavelet components are shown in figure 1. The x axis for each waveform in figure 1 represents time, whereas the y axis in each case is a linear amplitude scale.

Figure 1 (a): Original input signal - transformer inrush current.

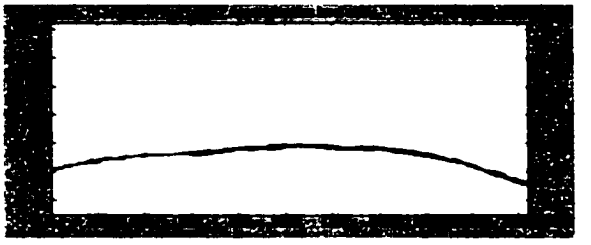

Figure 1(b): Approximation a10 (Level 0)

Figure 1(c): Detail d 10 (Level 1)

Figure 1(l): Detail d 1 (Level 10)

Figure 1 Wavelet decomposition of the signal using Daubechies db 4 wavelet function

A signal can be fully decomposed into n levels, given by $N = 2^n$, where N is the total number of data points. Since the inrush current waveform has 2048 data points,

$$N = 2048 = 2^{11}. \quad (1)$$

there are 11 dyadic wavelet levels the signal can be fully decomposed to [1]. Each of these wavelet levels correspond to a frequency band given by the equation:

$$f = 2^{v}\left(f_s/N\right) \quad (2)$$

where f is the higher frequency limit of the frequency band represented by the level v, f_s is the sampling frequency and N is the number of data points in the original input signal [1]. The maximum frequency that can be measured is given by the Nyquist theory as:

$$f_{max} = f_s/2 \quad (3)$$

where f_s is the sampling frequency.

Table 1 gives the frequency band information for the different levels of the wavelet analysis shown in figure 1, where the sampling frequency f_s =10.240 Hz.

Table 1

	Wavelet level	Frequency Band	Center Frequency
1	0 (a10)	DC - 5 Hz	2.5 Hz
2	1 (d10)	5 - 10 Hz	7.5 Hz
3	2 (d9)	10 - 20 Hz	15 Hz
4	3 (d8)	20 - 40 Hz	30 Hz
5	4 (d7)	40 - 80 Hz	60 Hz
6	5 (d6)	80 - 160 Hz	120 Hz
7	6 (d5)	160 - 320 Hz	240 Hz
8	7 (d4)	320 - 640 Hz	480 Hz
9	8 (d3)	640 - 1280 Hz	960 Hz
10	9 (d2)	1280 - 2560 Hz	1920 Hz
11	10 (d1)	2560 - 5120 Hz	3840 Hz

Thus, it can be seen that the wavelet decomposition agrees with the Nyquist criteria and, hence has a maximum measurable frequency of one half of the sampling frequency.

This is in contrast to the usually used Fourier Transform or the windowed Fourier Transform - the Short Time Fourier Transform (STFT). In the Fourier Transform, the time-based signal is completely transformed into a frequency-based signal. Figure 2 shows a FFT analysis of the input signal.

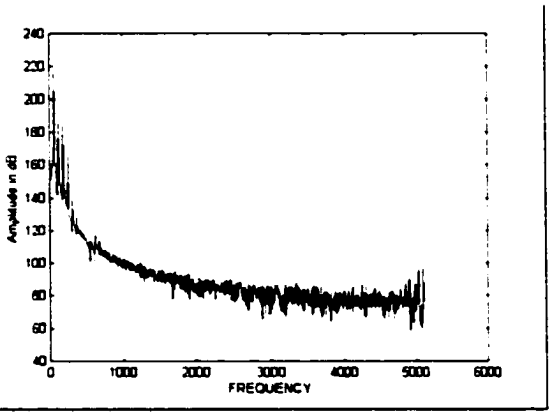

Figure 2: FFT analysis of the transformer inrush current waveform in figure 1

The maximum frequency of measurement using the FFT analysis is also equal to $f_{max} = f_s/2$, where f_s is the sampling frequency. The frequency composition is continuos and the exact reproduction of the signal requires all these frequency components.

The wavelet transform has been seen as a great tool that overcomes this problem of time location detection, which is not possible using the FFT transform. However in achieving a good location in time, it loses the frequency location but provides it in terms of frequency bands. As explained above, equation (3) gives the maximum frequency of a wavelet level instead of the center frequency stated in some papers [1],[8],[9]. To an engineer common questions that arise concern frequency bandwidth and the response characteristics at or near the "cut-off" frequencies. The authors have observed that this aspect of wavelets has not been discussed in an engineering point of view by researchers of wavelets. This paper explains the frequency characteristics of the filters used in wavelet decompositions and the energy distribution in each of the different levels. This paper is written in an electrical engineer's perspective and offers insight to the problems encountered.

III. QUESTIONS ENCOUNTERED IN WAVELET ANALYSIS

The inrush current signal (fig 1a) is a transient signal in the transformer and it has been a great concern for electrical engineers, as its amplitude is very much higher at higher percentage of remnant flux on the transformer core [10], [11]. This is sometimes very much higher than the full load current of the transformer. This transient magnetizing inrush current causes false tripping of the differential relay and hence shutting the power circuit off [9]. Wavelet analysis is being sought after, as it seems to offer a good solution to this problem. One of the areas of research being carried out in the area of power systems is the detection and identification of inrush current and distinguishing it from the fault current. The figure 3 shows a typical fault current measured.

Figure 3 Transformer fault current

The inrush current and the fault current can be distinguished from each other by the shape of their waveforms. The inrush current has intermittent peaks with valleys in between them. The inrush current is not symmetric in both the half cycles of the waveform. The fault current on the other hand is perfectly symmetric and has equal positive and negative half cycles.

The wavelet transform can be used to distinguish between the inrush current and the fault current. Applying db 4 and db 20 Daubechies wavelet transform to the original transformer inrush signal and the fault current signal, we get the following outputs as shown in figures 4 through 7.

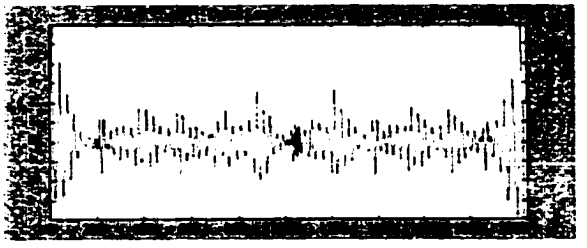

Figure 4. Wavelet decomposition Detail d 4 (Level 7) of the inrush current using Daubechies db 4 wavelet function

Figure 4 has an output that has large amplitude peaks corresponding to the peaks of the inrush current and smaller amplitude peaks corresponding to the valleys (null period) in between the peaks. These are clearly distinguishable and unique to the inrush current helping the engineer to distinctly discriminate the null period.

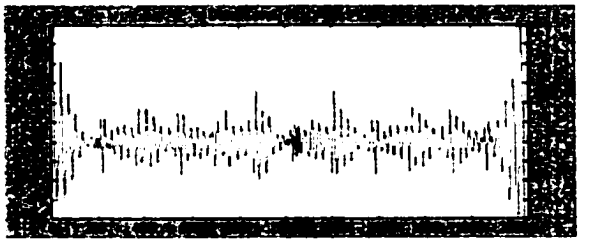

Figure 5 Wavelet decomposition Detail d 4 (Level 7) of the inrush current using Daubechies db 20 wavelet function

It can be clearly seen that the db 20 decomposition that has higher number of coefficients has averaged out the detail d 4 (level 7) (fig 6) output for the transformer inrush current. The output appears to have a uniform amplitude and hence using the wavelet having a large number of coefficients such as a db 20 is not a good choice for this application.

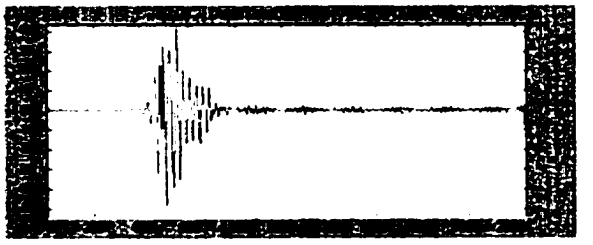

Figure 6 Wavelet decomposition Detail d 4 (Level 7) of the fault current signal using Daubechies db 4 wavelet function

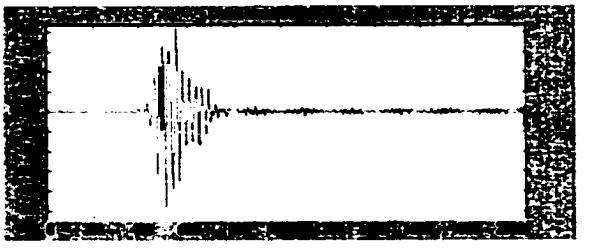

Figure 7 Wavelet decomposition Detail d 4 (Level 7) of the fault current signal using Daubechies db 20 wavelet function

Outputs for a fault current (fig 6 and fig 7) do not show the kind of behavior the decomposition of the magnetizing inrush current shows. It doesn't show any distinctive behavior except for a few large spikes at the state of

transition from the normal current to the fault current. The waveform after the initial spurt decays and remains same for all periods of time. This method of discriminating the magnetizing inrush current from the transformer fault current is better than the existing second harmonic components method used for most of the differential protective schemes. In the wavelet transform, the detection principle is based on the null period that exists in the inrush current.

Hence for applications where the information at a specific instance of time or for a very short period of time is to be retrieved, then the lower db 4 wavelets with less number of coefficients is a better option to use than wavelets with more number of coefficients such as db 20. Hence db 4 wavelets are a good choice for accurately detecting fast transients and short time information signals.

For an information spread over a long period of time such as a signal constituent of its fundamental frequency and its harmonics, the wavelet decomposition can be used to identify these frequencies (though not exactly but can be identified as to lie within the specific frequency bands). Here the db 20 with more number of coefficients is a good choice, as it tends to give us a smoother output than the output obtained by the use of a db 4 decomposition.

To analyze the db20 and db4, we shall consider a known signal simulated using Matlab, having a fundamental frequency combined with its fifth and eleventh harmonic frequency components given by:

$$f(t) = \sqrt{2}\sin(2\pi 60t + 60^{\circ}) + \sqrt{2}\sin(2\pi 300t) + \sqrt{2}\sin(2\pi 660t) \qquad (4)$$

Let us consider the signal for 3 cycles of 60 Hz having 512 data points with a sampling frequency of 10,240 Hz. The wavelet decomposition using the Daubechies wavelet function db 20 of the above signal gives us 9 levels.

Calculating the rms value of the signal $f(t)$:

$$f(t) = \sqrt{2}\sin(2\pi 60t + 60^{\circ}) + \sqrt{2}\sin(2\pi 300t) + \sqrt{2}\sin(2\pi 660t)$$

$$rms(f(t)) \equiv 1.7326$$

The rms value for each of the individual wavelet levels of the above wavelet decomposition using Daubechies db 20 wavelet function is given by table 3.

Table 3

Wavelet level	Frequency band	Rms value
0 (a8)	0-20 Hz	0.0086
1 (d8)	20 - 40 Hz	0.0062
2 (d7)	40 - 80 Hz	0.9799
3 (d6)	80 - 160 Hz	0.1984
4 (d5)	160 - 320 Hz	0.8171
5 (d4)	320 - 640 Hz	0.8637
6 (d3)	640 - 1280 Hz	0.7653
7 (d2)	1280 - 2560 Hz	0.0139
8 (d1)	2560 - 5120 Hz	3.44×10^{-5}

The square root of the sum total of all the rms values is

$$\sqrt{\Sigma(rms\ value)^2} = \sqrt{\begin{matrix}(0.0086)^2 + (0.0062)^2 + (0.9799)^2 + (0.1984)^2 \\ + (0.8171)^2 + (0.8637)^2 + (0.7653)^2 + (0.0139)^2 \\ + (3.449 \times 10^{-5})\end{matrix}}$$

$$rms(f(t)) = \sqrt{\Sigma(rms)^2} \equiv 1.7318$$

The value got by the wavelet decomposition is in good agreement with the rms value of the function $f(t)$.

The Daubechies db 4 wavelet decomposition for the same signal $f(t)$, also gives the total rms value as 1.7318.

This shows that the energy is distributed among the different wavelet levels with the total energy being the same in both the cases of wavelet decomposition. However, an interesting observation can be done on how the energy is distributed in the wavelet decomposition db 4 and db 20

In the case of db 20 wavelet decomposition of the signal having 60 Hz, 300 Hz and 660 Hz frequency components, the energy can be seen to be concentrated in level 2 (40 Hz to 80 Hz), level 4 (160 Hz to 320 Hz), level 6 (640 Hz to 1280 Hz) and level 5 (320 Hz to 640 Hz) of the wavelet decomposition.

Thus it can be seen that the db 20 wavelet decomposition of the original signal into different wavelet levels using filters is not ideal but has a frequency characteristics that are important for the knowledge of an engineer. The bandwidth cut-off points and the roll over characteristics of the filters used in wavelet decomposition are essential for using the wavelet in signal analysis.

For Daubechies db 4 wavelet decomposition, the leakage is more compared to the db 20 wavelet decomposition.

This shows that even when the total energy is same in both the db 4 and db 20 case, the energy distribution varies within the wavelet levels.

To find the bandwidth characteristics of a db 4 wavelet level and db 20 wavelet level, lets consider a sinusoidal signal:

$$f(t) = \sqrt{2}\sin(2\pi ft) \qquad (5)$$

and sweep its frequency between the minimum and maximum frequency of the wavelet level frequency band. The energy of the wavelet level 4 is calculated for each step and the amplitude in dB vs frequency in Hz characteristics plotted. This amplitude level at extreme end frequencies gives the cut-off level.

Table 4 below gives the frequency sweep and its corresponding energy amplitudes both in rms and in decibel (db) values for the wavelet level 4 of the wavelet decomposition db 20.

Table 4

	Frequency (Hz)	Rms value	Decibel value (db)
1	120	0.1918	-14.34
2	140	0.4368	-7.194
3	160	0.2211	-13.11
4	180	0.8995	-0.920
5	200	0.9787	-0.187
6	220	0.9918	-0.0715
7	240	0.9805	-0.1710
8	260	0.9520	-0.4272
9	280	0.9000	-0.9151
10	300	0.8200	-1.724
11	320	1.000	0.00
12	340	0.5726	-4.843
13	360	0.4363	-7.204

Figure 8 below gives frequency characteristics plot of the above data and shows the cut off frequency and its amplitude level.

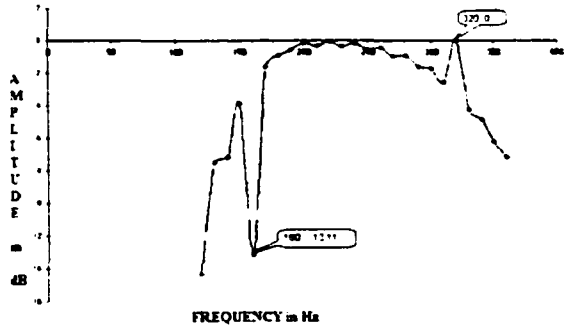

Figure 8: Frequency characteristics db 20 Detail 5 (Level 4)

Figure 9 below shows a frequency characteristics plot of detail 6 (level 5). The frequency range of this level is from 320 Hz to 640 Hz.

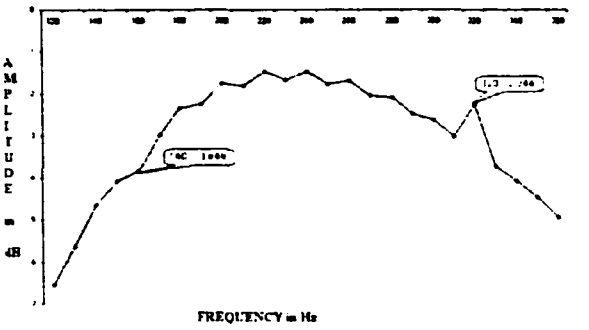

Figure 9: Frequency characteristics db 20 Detail 6 (Level 5)

Let us now decompose the signal using wavelet db 4 and the energy distribution is calculated and the frequency characteristics plotted.

Figure 10 below gives frequency characteristics plot db 4 Detail 5 (level 4) and shows the cut off frequency and its amplitude level.

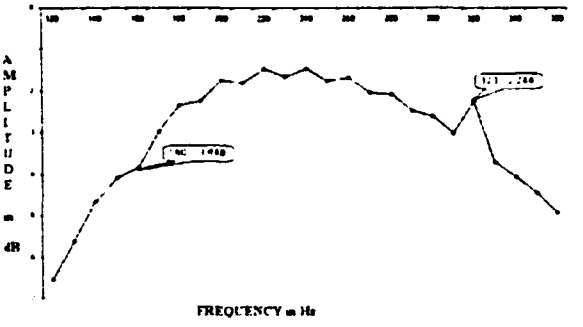

Figure 10: Frequency Characteristics db 4 Detail 5 (level 4)

Figure 11 shows the frequency characteristics for the wavelet decomposition Daubechies db 4 for detail 6 (Level 5).

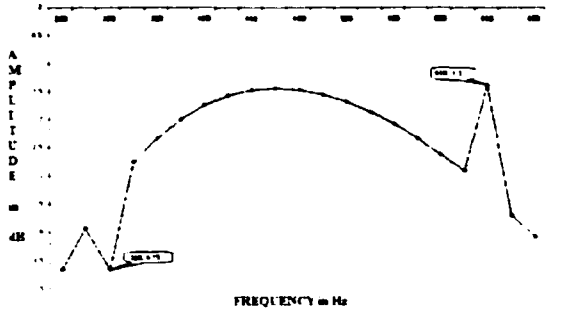

Figure 11: Frequency characteristics db 4 Detail 6 (level 5)

Comparing the above results, we find that the frequency characteristics of the db 4 and the db 20 decompositions are different. The frequency

characteristic plots of both the wavelet levels in db 20 resemble each other. As it can be seen, the lower end frequency slope is steeper and at the cut-off frequency, the amplitude is more than 10 db below the maximum db value. However on the higher frequency end, the curve rises up to a maximum value and then drops steeply after the cut-off frequency. Overlapping both the plots, it can be seen that the db 20 wavelet function exhibits the non-overlapping bandwidths with a very small roll over to the next band. But for a db 4 wavelet, the bandwidth characteristics are poorer and hence a lot of leakage can be seen between the bands. This indicates that a careful selection of the number of data points and the sampling frequency have to be made to avoid the frequency of interest falling on the edges of the band. It is better for the frequency to be at the center of the band to avoid loss of information.

For example, if a signal with its frequency of interest 60 Hz is sampled at a sampling frequency f_S = 7680 Hz and the number of data points N = 512, the wavelet level 2 (detail 7) would have a frequency bandwidth 30 Hz to 60 Hz. The frequency of interest 60 Hz is the cut-off frequency for the band and hence, the measurements made may not be accurate due to the frequency characteristics of the wavelet level. A sampling frequency f_S = 10240 and the number of data points N = 512, will make the wavelet level 2 (detail 7) have a frequency bandwidth 40 Hz to 80 Hz. The frequency of interest 60 Hz now lies at the center of the bandwidth and as seen in the frequency characteristic plots, the amplitude is near the maximum level and hence accuracy is improved.

IV. CONCLUSION

The use of wavelets in signal measurement, detection and analysis has been increasing and yet a few fundamental questions still need to be answered. This paper has identified certain issues regarding the frequency characteristics of wavelets.

Quantitative analysis of wavelet signals show that the db 20 wavelet has less leakage compared to the db 4. The selection of sampling frequency and the number of data points are important. Energy distributions in wavelet levels decomposed were studied and it was found that the total energy was the same but it was interesting to observe the energy distribution between energy levels.

V. REFERENCES

[1]. Wilkinson, W.A. and M.D. Cox. "Discrete Wavelet Analysis of Power System Transients." IEEE Transactions on Power Systems, 1996.

[2]. Galli, A.W. and O.M.Nielsen. "Wavelet Analysis for Power System Transients." IEEE Computer Applications in Power, Vol. 12, No. 1, January 1999.

[3]. Yoon, W. and M.J. Devaney. "Power Measurement Using the Wavelet Transform." IEEE Transactions on Instrumentation and Measurement, Vol. 47, No. 5, October 1998.

[4]. Angrisani, L., P. Daponte, M. D'Apuzzo and A. Testa. "A Measurement Method Based On The Wavelet Transform For Power Quality Analysis." IEEE Transactions on Power Delivery, Vol. 13, No. 4, October 1998.

[5]. Bentley, P.M. and J.T.E. McDonnell. "Wavelet Transforms, an Introduction." Electronics And Communication Engineering, Vol. 6, No. 4, August 1994.

[6]. Daubechies, I. "The Wavelet Transform, Time-Frequency Localization and Signal Analysis." IEEE Transactions on Information Theory, Vol. 36, No. 5, September 1990.

[7]. Misiti, M., Y. Misiti, G. Oppenheim and J. Poggi Wavelet Toolbox – User's Guide, Natick, MA: The MathWorks, Inc., 1984-1997.

[8]. NewLand, D.E. An Introduction to Random Vibrations, Spectral and Wavelet Analysis, 3rd ed. New York: John Wiley and Sons, Inc., 1993.

[9]. Gomez-Morante, M. and D.W. Nicoletti. "A Wavelet-based Differential Transformer Protection." IEEE Transactions on Power Delivery, Vol. 14, No. 4, October 1999.

[10]. Wai, C.T. and Q. Li "A dyadic Wavelet Method For Transformer Inrush Current Detection." NTU EEE Review.

[11]. Wai, C.T., Q. Li and K.K.L. Keerthipala. "Transformer Inrush Current Investigation Based On Wavelet Analysis." AUPEC, September 1998.

[12]. Perrier, V., T. Philipovitch, C. Basdevant "Wavelet Spectra compared to Fourier Spectra." Journal of Mathematical Physics, Vol. 36, No. 3, 1995.

[13]. Sarkar, T.K., C. Su, R. Adve, M. Salazar-Palma, L. Garcia-Castillo, R. R. Boix. "A Tutorial on Wavelets from and Electrical Engineering Perspective, Part 1 Discrete Wavelet Techniques." IEEE Antennas and Propagation Magazine, Vol. 40, No. 5, October 1998.

[14]. Bruce, A. D. Donoho, H. Gao "Wavelet Analysis." IEEE Spectrum, October 1996.

VI. BIOGRAPHY

Chethan Parameswariah, (M'98) a graduate student pursuing his Ph.D. in electrical engineering at Louisiana Tech University was born in Bangalore, India in May 1973. He graduated with his bachelors in electronics from R. V. College of Engineering, Bangalore University, India in Feb 1995. He moved to the US in Aug 1997 to pursue his education. He graduated in Nov 1999 with his masters in electrical engineering from Louisiana Tech University, Ruston, LA. He has worked on the development of an electric car and is currently working on a project to design a fiber optic based sensor for NASA.

Mickey Cox (SM'88) received the B.S. and M.S. degrees from Louisiana Tech University, Ruston, and the Ph.D. degree from Louisiana State University, Baton Rouge, in 1976, 1978, and 1986, respectively, all in electrical engineering. In 1985 he joined the faculty of Louisiana Tech university and is now a Professor of Electrical Engineering. His research interests are harmonics, power quality, and instrumentation and measurements.